CROSSLINKED LIGNIN-STARCH POLYMERS WITH ALTERNATIVE APPLICATIONS

A Thesis Submitted to the
Faculty of Graduate Studies of
Lakehead University

by

Jonathan Alejandro Díaz Baca

Submitted in partial fulfillment of requirements for the degree of
Doctor of Philosophy in Biotechnology

January/16/2023

but test everything; hold fast what is good.

Dedication

To my parents for their immensurable love, support, and dedication. My family, my strength.

Para mis padres, por su inmensurable amor, apoyo, y dedicación. Mi familia, mi fortaleza.

Abstract

Lignin is a complex biopolymer obtained as a by-product from the delignification of wood and grasses. Starch is also a natural polymer of amylose and amylopectin found in many plants, featuring a relatively simple structure and limited solubility in water. Lignin and starch are abundant and inexpensive biopolymers that are often considered sustainable alternatives to oil-based and synthetic polymers. Despite their abundance, and owing to their physicochemical properties, starch and lignin have limited usages as their pristine forms in industrial, high-performance, and food applications. In the last ten years, studies regarding the combination of starch and lignin for producing reinforced materials such as films, coatings, and adhesives have increased significantly. The incorporation of lignin into starch matrices produced materials that were more resistant to water, UV radiation, mechanical stress, and thermal changes. This thesis explores the state of the art for the production of starch-lignin materials, focusing on the physicochemical properties of the starch-lignin materials and the outcomes, challenges, and opportunities for this field.

In the first research study of this thesis, a new process for the isolation of lignin from the tall oil soap (TOS) generated in the kraft pulping process was developed (i.e., LignoTall). The properties and characteristics of the newly isolated lignin (tall oil lignin, (TOL)) were compared against kraft lignin (KL), and a new application was proposed for TOL. In a subsequent study, TOL and potato starch were polymerized with a sulphonate-containing monomer to generate flocculants for colloidal systems. The phenolic substructures of TOL and the anhydroglucose unit of starch were covalently polymerized by the monomer to generate a three-block copolymer, as confirmed by ^{1}H, COSY, HSQC, HSQC-TOCSY, and HMBC NMR analysis. Also, the structure of the copolymers was fundamentally assessed. The results of this research study validated a new approach for

preparing a lignin-starch polymer, which was successfully tested as a flocculant in a colloidal system. In addition, a temperature-responsive macromolecule (KLS) compounded by crosslinking of KL and potato starch (KLS) was generated and studied in another study. The crosslinking of KL and starch was achieved through glycerol ether cross-bonds, which was confirmed by NMR experiments and quantified by X-ray photoelectron spectroscopy (XPS) analysis. Moreover, the viscoelastic properties of KLS water dispersions were determined by rheological analysis. It was found that KLS formed a thermo-responsive structured network because of its multiple functional groups and large molecular weight. Furthermore, the extended globular shape of KLS prompted the development of a gel-like structure when submitted to heating-cooling conditions. Overall, the outcome of this thesis contributes to the knowledge of the production of soluble lignin-starch materials, describing new methods for generating covalently crosslinked lignin-starch macromolecules. Also, the introduction of the LignoTall process for generating TOL opens windows of opportunities for the transformation and application of a new type of lignin with unique properties.

Acknowledgments

First of all, I would like to express my profound gratitude to my supervisor Prof. Pedram Fatehi, for accepting me into his research group and for his tireless guidance, inspiration, support, and effort. I truly admire your commitment, perseverance, and achievements. You are a role model for me. My appreciation goes beyond the professional life and sets on a personal level, knowing that I have a mentor and a friend. Thank you for always providing all the necessary support for the progress of my Ph.D. studies, including but not limited to materials, equipment, and financial and emotional support.

I would also like to thank my thesis committee members, Dr. Sudip K. Rakshit, Dr. Ehsan Behzadfar, and Dr. Hongbin Liu, for their valuable contribution to my Ph.D. research and this thesis work.

I would like to extend my appreciation to Dr. Weijue Gao. Her support, collaboration, and valuable contribution have been present all along in my research. I would also like to specially acknowledge Dr. Ayyoub Salaghi and Dr. Mohan Konduri for their significant contribution to my development as a researcher, and for their priceless friendship.

I would like to thank my fellow lab colleagues, past and present. All of you are a fundamental part of my professional and personal growth. Thank you for every piece of advice, and thank you for your camaraderie, kindness, and professionalism showed from my first day till my last day in the group.

Special thanks to Dr. Guoseheng Wu, and Mr. Michael Sorokopud from the LUIL department of Lakehead University for their very much appreciated technical assistance. Also, I would like to especially thank Dr. Brenda Magajna for her unconditional support as Ph.D. Program Facilitator

and International Student Liaison. My extended thanks to the office of Lakehead International for their continuous assistance.

Thanks to my parents Reyna and Martin, sister Sugey, and brother Brayan, without you, this achievement would not have been possible.

Thanks to my friends, you were always there. Your friendship is my guiding anchor.

Above all else, I would like to express my love, immense gratitude, and profound admiration for Denisse, my dear life partner. There are no words to describe how important you were during my Ph.D. studies; your kind-heartedness, support, and love were always there with me. Denisse, my accomplishments are yours as well; thank you for all.

At last, I would like to acknowledge the financial support from CONACyT-Mexico and Instituto de Innovación y Competitividad-Chihuahua, for funding my Ph.D. studies entirely and financially assisting my living allowances.

Table of contents

List of Figures:

List of Tables:

Chapter 1: Introduction

1.1.Overview

In the last 15 years, there has been a growing interest in substituting traditional fossil fuel-based materials with biobased chemicals.[1–3] In the year 2020, the United Nations established a sustainable development agenda, in which goal 13 calls for impactful actions, such as the development of new technology, that must be taken to reduce greenhouse gas emissions and stop climate change.[4] The current focus of the biobased economy is a gradual change from energy production to the production of high-value biobased materials and chemicals.[5] For instance, the biorefining industry (e.g., pulp and paper, starch, and sugar industries) is shifting towards the production of high-value biobased materials employing a series of processes to convert different biomass feedstocks into biobased products.[6,7] New and more efficient approaches need to be developed in order to prioritize the production of advanced biobased materials, prioritizing the sustainability of biorefining processes.[8,9]

Biopolymers can be obtained as main products, by-products, or in the form of wastes from the biorefining process.[10,11] Among these biopolymers, lignin is obtained as a by-product of the pulping production process and is an aromatic polymer constituting approximately 30% of the lignocellulose biomass.[12] Lignin is composed of phenylpropane units rich in functional groups, such as phenoxy, methoxy, carboxyl, and carbonyl, arranged in a tridimensional conformation.[13] Owing to its chemical properties and extensive availability, lignin is considered a promising green alternative to oil-based and synthetic chemicals.[14] In this thesis, a new method is introduced for separating lignin from the tall oil produced during the kraft pulping process, which is denoted as the LignoTall process.

Kraft pulping is a biorefining process that generates several products, including cellulose, lignin, and tall oil when softwood species are used as biomass resources.[15] During the tall oil recovery, the saponification of fatty acids generates a by-product namely tall oil soap (TOS), which contains tall oil, lignin, water, and inorganic compounds.[16,17] Currently, the lignin contained in TOS is burned in the recovery section of the kraft process.[18] It is unclear if the lignin contained in TOS has any potential for its valorization, and the information regarding its physicochemical characteristics is limited. Therefore, the study and characterization of tall oil lignin (TOL) obtained via the LignoTall process were carried out in this Ph.D. work. Moreover, the characteristics of TOL were compared with those of kraft lignin (KL) as both polymers were obtained through the acidification process of black liquor.

Another extensively utilized biopolymer is starch, a polysaccharide composed of anhydroglucose units (AGU) present in many plants as an energy-reserved macromolecule.[19] Starch is the second most abundant carbohydrate, traditionally used in green processes because of its biodegradability, extensive accessibility, and low production cost.[20] Regardless of the abundance, availability, and low production cost of lignin and starch, both biopolymers require chemical modifications to strengthen their properties and be functionally suitable for commercial applications. The structural complexity, variability and low water solubility of lignin restrict many possible water-based applications, such as the flocculation of suspended particles.[21] Likewise, starch is chemically modified to increase its solubility in water, and to enhance its mechanical, thermal, and flocculation properties.[22,23]

Since TOL possesses a highly hydrophobic behaviour, modifying it with a highly hydrophilic polymer, such as starch, is a logical option for increasing its hydrophilicity.[24] Starch has many hydroxyl groups, which are highly convenient for modification.[25] The free radical polymerization

of monomers, such as acrylic acid, and methacryloyloxyethyl trimethylammonium chloride, has been successfully carried out separately on lignin and starch to improve their properties,[26,27] for instance, water solubility and flocculation efficiency.[23,28] Hence, the free radical polymerization of TOL and starch with a sulphonate-containing monomer was the subject of study in this thesis to generate a sustainable biopolymeric flocculant.

The crosslinking of lignin with starch is another strategy that has gained attention in recent years for overcoming the difficult processability, retrogradation, syneresis, and low mechanical and thermal resistance of starch-based material.[29,30] For example, KL was used as a filler in crosslinked-starch fertilizer films, and starch-based packaging materials, as well as to produce water-resistant adhesives.[30–32] However, lignin had a minor role in those materials as it was used only in a small fraction of the material's compositions. Moreover, most studies utilized physical blending methods to produce solid-state materials (e.g., films, coatings, or adhesives), which frequently display multiphase and miscibility challenges.[33,34] In contrast, the study of water-based systems has not been investigated yet since it is not possible to produce such materials with the physical blending of KL and starch. Consequently, in this thesis, covalently crosslinked KL-starch macromolecules were fabricated, comprehensively characterized, and studied in aqueous systems. In this **chapter**, a summary of chapters two to six is presented, along with the research motivation, objectives and novelty of this thesis.

Chapter two includes a comprehensive review of the relevant literature for the field of lignin-starch biomaterials. This chapter describes the current status, sources, and chemical modifications of lignin and starch, particularly those regarding the production of starch-lignin biomaterials. This chapter focuses on the production pathways and the physicochemical and mechanical properties of starch-lignin biomaterials. The discussion is also extended to the different methodologies and

technologies used to characterize lignin-starch biomaterials, pointing to their advantages, disadvantages, and expected outcomes. Furthermore, the challenges associated with the design and manufacture of lignin-starch biomaterials, as well as the opportunities and future perspectives on their development, are critically reviewed.

Chapter three introduces a new process to produce tall oil, sulphate salts, and tall oil lignin (TOL), namely LignoTall. This process offers the methodology for its integration into the kraft pulping process. Additionally, it provides information about how the spent liquor generated in LignoTall can be reintegrated into the pulping process. This chapter provides insights into the physicochemical similarities and differences between TOL and KL. Although TOL and KL possess some similarities because they both are from softwood and were generated from black liquor, the differences are remarkable as they were isolated following different methods. TOL showed a higher molecular weight, sulphur content, and concentration of carboxylate groups and a lower concentration of methoxy groups than KL. The results reveal that TOL can be used for manufacturing reinforced natural rubber and epoxy resins, especially because of its sulphur content and hydrophobic nature.

Chapter four focuses on the generation of sustainable sulphonated lignin-starch biomacromolecules and their utilization as flocculants of suspended aluminum oxide particles. The biomacromolecules were generated via the polymerization of TOL and starch with a sulphonate-containing monomer in a three-component system. This chapter centers on the comprehensive characterization and flocculation performance of the produced lignin-starch biomacromolecules. Advanced characterization methods, such as ^{1}H, COSY, HSQC, HSQC-TOCSY, and HMBC NMR, were carried out to confirm the copolymerization reaction and to elucidate the chemical structure of the lignin-starch biomacromolecules. Moreover, the adsorption, flocculation, and

sedimentation behaviour of the lignin-starch biomacromolecules on aluminum oxide were fundamentally analyzed via quartz crystal microbalance with dissipation (QCM-D), focused beam reflectance measurements (FBRM), and vertical scan (Turbiscan) and dispersion stability (LUMiSizer) analyzers. The result of this research offers a new approach for the generation of lignin-starch polymers, which can be used for removing inorganic suspended particles for water decontamination purposes**.**

Chapter five discusses the chemical structure, physicochemical characteristics, and viscoelastic properties of lignin-starch crosslinked macromolecules. This chapter presents the development of temperature-responsive, high molecular-weight macromolecules through the crosslinking of KL and starch with epichlorohydrin. The existence of glycerol ether cross-linkages between starch and KL, as well as the changes in the aromatic and anhydroglucose units of KL and starch, were validated by ^{1}H, HSQC, ^{31}P NMR and XPS analyses. Furthermore, the thermo-responsive properties of the crosslinked macromolecules were revealed by water solubility analysis and rheological characterization. The KL-starch macromolecules showed a structured network, which was stabilized by hydrophobic and hydrogen bond interactions among the functional groups of lignin and starch. Ultimately, temperature-responsive properties, such as temperature-dependence solubility and gel formation structures during heating-cooling treatments, were also monitored for the KL-starch macromolecules.

Chapter six states the overall conclusions from this thesis and provides a perspective for future studies in this field.

1.2. Objectives

The objectives of this thesis are to:

1. develop a new method for isolating lignin from the tall oil production of the kraft pulping process (i.e., LignoTall) and evaluate the properties of generated lignin
2. produce water-soluble sulphonated TOL-starch polymer with a high molecular weight and understand its chemical structure
3. evaluate the correlation of the chemical structure of sulphonated TOL-starch polymers and their interactions as flocculants of aluminum oxide particles in colloidal systems
4. generate a high molecular weight macromolecule of crosslinked kraft lignin and starch
5. study the chemical structure, physicochemical characteristics, thermal properties, and rheological behaviour of KL-starch macromolecules

1.3. Novelty

The novelty of this thesis work was 1) the discovery of a new type of lignin in a kraft pulping operation, tall oil lignin (TOL), 2) the investigation of the crosslinking pathways of lignin and starch and the possible application of such products.

1.4. References

(1) Wilson, M. P.; Schwarzman, M. R. Toward a New U.S. Chemicals Policy: Rebuilding the Foundation to Advance New Science, Green Chemistry, and Environmental Health. *Environmental Health Perspectives* **2009**, *117* (8), 1202–1209. https://doi.org/10.1289/ehp.0800404.

(2) Weiss, M.; Haufe, J.; Carus, M.; Brandão, M.; Bringezu, S.; Hermann, B.; Patel, M. K. A Review of the Environmental Impacts of Biobased Materials. *Journal of Industrial Ecology* **2012**, *16*, S169–S181. https://doi.org/10.1111/j.1530-9290.2012.00468.x.

(3) Ferreira-Filipe, D. A.; Paço, A.; Duarte, A. C.; Rocha-Santos, T.; Patrício Silva, A. L. Are Biobased Plastics Green Alternatives?—A Critical Review. *IJERPH* **2021**, *18* (15), 7729. https://doi.org/10.3390/ijerph18157729.

(4) United Nations. *Take Action for the Sustainable Development Goals*. United Nations Sustainable Development. https://www.un.org/sustainabledevelopment/sustainable-development-goals/ (accessed 2022-10-24).

(5) Diep, N. Q.; Sakanishi, K.; Nakagoshi, N.; Fujimoto, S.; Minowa, T.; Tran, X. D. Biorefinery : Concepts, Current Status, and Development Trends. *International Journal of Biomass and Renewables* **2012**, *1* (2), 1–8.
(6) Blair, M. J.; Mabee, W. E. Techno-economic and Market Analysis of Two Emerging Forest Biorefining Technologies. *Biofuels, Bioprod. Bioref.* **2021**, *15* (5), 1301–1317. https://doi.org/10.1002/bbb.2218.
(7) Annevelink, B.; Chavez, L. G.; van Ree, R.; Gursel, I. V. Global Biorefinery Status Report 2022. *IEA Bioenergy Task 42 Biorefining in a circular economy*, 94.
(8) Gajula, S.; Reddy, C. R. K. More Sustainable Biomass Production and Biorefining to Boost the Bioeconomy. *Biofuels, Bioprod. Bioref.* **2021**, *15* (5), 1221–1232. https://doi.org/10.1002/bbb.2227.
(9) Clark, J. H.; Luque, R.; Matharu, A. S. Green Chemistry, Biofuels, and Biorefinery. *Annu. Rev. Chem. Biomol. Eng.* **2012**, *3* (1), 183–207. https://doi.org/10.1146/annurev-chembioeng-062011-081014.
(10) Baranwal, J.; Barse, B.; Fais, A.; Delogu, G. L.; Kumar, A. Biopolymer: A Sustainable Material for Food and Medical Applications. *Polymers* **2022**, *14* (5), 983. https://doi.org/10.3390/polym14050983.
(11) Demuner, I. F.; Colodette, J. L.; Demuner, A. J.; Jardim, C. M. Biorefinery Review: Wide-Reaching Products Through Kraft Lignin. *BioResources* **2019**, *14* (3), 7543–7581.
(12) Haile, A.; Gelebo, G. G.; Tesfaye, T.; Mengie, W.; Mebrate, M. A.; Abuhay, A.; Limeneh, D. Y. Pulp and Paper Mill Wastes: Utilizations and Prospects for High Value-Added Biomaterials. *Bioresour. Bioprocess.* **2021**, *8* (1), 35. https://doi.org/10.1186/s40643-021-00385-3.
(13) Katahira, R.; Elder, T. J.; Beckham, G. T. Chapter 1. A Brief Introduction to Lignin Structure. In *Energy and Environment Series*; Beckham, G. T., Ed.; Royal Society of Chemistry: Cambridge, 2018; pp 1–20. https://doi.org/10.1039/9781788010351-00001.
(14) Moretti, C.; Corona, B.; Hoefnagels, R.; Vural-Gürsel, I.; Gosselink, R.; Junginger, M. Review of Life Cycle Assessments of Lignin and Derived Products: Lessons Learned. *Science of The Total Environment* **2021**, *770*, 144656. https://doi.org/10.1016/j.scitotenv.2020.144656.
(15) Galbe, M.; Wallberg, O. Pretreatment for Biorefineries: A Review of Common Methods for Efficient Utilisation of Lignocellulosic Materials. *Biotechnol Biofuels* **2019**, *12* (1), 2–26. https://doi.org/10.1186/s13068-019-1634-1.
(16) Aro, T.; Fatehi, P. Tall Oil Production from Black Liquor: Challenges and Opportunities. *Separation and Purification Technology* **2017**, *175*, 469–480. https://doi.org/10.1016/j.seppur.2016.10.027.
(17) Evdokimov, A. N.; Kurzin, A. V.; Trifonova, A. D.; Popova, L. M.; Buisman, G. J. H. Desulfurization of Black Liquor Soap for Production of Crude Tall Oil with Lower Sulfur Content. *Wood Sci Technol* **2017**, *51* (6), 1353–1363. https://doi.org/10.1007/s00226-017-0912-y.
(18) Niemeläinen, M. Tall Oil Depitching in Kraft Pulp Mill, Aalto University, Espoo, Finland, 2018. https://aaltodoc.aalto.fi:443/handle/123456789/33676 (accessed 2019-07-13).
(19) Al-Douri, Y. Fabrication and Analysis of Starch-Based Green Materials. In *Nanoparticles in Analytical and Medical Devices*; Elsevier, 2021; pp 301–318. https://doi.org/10.1016/B978-0-12-821163-2.00020-0.

(20) Falua, K. J.; Pokharel, A.; Babaei-Ghazvini, A.; Ai, Y.; Acharya, B. Valorization of Starch to Biobased Materials: A Review. *Polymers* **2022**, *14* (11), 2215. https://doi.org/10.3390/polym14112215.
(21) Chen, J.; Eraghi Kazzaz, A.; AlipoorMazandarani, N.; Hosseinpour Feizi, Z.; Fatehi, P. Production of Flocculants, Adsorbents, and Dispersants from Lignin. *Molecules* **2018**, *23* (4), 868. https://doi.org/10.3390/molecules23040868.
(22) Lermen, F. H.; de Souza Matias, G.; Bissaro, C. A.; Ribeiro, J. L. D.; Gonçalves, K. Y.; Matos, C.; Filho, N. A.; de Matos Jorge, L. M.; Coelho, T. M. The Characteristics and Industrial Applications of Natural and Hydrophobic Modified Starch. *Starch Stärke* **2022**, 2200022. https://doi.org/10.1002/star.202200022.
(23) Sarkar, A. K.; Ghorai, S.; Patra, A. S.; Mishra, B. K.; Mandre, N. R.; Pal, S. Modified Amylopectin Based Flocculant for the Treatment of Synthetic Effluent and Industrial Wastewaters. *Int. J. Biol. Macromol.* **2015**, *72*, 356–363. https://doi.org/10.1016/j.ijbiomac.2014.08.019.
(24) Wang, L.; Shen, J.; Men, Y.; Wu, Y.; Peng, Q.; Wang, X.; Yang, R.; Mahmood, K.; Liu, Z. Corn Starch-Based Graft Copolymers Prepared via ATRP at the Molecular Level. *Polym. Chem.* **2015**, *6* (18), 3480–3488. https://doi.org/10.1039/C5PY00184F.
(25) Singh, G. P.; Bangar, S. P.; Yang, T.; Trif, M.; Kumar, V.; Kumar, D. Effect on the Properties of Edible Starch-Based Films by the Incorporation of Additives: A Review. *Polymers* **2022**, *14* (10), 1987. https://doi.org/10.3390/polym14101987.
(26) Kaewtatip, K.; Tanrattanakul, V. Preparation of Cassava Starch Grafted with Polystyrene by Suspension Polymerization. *Carbohydr. Polym* **2008**, *73* (4), 647–655. https://doi.org/10.1016/j.carbpol.2008.01.006.
(27) Gupta, C.; Sverdlove, M. J.; Washburn, N. R. Molecular Architecture Requirements for Polymer-Grafted Lignin Superplasticizers. *Soft Matter* **2015**, *11* (13), 2691–2699. https://doi.org/10.1039/C4SM02675F.
(28) Ataie, M.; Sutherland, K.; Pakzad, L.; Fatehi, P. Experimental and Modeling Analysis of Lignin Derived Polymer in Flocculating Aluminium Oxide Particles. *Sep. Purif. Technol.* **2020**, *247*, 116944. https://doi.org/10.1016/j.seppur.2020.116944.
(29) de S. M. de Freitas, A.; Rodrigues, J. S.; Maciel, C. C.; Pires, A. A. F.; Lemes, A. P.; Ferreira, M.; Botaro, V. R. Improvements in Thermal and Mechanical Properties of Composites Based on Thermoplastic Starch and Kraft Lignin. *Int. J. Biol. Macromol.* **2021**, *184*, 863–873. https://doi.org/10.1016/j.ijbiomac.2021.06.153.
(30) Chen, X.; Pizzi, A.; Zhang, B.; Zhou, X.; Fredon, E.; Gerardin, C.; Du, G. Particleboard Bio-Adhesive by Glyoxalated Lignin and Oxidized Dialdehyde Starch Crosslinked by Urea. *Wood Sci. Technol.* **2022**, *56* (1), 63–85. https://doi.org/10.1007/s00226-021-01344-z.
(31) Javed, A.; Ullsten, H.; Rättö, P.; Järnström, L. Lignin-Containing Coatings for Packaging Materials. *Nord. Pulp Pap. Res. J.* **2018**, *33* (3), 548–556. https://doi.org/10.1515/npprj-2018-3042.
(32) Majeed, Z.; Mansor, N.; Ajab, Z.; Man, Z. Lignin Macromolecule's Implication in Slowing the Biodegradability of Urea-Crosslinked Starch Films Applied as Slow-Release Fertilizer: Lignin Macromolecule's Implication in Biodegradability of UcS Films. *Starch - Stärke* **2017**, *69* (11–12), 1600362. https://doi.org/10.1002/star.201600362.
(33) Acosta, J. L. E.; Chávez, P. I. T.; Ramírez-Wong, B.; Bello-Pérez, L. A.; Ríos, A. V.; Millán, E. C.; Jatomea, M. P.; Osuna, A. I. L. Mechanical, Thermal, and Antioxidant Properties of

Composite Films Prepared from Durum Wheat Starch and Lignin. *Starch - Stärke* **2015**, *67* (5–6), 502–511. https://doi.org/10.1002/star.201500009.

(34) Nasiri, A.; Wearing, J.; Dubé, M. A. Using Lignin to Modify Starch-Based Adhesive Performance. *ChemEngineering* **2020**, *4* (1), 3. https://doi.org/10.3390/chemengineering4010003.

Chapter 2: Production and Characterization of Starch-Lignin Based Materials: A Review

Jonathan A. Diaz-Baca, Pedram Fatehi*

Submitted to *J. Chem. Eng.* 2022

Green Processes Research Centre and Chemical Engineering Department,
Lakehead University, 955 Oliver Road,
Thunder Bay, ON, Canada, P7B5E1

* Corresponding author: email: pfatehi@lakeheadu.ca

The contribution of Jonathan A. Diaz-Baca to this work was the conception of the original draft, gathering and interpreting literature review, and formal analysis.

2.1. Abstract

Starch and lignin are abundant and inexpensive natural polymers frequently considered as green alternatives to oil-based and synthetic polymers. Despite their availability, and owing to their physicochemical properties, starch and lignin are not utilized in their pristine form for high-performance applications. Therefore, they are transformed into starch- and lignin-based materials by chemical and physical modifications, which widen their properties and functionality. In the last decade, the combination of starch and lignin for producing reinforced materials has gained significant attention. The reinforcing of starch matrices with lignin has received primary focus because of the enhanced water sensitivity, UV protection, and mechanical and thermal resistance that lignin introduces to starch-based materials. This review paper aims to assess the production and characterization technologies for starch-lignin materials, highlighting their physicochemical properties, outcomes, challenges, and opportunities. First, this paper describes the current status, sources, and chemical modifications of lignin and starch. Next, the discussion is oriented toward starch-lignin materials and their production approaches, such as blends, composites, plasticized/crosslinked films, and coupled polymers. Special attention will be given to the characterization methods of starch-lignin materials, focusing on their advantages, disadvantages, and expected outcomes. Finally, the challenges, opportunities, and future perspectives on developing of starch-lignin materials, such as fibres, adhesives, coatings, films, and controlled delivery systems, are discussed.

2.2. Introduction

The interest in substituting traditional fossil fuel-based materials with biobased chemicals has been increasing in the last 15 years.[1–4] This switching has become more necessary because of the concerns about greenhouse gas emissions and supply chain uncertainty. As stated in goal 13 of the 2030 United Nations sustainable development agenda, impactful actions like developing new technology must be taken to reduce greenhouse gas emissions and stop climate change.[5] However, the benefits of substituting fossil-fuel synthetic materials with biobased chemicals still need to be evaluated against the associated environmental impacts.[2,6,7] Different aspects, such as technical, economic, and social issues must be systematically studied before switching to a biobased economy.[8] The current focus of the biobased economy is a gradual change from energy production to the production of high-value biobased materials and chemicals.[9]

A major example of shifting towards the biobased economy and production of high-value biobased materials is noted in the biorefining industry.[10] Biorefining is a group of processes where different biomass feedstocks are converted into a spectrum of biobased products such as chemicals, materials, and energy in an analogous process to the actual petroleum refineries.[11] Biorefineries offer the possibility of using forest and agricultural wastes as new resources in integrated facilities capable of producing multiple products in a sequential process.[12–14] Traditionally, well-established industries, such as pulp and paper, starch, and sugar, use conventional conversion processes for biorefining.[9] However, developing a more efficient approach, where the conversion of biomass to biobased chemicals is prioritized before the energy conversion, is part of the strategies for maximizing the sustainability potential of biorefining.[15,16] The new strategies and priorities are the response to the increasing demand for high value bio-based materials and the current low cost of

bioenergy (e.g., bioethanol).[15] Therefore, by applying the principles of green chemistry (utilizing a more energy-efficient process, using renewable feedstocks, reducing the production of derivatives, and producing chemicals more susceptible to degradation) to biorefining, decisive steps can be taken to mitigate climate change while meeting the industry demands.[16,17]

Biopolymers are found in different living organisms and can be extracted as main products, by-products, or wastes by various processes, including biorefining.[18,19] Lignin is an aromatic biopolymer constituting approximately 30% of the lignocellulose biomass. Biologically, lignin offers rigidity and protective properties to the cell walls in vascular plants.[20] As the second most abundant biopolymer, it is highly available and mainly obtained as a by-product from the delignification of wood in the pulping production process.[21] Lignin is chemically composed of phenylpropane units arranged in complicated tridimensional structures. Lignin is rich in functional groups such as phenoxy, methoxy, carboxyl, and carbonyl.[22] Owing to its chemical properties and extensive availability, lignin is strongly considered a green alternative to oil-based and synthetic chemicals and materials.[23,24] Starch is another biopolymer highly utilized in diverse applications in green chemistry.[25] Starch is a polysaccharide made of anhydroglucose units (AGU) and the second most abundant carbohydrate present in many plants, where it functions as an energy reserve macromolecule.[26] Starch's biodegradability, extensive accessibility, and low cost make it often a preferred feedstock of green polymeric formulations.[27,28]

Despite the abundant availability and low production cost of lignin and starch, the industrial use of these natural polymers requires their chemical modification to strengthen their properties and be functionally suitable.[29,30] The structural complexity and variability of lignin restrict many possible applications, which is why it needed to modify its structure.[31] The chemical modification of lignin is often considered to be included in biorefining processes to create new lignin-based

green polymers with enhanced physicochemical properties proper for high-value utilizations.[32,33] For instance, carbon fibres,[34] polymer alloys, [35] adhesives,[36] resins,[37] fillers,[38] flocculants,[39] or dispersants[40] are among the most produced and studied lignin-based materials. Regarding starch, although more than 50% of commercial starch is used for non-food applications, its natural properties do not always meet the requirements for a wide variety of specialized applications.[41] Also, the industrial use of starch needs to be carefully targeted because starch is an important component of human food.[39,42] Generally, starch is chemically modified to increase its solubility in water and enhance its mechanical, thermal, and reactive properties.[43] Starch-based green polymers are mostly used as glues,[44] flocculants,[45] dispersants,[46] films,[47] hydrogels,[48] and packaging materials.[49]

As will be presented in this review paper, the combination of lignin with starch has received great attention in the last decade. Most studies have focused on reinforcing the starch matrices with lignin to enhance moisture/water sensitivity, thermolability, UV protection, and mechanical weakness. Therefore, this review article aims to explore the available information associated with the production of starch-lignin materials as a new approach to producing biobased materials. Moreover, the challenges, current trends, and future opportunities associated with the production of starch-lignin materials are also discussed. First, this review paper discusses the general description, sources, and chemical modification of lignin and starch. Furthermore, the analysis is directed to the starch-lignin materials and their production approaches, followed by the review of the characterization methods and structural elucidation of starch-lignin macromolecules.

2.3. Lignin

2.3.1. Structure

Lignin is a complex polymer of phenylpropanoid units, constitutes 10 to 29 wt.% of the lignocellulosic biomass and is the second most abundant natural polymer globally.[50] It provides structural rigidity, resistance to mechanical stress, photodegradation and biological attacks on the plant cell walls.[20] Furthermore, it promotes hydrophobicity and plays a vital role in mineral and water transportation in vascular plants. In the lignocellulose matrix, lignin is cross-linked with hemicellulose forming lignin-carbohydrate complexes that support cellulose fibres as schematized in Figure 2.1.[51] The proportion of lignin in biomass depends on the biological origin of lignocellulose species, varying from high, medium and low for softwood, hardwood, and herbaceous species.[52,53]

Lignin is typically constituted of three main phenylpropanoid units or monolignols, synapyl, coniferyl and p-coumaryl alcohols, which are the bases for the phenylpropanoid units hydroxyphenyl (H), guaiacyl (G) and syringyl (S) units in lignin, respectively (Figure 2.1).[54] In minor quantities, other units are available in lignin,[55] such as, flavonoids, stilbenes, and hydroxyphenylpropanoid compounds. The phenylpropane units are bound via a different ether, such as β–O–4, α–O–4, and 4–O–5, and C–C linkages, such as β–β, β–5, β–1 and 5–5.[56]

Moreover, the presence of different functional groups, such as hydroxyl, phenoxyl, carbonyl, carboxyl and methoxy groups, confer lignin reactivity and physicochemical properties of lignin.[52,57,58] The molecular weight (Mw) of native lignin (i.e., lignin isolated from biomass with minimal structural changes) is relatively low (2500 to 10000 g/mol) compared to other biopolymers (e.g., starch).[59] The different compositions and stereochemical configurations of

lignin macromolecules are relative to their biological origin, for instance, softwood, hardwood, or herbaceous lignin. Generally, softwood lignin contains mostly G units, and hardwood lignin is constituted by G and S units. In contrast, herbaceous lignin presents a diversified composition with the G, S and H units.[60] Moreover, softwood lignin generally contains more C–C linkages than hardwood lignin, significantly impacting the rigidity and resistance to cleavage and fractionation processes.[55,60]

2.3.2. Types of lignin

In industry, lignocellulosic biomass is fractionated to separate its three main components, cellulose, lignin, and hemicellulose, for use in different products.[61] In particular, lignin has been traditionally obtained as a by-product from the delignification of wood and non-wood biomass in the pulp and paper production process. However, the recent advancements in biorefining and lignin-focused processes have triggered the progress of innovative and efficient lignin isolation processes.[50,62,63] The obtained lignin from conventional and new strategies are denoted as technical lignins, commonly named after the fractionation method (e.g., kraft lignin from lignin obtained in a kraft pulping process). The isolation method greatly influences the chemical structure and physicochemical properties of technical lignins, which are significantly different from each other and native lignin.[64,65] Hence, it is essential to understand the nature of lignin because it will affect its composition, functional groups and potential modifications and applications.

Kraft lignin (KL) is isolated from the kraft pulping process, the most predominantly pulping process in use worldwide.[66] During the kraft pulping, a spent effluent (i.e., black liquor) containing solubilized lignin is generated and later precipitated via acidification for KL collection. Recently, the LignoBoost and LignoForce methods were developed to facilitate commercial production of

lignin, focusing on optimizing lignin precipitation from black liquor in the kraft pulping process.[67,68]

In the LignoBoost technology, the black liquor is cooled down to 60-80 °C and its pH is adjusted (~10) with CO_2, which precipitates the lignin particles. Afterwards, the lignin is filtered and redispersed in a diluted H_2SO_4 solution to be ultimately filter-pressed and acid washed again.[68] In the LignoForce system, lignin is isolated over three main steps, first by oxidation with O_2, second by acidification using CO_2, and last by a washing step with a diluted H_2SO_4 medium.[67] In comparison to LignoBoost, the filtration of the black liquor is carried out before the lignin precipitation and the oxidation treatment is included. LignoBoost and LignoForce lignin contains fewer impurities and less heterogeneous structure than conventional KL making them more attractive for potential commercial uses. The obtained KL is highly condensed, partially water-soluble with a low amount of β-O-4 inter unit linkages, and it contains thiol functional groups provided by the sulphur salts used during the pulping operation.[69,70]

Lignosulphonate is another available technical lignin, which is generated and isolated from the sulphite process. Compared to KL, lignosulphonates have a higher degree of sulphonation due to sulphurous acid and sulphite salts used in the pulping process.[71,72] The high concentration of sulphonate groups provides anionic charges and water solubility to lignosulphonates.[73]

Soda lignin is generated in soda pulping operations and mainly from non-woody biomass. The main characteristic of soda lignin is the absence of sulphur in its structure and its comparatively lower Mw than KL or lignosulphonates.[74,75] Lignin can also be generated in a solvent-based pulping process, such as organosolv pulping.[76,77] Generally, organosolv lignin has a low Mw (7000 to 17000 g/mol), is more oxidized and shows limited water-solubility.[78,79] The involvement of

organic acids and solvents elevates the production costs of organosolv lignin production, limiting its availability for industrial usage.[80]

Amongst technical lignins, lignosulphonates are one of the most dominant types accounting for 69% of the market share in 2020 [81], and KL comes second in use with a 15-20 % share.[66] However, KL has the highest forecasted growth rate in the next ten years owing to the commercial production of KL and advancement in the development of KL-derived high value-products, such as adhesives, bioplastics, and carbon fibres.[82] Through chemical modifications and reactivity enhancement, the properties of KL-based material can be effectively tailored to meet the market demand.

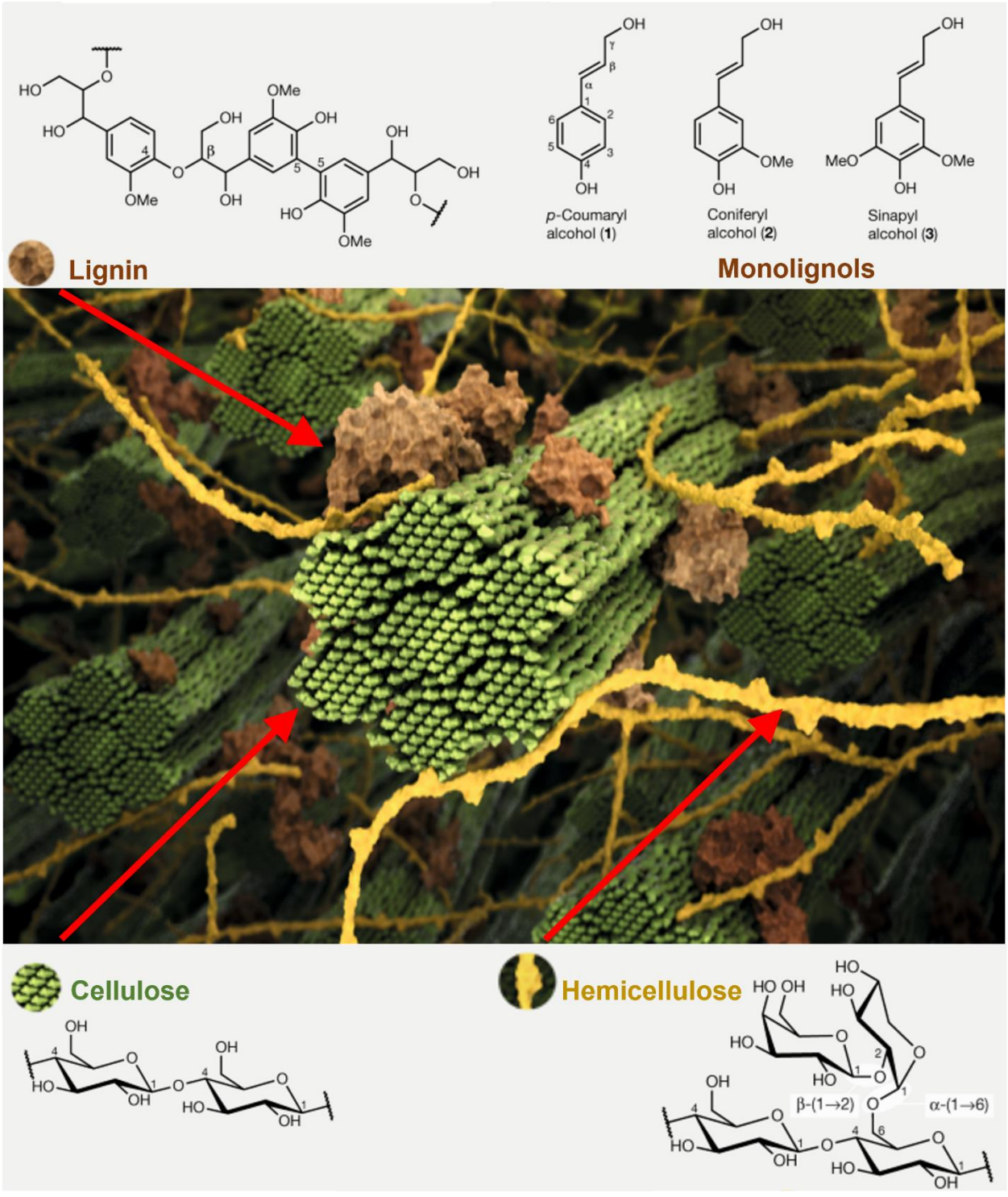

Figure 2.1. The simulation-inspired structure of lignocellulosic biomass and its components. Lignin (brown) cross-linked with hemicellulose (yellow) forming lignin-carbohydrate complexes

which surround and supports the cellulose fibers (green). *p*-Coumaryl, coniferyl and sinapyl are the main monolignols found in lignin.[54,83]

2.3.3. Lignin modification reactions

Despite the abundant availability and low production cost of KL,[66] the use of this natural by-product has been limited to fuel and energy supplies at commercial scales yet.[66] However, KL has the potential to replace many oil-based chemicals due to its unique characteristics, such as high hydroxyl and phenoxyl group contents.[60,84,85] However, the structural complexity of KL limits its potential application. As a result, there is a need to develop new modified KL-polymers with physicochemical properties suitable for their utilization in high-value applications including carbon fibres, polymer alloys, fillers, resins, flocculants, or dispersants.[86–88] Various methodologies including chemical, electrochemical, photochemical, and biological, have been studied for the modification of KL.[89] Nevertheless, to remain within the scope of this work, the discussion will be focused only on the chemical methods. The principal chemical pathways to produce modified KL-polymers are grafting, copolymerization, and coupling reactions, as depicted in Figure 2.2.[31,32,87] After modifications, KL can show varied charge densities, molecular weights, and degrees of hydrophilicity-hydrophobicity, which are essential features of its functionality and efficiency. The lignin-based material inherits some unique qualities from lignin, such as hydrophobicity, thermal resistance, UV protection, and three-dimensional structure.[90,91]

The grafting of anionic, cationic, or non-ionic groups onto KL has been widely studied as a modification reaction.[92,93] In brief, most grafting methods target the hydroxyl and/or phenoxyl groups of KL to enhance its functionality and water-solubility primarily for water-based applications, such as flocculation or dispersants. Anionic KL is produced by attaching negatively charged functional groups to the KL structure through different reaction pathways depending on

the grafted reagents (e.g., carboxyethylation, carboxymethylation, sulphonation).[94–96] The synthesis of cationic KL is mainly carried out via amination reactions,[97–99] including reagents like methylamine, dimethylamine, diethylenetriamine, formaldehyde, and dioxane into the KL chains.[100] Non-ionic grafting reactions of KL include alkylation, esterification, etherification, epoxidation and phenolation.[87] Non-ionic reactions are generally achieved by attaching the desired monomer (e.g., alkyl, epoxy, or phenol) onto KL's hydroxy groups (principally phenolic).[95,101,102] Owing to the diminution of the hydroxy groups and the incorporation of new functional groups to KL, its reactivity is increased. Functionalized KL can be used directly for its proposed application or can be used as a required functionalized molecule for further modifications.

The copolymerization of KL consists of grafting the KL backbone (macromonomer) to a monomer, which will be polymerized to produce KL-based graft copolymers. The polymerization of KL can be performed by free radical, controlled radical, or ring-opening polymerization methods.[103] Free radical polymerization has been widely investigated in KL. The main advantage of this method is that it can be conducted in aqueous-based systems with an acidic or basic environment.[104–107] This method requires the presence of initiator chemicals, such as potassium persulphate, sodium bisulphite, calcium chloride/hydrogen peroxide or radiation, such as gamma rays.[100] The controlled radical polymerization reactions, atom transfer radical polymerization (ATRP) and reversible addition-fragmentation chain transfer (RAFT) polymerization enable the control over the length of grafted polymeric chains and grafting ratios. ATRP is typically performed in a water/organic medium (e.g., water/ dimethylformamide (DMF)) in the presence of KL and the monomer, initiator with a transferable halogen, usually alkyl halides and a transition metal catalyst, such as copper complexes (Cu(I)Br/PMDTA CuCl /BPY).[108,109] Whereas RAFT often targets the insertion of a RAFT moiety through the esterification of KL. The RAFT reaction

is commonly carried out in DMF as a reaction medium and using an azo compound, such as azobisisobutyronitrile as the initiator.[110,111] The ring-opening polymerization (ROP) is a reaction where KL functions as a reactive center for the cyclic monomers (e.g., lactide or caprolactone), which will form a growing polymeric chain by a ring-opening mechanism.[112] Frequently used catalysts for this reaction are organotin compounds, such as triazabicyclodecene or stannous octoate, stannous hexanoate, and stannous chloride, used in an organic solvent medium.[113,114] In general, introducing synthetic polymerized chains to KL-based polymers increases the water or solvent solubility and Mw of KL, boosting its application as dispersants, adsorbents, flocculants, emulsifiers, hydrogels, resins, fibres, and thermoplastics.[114–118] More detailed and lignin-polymerization-oriented review papers are available in the literature for further consultation.[103,109]

Crosslinking of KL consists of coupling reactions between KL and other polymers via crosslinking agents, such as citric acid, epichlorohydrin, diglycidyl ether, formaldehyde, or polyethylene glycol.[92,109,119] The crosslinking of KL occurs at the hydroxy and phenoxy groups, forming stable covalent linkages between KL and the crosslinker, which will bond or be bonded to the other polymer.[86] The properties of the resultant copolymers are highly influenced by the KL content and the concentration of the crosslinking reagents during the reaction. Commonly, the thermal behaviour, rheological properties, and solvent- and water-solubility and uptake of KL are targeted and altered utilizing the crosslinking copolymerization.[101,120] These targeted properties will depend highly on the grafted polymer's nature. For instance, a hydrophilic polymer coupled to KL will increase its water solubility.[86,121,122] Through coupling reactions, different natural (e.g., chitosan or cellulose) and synthetic, e.g., polyvinyl alcohol (PVA), polyethylene glycol (PEG), polyurethane (PU) polymers, have been crosslinked with KL for diverse purposes, most commonly for films, hydrogel and membranes formation.[123–126]

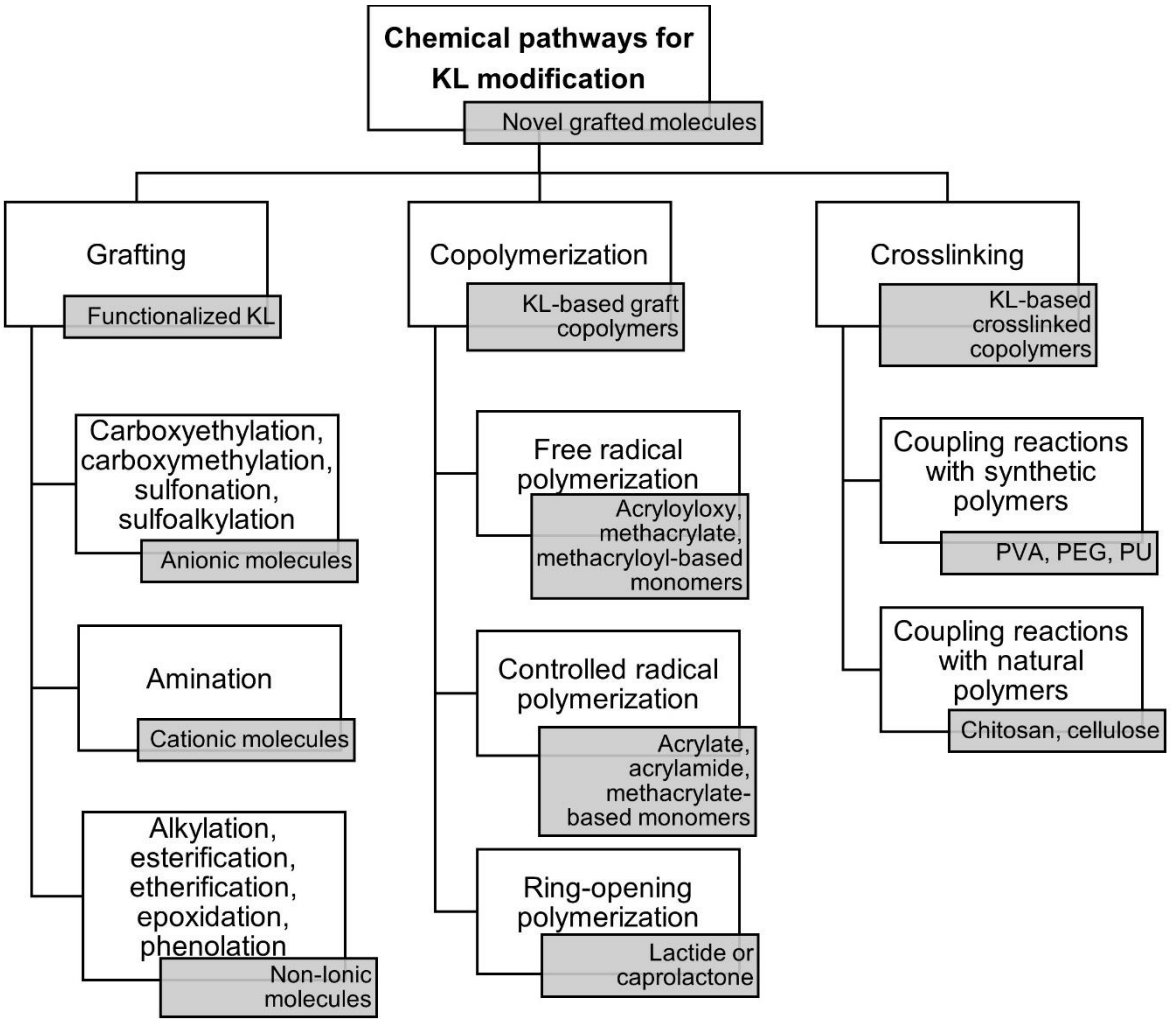

Figure 2.2. Summary of chemical pathways for the modification of KL

As a result of the combination of KL and other natural or synthetic polymers via copolymerization or crosslinking, the KL-based polymer possesses the characteristics of each polymer, which maximizes its properties and increases its applicability. These KL copolymers might be valuable for wastewater, coatings, agricultural, biomedical, or packaging applications. However, exploring the use of a greater variety of natural polymers and the viability of these materials in active compound-delivery systems and solution-based applications, particularly for removing contaminants from water, is of great interest and still underdeveloped.

2.4. Starch

2.4.1. Structure

Starch is a homopolysaccharide found in plant cells as the most important energy reserve macromolecule. It is constituted of long chains of anhydroglucose repetitive units (AGU) bonded by α-(1→4)-glycosidic linkages.[127] Native starch is synthesized and assembled in the form of water-insoluble semicrystalline particles known as starch granules, as depicted in Figure 2.3. Granular starch is presented in higher concentrations in the seeds, roots and fruits of different plant species.[127,128] The external structure of starch granules varies from spherical to polygonal, ellipsoidal or irregular shapes, while the internal structure is dense and semicrystalline.[129] The shape and crystallinity of starch depend mainly on its biological origin.[130] The macromolecular structure of starch is constructed by two polymeric fractions, amylose and amylopectin.[131] Amylose constitutes amorphous fractions, formed mainly by long linear polymeric chains with very few branches (Figure 2.3). The Mw of amylose has been found within an extensive range of 1×10^5 to 100×10^6 g/mol, depending on its biological origin and molecular degradation during its production process.[128] Amylopectin has a more complex and branched structure than amylose, and it is packed into a crystalline lamella with α-(1→6)-glycosidic linkages branching every 25 AGU units, approximately.[26] The Mw of amylopectin is much larger than amylose, ranging from 1×10^7 to 1×10^9 g/mol, but the polymeric chains are much shorter.[132]

The ratio of amylose to amylopectin in starch is of great interest, as it significantly influences its physical and chemical properties (e.g., viscosity and gel-formation capacity) and applications.[133] The amylose and amylopectin ratio in starch also vary with the different botanical species.[133] According to this ratio, starch is classified by its amylose content; low (<15%) are grouped as waxy starches, medium (20 to 35%) are considered regular starches, and high-amylose starches

contain > 40% amylose.[132,134] Starches with higher amylose content tend to produce tougher gels and stronger films. In contrast, starches with higher amylopectin show more resistance to retrogradation and have stickier textures.[135]

2.4.2. Sources of starch

The physical structure of granules, the chemical compositions, chemical structure, physicochemical properties and applications of starch differ considerably amongst vegetable species and plants part (e.g., seeds, stems and roots).[136] The source of starch is critical for understanding its properties and utilization approach in value-added applications. Corn, cassava, wheat, and potato are the principal crop sources along with a smaller proportion from rice and pulse for starch extraction for industry use.[137–139] In general, cereal-derived starches have higher protein and fatter components than potato or cassava.[140] A minor component of starch is minerals, such as phosphorus. Potato starch contains around 0.1 % phosphate, covalently linked to the amylopectin fractions.[141] Phosphate monoesters in amylopectin directly affect starch properties.[142,143] A higher hydration rate and swelling are caused by the negative charges of the phosphate groups in amylose.[137]

The amylose/amylopectin ratio of starch also varies with the botanical source, significantly impacting the purpose and application of starch. The amylose content varies between 22 and 90% in corn starch, similar to potato starch (from 17 to 92%). Wheat starch has shown a lower maximum amylose content (as high as 74%), followed by rice with 56% and cassava with 30%.[140,144–146] The variation in amylose/amylopectin content is the result of a natural evolutive selection process. However, with the current technology, it is possible to alter this ratio through genetic modification techniques.[147,148] As the rheological properties of starch are greatly

influenced by the source and amylose/amylopectin ratio, it is determinant to carefully select the starch type to better design the properties and final applications of the starch-based materials. [149,150]

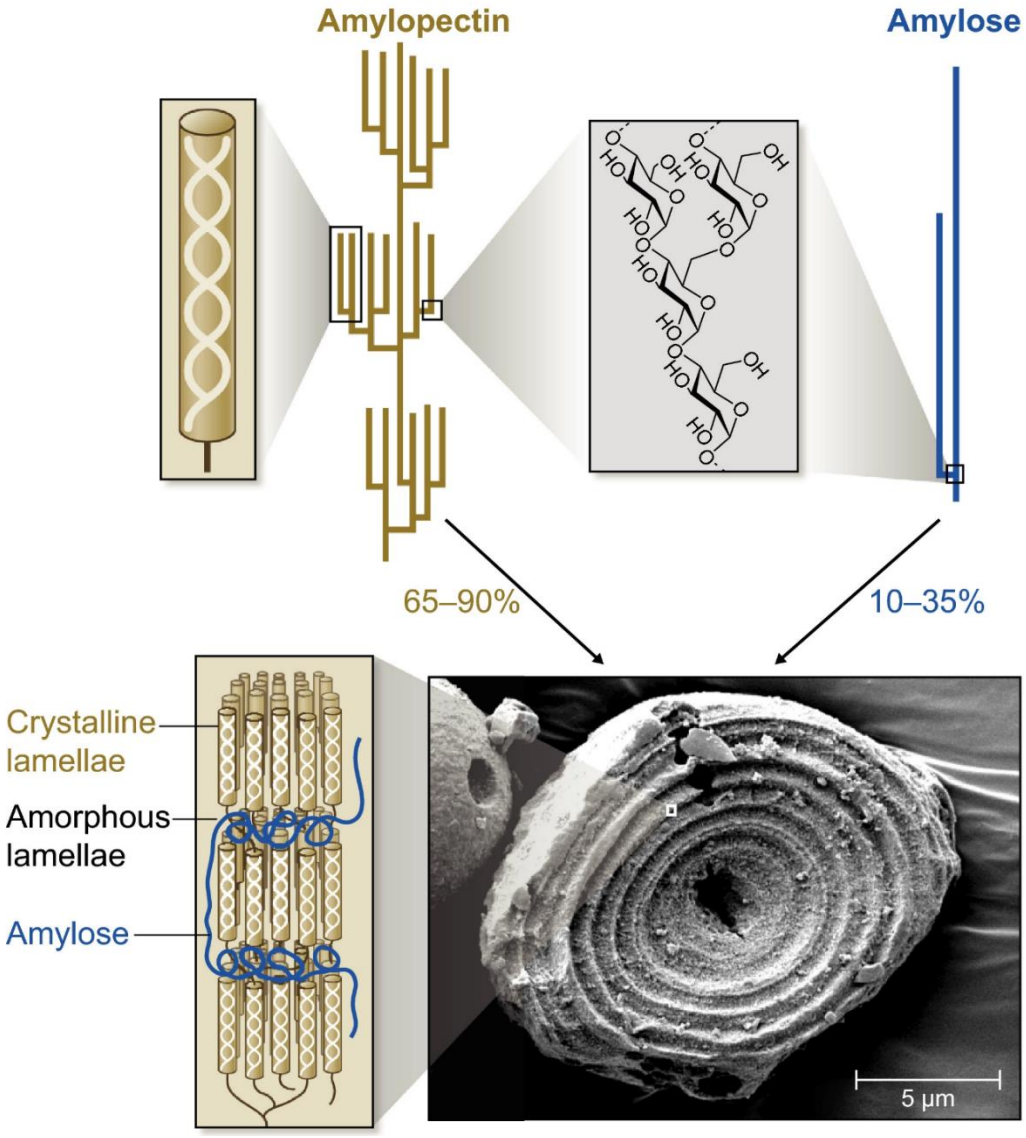

Figure 2.3. Native starch assembles in the form of granules. The macromolecular structure of starch is composed of amylose (amorphous fraction) and amylopectin (crystalline lamella).[136,144]

2.4.3. Starch modification reactions

Starch is an abundant and inexpensive ingredient in food products and non-food industrial applications.[151] Of the commercially produced starch, 45% is used for food applications, and the other 55% is related to non-food applications.[41] Among non-food applications, starch is used as glue, flocculant, dispersant-stabilizer, reinforcer agent, packaging material and drug delivery matrices. However, native starches properties do not always satisfy the needs of a wide range of specialized applications. Generally, starch is chemically modified to increase its solubility in water, resist mechanical shearing, acid hydrolysis, thermal and enzymatic degradation, and reduce retrogradation proclivity to fulfill the required properties of various applications. Out of the total consumption market of starch, 18% is modified starch, and its market value is almost triple as much as that of native starch.[152]

The most common chemical modification routes for producing starch-based polymers are esterification-etherification, copolymerization, and crosslinking (Figure 2.4).[153] The considerable number of hydroxyl groups in starch makes the chemical modification reactions possible.[154] In esterification, the addition of ester groups to the backbone of starch is conducted by reacting with organic or inorganic acids and their derivatives (e.g., acid chlorides, acetic anhydride, citric acid and malic anhydride).[155] The attachment of ether linkages to produce ionic starch is performed via the introduction of anionic (e.g., carboxymethyl and sulphonic) or cationic functional groups (e.g., ammonium, amino and imino).[156] Non-ionic starch is also generated throughout etherification by adding hydroxyethyl and hydroxypropyl groups. These modifications enhance thermal stability, moisture and swelling resistance, and tensile strength.[157] Throughout the copolymerization process, different monomers (e.g., methacrylamide, acrylic acid, styrene and n-butyl acrylate) are polymerized and grafted to the backbone of starch following reaction mechanisms such as free-

radical, controlled/living, and ring-opening polymerization.[158–163] The starch-derived polymers are frequently used as thickeners, superabsorbents, or flocculants for water-based applications.[164–166] Specific review papers regarding the polymerization of starch can be consulted for more details and widened description of the topic.[159,167]

The crosslinking of starch can be carried out to form interchain covalent linkages between starch macromolecules or to covalently couple starch with another polymer through the utilization of crosslinking agents to produce a copolymer. Nevertheless, this paper is focused on the crosslinked starch copolymers and not on the crosslinked starches (i.e., starch homopolymers). Comprehensive information on this topic is available in the literature.[168] For the synthesis of crosslinked starch copolymers frequently used, coupling agents are epichlorohydrin, bromoacetyl bromide, citric acid, and maleic acid [169–173]. Starch-based biopolymers can be tailored and produced by coupling starch with natural polymers such as rubber,[174–177] chitosan,[170,178,179] and pectin[180,181] or non-natural, such as poly(ethylene glycol) (PEG),[182,183] poly(lactic acid) (PLA),[184] poly(vinyl alcohol) (PVA).[185] The coupling reactions result in the alteration of solubility, pasting, swelling, and degradability properties of starch, which expanded its applications in flocculants, absorbents, films, hydrogels, fibers, and drug delivery systems. The starch-based copolymers, such as starch-poly(ethylene glycol) or starch-chitosan, showed improved properties in comparison with the individual components (e.g., starch and chitosan). By coupling the two polymers, a synergistic effect can be obtained after combining the advantages of each polymer to overcome their native disadvantages and obtain a product with desirable characteristics.

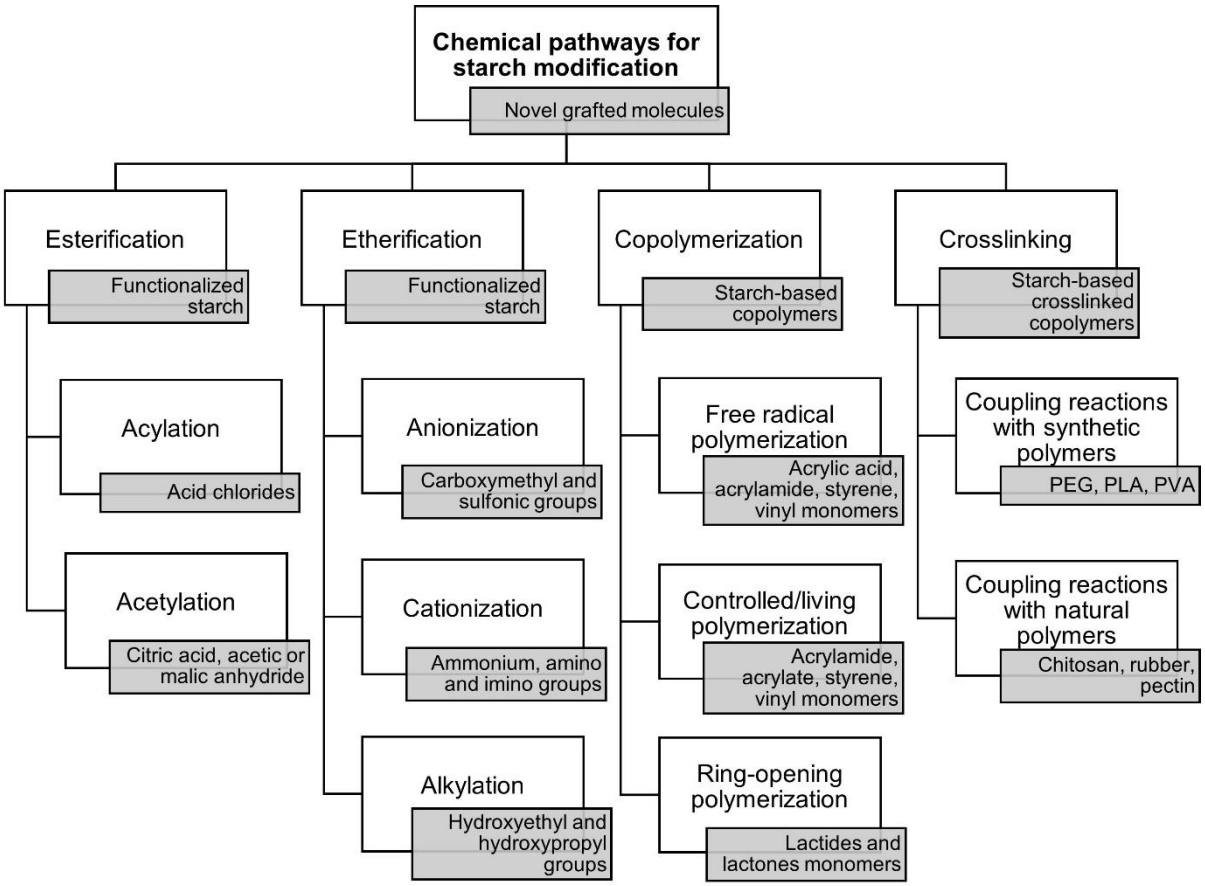

Figure 2.4. Summary of chemical pathways for the modification of starch

2.5. Starch-lignin materials

Combining starch with lignin has been proved to be an effective approach to overcoming the inherent undesirable characteristics of starch, such as moisture/water sensitivity, thermolability, and mechanical weakness. Most studies have focused on increasing water resistance and reducing the hydrophilicity of starch-based materials by reinforcing the starch matrix with lignin. Starch-lignin materials can be categorized into three major groups according to their properties and production routes: composite blends, films, and copolymers.

2.5.1. Starch-lignin blends

In starch-lignin composite blends, starch and lignin are combined via thermal methods without the aid of crosslinkers. The final products will be composites of starch matrices reinforced with lignin,

and the properties of such starch-lignin blends are listed in Table 2.1. Several studies were carried out in this respect. Stevens *et al.* mixed KL (solubilized in ammonium hydroxide) and corn starch (gelatinized at 70 °C) to produce foams by moulding compression-like method. Up to 20 wt.% of KL was used as filler to replace starch in the formulation, which induced thermal stability and decreased water absorption to the produced foams while keeping the structural strength of the composite.[186] Li *et al.* produced ternary composites by blending thermoplastic corn starch, PBAT (Poly (butylene adipate-co-terephthalate)) and corncob lignin (10, 20 and 30 wt.%). The composites were made by thermal compounding-extrusion method at 175 °C. Lignin acted as a compatibilizer, improving the interfacial interaction between starch and PBAT. The reinforced composites showed desirable characteristics, such as extended shelf-life, high thermal stability and hydrophobicity and enhanced mechanical properties.[187] Similarly, Wang *et al.* reinforced thermoplastic starch from cassava origin with 3 wt.% of lignin using a melt blending process. Thin pieces of the composite were produced with enhanced tensile strength and lower elongation at break.[188] However, due to the low lignin <5% and high starch >95% content in the formulation, the composites showed high water absorption. The previous works indicate that mechanically reinforcing starch matrixes with over 10 wt.% of lignin provides thermal stability and hydrophobicity to the starch-lignin composites.[189,190]

Table 2.1. Processes and properties of starch-lignin blends

Type of starch	**Type of lignin**	**Blending process**	**Blending ratio**		**Mixing conditions**	**Advantages**	**Disadvantages**	**Applications**	**Ref.**
			Starch	***Lignin***					

Corn starch	Indulin kraft lignin	Moulding-compression	98, 97, 90, 100	2, 3, 10, 20	Ammonium hydroxide, 70 °C, 15 min	Thermal stability, water resistance	Brittleness	Polystyrene foams replacement	[186]
Corn starch	Corncob lignin	Compounding-extrusion	50, 66, 34	50, 34, 66	Glycerol, 100-150 70 °C, extrusion 50 rpm/min	Thermal stability, hydrophobicity	Weak mechanical properties above 10% lignin content	PBAT-based composites for packaging	[187]
Cassava starch	Commercial lignin	Melt blending	99, 97, 95, 90, 85	1, 3, 5, 10, 15	Glycerol, mixing 10 min, 80-140 °C extrusion	Higher crystallization, higher tensile strength	Fast water absorption	Preparation of cabinet waste bags	[188]
Corn starch	Hardwood lignin	Blow moulding	75, 67	25, 33	Glycerol, 130 °C, 5 min	Water solubility, UV stability	Low content of natural polymers	PVA-based agricultural applications, packaging	[191]
Cassava starch	Kraft lignin	Compression molding	90	10	Glycerol, 160 °C, 10 min,	Mechanical propertie	High glycerol content	Bioplastics	[190]

					200 kg/cm^2	s, reduced water absorption			
Potato starch	Kraft-Lineo lignin	Thermo mechanical processing	75, 70	25, 30	Glycerol, 80 °C, 4 min, 40 rpm,	Tensile and elongation on strength, Thermal stability	Low content of starch and lignin	PVA-based Packaging materials	[192]
Corn starch	Lignosulphonate	Injection molding	99, 98, 96	1, 2, 4	Glycerol, 90 °C, 20 min, 100 rpm	Oxygen and water barrier properties	Partially biobased, complicate formulation	Polyolefin composite filler	[193]
Corn starch	Lignosulphonates	Thermal molding	90, 80, 70, 60, 50, 40	10, 20, 30, 40, 50, 60	Glycerol, 160 °C, 6 min, 50 rpm	Mechanical properties	Brittle material below 40 % starch content	Thermoplastic materials	[194]
Corn starch	LignoBoost lignin	Melt compounding	90	10	150 °C, 10 min, 60 rpm	Tensile strength, reduced water	Incompatibility within the matrix	PBAT-based Packaging materials	[189]

		uptake, antimicrobial

2.5.2. Starch-lignin plasticized films

The production of starch-based polymers for short-term shelf life, such as films, is currently extensively explored. Starch is widely used for film formation due to its flexibility and desirable optical and gas barrier properties. However, the mechanical properties of such films are often underachieved. The incorporation of lignin can promote the development of starch-based films with superior properties, as detailed in Table 2.2.

Significant advances were made from 1997 to 2004 regarding the fundamentals of processing and application of starch-lignin films.[195–198] Two initial strategies were taken to produce films, water-based moulding-extrusion and dimethyl sulfoxide (DMSO)-based solvent casting. In the blending process, starch-lignin interactions are generally developed via hydrogen bonding, creating films with plasticizer effect, and this process was more pronounced for lignin fractions with small molecular weights. Thanks to thermoforming extrusion, casting and electron beam irradiation methods, it was possible to develop starch films reinforced with lignin. Regardless of the lignin type (i.e., lignosulphonates, kraft and alkali lignin), the mechanical properties of such films were superior to those of lignin-free films. Nevertheless, the water resistance of the films was only enhanced when fractionated KL was used, where the hydrophobic nature of the fractioned lignin introduced some advantages. For example, Çalgeris *et al.* used small quantities of alkali lignin (1 to 2.5 wt.%) to reinforce corn starch films, which improved the mechanical, thermal, and swelling properties, but undesirable incompatibility issues arose when the lignin content was increased to

2.5 wt. %.[199] Espinoza Acosta *et al.* studied the blending of fractionated organosolv lignin and wheat starch to prepare casted starch-based films.[200] Interestingly, improvements were observed in the thermal resistance, water solubility and antioxidant activity of the reinforced films, proving the effectiveness of lignin as a free-radical scavenger in the matrix.

Recently, Ni *et al.* produced lignin nanoparticles to reinforce corn starch/polyvinyl alcohol and polyethylene oxide films by the solution-casting method.[201] The hydrophobicity and thermal stability were enhanced after adding lignin nanoparticles. The hydrophobicity measured by the contact angle of water was increased from 65° to 120°, and the degradation rate of the films was delayed by approximately 50 °C. More remarkably, the UV blocking properties of the films showed advanced functionalities, reducing the UV transmittance of the films from 40% to 10-2.5%. These results demonstrate the growing functionalization strategies for designing and producing starch-lignin films. More advanced characterization and innovative formulation approaches will significantly advance high-value applications.

Table 2.2. Summary of the starch-lignin formulations for composite blends and plasticized films.

Blending strategy	Mix ratio, %		Other reaction conditions	Lignin type and function	Final Product	Improvements	Weak points	Ref.
	Lignin	Starch						
Moulding-extrusion, solvent casting	10, 20 30	90, 80 70	Glycerol, 120 °C extrusion. Casting 80 °C 5, h	Lignosulphonate. Plasticizer	Film	Mechanical properties	Water resistance not enhanced	[195]
Solution casting	20	80	Casting, 80 °C 5, h	Indulin kraft. Plasticizer, compatibilizer	Film	Mechanical properties, water absorption	Heterogeneous matrix. Brittle material	[196]

Casting-beam irradiation	40	60	. Mixing 50 °C, 12 h. Irradiated with a 225 kV accelerator	Kraft. Compatibilizer	Film	Homogeneity. No plasticizer needed	Brittle films	[197]
Fast casting	4	96	Glycerol, 90 °C, 0.5 h	LignoBoost. Reinforcer	Film	Higher tensile strength, hydrophobicity	Brittle films	[202]
Solution casting	1.2, 1.4, 2.0, 2.4	98.8, 98.6, 98.0, 97.6	Glycerol, 100 °C, 0.2 h	Kraft. Reinforcer	Drug release biofilms	Thermal, mechanical, and swelling properties	Phase separation, water absorption.	[199]
Solution casting	5, 10, 20	95, 90, 80	Glycerol, 120 °C, 0.3 h	Organosolv. Reinforcer, plasticizer	Film	Thermal resistance, Antioxidant properties	Migration of lignin out of the matrix	[200]
Melt compounding	2, 10	21, 18	Glycerol, PVA, 190-230 °C, 0.1 h	Kraft. Reinforcer	Film	Thermal properties	Lignin agglomeration	[203]
Solvent casting	2, 4, 8	98, 96, 92	Glycerol, DMSO, 80 °C, 0.1 h	Kraft. Reinforcer, additive	Biodegradable	Hydrophobicity, mechanical properties, biodegradability	Low interaction among polymers, multiphase matrix	[204]
Solvent casting	1, 2, 3, 4, 5	99, 98, 97, 96, 95	Glycerol, DMSO, 85 °C, 0.75 h	Kraft. Reinforcer	Food packaging film	Mechanical properties, heat seal strength	Partial compatibility. Mechanical	[205]

						water vapor permeability	properties influenced greatly by plasticizer	
Solution casting	20	80	Glycerol, 80 °C, NA	Soda. Plasticizer and reinforcer	Film	Mechanical and water barrier properties	Lignin's reinforcer effect surpassed by other components	206
Solution casting	10	90	Glycerol, 85 °C, NA	Organosolv. Reinforcer, antioxidant	Film	Hydrophobicity, antioxidant activity	Incompatibility of polymers. Lignin agglomeration	207
Solution casting	10	90	Glycerol, 90 °C 0.5 h	Soda. Reinforcer, UV-blocking	Film	Mechanical and thermal properties, UV blocking properties	Lignin agglomeration	208
Multilayer coating	17, 19	62, 55	Glycerol, AZC, 95 °C 1 h	LignoBoost. Hydrophobic additive	Coating	Water vapor transmission rate	Uneven and cracking texture	209
Solution casting	5, 10, 15, 20, 25, 30	95, 90, 85, 80, 75, 70	Glycerol, 100 °C, 0.5 h	Soda Reinforcer	Film	Mechanical properties, thermal resistance	Hydrophobicity not increased	210

Solvent casting	4	96	90 °C, 0.5 h	LignoBoost. Reinforcer	Film	Mechanical properties, hydrophobicity	Opaque film, aggregates formation	[211]
Solution casting	1, 3	91, 77, 70, 50	90 °C, 0.5 h, ultrasonication, 30 min	Organosolv, nanoparticles. Reinforcer, UV-blocking	Composite film	Hydrophobicity, thermal stability, UV blocking properties	Cluster aggregation	[201]

2.5.3. Starch-lignin crosslinked films

The films of starch crosslinked with lignin are made of polymeric networks capable of swelling and holding water. Crosslinked starch-lignin films are commonly designed as controlled-release advanced materials. Starch films are prone to thermal and enzymatic degradation, which limits its use in environments where high temperatures and microorganisms are present, for instance, slow-release fertilizers applied in the soil.[212] Crosslinking lignin to the starch matrix decreases the degradation rate, increases its resistance, and reduces its water uptake and water activity. However, some weak points might appear and need to be corrected. If the hydrophilicity of the starch-lignin matrix is not decreased sufficiently, excessive water swelling and uncontrolled release of the carried molecule will occurr.[213] Using appropriate lignin content and performing lignin modification to increase its hydrophobicity might be effective strategies to be taken to avoid those weak points. A summary of the crosslinked starch-lignin materials and their formulations is presented in Table 2.3.

An attempt to develop crosslinked starch-lignin films were made by Sarwono *et al.*[214] Tapioca starch was chemically modified with urea and borate and mixed with 10 wt.%, and the product showed lower water absorption and presented structural stability after 30 days of water immersion. The upgrades that lignin offered to the films opened windows of opportunities for controlled release applications. Majeed and coworkers generated crosslinked starch-KL films for the controlled release of fertilizers (e.g., urea).[215–217] Films were prepared using the urea- disodium tetraborate crosslinking system earlier developed by Sarwono *et al,*[218] which aimed to reduce the films' rapid biodegradability and slow the release of nitrogen in aerobic soil. The addition of 15 and 20 wt.% KL significantly reduced the enzymatic degradation of the starch-lignin matrix caused by α-amylase and lignin peroxidase, which resulted in a slower release rate of nitrogen.[216,219] These results demonstrate that a crosslinked matrix of starch and lignin can be used as a controlled release system of urea as fertilizer. However, the mechanisms involved in the protection of the matrix are not detailed yet, and more comprehensive biodegradation assays are needed.

The chemical modification of starch or lignin before their crosslinking has been used as a strategy to enhance the properties of the crosslinked films. For instance, hydroxyalkylated starch or lignin were used in different studies as the base material to produce crosslinked films. In one study, Shi and Li used hydroxymethylated lignin with starch and glutaraldehyde as a crosslinker to produce reinforced films. The elasticity, thermal stability and compatibility were improved after the cross-linking. However, the relatively high proportion (38 wt.%) of hydroxymethylated lignin caused the increment of the film's hydrophilicity.[220] In another study, Javed *et al.,* utilized hydroxypropylated starch, lignin, and ammonium zirconium carbonate (AZC) as the crosslinker to generate films for coating purposes. The water resistance of the films increases noticeably after the crosslinking of lignin. Nevertheless, the water vapour barrier and oxygen transmission rate of

the coating were not significantly improved. In general, it is observed that the hydroxyalkylation modification of starch and lignin will increase the hydrophilicity of the polymers, which helps to increase the polymer compatibility and can be useful for applications where water absorption is required such as hydrogels.

Crosslinked starch-lignin films have shown great potential as matrices for controlled release systems, and most studies have been focused on the controlled release of urea. However, the study of non-urea fertilizers, agrochemicals and drug delivery applications remains to be explored. The modification of the polymer prior to the crosslinking, particularly modification of lignin, can be a pathway to be followed in future research as it might help to reduce the incidences of agglomeration and phase incompatibility in the starch-lignin matrices.

Table 2.3. Summary of the starch-lignin formulations for crosslinked films.

Blending strategy	Crosslinker and amount	Ratio, %		Other reaction conditions	Lignin type and function	Final product	Main improvement	Weak point	Ref.
		Lignin	Starch						
Solution casting	Urea-Disodium tetraborate	5, 10, 15, 20	95, 90, 85, 80	80 °C, 3 h	Indulin kraft. Reinforcer	Fertilizer controlled release film	Reduction enzyme catalysis	Low viscosity	[214]
Solution casting	Urea-Disodium tetraborate, NA	5, 10, 15, 20	95, 90, 85, 80	80°C, 3 h	Indulin kraft. Reinforcer	Fertilizer controlled release film	Thermal stability, Reduction of biodegrada	Biodegradability was assed	[215]

							bility. Slow nitrogen release	with enzymes only	
Solution casting	Urea-borate, , 24%	5, 10, 15, 20	71, 66, 61, 56	80˚C, 3 h	Indulin kraft Reinforcer	Fertilizer controlled release film	Hydrophobicity	Incompatibility when lignin >15%	[218]
Solution casting	Urea-Disodium tetraborate, 20-25%	5, 10, 15, 20	73, 66, 62, 59	80˚C, 3 h	Indulin kraft. Reinforcer	Fertilizer controlled release film	Reduction of aerobic biodegradability. Slow urea release	Fungal growth	[216]
Solution casting	Urea-Disodium tetraborate, 25%	5, 10, 15, 20	70, 65, 60, 55	80˚C, 3 h	Indulin kraft. Reinforcer	Fertilizer controlled release film	Reduction of anaerobic biodegradability. Slow urea release	Unclear effectiveness with other fertilizers	[217]
Solution casting	Glutaraldehyde, 4%	36	60	Glycerol, 50 ˚C, 2 h	Kraft, hydroxymethyl.	Cross-linked film	Elasticity, thermal stability	High moisture	[220]

					Reinforcer, compatibilizer			absorption	
Solution casting	Ammonium zirconium carbonate	23 24	77, 76,	Glycerol, 95 ˚C 1 h	LignoBoost. Hydrophobic additive	Paper coating	Water barrier, decreased water solubility	Negative effect on oxygen transmission rate	[221]
Multilayer coating	Ammonium zirconium carbonate	22, 26	78, 74	Glycerol, 95 ˚C 1 h	LignoBoost. Hydrophobic additive	Paper coating	Water vapor transmission rate	Uneven and cracking texture	[209]
Solution casting	Urea-Disodium tetraborate, 20-25%	5, 10, 15, 20	73, 66, 62, 59	80˚C, 3 h	Kraft. Reinforcer	Fertilizer controlled release film	Reduction enzyme catalysis	Recommended lignin content >15% prone	[219]

	to incompatibility

2.5.4. Starch-lignin coupled polymers

In this system, starch-lignin coupled polymers consist of one or more chains of one polymer (e.g., lignin) grafted as branches onto the backbone structure of the other polymer (e.g., starch).[222] In general, after the coupling reactions, a three-dimensional polymeric network linked by covalent bonds is formed between lignin and starch.[223] The starch-lignin coupled polymers can be produced from the native or modified forms of lignin and starch by copolymerization or crosslinking reactions. A few reports are available in the literature describing the formation of these coupled polymers as described in Table 2.4.

The copolymerization of starch and lignin has been carried out following different techniques, such as radiation-induced grafting, enzymatic catalysis and free radical copolymerization. Using an electron beam radiation-mediated grafting of starch and lignin has been investigated to produce hydrogels.[224] The produced copolymer was reported to have reduced surface hydrophilicity and the retrogradation of starch.[225] However, the radiation methodology is challenging to operate at a large scale and causes chain cleavage and polymeric degradation of starch, which limits its end-use applications.[226,227] In addition, the physicochemical structure of the radiation-mediated starch-lignin copolymer has not been fully studied.

Shogren and Biswas reported the generation of a starch-lignin coupled polymer using corn starch and sodium lignosulphonates via enzymatic catalysis with an oxidoreductase laccase.[228] In this

system, phenoxy radical groups in the lignosulphonates were generated by the laccase, which oxidized and radicalized the starch hydroxyl groups, reacting and coupling both polymers. The highlighted property of the lignosulphonate-starch was its radical scavenger activity and antioxidant capacity, making it potentially applicable as a food additive, preservative, and in cosmetic products. However, the grafting percentage of lignosulphonates into starch was around 1% due to low enzymatic concentration. In more recent studies, free radical copolymerization was chosen for producing starch-lignin copolymer. Wu et al. fabricated a copolymer of lignosulphonates and corn starch for its application as a bio-based adhesive.[229] The performance of the bio-adhesive showed adhesion and moisture resistance enhanced, and the material showed thermo-responsive dissolution properties. Similar to the previous studies, there were not enough details regarding the chemical properties of the copolymer (e.g., chemical structure and Mw) even though the covalent bonding between lignosulphonates and starch was assessed by FT-IR and XRD techniques.

The coupling of lignin and starch with the aid of a crosslinker has been also explored recently. Chen et al. used urea to crosslink lignin and starch.[230] For this purpose, significant modifications in both polymers were made before the crosslinking. Starch was obtained as dialdehyde starch, and KL was glyoxalated to increase the reactivity and binding properties. The viscosity and thermal stability were enhanced after the crosslinking, which is beneficial for its end-use as adhesives. However, it was suggested that a higher crosslinking degree was needed to meet the mechanical properties required in wood adhesives. Similarly, kraft lignin and starch were crosslinked to produce a bio-adhesive.[231] Using sodium tetraborate decahydrate as a crosslinker, the crosslinked starch-lignin adhesive showed stronger adhesive properties and higher water resistance than lignin-free formulations. Enhancing the water resistance of the adhesive broadens

its application possibilities in packaging materials, such as corrugated cardboard. Still, the water resistance is directly related to the lignin content but increasing its proportion in the material leads to brittleness and a reduction of adhesion capacity.

Table 2.4. Summary of the starch-lignin formulation for coupled polymers.

Reaction type	Copolymerization mediator	Ratio, %		Other reaction conditions	Lignin type and function	Proof of reaction	Final Product	Main improvement	Weak point	Ref.
		Lignin	Starch							
Radiation induced grafting	Electron beam irradiation	1	99	Glycerol, 105-115, °C, irradiation 50-400 kGy per pass	Cinnamyl alcohol model compounds	Size exclusion chromatography	Cross linked gel	Gelling properties	Model compound not reflective of lignin size and complexity	227
Radiation induced grafting	Electron beam irradiation	1	99	105-115, °C, irradiation 50-400 kGy per pass	Cinnamyl alcohol model compounds	Size exclusion chromatography	Cross linked gel	Gelling properties, no glycerol needed	Model compound not reflective of lignin size and	226

									complexity	
Enzymatic catalysis	*Trametes versicolor* laccase	17	83	30 °C, 4 h, pH 5.0	Lignosulphonate. Radical scavenging	UV spectroscopy	Graft copolymer	Antioxidant activity	Low grafting ratio	[228]
Free radical copolymerization	Ammonium persulphate	5, 10, 15, 20, 25	95, 90, 85, 80, 75	80 °C, 6 h, pH 4	Lignosulphonate. Reinforcer, adhesive	FT-IR, XRD	Bio-based adhesive	Moisture resistance. Viscosity and adhesion	Storage affects the thermodynamic equilibrium	[229]
Crosslinking	Sodium tetraborate decahydrate	5, 10, 15, 20, 25, 30, 35,	95, 90, 85, 80, 75, 70, 65,	Stein Hall process, 40-50 °C, 0.1 h	Kraft. Reinforcer, adhesive	Not performed	Bio-based adhesive	Mechanical strength, water resistance,	>5% concentrations of lignin, brittle and weaker adhesive	[231]
Crosslinking	Urea-glycerol	50	25	Lignin glyoxalat	Desulphurized	FT-IR, MALD	Bio-based	Mechanical	Higher crosslin	[230]

	diglycidyl ether	ion, 2 h, stirring	kraft. Scaffold, adhesive	I-ToF spectro metry	adhes ive	properti es, adhesio n charact eristics	king is require d

2.5.5. Achievements and challenges of starch-lignin materials

The reviewed literature shows that most works combining lignin and starch adopted the approach of physical blending via non-covalent interactions using plasticizers, such as glycerol to produce starch-lignin materials. As seen in Tables 2.1 to 2.4, the number of studies regarding the production, characterization, and utilization of covalently linked starch-lignin polymers is smaller than those regarding the study of films of composite materials. Among these materials, crucial properties such as tensile strength, thermal resistance, hydrophobicity, and water resistance were successfully developed and enhanced. Yet, there are still significant improvements to be made. For instance, there is great variability in the selection of the lignin type, where sodium lignosulphonates have been the preferred lignin mainly because of their water solubility and ease of use. However, due to its hydrophilicity nature, lignosulphonate-starch materials showed low water resistance. Thus, using KL would be more suitable if the objective or application of the final product requires the development of hydrophobicity and water resistance.

From the revised literature, it is evident that the starch's content in most formulations is dominant, with contents around 80 wt.% of the total mass. One reason for the lignin's low content in starch composite is that when its content increases above 20 wt.%, issues, such as particle agglomeration, incompatibility between starch and lignin, and brittleness, seem to be recurrent. Different strategies

are required to solve the appearance of those problems. For example, increasing the crosslinking ratio, using modified lignin, or selecting chemical reaction methods, such as radical copolymerization are promising approaches to produce more resilient starch-lignin materials. Moreover, it is necessary to correlate the physicochemical and rheological properties of the starch-lignin polymers with their chemical structure, which will allow to achieve better performance by customizing the applications to the polymers' characteristics. As explained in this section, most studies combined starch and lignin to generate film-like materials. Nonetheless, the generation of new materials and applications, such as matrices for non-urea fertilizers, hydrogels for bioactive molecules delivery (e.g., drugs or agrochemicals), and solution-based applications (e.g., coating or flocculation) are of great importance and remain to be explored.

2.6. Methods for the characterization of starch-lignin copolymers

2.6.1. 1 Dimensional-Nuclear magnetic resonance

^{1}H-NMR. Nuclear magnetic resonance (NMR) has been extensively used to elucidate the structure of lignin and starch.[232,233] Proton NMR (^{1}H-NMR) was the primary method for the characterization of macromolecules in the past. It is still a proper routinary analysis due to its short experimental time and ease of sample preparation. The fingerprint regions in lignin (aromatic H, methoxy group, and aliphatic H) and starch (anomeric H in glycosidic linkage) can be identified by analyzing the ^{1}H-NMR spectra[234] as displayed in Figure 2.5a.

The polymeric nature of both lignin and starch and their diversity of protons causes the ^{1}H-NMR spectrum results to appear with some overlapping, which makes the structural elucidation difficult, and, to some extent, inaccurate.[235] Hence, the sample preparation procedure is critical, and the low solubility of starch and lignin is a major challenge for their NMR characterization. Because the resolution, signal to-noise ratio, and overall quality of the NMR analysis is limited by sample

solubility, different solvents and solvent mixtures have been used to prepare starch and lignin-based samples for NMR analysis.[235] The most effectively used solvents are deuterated dimethyl sulfoxide (DMSO-d6), chloroform-d, and deuterium oxide (D_2O). Also, the mixtures, such as D_2O/DMSO-d6 DMSO-d6/LiBr, DMSO-d6/pyridine-d5, and chloroform-d/pyridine are proven to be effective for preparation of starch and lignin samples for NMR analysis.[232,236] The selection of the ideal solvent should be based on the physicochemical characteristics of the samples, focusing on their solubility in polar or non-polar solvents, which will determine the adequate choice.

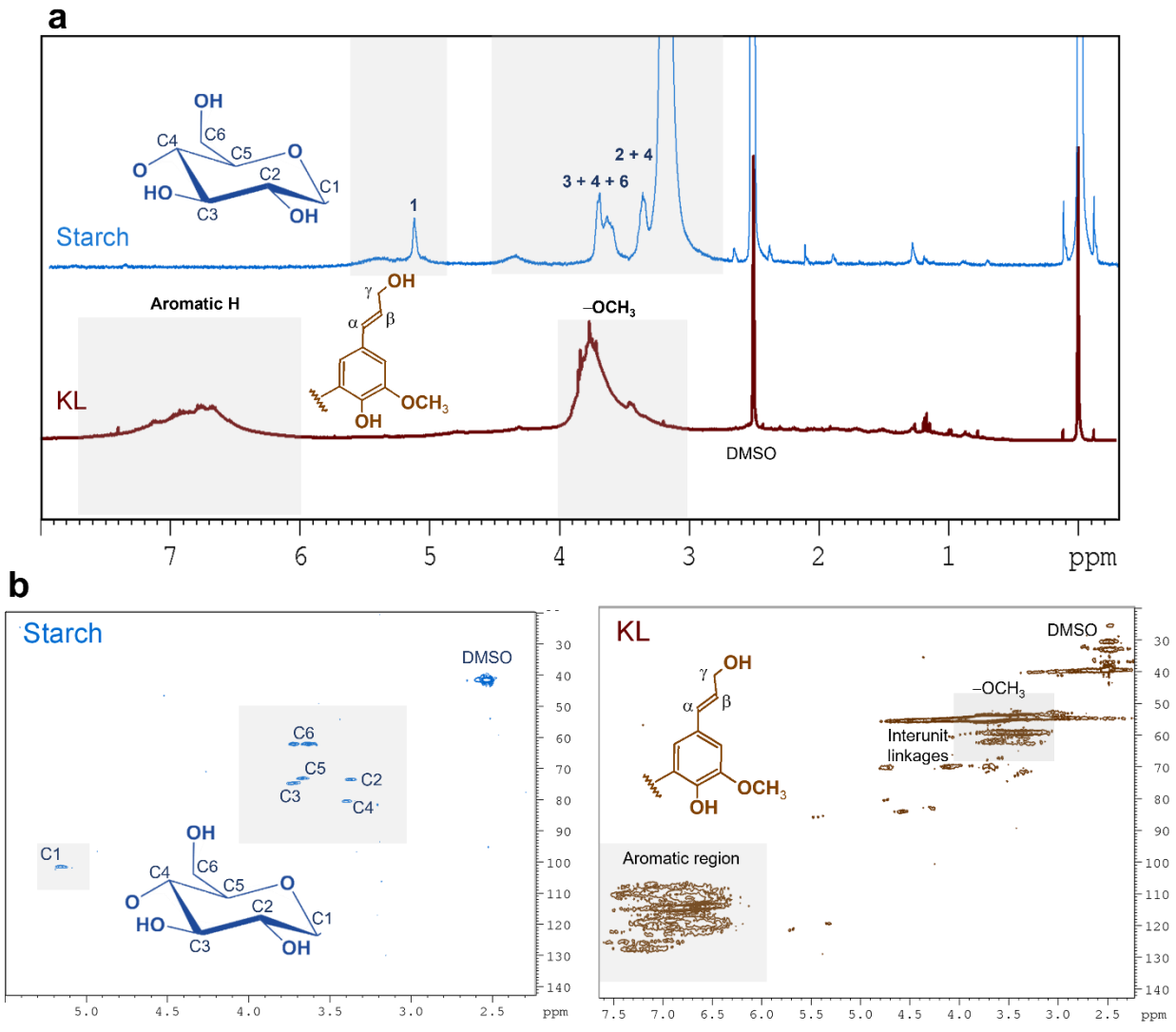

Figure 2.5. (a) ^{1}H-NMR spectra of starch and KL dissolved in d6-DMSO/LiBr and d6-DMSO, respectively. (b) 2D HSQC-NMR of the fingerprint regions of starch and KL.

^{31}P-NMR. The quantitative analysis of the chemical structure of lignin has been performed via ^{31}P-NMR spectroscopy.[237,238] The concentration of the hydroxyl functional groups in lignin can be quantified after their phosphitylation (Figure 2.6). In general, the experiment requires the phosphitylation of the hydroxyl groups in lignin using a phosphitylating reagent, such as 2-chloro-4,4,5,5-tetramethyl-1,3,2-dioxaphospholane (TMDP). After the phosphorylation, the ^{31}P signals can be detected in lignin by ^{31}P-NMR spectroscopy at the130–150 ppm region, which can be used to identify and quantify the concentration of the hydroxyl groups in lignin.[239] A protocol for phosphitylation and P-NMR analysis has been established and is now widely used in lignin chemistry.[55,240] Compared to wet-chemical techniques, the quantitative ^{31}P-NMR allows the identification and quantification of aliphatic hydroxyl groups and the phenolic hydroxyl groups of the different lignin subunits, such as syringyl, guaiacyl and p-hydroxyphenyl.

In starch, ^{31}P-NMR spectroscopy is used for quantifying the phosphorus content, which are present mainly in the form of phosphate esters and phospholipids depending on the botanical source.[241] Also, ^{31}P-NMR analysis can be used to quantify the phosphorus content and degree of substitution of synthetically phosphorylated starch.[242] Usually, phosphate monoesters are located on the C6 and C3 of the anhydroglucose unit (AGU) in starch, and their signal appears at the -5.0 to 10.0 ppm region as observed in Figure 2.6a.[243]

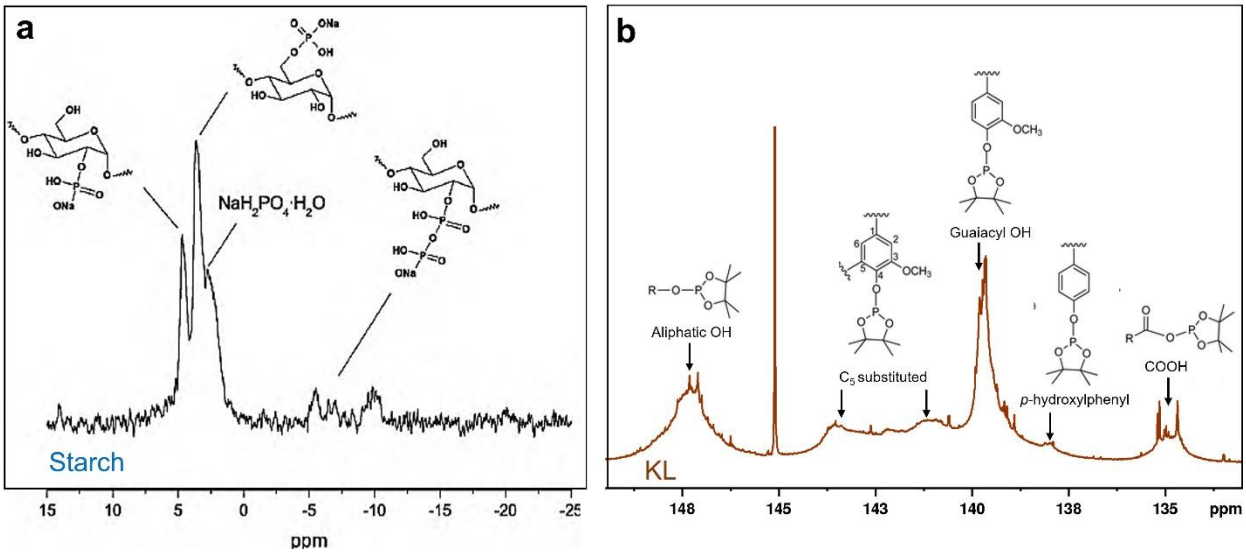

Figure 2.6. (a) ^{31}P-NMR spectrum of monostarch monophosphate dissolved in D_2O.[243] (b) ^{31}P-NMR spectrum of phosphitylated KL and the identification of the hydroxyl groups after reacting with TMDP in chloroform-d/pyridine solvent mixture.

2.6.2. 2 dimensional-Nuclear magnetic resonance

Comprehensive structural elucidation on lignin and starch are currently carried out using two-dimensional NMR techniques (2D-NMR).[244–246] 2D-NMR is the most widely used tool for the structural characterization of lignin and starch owing to the rich and less overlapped data compared to 1D-NMR, as observed in Figure 2.5.[247] Because of the higher resolution of 2D-NMR spectra, the signal assignment is more reliable and precise. Moreover, there is a large amount of data available in the literature for lignin and starch that makes the assignment of signal correlations a less ambiguous process. This method mainly for the identification of lignin's major structures and its interunit linkages, and starch's C1-C6 in the glycosidic linkages between the AGU.[248,249] In this review paper, the most utilized 2D-NMR methods for starch and lignin, such as ^{1}H–^{1}H COSY, ^{1}H-^{13}C HSQC, ^{1}H-^{13}C HSQC-TOCSY, and ^{1}H-^{13}C HMBC are discussed.

^{1}H–^{1}H COSY. The 2D correlational spectroscopy (^{1}H–^{1}H COSY) is a valuable tool that helps to separate and observe the proton signals in lignin and starch, which would be usually highly overlapped in 1D-NMR.[250,251] Using ^{1}H–^{1}H COSY, the signals of adjacent proton resonances of lignin and starch can be identified more easily as observed in Figure 2.7. In ^{1}H–^{1}H COSY, both axes correspond to the proton signal, and the contour cluster signals appearing in diagonal (diagonal-peak) correspond to the 1D-NMR spectrum.[244] Whereas the symmetrical off-diagonal contour signals (cross-peaks) are found from coupling proton shifts on the X and Y axes.[246] The connection between diagonal- and cross-peaks establishes their vicinity among the carbon chain in the chemical structure of lignin and starch.[252]

For example, as depicted in Figure 2.7a, the cross-peak found at 3.4 and 5.2 ppm is attributed to the coupling of H in C1 with the H in C2, respectively, which reveals the connectivity of the protons in the AGU of starch.[249] However, the region between 3.5 to 4.0 ppm is highly overcrowded, making the identification of signals more challenging. In the case of lignin, the cross-peaks at 6.5 and 7.5 ppm are assigned to the H in the $C_{2\text{-}6}$ of the phenolic ring,[247] as seen in Figure 2.7b. Additionally, the connectivity among the KL interunit linkages is observed from the cross-peak of 4.9 and 5.8 ppm corresponding to the H in the C_{α} and C_{β}, respectively.[253] These COSY NMR assignments provide aids to elucidate the structure of starch-lignin materials, particularly by resolving the overlapped signal obtained by 1D-NMR analysis and offering information about the interunit linkages or crosslinks.

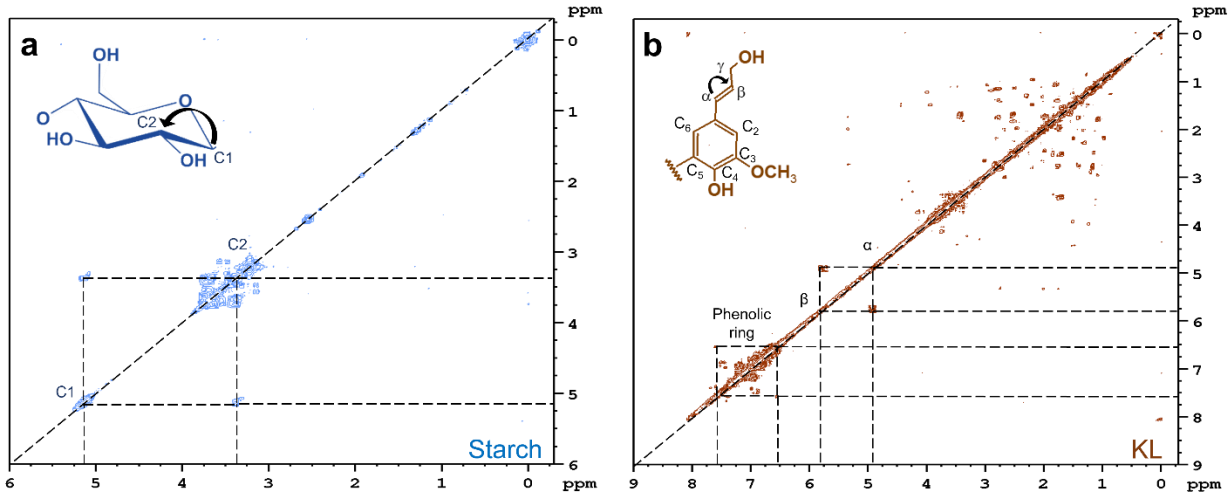

Figure 2.7. (a) ^{1}H–^{1}H COSY spectrum of starch dissolved in d6-DMSO/LiBr. (b) ^{1}H–^{1}H COSY spectrum of KL dissolved in d6-DMSO.

^{1}H-^{13}C HSQC. The heteronuclear single quantum coherence (^{1}H-^{13}C HSQC) NMR is a versatile method extensively used to explain the structural features and transformations of lignin- and starch-based polymers.[245,254] The assignments of a given cross signal from ^{13}C and ^{1}H, the HSQC analysis possess a significantly improved resolution and offers more details for the identification of the corresponding signals of lignin and starch. The observations of specific protons attached to specific carbons provide the clear identification of linkages, major structures or specific C-H assignments.[255,256] Essential structural findings about the lignin-based, starch-based polymers and inter-molecular linkages have performed by means of ^{1}H-^{13}C HSQC. For instance, phenyl glycosidic structures, esters, and benzyl ethers groups have been identified with ^{1}H-^{13}C HSQC analysis in various lignin- and starch-based polymers.[58,232,257,258]

For starch, the structure of the AGU can be extensively elucidated by HSQC analysis. The signals for the C1-C6/H1-H6 are well-resolved and are observed at δC/δH 101.6/5.2, 73.7/3.4, 74.7/3.7, 80.6/3.4, 73.2/3.7, and 62.3/3.7 ppm, respectively (Figure 2.5a).[254] On the other hand, using

HSQC, several of the lignin's substructures can be identified with highly-resolved signals from the 2D spectrum. As presented in Figure 2.5b, the signals corresponding to the cross-peaks in the region of δC/δH 100-130/6.5-7.5 ppm are assigned to the G units in KL.[259] Another important signal in lignin's HSQC spectra is corresponding to the methoxy group, which is observable at δC/δH 58.1/3.7 ppm.[248] The methoxy's group signal is often used as the reference for lignin in lignin-based polymers, as regularly is a non-altered site in modified lignin, as discussed in section 1.2.3. Using HSQC as a central tool for the elucidation of the starch-lignin material is essential for understanding their structure, and the reaction mechanism, and obtaining valuable data for the development of these materials.

^{1}H-^{13}C HSQC-TOCSY. The HSQC total correlation spectroscopy (^{1}H-^{13}C HSQC-TOCSY) is an experiment in which the bond correlations between all spins in the same uninterrupted spin system can be detected by the appearance of cross-peaks.[260] The HSQC-TOCSY spectrum provides details that enhance the understanding of the structural interconnectivity of starch and lignin, observed by sets of cross-peaks as displayed in Figure 2.8. Similar to the way COSY NMR is interpreted, the intensity of the peaks is related to the distance between the coupled signals in the HSQC-TOCSY spectrum. However, because of the large amount of information contained in 2D TOCSY spectra, this experiment is less sensitive in comparison to other 2D-NMR experiments, and lower intensity can be found among the cross-peaks contours.[261] HSQC-TOCSY is a typical method used for supplementing the HSQC experiments, in particular, is a valuable tool for resolving carbohydrate rings, such as the AGU in starch, and monolignol units in lignin, as well as the lignin-carbohydrate complexes.[262,263]

The multiple bond correlation within the AGU in starch can be examined via HSQC-TOCSY since the C1 to C5 are part of the same spin system. For instance, it is observed in Figure 2.8a that the correlation from HO3 with the C2 to C5 ring carbons appeared as cross-peaks at δH 5.75 ppm with δC 74.1, 75.9, 77.5, and 79.5 ppm. Moreover, the assignments of the lignin inter-units, such as the coniferyl alcohol end groups can be accomplished through HSQC-TOCSY.[261,264] The uninterrupted spin system in the KL monolignol containing the multiple bond correlation of C_α, C_β, and C_γ is assigned by the cross-peaks at δC/δH 128.6/6.5, 128.6/6.3, and 61.5/4.2 ppm, as depicted in Figure 2.8b. The direct assignment of ^{13}C and ^{1}H chemical shifts of starch and lignin polymers is performed more easily by combining HSQC and HSQC-TOCSY experiments, which provides advantages of a clear assigning of highly overlapped regions by separating the signals from their correlations of the coupling networks.

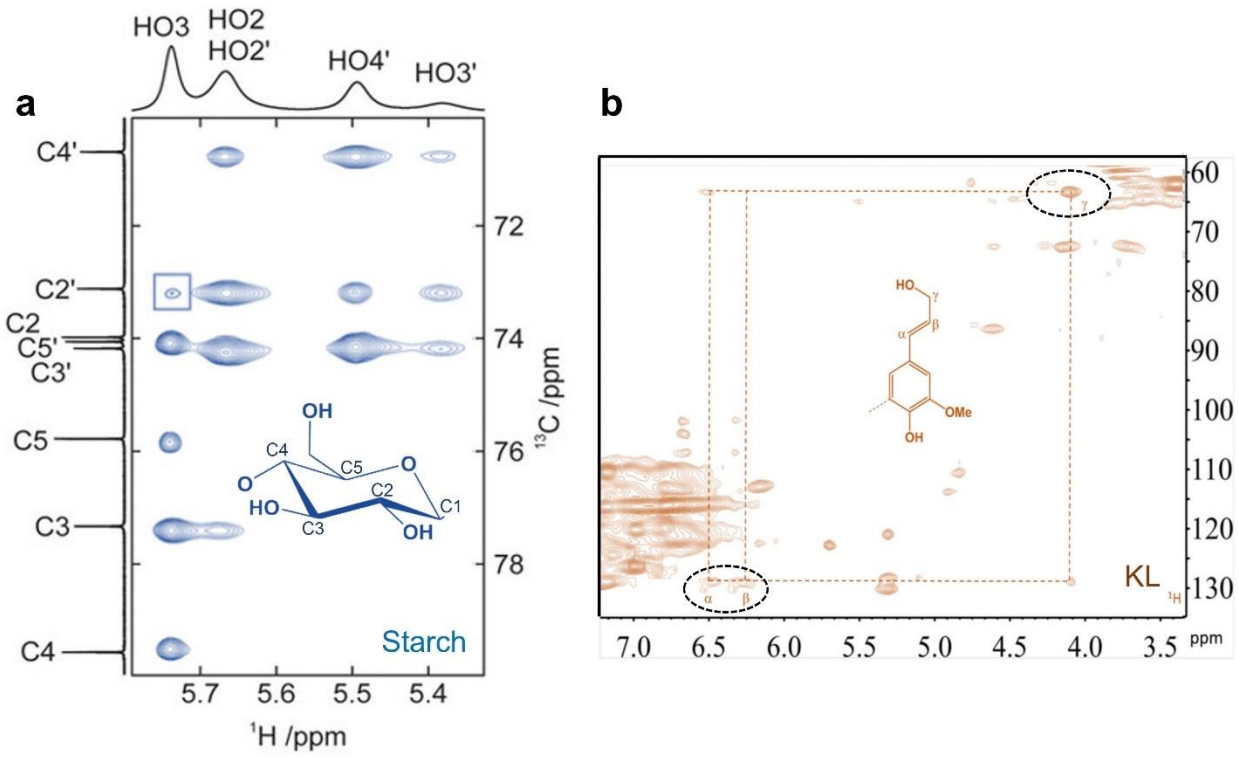

Figure 2.8. (a) ^{1}H-^{13}C HSQC-TOCSY spectrum of a disaccharide (i.e., α-d-Glcp-(1→4)-β-d-Glcp-OMe) sample representative of starch dissolved in H_2O/d6-DMSO solvent mixture.[265] (b) 2D

HSQC-NMR spectrum of the fingerprint region (i.e., coniferyl alcohol) of KL dissolved in d6-DMSO.[264]

^{1}H-^{13}C HMBC. In the heteronuclear multiple bond correlation spectroscopy (^{1}H-^{13}C HMBC), the H and C can be correlated from coupling vicinities with a maximum separation of up to three bonds, providing essential information about connectivity networks in lignin and starch.[266,267] The coupling interactions of three-bond correlations between H and C can offer compelling evidence of linkages where oxygen is involved as displayed in Figure 2.9. For example, ether linkages in lignin-carbohydrate complexes, or the glycosidic bond in starch, this characteristic is the main advantage of HMBC over other 2D-NMR experiments for the analysis of lignin and starch polymers.[268,269] However, such determinations are not easy and are commonly used as complementary experiments to HSQC and other 2D-NMR experiments. Furthermore, the often longer relaxation delays are required to make a particular structure visible in the spectrum, which could significantly reduce the intensity of the spectrum.[270] Extensive details can be obtained from the HMBC analysis, allowing the distinction between S and G and p-hydroxybenzyl in lignin, or the identification of the C involved in crosslinks in starch-based polymer, for instance.[271,272]

The HMBC spectrum of oxidized starch is observed in Figure 2.9a, where a crosslinked network resulting from the starch's modification is identified.[273] As seen, the cross-peaks appearing at δC/δH 74.0/5.1 and 71.0/5.1 ppm are assigned to the correlation of H1 with C5 and C2, respectively. Likewise, the crosslink between the C6 and H4 is identified by the cross-peak a δC/δH 179/4.1 ppm, which evidenced the crosslinked network. In the case of lignin, the HMBC signals are more saturated due to the high number of correlations occurring in the complex and heterogeneous lignin's structure. As is displayed in Figure 2.9b, two noticeable correlations are

observed for KL, corresponding to the phenolic structures and the methoxy group. The correlation between the H in the methoxy group and the C4 in the phenolic ring is assigned to the cross-peak at δC/δH 150/3.9 ppm. Moreover, the correlations between the C and H within the phenolic ring are identified with the cross-peaks at δC/δH 150/6.5-7.5 ppm. The appearance of new correlations or the absence of expected ones can be used as an indication of the success of different structural modifications, such as crosslinking or polymerization reactions in lignin and starch. Therefore, the collective use of ^{1}H-^{13}C HSQC, HSQC-TOCSY, and HMBC analysis form a powerful approach for the comprehensive elucidation of signal assignments and structural analysis of starch-lignin-based polymers.

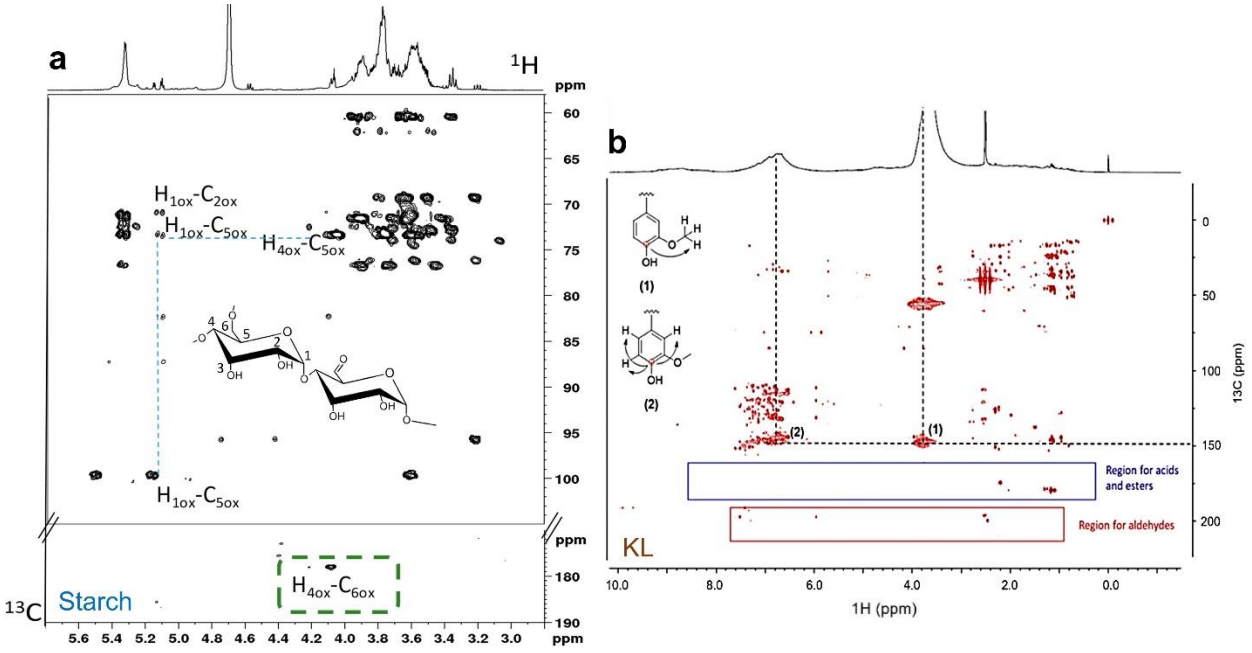

Figure 2.9. (a) ^{1}H-^{13}C HMBC spectrum of oxidized starch dissolved in in D_2O.[273] (b) ^{1}H-^{13}C HMBC spectrum of KL dissolved in d6-DMSO.[274]

2.6.3. Fourier transformed infrared spectroscopic

The attenuated total reflectance-Fourier transformed infrared (ATR-FTIR) spectroscopic method is an absorption technique used to identify or characterize the chemical structure of polymeric samples. ATR-FTIR is a technique that analyzes the vibrational (e.g., bending or stretching) properties of different bonds. Associated bands with -OH, C-H, C-O, C-C, C=O, C-O-C and C-O-H bonds, amongst others, can be detected by vibrational bending or stretching as described in Table 2.5.[275,276] The FT-IR method allows the identification of modified lignin- and starch-based polymers in a rapid and simple way. The ease, non-destructive, and solid-state characteristics of FT-IR makes it an ideal preliminary analysis for the characterization of lignin and starch-based polymers.[52,277] However, the IR-fingerprint spectral region of lignin and starch frequently overlaps between 900 and 1800 cm^{-1} and is hard to discriminate among many different linkages in both polymers.[278] Moreover, the intense overlapping might affect the intensity of the bands depending on the relative concentration.[279] Therefore, it is commonly suggested that FTIR results are combined with other characterization methods, such as NMR or XPS, to present more reliable and conclusive evidence for elucidating the structure of starch-lignin-based polymers.

Table 2.5. Assignment of FT-IR bands of the most important groups in starch-lignin materials

Polymer type	Wavenumber, cm^{-1}	Band assignment	Vibration type	Reference
Starch-lignin blend	3271	OH	Stretching	[190]
Starch-lignin blend	2924	C-H	Stretching	[190]
Starch-lignin crosslinked film	1600-1510	Aromatic ring	Stretching	[218]
Starch-lignin coupled polymer	1515	Benzene ring	Stretching	[229]

Starch-lignin coupled polymer	1616	C=O (–NH–C=O)	Stretching	[230]
Plasticized Starch-lignin film	1415	C-H_2	Bending	[211]
Plasticized Starch-lignin film	1150	C-O (C-O-H)	Stretching	[202]
Plasticized Starch-lignin film	1120	C-C	Stretching	[202]
Starch-lignin crosslinked film	1082	C-O	Deformation	[220]

2.6.4. X-ray photoelectron spectroscopy

X-ray photoelectron spectroscopy (XPS) is a surface analysis method that determines the elements and linkages present on the surface of materials and is commonly used for characterizing starch-lignin materials.[280,281] Two important characteristics can be obtained through XPS: the type and concentration of elements and the type and concentration of chemical bonds present in the material. By a survey scan, an element such as C (C_{1s}), O (O_{1s}), N (N_{1s}), Na (Na_{1s}) and S (S_{2s} and S_{2p}) can be detected, all of which are of great importance in lignin and starch polymers.[282] A low-resolution scan provides the percentage of each atom, whereas a high-resolution scan delivers the type and concentration of the different linkages. The signal of XPS spectra will commonly appear as atom-specific peaks, which can be deconvoluted in sub-peaks corresponding to the diverse atom-specific linkages involved in the chemical structure. Usually, the C 1s orbital is taken as the main peak for the study of starch and lignin polymers, located at the binding energy of 285.0 eV. The C 1s peak can be deconvoluted into several peaks corresponding to the main linkages of lignin and starch, such as C-C, C–O, O–C–O/C=O, and O=C–O.[283,284] The region of interest of the deconvoluted peaks is positioned at 284.8-284.5, 286.5-286.0, 287.6, and 288.5-288.9 eV, for C-C, C–O,

O–C–O/C=O, and O=C–O, respectively.[285,286] The relative surface content of those linkages can be also calculated from the spectral survey utilizing the relative sensitivity factor values, which are provided by the XPS machine company. However, XPS cannot detect H atoms, which is one of its limitations, often overcome by using H-NMR or HSQC as complementary methods. Nevertheless, its sensitivity, non-destructive and solid-state nature are desirable for the characterization of different lignin and starch-based polymers.[287–290]

2.6.5. Thermal-analytical methods

The thermogravimetric analysis (TGA) is used to measure the mass change and degradation of a sample as a function of time and temperature.[278] Moreover, the derivative thermogravimetric analysis (DTG) can be performed on the experiment generated in TGA to study phase transition temperatures.[291] TGA and DTG have been extensively employed to investigate the thermal stability of lignin and starch-based polymers.[201,292–294] From the different transition temperatures and the loss of mass rate, the temperature for the cleavage of specific moieties composing the starch-lignin materials can be the determined, as described in Table 2.6.[295] Using only a few milligrams of a sample (5 to 15 mg), TGA can be highly beneficial for obtaining information about the structure and thermal properties of the lignin and starch-based polymers.

Differential scanning calorimetry (DSC) is another effective thermos-analytical method to characterize lignin and starch-based polymers.[296,297] In DSC analysis, a sample is placed under constant heating and undergoes a series of physical transformations such as phase transitions (e.g., glass transition, melting). For starch-lignin materials, the glass transition temperature (T_g) and melting point (T_m) are frequently reported as an important part of their thermal characterization, as shown in Table 2.7.[298–301] The T_g is the temperature range where amorphous polymers are randomly rearranged from an ordered state to a more disordered state, generally appearing as a

step change in the heat flow curve. Different degrees of polymerization, MW, and grafting modifications are commonly parameters affecting the T_g.[302–304] The T_m is taken as the temperature range where a polymer changes from a solid to a liquid state, reflected by an endothermic step in the DSC curve (i.e., melting transition).[305] Knowing the T_g and T_m, of the starch-lignin materials provides valuable information for establishing suitable applications and analyzing the structural changes caused by the chemical modifications of these materials. However, for starch-based materials, the enthalpy of the T_g is often weak in dry samples, and the T_m occurred only in materials with plasticizers.[306] Thus, thorough measurements, elimination of heating history, and detailed data analysis must be performed to avoid misinterpretation of the results.

Table 2.6. Degradation temperature of the principal structures in different starch-lignin materials determined by DTG.

Material type	Degradation temperature, °C	Structure	Reference
Plasticized Starch-lignin film	200	Glycerol moieties	202
Starch-lignin crosslinked film	250	Urea crosslink	217
Plasticized Starch-lignin film	298	Glycerol moieties	204
Plasticized Starch-lignin film	320	AGU	211
Plasticized Starch-lignin film	350	Aliphatic side chains	205
Plasticized Starch-lignin film	430	Aromatic moieties	201
Starch-lignin crosslinked film	485	Aromatic moieties	216

Table 2.7. T_g and T_m of different starch-lignin materials determined by DSC

Material type	T_g, °C	T_m, °C	Reference
Starch-lignin blends	–30	120-123	[186]
Starch-lignin blends	148-170	180–220	[192]
Starch-lignin blends	-25	129-131	[189]
Starch-lignin blends	52	NR	[191]
Plasticized Starch-lignin film	NR	180	[199]
Plasticized Starch-lignin film	100-150	NR	[208]

NR, not reported in the study

2.6.6. Mechanical and thermomechanical properties

The mechanical properties of the starch-lignin materials including the tensile strength and elongation at break, are performance parameters frequently evaluated (Table 2.8). The tensile strength is the maximum tensile stress that a material can hold, while the elongation at break is the proportion of length change relative to the initial length of the material.[307] The tensile strength and elongation at break are determined by standard tensile stress-strain analysis following specific technical standards (e.g., ASTM D638, D638-M, D882–02, or ISO 527-1996).[199,203,208] The enhancement in the tensile strength and elongation at break are often aimed for starch-lignin materials. By studying the performance of the mechanical performance of the starch-lignin materials, the effect of lignin on the reinforced starch matrix can be assessed, as the ratio of lignin to starch, compatibility, and crosslinking degree are determinant factors affecting these parameters.

The most common approach for determining thermomechanical properties of starch-lignin materials is the dynamic mechanical analysis (DMA).[308] In the DMA, after applying a small cyclic deformation to the sample, it is possible to detect mechanical relaxations as a function of temperature, such as the Tan δ, the main mechanical relaxation associated with the T_g.[195,309] One important factor affecting the Tan δ is the incorporation of plasticizers and reinforces, such as lignin into the starch matrices, which is reflected as shifts in the temperature and maximum Tan δ peak (Tan δ_{max}).[191,194] However, as observed in Table 2.8 just a small proportion of the studies analyzing the mechanical properties of the starch-lignin materials performed DMA tests and reported the Tan δ_{max} and associated temperature. The significance of the Tan δ_{max} is related to its association with the segmental mobility of the polymers, such mobility is often affected by crosslinking and/or reinforcing agent, causing mobility restrictions.[310] Therefore, a higher crosslinking degree and the incorporation of a reinforcer agent will be observed as a decrease in Tan δ_{max}, while the temperature of the Tan δ_{max} will indicate the transition from an ordered to a disordered state of the starch-lignin material.

Table 2.8. Thermomechanical properties of starch-lignin materials determined by universal tensile tester and DMA

Material type	Tensile strength, Mpa	Elongation at break, %	Tan δ_{max}/Temperature °C	Ratio, %		Reference
				Lignin	Starch	
Starch-lignin blends	77.6 ± 9.3	214.0 ± 8.0	NR	2	98	[193]
Starch-lignin blends	14.9 ± 1.8	2.4 ± 0.0	NR	10	90	[189]
Starch-lignin blends	9.7 ± 0.25	94.2 ± 8.1	0.35 [a] /40	25	75	[191]
Starch-lignin blends	1.0 ± 0.1	92.8 ± 8.1	0.74 [a] /87	30	70	[194]

Starch-lignin blends	0.9 ± 0.1	212.0 ± 5.0	0.75 [a]/45	10	90	[195]
Plasticized Starch-lignin film	60.0 ± 3.6	97.0 ± 5.6	NR	2.4	97.6	[199]
Plasticized Starch-lignin film	1.1 ± 0.0	38.1 ± 0.85	NR	5	95	[200]
Plasticized Starch-lignin film	4.8 ± 0.1[a]	52.8 ± 0.5[a]	NR	10	90	[208]
Plasticized Starch-lignin film	8.0 ± 0.4	34.3 ± 1.1	NR	20	80	[210]
Starch-lignin crosslinked film	1.2 ± 0.0	114.5 ± 2.5	NR	10	65	[220]

[a] Parameter calculated with DMA

NR, not reported in the study

2.6.7. Rheological analysis

Rheology is the science that discusses the relationship between applied force (stress) and resulting deformation (strain) of materials under different environmental conditions.[311] The rheological characterization of lignin- and starch-based suspensions offers a perspective of their viscoelastic properties, which are often exemplified with a complex modulus and a phase angle.[312,313] The viscoelastic behaviour is given by the interactions between the different components in the system, exhibiting a combination of instant (elastic) or delayed (viscous) responses caused by a given amplitude and frequency.[314] Hence, the complex modulus representing the viscoelastic response is composed of the viscous modulus (G''), which describes the magnitude of energy loss by the material during deformation, and the elastic modulus (G') representing the amount of stored energy in the structure.[315]

The viscoelastic behaviour of lignin- and starch-based materials in solutions is often characterized by dynamic oscillatory rheology, using different shear rates, frequencies, and temperatures.[316–319] Determining the viscoelastic behaviour under various environmental conditions of lignin- and starch-based blends is an essential characterization stage for designing their applications.[320,321] Distinct experimental methods, such as strain, amplitude, frequency, and temperature sweeps, are typically performed to establish the viscoelastic properties under different conditions.[322,323] Among those properties, the viscous (G'') and elastic (G') moduli, and the yield stress, are frequently the most reported parameters for the lignin- and starch-based blends, as shown in Table 2.9. Notably, the rheological characterization of starch-lignin material is limited. As observed in Table 2.9, only one study amongst the revised works in this review paper performed a rheological analysis.

The rheological analysis of starch-lignin dispersions is a highly valuable tool for investigating the interaction between polymers, their correlation with their physicochemical properties, and their performance under different environmental conditions. However, as discussed earlier in this review, the development of starch-lignin polymers for solution-based applications is still in an early growth stage, and the information is limited. In these systems the rheological characterization is crucial, therefore, there exists a great window of opportunities for studying and developing starch-lignin materials throughout rheological characterization.

Table 2.9. Rheological properties of lignin- and starch-based in solution materials

Yield stress (G'/G''), Pa	G' vs G''	Viscosity behaviour	Blend type	Reference
NR	G'>G''	Shear-thinning	Starch-lignin coupled polymer	[229]

1.1 – 4.3	G'>G''	Shear-thinning	Lignin- cellulose suspension	316
NR	G'>G''	NR	Starch-carrageenan dispersion	318
4.0 – 5.0	G''>G'	Shear-thinning and shear-thickening	Starch-xyloglucan suspension	324
2.0 – 5.0	G''>G'	Shear-thinning	Lignin-polybutylene dispersion	317
0.1 – 0.2	G'>G''	Shear-thinning	Lignin-polyacrylonitrile solution	325

NR, not reported in the study

2.7. Conclusions, challenges, and future perspectives

The chemical approaches and characterization methods for the production and investigation of starch-lignin blends, composites, plasticized/crosslinked films, and coupled polymers were emphasized in this review paper. So far, there is an indication that the reinforcement of starch matrices with lignin is a promising strategy to overcome starch's downsides, such as moisture/water sensitivity, thermolability, and mechanical weakness. The inclusion of lignin into the starch matrices provides desirable properties, such as hydrophobicity, thermal stability, UV blocking and antioxidant capacity. However, the starch-lignin materials were predominantly generated with minimum lignin contents because of the challenges associated with the use of higher lignin content. The incorporation of larger lignin contents (>10 wt.%) generally resulted in the formation of lignin aggregates and an uneven distribution into the starch matrix causing brittle and cracking materials. Moreover, when the content of lignin was increased, often problems, such as incompatibility among polymers and phase separation, arose. It was also demonstrated that careful consideration is required when selecting the type of lignin for producing starch-lignin

materials. For instance, if the aim is to obtain a hydrophobic material, lignosulphonates should be avoided, while kraft lignin would be a more suitable choice.

Some significant challenges are evident in the characterization of starch-lignin materials. Chemical structural characterization persists as one of the biggest challenges in the field, particularly for solution-based methods (e.g., NMR or molecular weight analysis). Because of the low solubility of the starch-lignin material in traditional solvents, analyzing these materials becomes a greater challenge and this is reflected in the relatively small literature reporting these important characterization methods. The use of tailor-made solvent mixtures (e.g., LiBr/DMSO) capable of solubilizing the complicated starch-lignin matrix could be considered to overcome the insolubility issue. Another alternative is the utilization of non-solution methods, such as solid-state NMR, however, the low resolution and high costs associated with the analysis are concerns.[326] Overall, expanding the fundamental study of starch-lignin materials is required. The comprehensive elucidation of the physicochemical characteristics, and the correlation of such properties and performance, will help to accurately develop the formulations, significantly advancing to high-value applications of starch-lignin materials.

There are limited studies available regarding the production of starch-lignin coupled polymers. Among the explored methods, the chemically linked starch-lignin materials appear as a promising alternative to physical blending methods. The chemical coupling of starch and lignin might be an effective approach to avoid problems, like phase separation and polymer incompatibility. Overcoming these weaknesses will enhance the mechanical properties and performance of the starch-lignin materials. While this field is still in an early development stage, it is expected to grow in near future, which will open windows of opportunities for investigating different factors in the production of starch-lignin materials. Using modified lignin and starch polymers (e.g.,

sulphoalkylated lignin or aminated starch), trying different reaction pathways (e.g., controlled radical polymerization), and introducing other biopolymers into the formulation (e.g., chitosan or pectin) could be subjects future investigation.

So far, starch-lignin materials have demonstrated great potential as matrices for the controlled release of fertilizers, particularly urea. The controlled released fertilizers technology signifies a great benefit to agriculture as it can increase the efficiency of nutrients used by crops in a more ecological and environmentally sustainable way.[327,328] Although the study of starch-lignin controlled-release fertilizers is a topic not consolidated comprehensively, other significant factors, such as preparation methods, release approaches, and types of fertilizers remain to be investigated. Likewise, the generation and investigation of starch-lignin-controlled delivery systems with other agrochemicals, such as pesticides and herbicides, are an unexplored field with great potential. The suitability of the starch-lignin materials relies on their biodegradability in soil, and the fact that they will not accumulate over time. At the same time, they can offer desirable hydrophobicity and mechanical integrity required in these delivery systems. The cost-effect relationship is also advantageous, as starch and lignin are abundant and inexpensive raw materials. Moreover, drug-delivery systems are also of great importance; however, extensive research should be performed to assess the biocompatibility, toxicity, and health effects of the starch-lignin materials in the human body.

Starch-lignin materials provide valuable properties in particulate systems such as fibres, adhesives, coatings, and films material for packaging applications. Despite all the progress accomplished on starch-lignin materials, more research-oriented design and production of solution-based applications need to be closely considered, particularly for those of dispersion, flocculation, and emulsions products. Contrary to the particulate systems, starch-lignin materials in solution systems

requires the water solubility to be increased and the introduction of ionic groups to the chemical structure to develop more efficient products.

Ultimately, the research target for the starch-lignin material is to bring these products to the level of practical and commercial applications. However, the production of such materials is in infantry stage, as there are several gaps to be filled in the design, performance, and more importantly, fundamental knowledge concerning starch-lignin materials. It is imperative to implement more comprehensive studies of starch-lignin materials and to compare the results against traditional and commercial formulations so that their potential use, challenges, and benefits are identified and addressed properly. The performance of the new starch-lignin material should aim to comply with the current international standards criteria of a determined application, for instance, the ISO 18644:2016 for controlled-release fertilizers. Furthermore, the biodegradability and environmental impact of the starch-lignin material must be carefully considered in order to produce greener and more sustainable practices and technologies in future.

2.8. References

(1) Wilson, M. P.; Schwarzman, M. R. Toward a New U.S. Chemicals Policy: Rebuilding the Foundation to Advance New Science, Green Chemistry, and Environmental Health. *Environmental Health Perspectives* **2009**, *117* (8), 1202–1209. https://doi.org/10.1289/ehp.0800404.

(2) Weiss, M.; Haufe, J.; Carus, M.; Brandão, M.; Bringezu, S.; Hermann, B.; Patel, M. K. A Review of the Environmental Impacts of Biobased Materials. *Journal of Industrial Ecology* **2012**, *16*, S169–S181. https://doi.org/10.1111/j.1530-9290.2012.00468.x.

(3) Ferreira-Filipe, D. A.; Paço, A.; Duarte, A. C.; Rocha-Santos, T.; Patrício Silva, A. L. Are Biobased Plastics Green Alternatives?—A Critical Review. *IJERPH* **2021**, *18* (15), 7729. https://doi.org/10.3390/ijerph18157729.

(4) Fadlallah, S.; Sinha Roy, P.; Garnier, G.; Saito, K.; Allais, F. Are Lignin-Derived Monomers and Polymers Truly Sustainable? An in-Depth Green Metrics Calculations Approach. *Green Chem.* **2021**, *23* (4), 1495–1535. https://doi.org/10.1039/D0GC03982A.

(5) United Nations. *Take Action for the Sustainable Development Goals*. United Nations Sustainable Development. https://www.un.org/sustainabledevelopment/sustainable-development-goals/ (accessed 2022-10-24).

(6) Van Schoubroeck, S.; Van Dael, M.; Van Passel, S.; Malina, R. A Review of Sustainability Indicators for Biobased Chemicals. *Renewable and Sustainable Energy Reviews* **2018**, *94*, 115–126. https://doi.org/10.1016/j.rser.2018.06.007.
(7) Mann, G. S.; Singh, L. P.; Kumar, P.; Singh, S. Green Composites: A Review of Processing Technologies and Recent Applications. *Journal of Thermoplastic Composite Materials* **2020**, *33* (8), 1145–1171. https://doi.org/10.1177/0892705718816354.
(8) OECD. *Bio-based Economy*. Organisation for Economic Co-operation and Development. https://www.oecd.org/sti/emerging-tech/bio-basedeconomy.htm (accessed 2022-10-24).
(9) Diep, N. Q.; Sakanishi, K.; Nakagoshi, N.; Fujimoto, S.; Minowa, T.; Tran, X. D. Biorefinery : Concepts, Current Status, and Development Trends. *International Journal of Biomass and Renewables* **2012**, *1* (2), 1–8.
(10) Blair, M. J.; Mabee, W. E. Techno-economic and Market Analysis of Two Emerging Forest Biorefining Technologies. *Biofuels, Bioprod. Bioref.* **2021**, *15* (5), 1301–1317. https://doi.org/10.1002/bbb.2218.
(11) Annevelink, B.; Chavez, L. G.; van Ree, R.; Gursel, I. V. Global Biorefinery Status Report 2022. *IEA Bioenergy Task 42 Biorefining in a circular economy*, 94.
(12) Yoo, H. Y.; Kim, S. W. The Next-Generation Biomass for Biorefining. *BioRes.* **2021**, *16* (2), 2188–2199.
(13) Arpit Singh, T.; Sharma, M.; Sharma, M.; Dutt Sharma, G.; Kumar Passari, A.; Bhasin, S. Valorization of Agro-Industrial Residues for Production of Commercial Biorefinery Products. *Fuel* **2022**, *322*, 124284. https://doi.org/10.1016/j.fuel.2022.124284.
(14) Matharu, A. S.; de Melo, E. M.; Houghton, J. A. Opportunity for High Value-Added Chemicals from Food Supply Chain Wastes. *Bioresource Technology* **2016**, *215*, 123–130. https://doi.org/10.1016/j.biortech.2016.03.039.
(15) Gajula, S.; Reddy, C. R. K. More Sustainable Biomass Production and Biorefining to Boost the Bioeconomy. *Biofuels, Bioprod. Bioref.* **2021**, *15* (5), 1221–1232. https://doi.org/10.1002/bbb.2227.
(16) Clark, J. H.; Luque, R.; Matharu, A. S. Green Chemistry, Biofuels, and Biorefinery. *Annu. Rev. Chem. Biomol. Eng.* **2012**, *3* (1), 183–207. https://doi.org/10.1146/annurev-chembioeng-062011-081014.
(17) Heo, J. B.; Yun, H. R.; Lee, Y.-S.; Chung, C.-H. Strategic Biomodification for Raw Plant-Based Pretreatment Biorefining toward Sustainable Chemistry. *Critical Reviews in Biotechnology* **2022**, 1–14. https://doi.org/10.1080/07388551.2022.2092715.
(18) Baranwal, J.; Barse, B.; Fais, A.; Delogu, G. L.; Kumar, A. Biopolymer: A Sustainable Material for Food and Medical Applications. *Polymers* **2022**, *14* (5), 983. https://doi.org/10.3390/polym14050983.
(19) Demuner, I. F.; Colodette, J. L.; Demuner, A. J.; Jardim, C. M. Biorefinery Review: Wide-Reaching Products Through Kraft Lignin. *BioResources* **2019**, *14* (3), 7543–7581.
(20) Liu, Q.; Luo, L.; Zheng, L. Lignins: Biosynthesis and Biological Functions in Plants. *International Journal of Molecular Sciences* **2018**, *19* (2), 335. https://doi.org/10.3390/ijms19020335.
(21) Haile, A.; Gelebo, G. G.; Tesfaye, T.; Mengie, W.; Mebrate, M. A.; Abuhay, A.; Limeneh, D. Y. Pulp and Paper Mill Wastes: Utilizations and Prospects for High Value-Added Biomaterials. *Bioresour. Bioprocess.* **2021**, *8* (1), 35. https://doi.org/10.1186/s40643-021-00385-3.

(22) Katahira, R.; Elder, T. J.; Beckham, G. T. Chapter 1. A Brief Introduction to Lignin Structure. In *Energy and Environment Series*; Beckham, G. T., Ed.; Royal Society of Chemistry: Cambridge, 2018; pp 1–20. https://doi.org/10.1039/9781788010351-00001.
(23) Mariana, M.; Alfatah, T.; H.P.S., A. K.; Yahya, E. B.; Olaiya, N. G.; Nuryawan, A.; Mistar, E. M.; Abdullah, C. K.; Abdulmadjid, S. N.; Ismail, H. A Current Advancement on the Role of Lignin as Sustainable Reinforcement Material in Biopolymeric Blends. *Journal of Materials Research and Technology* **2021**, *15*, 2287–2316. https://doi.org/10.1016/j.jmrt.2021.08.139.
(24) Moretti, C.; Corona, B.; Hoefnagels, R.; Vural-Gürsel, I.; Gosselink, R.; Junginger, M. Review of Life Cycle Assessments of Lignin and Derived Products: Lessons Learned. *Science of The Total Environment* **2021**, *770*, 144656. https://doi.org/10.1016/j.scitotenv.2020.144656.
(25) Al-Douri, Y. Fabrication and Analysis of Starch-Based Green Materials. In *Nanoparticles in Analytical and Medical Devices*; Elsevier, 2021; pp 301–318. https://doi.org/10.1016/B978-0-12-821163-2.00020-0.
(26) Le Corre, D.; Bras, J.; Dufresne, A. Starch Nanoparticles: A Review. *Biomacromolecules* **2010**, *11* (5), 1139–1153. https://doi.org/10.1021/bm901428y.
(27) Salehizadeh, H.; Yan, N.; Farnood, R. Recent Advances in Polysaccharide Bio-Based Flocculants. *Biotechnology Advances* **2018**, *36* (1), 92–119. https://doi.org/10.1016/j.biotechadv.2017.10.002.
(28) Falua, K. J.; Pokharel, A.; Babaei-Ghazvini, A.; Ai, Y.; Acharya, B. Valorization of Starch to Biobased Materials: A Review. *Polymers* **2022**, *14* (11), 2215. https://doi.org/10.3390/polym14112215.
(29) Balakshin, M. Yu.; Capanema, E. A.; Sulaeva, I.; Schlee, P.; Huang, Z.; Feng, M.; Borghei, M.; Rojas, O. J.; Potthast, A.; Rosenau, T. New Opportunities in the Valorization of Technical Lignins. *ChemSusChem* **2021**, *14* (4), 1016–1036. https://doi.org/10.1002/cssc.202002553.
(30) Zha, D.; Guo, B.; Li, B.; Yin, P.; Li, P. Chemical and Physical Mechanism of Water Resistance for Thermoplastic Starch. *Prog. Chem.* **2019**, *31* (1), 156–166. https://doi.org/10.7536/PC180309.
(31) Ragauskas, A. J.; Beckham, G. T.; Biddy, M. J.; Chandra, R.; Chen, F.; Davis, M. F.; Davison, B. H.; Dixon, R. A.; Gilna, P.; Keller, M.; Langan, P.; Naskar, A. K.; Saddler, J. N.; Tschaplinski, T. J.; Tuskan, G. A.; Wyman, C. E. Lignin Valorization: Improving Lignin Processing in the Biorefinery. *Science* **2014**, *344* (6185), 1246843–1246843. https://doi.org/10.1126/science.1246843.
(32) Laurichesse, S.; Avérous, L. Chemical Modification of Lignins: Towards Biobased Polymers. *Progress in Polymer Science* **2014**, *39* (7), 1266–1290. https://doi.org/10.1016/j.progpolymsci.2013.11.004.
(33) Suota, M. J.; Kochepka, D. M.; Ganter Moura, M. G.; Pirich, C. L.; Matos, M.; Magalhães, W. L. E.; Ramos, L. P. Lignin Functionalization Strategies and the Potential Applications of Its Derivatives – A Review. *BioRes* **2021**, *16* (3), 6471–6511. https://doi.org/10.15376/biores.16.3.Suota.
(34) Souto, F.; Calado, V.; Pereira, N. Lignin-Based Carbon Fiber: A Current Overview. *Mater. Res. Express* **2018**, *5* (7), 072001. https://doi.org/10.1088/2053-1591/aaba00.
(35) Gonçalves, G. C.; Gimeno, F.; Dicharry, C.; Allouche, J.; Charrier-El Bouhtoury, F.; Dupin, J.-C. Design of Sol–Gel Hybrid Bio-Sourced Lignin/Silica Hydrophobic Nanocomposites

through a Dip-Coated Evaporation-Induced Self-Assembly Method. *ACS Sustainable Chem. Eng.* **2022**, *10* (38), 12783–12795. https://doi.org/10.1021/acssuschemeng.2c03770.

(36) Ang, A. F.; Ashaari, Z.; Lee, S. H.; Md Tahir, P.; Halis, R. Lignin-Based Copolymer Adhesives for Composite Wood Panels – A Review. *International Journal of Adhesion and Adhesives* **2019**, *95*, 102408. https://doi.org/10.1016/j.ijadhadh.2019.102408.

(37) Van Nieuwenhove, I.; Renders, T.; Lauwaert, J.; De Roo, T.; De Clercq, J.; Verberckmoes, A. Biobased Resins Using Lignin and Glyoxal. *ACS Sustainable Chem. Eng.* **2020**, *8* (51), 18789–18809. https://doi.org/10.1021/acssuschemeng.0c07227.

(38) Jeong, H.; Park, J.; Kim, S.; Lee, J.; Cho, J. W. Use of Acetylated Softwood Kraft Lignin as Filler in Synthetic Polymers. *Fibers Polym* **2012**, *13* (10), 1310–1318. https://doi.org/10.1007/s12221-012-1310-6.

(39) Wang, B.; Wang, S.-F.; Lam, S. S.; Sonne, C.; Yuan, T.-Q.; Song, G.-Y.; Sun, R.-C. A Review on Production of Lignin-Based FLocculants: Sustainable Feedstock and Low Carbon Footprint Applications. *Renewable Sustainable Energy Rev.* **2020**, *134*, 110384. https://doi.org/10.1016/j.rser.2020.110384.

(40) Zhu, W.; Chen, F.; He, T. Preparation of Lignin-Based Dye Dispersant with Favorable Heat Stability and Slight Fiber Staining. *J. Dispersion Sci. Technol.* https://doi.org/10.1080/01932691.2021.1924188.

(41) The European Starch Industry Association. *EU starch market data*. Starch Europe. https://www.starch.eu/the-european-starch-industry/ (accessed 2019-03-13).

(42) Yang, Z.; McClements, D. J.; Xu, Z.; Meng, M.; Li, C.; Chen, L.; Qiu, C.; Long, J.; Jin, Z. Carbohydrate-Based Functional Ingredients Derived from Starch: Current Status and Future Prospects. *Food Hydrocolloids* **2022**, *131*, 107729. https://doi.org/10.1016/j.foodhyd.2022.107729.

(43) Lermen, F. H.; de Souza Matias, G.; Bissaro, C. A.; Ribeiro, J. L. D.; Gonçalves, K. Y.; Matos, C.; Filho, N. A.; de Matos Jorge, L. M.; Coelho, T. M. The Characteristics and Industrial Applications of Natural and Hydrophobic Modified Starch. *Starch Stärke* **2022**, 2200022. https://doi.org/10.1002/star.202200022.

(44) Chen, L.; Xiong, Z.; Li, Q.; Din, Z.; Xiong, H. Sodium Dodecyl Sulfate Improves the Properties of Bio-Based Wood Adhesive Derived from Micronized Starch: Microstructure and Rheological Behaviors. *International Journal of Biological Macromolecules* **2019**, *140*, 1026–1036. https://doi.org/10.1016/j.ijbiomac.2019.08.167.

(45) Liu, Z.; Wei, H.; Li, A.; Yang, H. Evaluation of Structural Effects on the Flocculation Performance of a Co-Graft Starch-Based Flocculant. *Water Research* **2017**, *118*, 160–166. https://doi.org/10.1016/j.watres.2017.04.032.

(46) Zhu, J.; Zhang, G.; Li, J.; Zhao, F. Synthesis, Adsorption and Dispersion of a Dispersant Based on Starch for Coal–Water Slurry. *Colloids and Surfaces A: Physicochemical and Engineering Aspects* **2013**, *422*, 165–171. https://doi.org/10.1016/j.colsurfa.2013.01.033.

(47) Tang, J.; Zou, F.; Guo, L.; Wang, N.; Zhang, H.; Cui, B.; Liu, X. The Relationship between Linear Chain Length Distributions of Amylopectin and the Functional Properties of the Debranched Starch-Based Films. *Carbohydrate Polymers* **2022**, *279*, 119012. https://doi.org/10.1016/j.carbpol.2021.119012.

(48) Ma, C.; Xie, F.; Wei, L.; Zheng, C.; Liu, X.; Wang, L.; Liu, P. All-Starch-Based Hydrogel for Flexible Electronics: Strain-Sensitive Batteries and Self-Powered Sensors. *ACS Sustainable Chem. Eng.* **2022**, *10* (20), 6724–6735. https://doi.org/10.1021/acssuschemeng.2c00872.

(49) Tapia-Blácido, D. R.; Aguilar, G. J.; de Andrade, M. T.; Rodrigues-Júnior, M. F.; Guareschi-Martins, F. C. Trends and Challenges of Starch-Based Foams for Use as Food Packaging and Food Container. *Trends in Food Science & Technology* **2022**, *119*, 257–271. https://doi.org/10.1016/j.tifs.2021.12.005.

(50) Gall, D. L.; Ralph, J.; Donohue, T. J.; Noguera, D. R. Biochemical Transformation of Lignin for Deriving Valued Commodities from Lignocellulose. *Current Opinion in Biotechnology* **2017**, *45*, 120–126. https://doi.org/10.1016/j.copbio.2017.02.015.

(51) Labeeuw, L.; Martone, P. T.; Boucher, Y.; Case, R. J. Ancient Origin of the Biosynthesis of Lignin Precursors. *Biology Direct* **2015**, *10* (1), 23. https://doi.org/10.1186/s13062-015-0052-y.

(52) Boeriu, C. G.; Bravo, D.; Gosselink, R. J. A.; van Dam, J. E. G. Characterisation of Structure-Dependent Functional Properties of Lignin with Infrared Spectroscopy. *Industrial Crops and Products* **2004**, *20* (2), 205–218. https://doi.org/10.1016/j.indcrop.2004.04.022.

(53) *Lignin: Historical, Biological, and Materials Perspectives*; Glasser, W. G., Northey, R. A., Schultz, T. P., Eds.; ACS Symposium Series; American Chemical Society: Washington, DC, 1999; Vol. 742. https://doi.org/10.1021/bk-2000-0742.

(54) Langan, P.; Petridis, L.; O'Neill, H. M.; Pingali, S. V.; Foston, M.; Nishiyama, Y.; Schulz, R.; Lindner, B.; Hanson, B. L.; Harton, S.; Heller, W. T.; Urban, V.; Evans, B. R.; Gnanakaran, S.; Ragauskas, A. J.; Smith, J. C.; Davison, B. H. Common Processes Drive the Thermochemical Pretreatment of Lignocellulosic Biomass. *Green Chem.* **2013**, *16* (1), 63–68. https://doi.org/10.1039/C3GC41962B.

(55) Meng, X.; Crestini, C.; Ben, H.; Hao, N.; Pu, Y.; Ragauskas, A. J.; Argyropoulos, D. S. Determination of Hydroxyl Groups in Biorefinery Resources via Quantitative 31P NMR Spectroscopy. *Nat. Protoc.* **2019**, *14* (9), 2627–2647. https://doi.org/10.1038/s41596-019-0191-1.

(56) Hatakeyama, H.; Hatakeyama, T. Lignin Structure, Properties, and Applications. In *Biopolymers: Lignin, Proteins, Bioactive Nanocomposites*; Abe, A., Dusek, K., Kobayashi, S., Eds.; Advances in Polymer Science; Springer: Berlin, Heidelberg, 2010; pp 1–63. https://doi.org/10.1007/12_2009_12.

(57) Roopan, S. M. An Overview of Natural Renewable Bio-Polymer Lignin towards Nano and Biotechnological Applications. *International Journal of Biological Macromolecules* **2017**, *103*, 508–514. https://doi.org/10.1016/j.ijbiomac.2017.05.103.

(58) Ghavidel, N.; Konduri, M. K. R.; Fatehi, P. Chemical Reactivity and Sulfo-Functionalization Response of Enzymatically Produced Lignin. *Ind. Crops. Prod.* **2021**, *172*, 113950. https://doi.org/10.1016/j.indcrop.2021.113950.

(59) Tolbert, A.; Akinosho, H.; Khunsupat, R.; Naskar, A. K.; Ragauskas, A. J. Characterization and Analysis of the Molecular Weight of Lignin for Biorefining Studies. *Biofuels, Bioprod. Biorefin.* **2014**, *8* (6), 836–856. https://doi.org/10.1002/bbb.1500.

(60) Schutyser, W.; Renders, T.; Van den Bosch, S.; Koelewijn, S.-F.; Beckham, G. T.; Sels, B. F. Chemicals from Lignin: An Interplay of Lignocellulose Fractionation, Depolymerisation, and Upgrading. *Chemical Society Reviews* **2018**, *47* (3), 852–908. https://doi.org/10.1039/C7CS00566K.

(61) Chen, H. 3 - Lignocellulose Biorefinery Feedstock Engineering. In *Lignocellulose Biorefinery Engineering*; Chen, H., Ed.; Woodhead Publishing, 2015; pp 37–86. https://doi.org/10.1016/B978-0-08-100135-6.00003-X.

(62) Brännvall, E. The Limits of Delignification in Kraft Cooking. *Bioresources* **2017**, *12* (1), 2081–2107. https://doi.org/10.15376/biores.12.1.Brannvall.
(63) Bajpai, P. Biorefinery Opportunities in the Pulp and Paper Industry. In *Biorefinery in the Pulp and Paper Industry*; Elsevier, 2013; pp 11–15. https://doi.org/10.1016/B978-0-12-409508-3.00002-X.
(64) Constant, S.; Wienk, H. L. J.; Frissen, A. E.; Peinder, P. de; Boelens, R.; van Es, D. S.; Grisel, R. J. H.; Weckhuysen, B. M.; Huijgen, W. J. J.; Gosselink, R. J. A.; Bruijnincx, P. C. A. New Insights into the Structure and Composition of Technical Lignins: A Comparative Characterisation Study. *Green Chem.* **2016**, *18* (9), 2651–2665. https://doi.org/10.1039/C5GC03043A.
(65) Gordobil, O.; Moriana, R.; Zhang, L.; Labidi, J.; Sevastyanova, O. Assesment of Technical Lignins for Uses in Biofuels and Biomaterials: Structure-Related Properties, Proximate Analysis and Chemical Modification. *Industrial Crops and Products* **2016**, *83*, 155–165. https://doi.org/10.1016/j.indcrop.2015.12.048.
(66) Dessbesell, L.; Paleologou, M.; Leitch, M.; Pulkki, R.; Xu, C. (Charles). Global Lignin Supply Overview and Kraft Lignin Potential as an Alternative for Petroleum-Based Polymers. *Renewable Sustainable Energy Rev.* **2020**, *123*, 109768. https://doi.org/10.1016/j.rser.2020.109768.
(67) Kouisni, L.; Gagné, A.; Maki, K.; Holt-Hindle, P.; Paleologou, M. LignoForce System for the Recovery of Lignin from Black Liquor: Feedstock Options, Odor Profile, and Product Characterization. *ACS Sustainable Chem. Eng.* **2016**, *4* (10), 5152–5159. https://doi.org/10.1021/acssuschemeng.6b00907.
(68) Öhman, F.; Theliander, H.; Tomani, P.; Axegard, P. Method for Separating Lignin from Black Liquor. US8486224B2, July 16, 2013. https://patents.google.com/patent/US8486224B2/en (accessed 2020-05-22).
(69) Brazil, T. R.; Costa, R. N.; Massi, M.; Rezende, M. C. Structural, Morphological, and Thermal Characterization of Kraft Lignin and Its Charcoals Obtained at Different Heating Rates. *Materials Research Express* **2018**, *5* (4), 045502. https://doi.org/10.1088/2053-1591/aab7c2.
(70) Alekhina, M.; Ershova, O.; Ebert, A.; Heikkinen, S.; Sixta, H. Softwood Kraft Lignin for Value-Added Applications: Fractionation and Structural Characterization. *Industrial Crops and Products* **2015**, *66*, 220–228. https://doi.org/10.1016/j.indcrop.2014.12.021.
(71) Aro, T.; Fatehi, P. Production and Application of Lignosulfonates and Sulfonated Lignin. *ChemSusChem* **2017**, *10* (9), 1861–1877. https://doi.org/10.1002/cssc.201700082.
(72) Qin, Y.; Yu, L.; Wu, R.; Yang, D.; Qiu, X.; Zhu, J. Y. Biorefinery Lignosulfonates from Sulfite-Pretreated Softwoods as Dispersant for Graphite. *ACS Sustainable Chem. Eng.* **2016**, *4* (4), 2200–2205. https://doi.org/10.1021/acssuschemeng.5b01664.
(73) Ekeberg, D.; Gretland, K. S.; Gustafsson, J.; Bråten, S. M.; Fredheim, G. E. Characterisation of Lignosulphonates and Kraft Lignin by Hydrophobic Interaction Chromatography. *Anal. Chim. Acta* **2006**, *565* (1), 121–128. https://doi.org/10.1016/j.aca.2006.02.008.
(74) Li, X.; Wu, S. Chemical Structure and Pyrolysis Characteristics of the Soda-Alkali Lignin Fractions. *Bioresources* **2014**, *9* (4), 6277–6289. https://doi.org/10.15376/biores.9.4.6277-6289.
(75) Mousavioun, P.; Doherty, W. O. S. Chemical and Thermal Properties of Fractionated Bagasse Soda Lignin. *Industrial Crops and Products* **2010**, *31* (1), 52–58. https://doi.org/10.1016/j.indcrop.2009.09.001.

(76) Rossberg, C.; Janzon, R.; Saake, B.; Leschinsky, M. Effect of Process Parameters in Pilot Scale Operation on Properties of Organosolv Lignin. *Bioresources* **2019**, *14* (2), 4543–4559. https://doi.org/DOI: 10.15376/biores.14.2.4543-4559.

(77) Singh, S. K.; Dhepe, P. L. Isolation of Lignin by Organosolv Process from Different Varieties of Rice Husk: Understanding Their Physical and Chemical Properties. *Bioresour. Technol.* **2016**, *221*, 310–317. https://doi.org/10.1016/j.biortech.2016.09.042.

(78) Trubetskaya, A.; Lange, H.; Wittgens, B.; Brunsvik, A.; Crestini, C.; Rova, U.; Christakopoulos, P.; Leahy, J. J.; Matsakas, L. Structural and Thermal Characterization of Novel Organosolv Lignins from Wood and Herbaceous Sources. *Processes* **2020**, *8* (7), 860. https://doi.org/10.3390/pr8070860.

(79) Sadeghifar, H.; Wells, T.; Le, R. K.; Sadeghifar, F.; Yuan, J. S.; Jonas Ragauskas, A. Fractionation of Organosolv Lignin Using Acetone:Water and Properties of the Obtained Fractions. *ACS Sustainable Chem. Eng.* **2017**, *5* (1), 580–587. https://doi.org/10.1021/acssuschemeng.6b01955.

(80) Kautto, J.; Realff, M. J.; Ragauskas, A. J.; Kässi, T. Economic Analysis of an Organosolv Process for Bioethanol Production. *BioResources* **2014**, *9* (4), 6041–6072. https://doi.org/10.15376/biores.9.4.6041-6072.

(81) *Lignin Market By Product Type (Lignosulfonate, Kraft Lignin), By Application (Concrete Admixture, Animal Feed Binders, Dye Stuff), By Region - Global Forecast 2020-2030*. Fact.MR. https://www.factmr.com/report/4660/lignin-market (accessed 2022-09-09).

(82) *Lignin Market Size, Share & Trends Report 2022- 2028*. Global Market Insights Inc. https://www.gminsights.com/industry-analysis/lignin-market (accessed 2022-09-09).

(83) Petridis, L.; Smith, J. C. Molecular-Level Driving Forces in Lignocellulosic Biomass Deconstruction for Bioenergy. *Nat Rev Chem* **2018**, *2* (11), 382–389. https://doi.org/10.1038/s41570-018-0050-6.

(84) Konduri, M. K.; Kong, F.; Fatehi, P. Production of Carboxymethylated Lignin and Its Application as a Dispersant. *European Polymer Journal* **2015**, *70*, 371–383. https://doi.org/10.1016/j.eurpolymj.2015.07.028.

(85) Christopher, L. Integrated Forest Biorefineries: Current State and Development Potential. In *Integrated forest biorefineries: challenges and opportunities*; Royal Society of Chemistry: Cambridge, 2013; pp 1–66.

(86) Lizundia, E.; Sipponen, M. H.; Greca, L. G.; Balakshin, M.; Tardy, B. L.; Rojas, O. J.; Puglia, D. Multifunctional Lignin-Based Nanocomposites and Nanohybrids. *Green Chem.* **2021**, *23* (18), 6698–6760. https://doi.org/10.1039/d1gc01684a.

(87) Figueiredo, P.; Lintinen, K.; Hirvonen, J. T.; Kostiainen, M. A.; Santos, H. A. Properties and Chemical Modifications of Lignin: Towards Lignin-Based Nanomaterials for Biomedical Applications. *Progress in Materials Science* **2018**, *93*, 233–269. https://doi.org/10.1016/j.pmatsci.2017.12.001.

(88) Kai, D.; Tan, M. J.; Chee, P. L.; Chua, Y. K.; Yap, Y. L.; Loh, X. J. Towards Lignin-Based Functional Materials in a Sustainable World. *Green Chemistry* **2016**, *18* (5), 1175–1200. https://doi.org/10.1039/C5GC02616D.

(89) Nadányi, R.; Ház, A.; Lisý, A.; Jablonský, M.; Šurina, I.; Majová, V.; Baco, A. Lignin Modifications, Applications, and Possible Market Prices. *Energies* **2022**, *15* (18), 6520. https://doi.org/10.3390/en15186520.

(90) He, W.; Zhang, Y.; Fatehi, P. Sulfomethylated Kraft Lignin as a Flocculant for Cationic Dye. *Colloids and Surfaces A: Physicochemical and Engineering Aspects* **2016**, *503*, 19–27. https://doi.org/10.1016/j.colsurfa.2016.05.009.
(91) He, W.; Fatehi, P. Preparation of Sulfomethylated Softwood Kraft Lignin as a Dispersant for Cement Admixture. *RSC Advances* **2015**, *5* (58), 47031–47039. https://doi.org/10.1039/C5RA04526F.
(92) Qin, G.; Liu, Y.; Yin, F.; Hu, X.; Zhu, N.; Guo, K. Grafting Modification of Lignin via Ring-Opening Polymerization. *Prog. Chem.* **2020**, *32* (10), 1547–1556. https://doi.org/10.7536/PC200225.
(93) Zhai, J.; Hu, X.; Liu, C.; Zhu, N.; Guo, K. Grafting Modification of Lignin via Atom Transfer Radical Polymerization. *Prog. Chem.* **2019**, *31* (9), 1293–1302. https://doi.org/10.7536/PC190106.
(94) Bahrpaima, K.; Fatehi, P. Synthesis and Characterization of Carboxyethylated Lignosulfonate. *ChemSusChem* **2018**, *11* (17), 2967–2980. https://doi.org/10.1002/cssc.201800994.
(95) Gao, W.; Inwood, J. P. W.; Fatehi, P. Sulfonation of Phenolated Kraft Lignin to Produce Water Soluble Products. *Journal of Wood Chemistry and Technology* **2019**, *39* (4), 225–241. https://doi.org/10.1080/02773813.2019.1565866.
(96) Gan, L.; Zhou, M.; Yang, D.; Qiu, X. Preparation and Evaluation of Carboxymethylated Lignin as Dispersant for Aqueous Graphite Suspension Using Turbiscan Lab Analyzer. *Journal of Dispersion Science and Technology* **2013**, *34* (5), 644–650. https://doi.org/10.1080/01932691.2012.686248.
(97) Kajihara, M.; Aoki, D.; Matsushita, Y.; Fukushima, K. Synthesis and Characterization of Lignin-Based Cationic Dye-Flocculant: Research Article. *J. Appl. Polym. Sci.* **2018**, *135* (32), 46611. https://doi.org/10.1002/app.46611.
(98) Du, X.; Li, J.; Lindström, M. E. Modification of Industrial Softwood Kraft Lignin Using Mannich Reaction with and without Phenolation Pretreatment. *Industrial Crops and Products* **2014**, *52*, 729–735. https://doi.org/10.1016/j.indcrop.2013.11.035.
(99) Eraghi Kazzaz, A.; Fatehi, P. Fabrication of Amphoteric Lignin and Its Hydrophilicity/Oleophilicity at Oil/Water Interface. *Journal of Colloid and Interface Science* **2020**, *561*, 231–243. https://doi.org/10.1016/j.jcis.2019.11.111.
(100) Eraghi Kazzaz, A.; Hosseinpour Feizi, Z.; Fatehi, P. Grafting Strategies for Hydroxy Groups of Lignin for Producing Materials. *Green Chemistry* **2019**, *21* (21), 5714–5752. https://doi.org/10.1039/C9GC02598G.
(101) Lin, X.; Zhou, M.; Wang, S.; Lou, H.; Yang, D.; Qiu, X. Synthesis, Structure, and Dispersion Property of a Novel Lignin-Based Polyoxyethylene Ether from Kraft Lignin and Poly(Ethylene Glycol). *ACS Sustainable Chem. Eng.* **2014**, *2* (7), 1902–1909. https://doi.org/10.1021/sc500241g.
(102) Zhang, N.; Zhao, M.; Liu, G.; Wang, J.; Chen, Y.; Zhang, Z. Alkylated Lignin with Graft Copolymerization for Enhancing Toughness of PLA. *J Mater Sci* **2022**, *57* (19), 8687–8700. https://doi.org/10.1007/s10853-022-07101-2.
(103) Ganewatta, M. S.; Lokupitiya, H. N.; Tang, C. Lignin Biopolymers in the Age of Controlled Polymerization. *Polymers* **2019**, *11* (7), 1176. https://doi.org/10.3390/polym11071176.
(104) Wang, S.; Kong, F.; Gao, W.; Fatehi, P. Novel Process for Generating Cationic Lignin Based Flocculant. *Ind. Eng. Chem. Res.* **2018**, *57* (19), 6595–6608. https://doi.org/10.1021/acs.iecr.7b05381.

(105) Hasan, A.; Fatehi, P. Flocculation of Kaolin Particles with Cationic Lignin Polymers. *Sci. Rep.* **2019**, *9* (1). https://doi.org/10.1038/s41598-019-39135-z.
(106) Moore, C.; Gao, W.; Fatehi, P. Cationic Lignin Polymers as Flocculant for Municipal Wastewater. *Polymers* **2021**, *13* (22), 3871. https://doi.org/10.3390/polym13223871.
(107) Sabaghi, S.; Fatehi, P. Phenomenological Changes in Lignin Following Polymerization and Its Effects on Flocculating Clay Particles. *Biomacromolecules* **2019**, *20* (10), 3940–3951. https://doi.org/10.1021/acs.biomac.9b01016.
(108) Matyjaszewski, K.; Xia, J. Atom Transfer Radical Polymerization. *Chem. Rev.* **2001**, *101* (9), 2921–2990. https://doi.org/10.1021/cr940534g.
(109) Liu, H.; Chung, H. Lignin-Based Polymers via Graft Copolymerization. *J. Polym. Sci., Part A: Polym. Chem.* **2017**, *55* (21), 3515–3528. https://doi.org/10.1002/pola.28744.
(110) Hatton, F. L. Recent Advances in RAFT Polymerization of Monomers Derived from Renewable Resources. *Polym. Chem.* **2020**, *11* (2), 220–229. https://doi.org/10.1039/C9PY01128E.
(111) Gupta, C.; Washburn, N. R. Polymer-Grafted Lignin Surfactants Prepared via Reversible Addition–Fragmentation Chain-Transfer Polymerization. *Langmuir* **2014**, *30* (31), 9303–9312. https://doi.org/10.1021/la501696y.
(112) Li, M.; Pu, Y.; Chen, F.; Ragauskas, A. J. Synthesis and Characterization of Lignin-Grafted-Poly(ε-Caprolactone) from Different Biomass Sources. *New Biotechnology* **2021**, *60*, 189–199. https://doi.org/10.1016/j.nbt.2020.10.005.
(113) Perez-Arce, J.; Centeno-Pedrazo, A.; Labidi, J.; Ochoa-Gomez, J. R.; Garcia-Suarez, E. J. Lignin-Based Polyols with Controlled Microstructure by Cationic Ring Opening Polymerization. *Polymers* **2021**, *13* (4), 651. https://doi.org/10.3390/polym13040651.
(114) Parit, M.; Jiang, Z. Towards Lignin Derived Thermoplastic Polymers. *International Journal of Biological Macromolecules* **2020**, *165*, 3180–3197. https://doi.org/10.1016/j.ijbiomac.2020.09.173.
(115) Alipoormazandarani, N.; Fatehi, P. Adsorption Characteristics of Carboxymethylated Lignin on Rigid and Soft Surfaces Probed by Quartz Crystal Microbalance. *Langmuir* **2018**, *34* (50), 15293–15303. https://doi.org/10.1021/acs.langmuir.8b02694.
(116) Hopa, D. Y.; Fatehi, P. Using Sulfobutylated and Sulfomethylated Lignin as Dispersant for Kaolin Suspension. *Polymers* **2020**, *12* (9), 2046. https://doi.org/10.3390/polym12092046.
(117) Chen, N.; Liu, W.; Huang, J.; Qiu, X. Preparation of Octopus-like Lignin-Grafted Cationic Polyacrylamide Flocculant and Its Application for Water Flocculation. *Int. J. Biol. Macromol.* **2020**, *146*, 9–17. https://doi.org/10.1016/j.ijbiomac.2019.12.245.
(118) Xu, Y.; Li, N.; Wang, G.; Wang, C.; Chu, F. Synthesis of Lignin-Based MMA-Co-BA Hybrid Resins from Cornstalk Residue via RAFT Miniemulsion Polymerization and Their Characteristics. *Polymers* **2021**, *13* (6), 968. https://doi.org/10.3390/polym13060968.
(119) Penczek, S.; Moad, G. Glossary of Terms Related to Kinetics, Thermodynamics, and Mechanisms of Polymerization (IUPAC Recommendations 2008). *Pure and Applied Chemistry* **2008**, *80* (10), 2163–2193. https://doi.org/10.1351/pac200880102163.
(120) Popovic, A.; Rusmirovic, J.; Velickovic, Z.; Radovanovic, Z.; Ristic, M.; Pavlovic, V.; Marinkovic, A. Novel Amino-Functionalized Lignin Microspheres: High Performance Biosorbent with Enhanced Capacity for Heavy Metal Ion Removal. *International Journal of Biological Macromolecules* **2020**, *156*, 1160–1173. https://doi.org/10.1016/j.ijbiomac.2019.11.152.

(121) Ayoub, A.; Venditti, R.; Jameel, H.; Chang, H. Effect of Irradiation on the Composition and Thermal Properties of Softwood Kraft Lignin and Styrene Grafted Lignin. *Journal of Applied Polymer Science* **2014**, *131* (1). https://doi.org/10.1002/app.39743.
(122) Chile, L.; Kaser, S.; Hatzikiriakos, S.; Mehrkhodavandi, P. Synthesis and Thermorheological Analysis of Biobased Lignin-Graft-Poly(Lactide) Copolymers and Their Blends. *ACS Sustainable Chemistry & Engineering* **2018**, *6* (2), 1650–1661. https://doi.org/10.1021/acssuschemeng.7b02866.
(123) Shiyan, H.; Fang, G.; Li, S.; Liu, G.; Jiang, G. Cu(II) Ion Adsorption onto Hydroxymethylated Lignin-Chitosan Crosslinked Membrane. *BioResources* **2014**, *9* (3), 4971–4980. https://doi.org/10.15376/biores.9.3.4971-4980.
(124) Rico-García, D.; Ruiz-Rubio, L.; Pérez-Alvarez, L.; Hernández-Olmos, S. L.; Guerrero-Ramírez, G. L.; Vilas-Vilela, J. L. Lignin-Based Hydrogels: Synthesis and Applications. *Polymers* **2020**, *12* (1), 81. https://doi.org/10.3390/polym12010081.
(125) Ciolacu, D.; Oprea, A. M.; Anghel, N.; Cazacu, G.; Cazacu, M. New Cellulose–Lignin Hydrogels and Their Application in Controlled Release of Polyphenols. *Materials Science and Engineering: C* **2012**, *32* (3), 452–463. https://doi.org/10.1016/j.msec.2011.11.018.
(126) Dudeja, I.; Mankoo, R. K.; Singh, A.; Kaur, J. Development, Characterisation and Biodegradability of Rice Straw Lignin Based Sustainable Biopolymeric Films. *Int J of Food Sci Tech* **2022**, ijfs.16105. https://doi.org/10.1111/ijfs.16105.
(127) Apriyanto, A.; Compart, J.; Fettke, J. A Review of Starch, a Unique Biopolymer - Structure, Metabolism and in Planta Modifications. *Plant Science* **2022**, *318*. https://doi.org/10.1016/j.plantsci.2022.111223.
(128) Buleon, A.; Colonna, P.; Planchot, V.; Ball, S. Starch Granules: Structure and Biosynthesis. *International Journal of Biological Macromolecules* **1998**, *23* (2), 85–112. https://doi.org/10.1016/S0141-8130(98)00040-3.
(129) Bertoft, E. Understanding Starch Structure: Recent Progress. *AGRONOMY-BASEL* **2017**, *7* (3). https://doi.org/10.3390/agronomy7030056.
(130) Perez, S.; Bertoft, E. The Molecular Structures of Starch Components and Their Contribution to the Architecture of Starch Granules: A Comprehensive Review. *Starch - Stärke* **2010**, *62* (8), 389–420. https://doi.org/10.1002/star.201000013.
(131) Robyt, J. F. Starch: Structure, Properties, Chemistry, and Enzymology. In *Glycoscience: Chemistry and Chemical Biology*; Fraser-Reid, B. O., Tatsuta, K., Thiem, J., Eds.; Springer: Berlin, Heidelberg, 2008; pp 1437–1472. https://doi.org/10.1007/978-3-540-30429-6_35.
(132) Tester, R.; Karkalas, J.; Qi, X. Starch - Composition, Fine Structure and Architecture. *Journal of Cereal Science* **2004**, *39* (2), 151–165. https://doi.org/10.1016/j.jcs.2003.12.001.
(133) Luchese, C. L.; Benelli, P.; Spada, J. C.; Tessaro, I. C. Impact of the Starch Source on the Physicochemical Properties and Biodegradability of Different Starch-Based Films. *Journal of Applied Polymer Science* **2018**, *135* (33), 46564. https://doi.org/10.1002/app.46564.
(134) Zhu, F.; Xie, Q. Structure of New Zealand Sweetpotato Starch. *Carbohydrate Polymers* **2018**, *188*, 181–187. https://doi.org/10.1016/j.carbpol.2018.01.091.
(135) Van Hung, P.; Maeda, T.; Morita, N. Waxy and High-Amylose Wheat Starches and Flours—Characteristics, Functionality and Application. *Trends in Food Science & Technology* **2006**, *17* (8), 448–456. https://doi.org/10.1016/j.tifs.2005.12.006.
(136) Seung, D. Amylose in Starch: Towards an Understanding of Biosynthesis, Structure and Function. *New Phytologist* **2020**, *228* (5), 1490–1504. https://doi.org/10.1111/nph.16858.

(137) Waterschoot, J.; Gomand, S.; Fierens, E.; Delcour, J. Production, Structure, Physicochemical and Functional Properties of Maize, Cassava, Wheat, Potato and Rice Starches. *Starch - Stärke* **2015**, *67* (1–2), 14–29. https://doi.org/10.1002/star.201300238.
(138) Dong, H.; Zhang, Q.; Gao, J.; Chen, L.; Vasanthan, T. Comparison of Morphology and Rheology of Starch Nanoparticles Prepared from Pulse and Cereal Starches by Rapid Antisolvent Nanoprecipitation. *Food Hydrocolloids* **2021**, *119*, 106828. https://doi.org/10.1016/j.foodhyd.2021.106828.
(139) Shevkani, K.; Singh, N.; Bajaj, R.; Kaur, A. Wheat Starch Production, Structure, Functionality and Applications-a Review. *International Journal of Food Science and Technology* **2017**, *52* (1), 38–58. https://doi.org/10.1111/ijfs.13266.
(140) Zhu, F. Composition, Structure, Physicochemical Properties, and Modifications of Cassava Starch. *Carbohydrate Polymers* **2015**, *122*, 456–480. https://doi.org/10.1016/j.carbpol.2014.10.063.
(141) Noda, T.; Matsuura-Endo, C.; Ishiguro, K. Physicochemical Properties of Potato Starches Manufactured in Hokkaido Factories. *J Food Sci Technol* **2019**, *56* (5), 2501–2507. https://doi.org/10.1007/s13197-019-03727-4.
(142) Jacobsen, H. B.; Madsen, M. H.; Christiansen, J.; Nielsen, T. H. The Degree of Starch Phosphorylation as Influenced by Phosphate Deprivation of Potato (Solanum Tuberosum L.) Plants. *Potato Res.* **1998**, *41* (2), 109–116. https://doi.org/10.1007/BF02358433.
(143) Yang, L.; Xia, Y.; Junejo, S.; Zhou, Y. Composition, Structure and Physicochemical Properties of Three Coloured Potato Starches. *International Journal of Food Science and Technology* **2018**, *53* (10), 2325–2334. https://doi.org/10.1111/ijfs.13824.
(144) Hoover, R. Composition, Molecular Structure, and Physicochemical Properties of Tuber and Root Starches: A Review. *Carbohydrate Polymers* **2001**, *45* (3), 253–267. https://doi.org/10.1016/S0144-8617(00)00260-5.
(145) Patindol, J.; Siebenmorgen, T.; Wang, Y. Impact of Environmental Factors on Rice Starch Structure: A Review. *Starch - Stärke* **2015**, *67* (1–2), 42–54. https://doi.org/10.1002/star.201400174.
(146) Yu, S.; Ma, Y.; Menager, L.; Sun, D. Physicochemical Properties of Starch and Flour from Different Rice Cultivars. *FOOD AND BIOPROCESS TECHNOLOGY* **2012**, *5* (2), 626–637. https://doi.org/10.1007/s11947-010-0330-8.
(147) Sun, Y.; Jiao, G.; Liu, Z.; Zhang, X.; Li, J.; Guo, X.; Du, W.; Du, J.; Francis, F.; Zhao, Y.; Xia, L. Generation of High-Amylose Rice through CRISPR/Cas9-Mediated Targeted Mutagenesis of Starch Branching Enzymes. *Front Plant Sci* **2017**, *8*, 298. https://doi.org/10.3389/fpls.2017.00298.
(148) Regina, A.; Berbezy, P.; Kosar-Hashemi, B.; Li, S.; Cmiel, M.; Larroque, O.; Bird, A. R.; Swain, S. M.; Cavanagh, C.; Jobling, S. A.; Li, Z.; Morell, M. A Genetic Strategy Generating Wheat with Very High Amylose Content. *Plant Biotechnol J* **2015**, *13* (9), 1276–1286. https://doi.org/10.1111/pbi.12345.
(149) Cornejo-Ramírez, Y. I.; Martínez-Cruz, O.; Del Toro-Sánchez, C. L.; Wong-Corral, F. J.; Borboa-Flores, J.; Cinco-Moroyoqui, F. J. The Structural Characteristics of Starches and Their Functional Properties. *CyTA - Journal of Food* **2018**, *16* (1), 1003–1017. https://doi.org/10.1080/19476337.2018.1518343.
(150) Hoover, R.; Hughes, T.; Chung, H.; Liu, Q. Composition, Molecular Structure, Properties, and Modification of Pulse Starches: A Review. *Food Research International* **2010**, *43* (2), 399–413. https://doi.org/10.1016/j.foodres.2009.09.001.

(151) Sudharsan, K.; Chandra Mohan, C.; Azhagu Saravana Babu, P.; Archana, G.; Sabina, K.; Sivarajan, M.; Sukumar, M. Production and Characterization of Cellulose Reinforced Starch (CRT) Films. *International Journal of Biological Macromolecules* **2016**, *83*, 385–395. https://doi.org/10.1016/j.ijbiomac.2015.11.037.
(152) Starch Europe. *The European starch industry*. Starch Europe. https://starch.eu/the-european-starch-industry/ (accessed 2022-09-06).
(153) Adewale, P.; Yancheshmeh, M.; Lam, E. Starch Modification for Non-Food, Industrial Applications: Market Intelligence and Critical Review. *Carbohydrate Polymers* **2022**, *291*. https://doi.org/10.1016/j.carbpol.2022.119590.
(154) Masina, N.; Choonara, Y.; Kumar, P.; du Toit, L.; Govender, M.; Indermun, S.; Pillay, V. A Review of the Chemical Modification Techniques of Starch. *Carbohydrate Polymers* **2017**, *157*, 1226–1236. https://doi.org/10.1016/j.carbpol.2016.09.094.
(155) Ruhul Amin, Md.; Anannya, F. R.; Mahmud, Md. A.; Raian, S. Esterification of Starch in Search of a Biodegradable Thermoplastic Material. *J Polym Res* **2020**, *27* (1), 3. https://doi.org/10.1007/s10965-019-1983-2.
(156) Gilet, A.; Quettier, C.; Wiatz, V.; Bricout, H.; Ferreira, M.; Rousseau, C.; Monflier, E.; Tilloy, S. Unconventional Media and Technologies for Starch Etherification and Esterification. *Green Chem.* **2018**, *20* (6), 1152–1168. https://doi.org/10.1039/C7GC03135A.
(157) Ojogbo, E.; Ogunsona, E.; Mekonnen, T. Chemical and Physical Modifications of Starch for Renewable Polymeric Materials. *Material Today Sustainability* **2020**, *7–8*. https://doi.org/10.1016/j.mtsust.2019.100028.
(158) Haroon, M.; Wang, L.; Yu, H.; Abbasi, N. M.; Zain-ul-Abdin, Z.-A.; Saleem, M.; Khan, R. U.; Ullah, R. S.; Chen, Q.; Wu, J. Chemical Modification of Starch and Its Application as an Adsorbent Material. *RSC Advances* **2016**, *6* (82), 78264–78285. https://doi.org/10.1039/C6RA16795K.
(159) Noordergraaf, I.-W.; Fourie, Tori.; Raffa, P. Free-Radical Graft Polymerization onto Starch as a Tool to Tune Properties in Relation to Potential Applications. A Review. *Processes* **2018**, *6* (4), 31. https://doi.org/10.3390/pr6040031.
(160) Wang, L.; Wu, Y.; Men, Y.; Shen, J.; Liu, Z. Thermal-Sensitive Starch-g-PNIPAM Prepared by Cu(0) Catalyzed SET-LRP at Molecular Level. *RSC Adv.* **2015**, *5* (87), 70758–70765. https://doi.org/10.1039/C5RA14765D.
(161) Wang, L.; Shen, J.; Men, Y.; Wu, Y.; Peng, Q.; Wang, X.; Yang, R.; Mahmood, K.; Liu, Z. Corn Starch-Based Graft Copolymers Prepared via ATRP at the Molecular Level. *Polym. Chem.* **2015**, *6* (18), 3480–3488. https://doi.org/10.1039/C5PY00184F.
(162) Lu, D.; Xiao, C.; Sun, F. Controlled Grafting of Poly(Vinyl Acetate) onto Starch via RAFT Polymerization. *J. Appl. Polym. Sci.* **2012**, *124* (4), 3450–3455. https://doi.org/10.1002/app.35423.
(163) Xu, Q.; Wang, Q.; Liu, L. Ring-Opening Graft Polymerization OfL-Lactide onto Starch Granules in an Ionic Liquid. *J. Appl. Polym. Sci.* **2008**, *107* (4), 2704–2713. https://doi.org/10.1002/app.27341.
(164) Jyothi, A. N. Starch Graft Copolymers: Novel Applications in Industry. *Composite Interfaces* **2010**, *17* (2–3), 165–174. https://doi.org/10.1163/092764410X490581.
(165) Lele, V. V.; Kumari, S.; Niju, H. Syntheses, Characterization and Applications of Graft Copolymers of Sago Starch - A Review. *Starch - Stärke* **2018**, *70* (7–8), 1700133. https://doi.org/10.1002/star.201700133.

(166) Wang, J.-P.; Yuan, S.-J.; Wang, Y.; Yu, H.-Q. Synthesis, Characterization and Application of a Novel Starch-Based Flocculant with High Flocculation and Dewatering Properties. *Water Research* **2013**, *47* (8), 2643–2648. https://doi.org/10.1016/j.watres.2013.01.050.
(167) Meimoun, J.; Wiatz, V.; Saint-Loup, R.; Parcq, J.; Favrelle, A.; Bonnet, F.; Zinck, P. Modification of Starch by Graft Copolymerization: Starch Graft Copolymerization. *Starch/Staerke* **2018**, *70* (1–2), 1600351. https://doi.org/10.1002/star.201600351.
(168) Shah, N.; Mewada, R. K.; Mehta, T. Crosslinking of Starch and Its Effect on Viscosity Behaviour. *Reviews in Chemical Engineering* **2016**, *32* (2). https://doi.org/10.1515/revce-2015-0047.
(169) Haq, F.; Yu, H.; Wang, L.; Teng, L.; Haroon, M.; Khan, R. U.; Mehmood, S.; Bilal-Ul-Amin; Ullah, R. S.; Khan, A.; Nazir, A. Advances in Chemical Modifications of Starches and Their Applications. *Carbohydrate Research* **2019**, *476*, 12–35. https://doi.org/10.1016/j.carres.2019.02.007.
(170) You, L.; Lu, F.; Li, D.; Qiao, Z.; Yin, Y. Preparation and Flocculation Properties of Cationic Starch/Chitosan Crosslinking-Copolymer. *J. Hazard. Mater.* **2009**, *172* (1), 38–45. https://doi.org/10.1016/j.jhazmat.2009.06.120.
(171) Wang, J.; Zhai, W.; Zheng, W. Preparation of Granular Cold-Water-Soluble Corn Starch by Surface Modification with Poly(Ethylene Glycol). *Starch/Stärke* **2011**, *63* (10), 625–631. https://doi.org/10.1002/star.201100033.
(172) Riyajan, S.-A.; Sukhlaaied, W.; Keawmang, W. Preparation and Properties of a Hydrogel of Maleated Poly(Vinyl Alcohol) (PVAM) Grafted with Cassava Starch. *Carbohydrate Polymers* **2015**, *122*, 301–307. https://doi.org/10.1016/j.carbpol.2014.12.012.
(173) Chen, Q.; Gao, X.; Zhao, Y.; Liu, Z.; Xie, G.; Liang, C.; Wang, J. Starch Nanocrystals Grafted with Epichlorohydrin Dimethylamine for Methyl Blue Dye Removal. *Starch Stärke* **2022**, *74* (3–4), 2100200. https://doi.org/10.1002/star.202100200.
(174) Chalid, M.; Husnil, Y. A.; Puspitasari, S.; Cifriadi, A. Experimental and Modelling Study of the Effect of Adding Starch-Modified Natural Rubber Hybrid to the Vulcanization of Sorghum Fibers-Filled Natural Rubber. *Polymers* **2020**, *12* (12), 3017. https://doi.org/10.3390/polym12123017.
(175) Riyajan, S.-A. Chemical Modification of Poly (Vinyl Alcohol) with Starch/Natural Rubber and Its Application for the Encapsulation of Urea Fertilizer. *KGK-Kautsch. Gummi Kunstst.* **2016**, *69* (11–12), 49–54.
(176) Riyajan, S.-A.; Keawittarit, P. A Novel Natural Rubber-Graft-Cassava Starch Foam for Oil/Gasohol Absorption. *Polym. Int.* **2016**, *65* (5), 491–502. https://doi.org/10.1002/pi.5062.
(177) Riyajan, S.-A.; Sangwan, W.; Leejarkpai, T. Synthesis and Properties of a Novel Epoxidised Natural Rubber-g-Cassava Starch Polymer and Its Use as an Impact Strengthening Agent. *Plast. Rubber Compos.* **2016**, *45* (6), 277–285. https://doi.org/10.1080/14658011.2016.1186860.
(178) Han, Y.; Chen, S.; Yang, M.; Zou, H.; Zhang, Y. Inorganic Matter Modified Water-Based Copolymer Prepared by Chitosan-Starch-CMC-Na-PVAL as an Environment-Friendly Coating Material. *Carbohydr. Polym.* **2020**, *234*, 115925. https://doi.org/10.1016/j.carbpol.2020.115925.
(179) Yongsheng, M.; Lintong, W.; Yunchen, Z.; Huayu, Q. Synthesis and Application of Chitosan-Starch Graft Copolymers as Paper Strengthening Agent. In *Second International*

Papermaking and Environment Conference, Proceeding, Books a and B; Wang, L., Ni, Y., Hou, Q., Liu, Z., Eds.; China Light Industry Press: Beijing, 2008; pp 698–701.

(180) Da Roz, A. L.; Veiga-Santos, P.; Ferreira, A. M.; Ribeiro Antunes, T. C.; Leite, F. de L.; Yamaji, F. M.; Felix de Carvalho, A. J. Water Susceptibility and Mechanical Properties of Thermoplastic Starch-Pectin Blends Reactively Extruded with Edible Citric Acid. *Mater. Res.-Ibero-am. J. Mater.* **2016**, *19* (1), 138–142. https://doi.org/10.1590/1980-5373-MR-2015-0215.

(181) Soares, G. A.; de Castro, A. D.; Cury, B. S. F.; Evangelista, R. C. Blends of Cross-Linked High Amylose Starch/Pectin Loaded with Diclofenac. *Carbohydr. Polym.* **2013**, *91* (1), 135–142. https://doi.org/10.1016/j.carbpol.2012.08.014.

(182) Wang, J.; Zhai, W.; Zheng, W. Poly(Ethylene Glycol) Grafted Starch Introducing a Novel Interphase in Poly(Lactic Acid)/Poly(Ethylene Glycol)/Starch Ternary Composites. *J Polym Environ* **2012**, *20* (2), 528–539. https://doi.org/10.1007/s10924-012-0416-7.

(183) Movagharnezhad, N.; Najafi Moghadam, P. Synthesis of Methoxy Poly (Ethylene Glycol)/Starch Grafted Copolymers and Investigation of Their Drug Release Behavior. *Starch - Stärke* **2016**, *68* (3–4), 314–320. https://doi.org/10.1002/star.201400044.

(184) Wootthikanokkhan, J.; Kasemwananimit, P.; Sombatsompop, N.; Kositchaiyong, A.; Isarankura na Ayutthaya, S.; Kaabbuathong, N. Preparation of Modified Starch-Grafted Poly(Lactic Acid) and a Study on Compatibilizing Efficacy of the Copolymers in Poly(Lactic Acid)/Thermoplastic Starch Blends. *J. Appl. Polym. Sci.* **2012**, *126* (S1), E389–E396. https://doi.org/10.1002/app.36896.

(185) Das, K.; Ray, D.; Bandyopadhyay, N. R.; Gupta, A.; Sengupta, S.; Sahoo, S.; Mohanty, A.; Misra, M. Preparation and Characterization of Cross-Linked Starch/Poly(Vinyl Alcohol) Green Films with Low Moisture Absorption. *Ind. Eng. Chem. Res.* **2010**, *49* (5), 2176–2185. https://doi.org/10.1021/ie901092n.

(186) Stevens, E. S.; Klamczynski, A.; Glenn, G. M. Starch-Lignin Foams. *Express Polym. Lett.* **2010**, *4* (5), 311–320. https://doi.org/10.3144/expresspolymlett.2010.39.

(187) Li, M.; Jia, Y.; Shen, X.; Shen, T.; Tan, Z.; Zhuang, W.; Zhao, G.; Zhu, C.; Ying, H. Investigation into Lignin Modified PBAT/Thermoplastic Starch Composites: Thermal, Mechanical, Rheological and Water Absorption Properties. *Ind. Crops. Prod.* **2021**, *171*, 113916. https://doi.org/10.1016/j.indcrop.2021.113916.

(188) Wang, L.; He, J.; Wang, Q.; Zhang, J.; Feng, J. Lignin Reinforced, Water Resistant, and Biodegradable Cassava Starch/PBAT Sandwich Composite Pieces. *J. Polym. Eng.* **2021**, *41* (9), 818–826. https://doi.org/10.1515/polyeng-2021-0094.

(189) Spiridon, I.; Anghel, N. C.; Darie-Nita, R. N.; Iwańczuk, A.; Ursu, R. G.; Spiridon, I. A. New Composites Based on Starch/Ecoflex®/Biomass Wastes: Mechanical, Thermal, Morphological and Antimicrobial Properties. *Int. J. Biol. Macromol.* **2020**, *156*, 1435–1444. https://doi.org/10.1016/j.ijbiomac.2019.11.185.

(190) Kaewtatip, K.; Thongmee, J. Effect of Kraft Lignin and Esterified Lignin on the Properties of Thermoplastic Starch. *Mater. Des.* **2013**, *49*, 701–704. https://doi.org/10.1016/j.matdes.2013.02.010.

(191) Julinová, M.; Slavík, R.; Vyoralová, M.; Kalendová, A.; Alexy, P. Utilization of Waste Lignin and Hydrolysate From Chromium Tanned Waste in Blends of Hot-Melt Extruded PVA-Starch. *J. Polym. Environ.* **2018**, *26* (4), 1459–1472. https://doi.org/10.1007/s10924-017-1050-1.

(192) Janik, W.; Wojtala, A.; Pietruszka, A.; Dudek, G.; Sabura, E. Environmentally Friendly Melt-Processed Chitosan/Starch Composites Modified with PVA and Lignin. *Polymers* **2021**, *13* (16), 2685. https://doi.org/10.3390/polym13162685.
(193) Privas, E.; Leroux, F.; Navard, P. Preparation and Properties of Blends Composed of Lignosulfonated Layered Double Hydroxide/Plasticized Starch and Thermoplastics. *Carbohydr. Polym* **2013**, *96* (1), 91–100. https://doi.org/10.1016/j.carbpol.2013.03.042.
(194) Morais, L. C.; Consolin-Filho, N.; Sartori, R. A.; Cadaxo-Sobrinho, E. S.; Souza, T. M. H.; Regiani, A. M.; Curvelo, A. A. S. Thermoplastic Starch-Glycerol-Lignosulfonate Blends: Mixtures of Thermally Molded Blends Studied in a Ternary Diagram. *J. Thermoplast. Compos. Mater.* **2010**, *23* (5), 699–716. https://doi.org/10.1177/0892705709353721.
(195) Baumberger, S.; Lapierre, C.; Monties, B.; Lourdin, D.; Colonna, P. Preparation and Properties of Thermally Moulded and Cast Lignosulfonates-Starch Blends. *Ind. Crops. Prod.* **1997**, *6* (3), 253–258. https://doi.org/10.1016/S0926-6690(97)00015-0.
(196) Baumberger, S.; Lapierre, C.; Monties, B. Utilization of Pine Kraft Lignin in Starch Composites: Impact of Structural Heterogeneity. *J. Agric. Food Chem.* **1998**, *46* (6), 2234–2240. https://doi.org/10.1021/jf971067h.
(197) Lepifre, S.; Baumberger, S.; Pollet, B.; Cazaux, F.; Coqueret, X.; Lapierre, C. Reactivity of Sulphur-Free Alkali Lignins within Starch Films. *Ind. Crop. Prod.* **2004**, *20* (2), 219–230. https://doi.org/10.1016/j.indcrop.2004.04.023.
(198) Baumberger, S.; Lapierre, C.; Monties, B.; Della Valle, G. Use of Kraft Lignin as Filler for Starch Films. *Polym. Degrad. Stabil.* **1998**, *59* (1–3), 273–277. https://doi.org/10.1016/S0141-3910(97)00193-6.
(199) Çalgeris, İ.; Çakmakçı, E.; Ogan, A.; Kahraman, M. V.; Kayaman-Apohan, N. Preparation and Drug Release Properties of Lignin–Starch Biodegradable Films. *Starch - Stärke* **2012**, *64* (5), 399–407. https://doi.org/10.1002/star.201100158.
(200) Espinoza Acosta, J. L.; Torres Chávez, P. I.; Ramírez-Wong, B.; Bello-Pérez, L. A.; Vega Ríos, A.; Carvajal Millán, E.; Plascencia Jatomea, M.; Ledesma Osuna, A. I. Mechanical, Thermal, and Antioxidant Properties of Composite Films Prepared from Durum Wheat Starch and Lignin. *Starch - Stärke* **2015**, *67* (5–6), 502–511. https://doi.org/10.1002/star.201500009.
(201) Ni, S.; Bian, H.; Zhang, Y.; Fu, Y.; Liu, W.; Qin, M.; Xiao, H. Starch-Based Composite Films with Enhanced Hydrophobicity, Thermal Stability, and UV-Shielding Efficacy Induced by Lignin Nanoparticles. *Biomacromolecules* **2022**, *23* (3), 829–838. https://doi.org/10.1021/acs.biomac.1c01288.
(202) Spiridon, I.; Teaca, C.-A.; Bodirlau, R. Preparation and Characterization of Adipic Acid-Modified Starch Microparticles/Plasticized Starch Composite Films Reinforced by Lignin. *J. Mater. Sci.* **2011**, *46* (10), 3241–3251. https://doi.org/10.1007/s10853-010-5210-0.
(203) Wulandari, R.; Ratnawati. Effects of Processing Temperature and Lignin on Properties of Starch/PVA/Lignin Film Prepared by Melt Compounding. *J. Phys.: Conf. Ser.* **2019**, *1295* (1), 012058. https://doi.org/10.1088/1742-6596/1295/1/012058.
(204) de S. M. de Freitas, A.; Rodrigues, J. S.; Maciel, C. C.; Pires, A. A. F.; Lemes, A. P.; Ferreira, M.; Botaro, V. R. Improvements in Thermal and Mechanical Properties of Composites Based on Thermoplastic Starch and Kraft Lignin. *Int. J. Biol. Macromol.* **2021**, *184*, 863–873. https://doi.org/10.1016/j.ijbiomac.2021.06.153.
(205) Bhat, R.; Abdullah, N.; Din, R. H.; Tay, G.-S. Producing Novel Sago Starch Based Food Packaging Films by Incorporating Lignin Isolated from Oil Palm Black Liquor Waste.

Journal of Food Engineering **2013**, *119* (4), 707–713. https://doi.org/10.1016/j.jfoodeng.2013.06.043.

(206) Miranda, C. S.; Ferreira, M. S.; Magalhães, M. T.; Bispo, A. P. G.; Oliveira, J. C.; Silva, J. B. A.; José, N. M. Starch-Based Films Plasticized with Glycerol and Lignin from Piassava Fiber Reinforced with Nanocrystals from Eucalyptus. *Materials Today: Proceedings* **2015**, *2* (1), 134–140. https://doi.org/10.1016/j.matpr.2015.04.038.

(207) Marques de Farias, P.; Barros de Vasconcelos, L.; da Silva Ferreira, M. E.; Alves Filho, E. G.; De Freitas, V. A. A.; Tapia-Blácido, D. R. Nopal Cladode as a Novel Reinforcing and Antioxidant Agent for Starch-Based Films: A Comparison with Lignin and Propolis Extract. *International Journal of Biological Macromolecules* **2021**, *183*, 614–626. https://doi.org/10.1016/j.ijbiomac.2021.04.143.

(208) Mousavi, S. N.; Nazarnezhad, N.; Asadpour, G.; Ramamoorthy, S. K.; Zamani, A. Ultrafine Friction Grinding of Lignin for Development of Starch Biocomposite Films. *Polymers* **2021**, *13* (12), 2024. https://doi.org/10.3390/polym13122024.

(209) Javed, A.; Rättö, P.; Järnström, L.; Ullsten, H. Lignin-Containing Coatings for Packaging Materials—Pilot Trials. *Polymers* **2021**, *13* (10), 1595. https://doi.org/10.3390/polym13101595.

(210) Roostazadeh, R.; Behzad, T.; Karimi, K. Isolation and Characterization of Lignin-Rich Particles as Byproducts of Bioethanol Production from Wheat Straw to Reinforce Starch Composite Films. *Industrial Crops and Products* **2022**, *186*, 115175. https://doi.org/10.1016/j.indcrop.2022.115175.

(211) Bodirlau, R.; Teaca, C.-A.; Spiridon, I. Influence of Natural Fillers on the Properties of Starch-Based Biocomposite Films. *Composites, Part B* **2013**, *44* (1), 575–583. https://doi.org/10.1016/j.compositesb.2012.02.039.

(212) Majeed, Z.; Ramli, N.; Mansor, N.; Man, Z. Lignin Loading Effect on Biodegradability and Nitrogen Release Properties of Urea Modified Tapioca Starch in Wet Soil; Abdullah, M., Jamaludin, L., Abdullah, A., AbdRazak, R., Hussin, K., Eds.; 2014; Vol. 594–595, pp 798–802. https://doi.org/10.4028/www.scientific.net/KEM.594-595.798.

(213) Majeed, Z.; Ramli, N.; Mansor, N.; Man, Z. Starch Biodegradation in a Lignin Modified Slow Release Fertilizer: Effect of Thickness; Ahmed, I., Ed.; 2014; Vol. 625, pp 830–833. https://doi.org/10.4028/www.scientific.net/AMM.625.830.

(214) Sarwono, A.; Zakaria, M.; Mohammad Azmi, B. Improvement of Hydrophobicity of Urea Modified Tapioca Starch Film with Lignin for Slow Release Fertilizer. *Adv. Mater. Res. (Durnten-Zurich, Switz.)* **2013**, *626*, 350–354. https://doi.org/10.4028/www.scientific.net/AMR.626.350.

(215) Majeed, Z.; Mansor, N.; Man, Z.; Wahid, S. A. Lignin Reinforcement of Urea-Crosslinked Starch Films for Reduction of Starch Biodegradability to Improve Slow Nitrogen Release Properties under Natural Aerobic Soil Condition. *e-Polym.* **2016**, *16* (2), 159–170. https://doi.org/10.1515/epoly-2015-0231.

(216) Majeed, Z.; Mansor, N.; Ajab, Z.; Man, Z. Lignin Macromolecule's Implication in Slowing the Biodegradability of Urea-Crosslinked Starch Films Applied as Slow-Release Fertilizer: Lignin Macromolecule's Implication in Biodegradability of UcS Films. *Starch - Stärke* **2017**, *69* (11–12), 1600362. https://doi.org/10.1002/star.201600362.

(217) Majeed, Z.; Mansor, N.; Ajab, Z.; Man, Z.; Sarwono, A. Kraft Lignin Ameliorates Degradation Resistance of Starch in Urea Delivery Biocomposites. *Polym. Test.* **2018**, *65*, 398–406. https://doi.org/10.1016/j.polymertesting.2017.12.011.

(218) Sarwono, A.; Man, Z.; Bustam, M. A.; Subbarao, D.; Idris, A.; Muhammad, N.; Khan, A. S.; Ullah, Z. Swelling Mechanism of Urea Cross-Linked Starch-Lignin Films in Water. *Environ. Technol.* **2018**, *39* (12), 1522–1532. https://doi.org/10.1080/09593330.2017.1332108.

(219) Majeed, Z.; Ajab, Z.; Guan, Q.; Abbasi, A.; Mahmood, Q.; Mahnashi, M.; Alyami, B.; Alqarni, A.; Alqahtani, Y.; Mansor, N. Reduction in Lignin Peroxidase Activity Revealed by Effects of Lignin Content in Urea Crosslinked Starch under Aerobic Biodegradation in Soil. *BioResources* **2021**, *16* (1), 1940–1948. https://doi.org/10.15376/biores.16.1.1940-1948.

(220) Shi, R.; Li, B. Synthesis and Characterization of Cross-Linked Starch/Lignin Film. *Starch - Stärke* **2016**, *68* (11–12), 1224–1232. https://doi.org/10.1002/star.201500331.

(221) Javed, A.; Ullsten, H.; Rättö, P.; Järnström, L. Lignin-Containing Coatings for Packaging Materials. *Nord. Pulp Pap. Res. J.* **2018**, *33* (3), 548–556. https://doi.org/10.1515/npprj-2018-3042.

(222) Hagiopol, C. Copolymers. In *Reference Module in Materials Science and Materials Engineering*; Elsevier, 2016. https://doi.org/10.1016/B978-0-12-803581-8.01126-7.

(223) Sharma, S.; Dua, A.; Malik, A. Polyaspartic Acid Based Superabsorbent Polymers. *European Polymer Journal* **2014**, *59*, 363–376. https://doi.org/10.1016/j.eurpolymj.2014.07.043.

(224) Froment, M.; Gors, C.; Cazaux, F.; Coqueret, X.; Lepifre, S.; Baumberger, S.; Lapierre, C.; Linz, C.; Lacrampe, M.-F.; Krawczak, P. Reduction of Starch Hydrophilicity by Grafting Lignin Derivatives under EB Irradiation: A Study of Model Compounds. In *Starch: Achievements in Understanding of Structure and Functionality*; Yuryev, V., Tomasik, P., Bertoft, E., Eds.; Nova Science Publishers, Inc: Hauppauge, 2007; pp 167-+.

(225) Khandal, D.; Bliard, C.; Coqueret, X.; Mikus, P.-Y.; Dole, P.; Baumberger, S.; Soulestin, J.; Lacrampe, M. F. LignoStarch Tailored Modification of Starch by Radiation-Grafting of Lignin; ANR, 2012.

(226) Khandal, D.; Mikus, P.-Y.; Dole, P.; Coqueret, X. Radiation Processing of Thermoplastic Starch by Blending Aromatic Additives: Effect of Blend Composition and Radiation Parameters. *Radiation Physics and Chemistry* **2013**, *84*, 218–222. https://doi.org/10.1016/j.radphyschem.2012.05.007.

(227) Khandal, D.; Mikus, P.-Y.; Dole, P.; Bliard, C.; Soulestin, J.; Lacrampe, M.-F.; Baumberger, S.; Coqueret, X. Tailoring the Properties of Thermoplastic Starch by Blending with Cinnamyl Alcohol and Radiation Processing: An Insight into the Competitive Grafting and Scission Reactions. *Radiation Physics and Chemistry* **2012**, *81* (8), 986–990. https://doi.org/10.1016/j.radphyschem.2011.10.028.

(228) Shogren, R. L.; Biswas, A. Preparation of Starch-Sodium Lignosulfonate Graft Copolymers via Laccase Catalysis and Characterization of Antioxidant Activity. *Carbohydr. Polym.* **2013**, *91* (2), 581–585. https://doi.org/10.1016/j.carbpol.2012.08.079.

(229) Wu, Q.; Shao, W.; Xia, N.; Wang, P.; Kong, F. A Separable Paper Adhesive Based on the Starch—lignin Composite. *Carbohydr. Polym* **2020**, *229*, 115488. https://doi.org/10.1016/j.carbpol.2019.115488.

(230) Chen, X.; Pizzi, A.; Zhang, B.; Zhou, X.; Fredon, E.; Gerardin, C.; Du, G. Particleboard Bio-Adhesive by Glyoxalated Lignin and Oxidized Dialdehyde Starch Crosslinked by Urea. *Wood Sci. Technol.* **2022**, *56* (1), 63–85. https://doi.org/10.1007/s00226-021-01344-z.

(231) Nasiri, A.; Wearing, J.; Dubé, M. A. Using Lignin to Modify Starch-Based Adhesive Performance. *ChemEngineering* **2020**, *4* (1), 3. https://doi.org/10.3390/chemengineering4010003.
(232) Yao, H.-Y.-Y.; Wang, J.-Q.; Yin, J.-Y.; Nie, S.-P.; Xie, M.-Y. A Review of NMR Analysis in Polysaccharide Structure and Conformation: Progress, Challenge and Perspective. *Food Research International* **2021**, *143*, 110290. https://doi.org/10.1016/j.foodres.2021.110290.
(233) Lu, Y.; Lu, Y.-C.; Hu, H.-Q.; Xie, F.-J.; Wei, X.-Y.; Fan, X. *Structural Characterization of Lignin and Its Degradation Products with Spectroscopic Methods*. Journal of Spectroscopy. https://doi.org/10.1155/2017/8951658.
(234) Cheng, H. N.; Neiss, T. G. Solution NMR Spectroscopy of Food Polysaccharides. *Polymer Reviews* **2012**, *52* (2), 81–114. https://doi.org/10.1080/15583724.2012.668154.
(235) Wen, J.-L.; Sun, S.-L.; Xue, B.-L.; Sun, R.-C. Recent Advances in Characterization of Lignin Polymer by Solution-State Nuclear Magnetic Resonance (NMR) Methodology. *Materials (Basel)* **2013**, *6* (1), 359–391. https://doi.org/10.3390/ma6010359.
(236) Yuan, T.-Q.; Xu, F.; Sun, R.-C. Role of Lignin in a Biorefinery: Separation Characterization and Valorization: Separation, Characterization, and Valorization of Lignin for Biorefinery. *J. Chem. Technol. Biotechnol.* **2013**, *88* (3), 346–352. https://doi.org/10.1002/jctb.3996.
(237) Kong, F.; Wang, S.; Price, J. T.; Konduri, M. K. R.; Fatehi, P. Water Soluble Kraft Lignin–Acrylic Acid Copolymer: Synthesis and Characterization. *Green Chem.* **2015**, *17* (8), 4355–4366. https://doi.org/10.1039/C5GC00228A.
(238) Argyropoulos, D. S.; Pajer, N.; Crestini, C. Quantitative 31P NMR Analysis of Lignins and Tannins. *JoVE (Journal of Visualized Experiments)* **2021**, No. 174, e62696. https://doi.org/10.3791/62696.
(239) Ahvazi, B.; Wojciechowicz, O.; Ton-That, T.-M.; Hawari, J. Preparation of Lignopolyols from Wheat Straw Soda Lignin. *J. Agric. Food Chem.* **2011**, *59* (19), 10505–10516. https://doi.org/10.1021/jf202452m.
(240) Araneda, J. F.; Burton, I. W.; Paleologou, M.; Riegel, S. D.; Leclerc, M. C. Analysis of Lignins Using ^{31}P Benchtop NMR Spectroscopy: Quantitative Assessment of Substructures and Comparison to High-Field NMR. *Can. J. Chem.* **2022**, *100* (11), 799–808. https://doi.org/10.1139/cjc-2022-0041.
(241) Lim, S.; Kasemsuwan, T.; Jane, J. Characterization of Phosphorus in Starch by 31P-Nuclear Magnetic Resonance Spectroscopy. *Cereal chemistry.* **1994**, *71* (5), 488–493.
(242) Sang, Y.; Prakash, O.; Seib, P. A. Characterization of Phosphorylated Cross-Linked Resistant Starch by 31P Nuclear Magnetic Resonance (31P NMR) Spectroscopy. *Carbohydrate Polymers* **2007**, *67* (2), 201–212. https://doi.org/10.1016/j.carbpol.2006.05.009.
(243) Passauer, L.; Liebner, F.; Fischer, K. Starch Phosphate Hydrogels. Part I: Synthesis by Mono-Phosphorylation and Cross-Linking of Starch. *Starch - StÃ¤rke* **2009**, *61* (11), 621–627. https://doi.org/10.1002/star.200900168.
(244) Speciale, I.; Notaro, A.; Garcia-Vello, P.; Di Lorenzo, F.; Armiento, S.; Molinaro, A.; Marchetti, R.; Silipo, A.; De Castro, C. Liquid-State NMR Spectroscopy for Complex Carbohydrate Structural Analysis: A Hitchhiker's Guide. *Carbohydrate Polymers* **2022**, *277*, 118885. https://doi.org/10.1016/j.carbpol.2021.118885.
(245) Zhang, L.; Gellerstedt, G. Quantitative 2D HSQC NMR Determination of Polymer Structures by Selecting Suitable Internal Standard References. *Magnetic Resonance in Chemistry* **2007**, *45* (1), 37–45. https://doi.org/10.1002/mrc.1914.

(246) Dufour, G.; Evrard, B.; de Tullio, P. 2D-Cosy NMR Spectroscopy as a Quantitative Tool in Biological Matrix: Application to Cyclodextrins. *AAPS J* **2015**, *17* (6), 1501–1510. https://doi.org/10.1208/s12248-015-9806-9.
(247) Mansfield, S. D.; Kim, H.; Lu, F.; Ralph, J. Whole Plant Cell Wall Characterization Using Solution-State 2D NMR. *Nat Protoc* **2012**, *7* (9), 1579–1589. https://doi.org/10.1038/nprot.2012.064.
(248) Faleva, A. V.; Kozhevnikov, A. Yu.; Pokryshkin, S. A.; Falev, D. I.; Shestakov, S. L.; Popova, J. A. Structural Characteristics of Different Softwood Lignins According to 1D and 2D NMR Spectroscopy. *J. Wood Chem. Technol.* **2020**, *40* (3), 178–189. https://doi.org/10.1080/02773813.2020.1722702.
(249) Bai, Y.; Shi, Y.-C. Chemical Structures in Pyrodextrin Determined by Nuclear Magnetic Resonance Spectroscopy. *Carbohydrate Polymers* **2016**, *151*, 426–433. https://doi.org/10.1016/j.carbpol.2016.05.058.
(250) Lundquist, K.; Stern, K. Analysis of Lignins by 1H NMR Spectroscopy. *Nordic Pulp & Paper Research Journal* **1989**, *4* (3), 210–213. https://doi.org/10.3183/npprj-1989-04-03-p210-213.
(251) McIntyre, D. D.; Vogel, H. J. Two-Dimensional Nuclear Magnetic Resonance Studies of Starch and Starch Products. *Starch/Stärke* **1990**, *42* (8), 287–293. https://doi.org/10.1002/star.19900420802.
(252) Kempgens, P. The Theory of Cosy NMR Experiments Revisited : Application to an AX Spin System of Quadrupolar Nuclei. *Concepts in Magnetic Resonance Part A* **2010**, *36A* (3), 170–177. https://doi.org/10.1002/cmr.a.20159.
(253) Rietzler, B.; Karlsson, M.; Kwan, I.; Lawoko, M.; Ek, M. Fundamental Insights on the Physical and Chemical Properties of Organosolv Lignin from Norway Spruce Bark. *Biomacromolecules* **2022**, *23* (8), 3349–3358. https://doi.org/10.1021/acs.biomac.2c00457.
(254) Koev, T. T.; Muñoz-García, J. C.; Iuga, D.; Khimyak, Y. Z.; Warren, F. J. Structural Heterogeneities in Starch Hydrogels. *Carbohydrate Polymers* **2020**, *249*, 116834. https://doi.org/10.1016/j.carbpol.2020.116834.
(255) Pfeifer, A.; Hampe, R.; Heinze, T. Synthesis and Characterization of Novel Water-Soluble and Bactericidic Cationic Starch Esters. *Starch - Stärke* **2017**, *69* (9–10), 1700029. https://doi.org/10.1002/star.201700029.
(256) Lancefield, C. S.; Wienk, H. L. J.; Boelens, R.; Weckhuysen, B. M.; Bruijnincx, P. C. A. Identification of a Diagnostic Structural Motif Reveals a New Reaction Intermediate and Condensation Pathway in Kraft Lignin Formation. *Chem. Sci.* **2018**, *9* (30), 6348–6360. https://doi.org/10.1039/C8SC02000K.
(257) Yuan, T.-Q.; Sun, S.-N.; Xu, F.; Sun, R.-C. Characterization of Lignin Structures and Lignin–Carbohydrate Complex (LCC) Linkages by Quantitative 13C and 2D HSQC NMR Spectroscopy. *J. Agric. Food Chem.* **2011**, *59* (19), 10604–10614. https://doi.org/10.1021/jf2031549.
(258) Kim, H.; Padmakshan, D.; Li, Y.; Rencoret, J.; Hatfield, R. D.; Ralph, J. Characterization and Elimination of Undesirable Protein Residues in Plant Cell Wall Materials for Enhancing Lignin Analysis by Solution-State Nuclear Magnetic Resonance Spectroscopy. *Biomacromolecules* **2017**, *18* (12), 4184–4195. https://doi.org/10.1021/acs.biomac.7b01223.

(259) Zhao, C.; Huang, J.; Yang, L.; Yue, F.; Lu, F. Revealing Structural Differences between Alkaline and Kraft Lignins by HSQC NMR. *Ind. Eng. Chem. Res.* **2019**, *58* (14), 5707–5714. https://doi.org/10.1021/acs.iecr.9b00499.
(260) Buedenbender, L.; Habener, L. J.; Grkovic, T.; Kurtböke, D. İ.; Duffy, S.; Avery, V. M.; Carroll, A. R. HSQC–TOCSY Fingerprinting for Prioritization of Polyketide- and Peptide-Producing Microbial Isolates. *J. Nat. Prod.* **2018**, *81* (4), 957–965. https://doi.org/10.1021/acs.jnatprod.7b01063.
(261) Ede, R. M.; Ralph, J. Assignment of 2D TOCSY Spectra of Lignins: The Role of Lignin Model Compounds. *Magn. Reson. Chem.* **1996**, *34* (4), 261–268. https://doi.org/10.1002/(SICI)1097-458X(199604)34:4<261::AID-OMR864>3.0.CO;2-J.
(262) Petersen, B. O.; Motawie, M. S.; Møller, B. L.; Hindsgaul, O.; Meier, S. NMR Characterization of Chemically Synthesized Branched α-Dextrin Model Compounds. *Carbohydr. Res.* **2015**, *403*, 149–156. https://doi.org/10.1016/j.carres.2014.05.011.
(263) Nishimura, H.; Kamiya, A.; Nagata, T.; Katahira, M.; Watanabe, T. Direct Evidence for α Ether Linkage between Lignin and Carbohydrates in Wood Cell Walls. *Sci. Rep.* **2018**, *8* (1), 6538. https://doi.org/10.1038/s41598-018-24328-9.
(264) Giummarella, N.; Lindén, P. A.; Areskogh, D.; Lawoko, M. Fractional Profiling of Kraft Lignin Structure: Unravelling Insights on Lignin Reaction Mechanisms. *ACS Sustainable Chem. Eng.* **2020**, *8* (2), 1112–1120. https://doi.org/10.1021/acssuschemeng.9b06027.
(265) Rönnols, J.; Engström, O.; Schnupf, U.; Säwén, E.; Brady, J. W.; Widmalm, G. Inter-residual Hydrogen Bonding in Carbohydrates Unraveled by NMR Spectroscopy and Molecular Dynamics Simulations. *ChemBioChem* **2019**, *20* (19), 2519–2528. https://doi.org/10.1002/cbic.201900301.
(266) Claridge, T. D. W. Structure Elucidation and Spectrum Assignment. In *High-Resolution NMR Techniques in Organic Chemistry*; Elsevier, 2016; pp 499–525. https://doi.org/10.1016/B978-0-08-099986-9.00013-0.
(267) Nilsson, G. S.; Gorton, L.; Bergquist, K.-E.; Nilsson, U. Determination of the Degree of Branching in Normal and Amylopectin Type Potato Starch with 1H-NMR Spectroscopy Improved Resolution and Two-Dimensional Spectroscopy. *Starch - Stärke* **1996**, *48* (10), 352–357. https://doi.org/10.1002/star.19960481003.
(268) Balakshin, M. Y.; Capanema, E. A.; Chang, H. MWL Fraction with a High Concentration of Lignin-Carbohydrate Linkages: Isolation and 2D NMR Spectroscopic Analysis. **2007**, *61* (1), 1–7. https://doi.org/10.1515/HF.2007.001.
(269) Giummarella, N.; Pu, Y.; Ragauskas, A. J.; Lawoko, M. A Critical Review on the Analysis of Lignin Carbohydrate Bonds. *Green Chem.* **2019**, *21* (7), 1573–1595. https://doi.org/10.1039/C8GC03606C.
(270) Dais, P.; Spyros, A. Nuclear Magnetic Resonance. In *Chemical Analysis of Food: Techniques and Applications*; Elsevier, 2012; pp 91–115. https://doi.org/10.1016/B978-0-12-384862-8.00004-2.
(271) Jiang, B.; Zhang, Y.; Guo, T.; Zhao, H.; Jin, Y. Structural Characterization of Lignin and Lignin-Carbohydrate Complex (LCC) from Ginkgo Shells (Ginkgo Biloba L.) by Comprehensive NMR Spectroscopy. *Polymers* **2018**, *10* (7), 736. https://doi.org/10.3390/polym10070736.
(272) Suchao-in, K.; Koombhongse, P.; Chirachanchai, S. Starch Grafted Poly(Butylene Succinate) via Conjugating Reaction and Its Role on Enhancing the Compatibility. *Carbohydrate Polymers* **2014**, *102*, 95–102. https://doi.org/10.1016/j.carbpol.2013.11.001.

(273) Boccia, A. C.; Scavia, G.; Schizzi, I.; Conzatti, L. Biobased Cryogels from Enzymatically Oxidized Starch: Functionalized Materials as Carriers of Active Molecules. *Molecules* **2020**, *25* (11), 2557. https://doi.org/10.3390/molecules25112557.
(274) Romanenko, I.; Kurz, F.; Baumgarten, R.; Jevtovikj, I.; Lindner, J.-P.; Kundu, A.; Kindler, A.; Schunk, S. A. Lignin Depolymerization in the Presence of Base, Hydrogenation Catalysts, and Ethanol. *Catalysts* **2022**, *12* (2), 158. https://doi.org/10.3390/catal12020158.
(275) Stark, N. M.; Yelle, D. J.; Agarwal, U. P. Techniques for Characterizing Lignin. In *Lignin in Polymer Composites*; Elsevier, 2016; pp 49–66. https://doi.org/10.1016/B978-0-323-35565-0.00004-7.
(276) Derkacheva, O.; Sukhov, D. Investigation of Lignins by FTIR Spectroscopy. *Macromolecular Symposia* **2008**, *265* (1), 61–68. https://doi.org/10.1002/masy.200850507.
(277) Pozo, C.; Rodríguez-Llamazares, S.; Bouza, R.; Barral, L.; Castaño, J.; Müller, N.; Restrepo, I. Study of the Structural Order of Native Starch Granules Using Combined FTIR and XRD Analysis. *J Polym Res* **2018**, *25* (12), 266. https://doi.org/10.1007/s10965-018-1651-y.
(278) Vasile, C.; Gosselink, R. J. A.; Quintus, P.; Koukios, E. G.; Koullas, D. P.; Avgerinos, E.; Abacherli, D. A. Analytical Methods for Lignin Characterization. I. Thermogravimetry. *Cellulose Chemistry and Technology* **2006**, *40* (6), 421–429.
(279) Bikmurzin, R.; Bandzevičiūtė, R.; Maršalka, A.; Maneikis, A.; Kalėdienė, L. FT-IR Method Limitations for β-Glucan Analysis. *Molecules* **2022**, *27* (14), 4616. https://doi.org/10.3390/molecules27144616.
(280) Johansson, L.-S.; Campbell, J. M.; Koljonen, K.; Stenius, P. Evaluation of Surface Lignin on Cellulose Fibers with XPS. *Applied Surface Science* **1999**, *144–145*, 92–95. https://doi.org/10.1016/S0169-4332(98)00920-9.
(281) Hao, Y.; Chen, Y.; Li, Q.; Gao, Q. Synthesis, Characterization and Hydrophobicity of Esterified Waxy Potato Starch Nanocrystals. *Ind. Crop. Prod.* **2019**, *130*, 111–117. https://doi.org/10.1016/j.indcrop.2018.12.073.
(282) Arefmanesh, M.; Vuong, T. V.; Mobley, J. K.; Alinejad, M.; Master, E. R.; Nejad, M. Bromide-Based Ionic Liquid Treatment of Hardwood Organosolv Lignin Yielded a More Reactive Biobased Polyol. *Ind. Eng. Chem. Res.* **2020**, *59* (42), 18740–18747. https://doi.org/10.1021/acs.iecr.0c03718.
(283) Zhang, J.; Tian, Z.; Ji, X.; Zhang, F. Fabrication Mechanisms of Lignin Nanoparticles and Their Ultraviolet Protection Ability in PVA Composite Film. *Polymers* **2022**, *14* (19), 4196. https://doi.org/10.3390/polym14194196.
(284) Luo, Z.; Cheng, W.; Chen, H.; Fu, X.; Peng, X.; Luo, F.; Nie, L. Preparation and Properties of Enzyme-Modified Cassava Starch–Zinc Complexes. *J. Agric. Food Chem.* **2013**, *61* (19), 4631–4638. https://doi.org/10.1021/jf4016015.
(285) Myint, A. A.; Lee, H. W.; Seo, B.; Son, W.-S.; Yoon, J.; Yoon, T. J.; Park, H. J.; Yu, J.; Yoon, J.; Lee, Y.-W. One Pot Synthesis of Environmentally Friendly Lignin Nanoparticles with Compressed Liquid Carbon Dioxide as an Antisolvent. *Green Chem.* **2016**, *18* (7), 2129–2146. https://doi.org/10.1039/C5GC02398J.
(286) Wei, B.; Xu, X.; Jin, Z.; Tian, Y. Surface Chemical Compositions and Dispersity of Starch Nanocrystals Formed by Sulfuric and Hydrochloric Acid Hydrolysis. *PLoS ONE* **2014**, *9* (2), e86024. https://doi.org/10.1371/journal.pone.0086024.
(287) Pylypchuk, I. V.; Lindén, P. A.; Lindström, M. E.; Sevastyanova, O. New Insight into the Surface Structure of Lignin Nanoparticles Revealed by 1H Liquid-State NMR

Spectroscopy. *ACS Sustainable Chem. Eng.* **2020**, *8* (36), 13805–13812. https://doi.org/10.1021/acssuschemeng.0c05119.
(288) Ying, W.; Shi, Z.; Yang, H.; Xu, G.; Zheng, Z.; Yang, J. Effect of Alkaline Lignin Modification on Cellulase–Lignin Interactions and Enzymatic Saccharification Yield. *Biotechnology for Biofuels* **2018**, *11* (1), 214. https://doi.org/10.1186/s13068-018-1217-6.
(289) Gao, W.; Liu, P.; Wang, B.; Kang, X.; Zhu, J.; Cui, B.; Abd El-Aty, A. M. Synthesis, Physicochemical and Emulsifying Properties of C-3 Octenyl Succinic Anhydride-Modified Corn Starch. *Food Hydrocolloids* **2021**, *120*, 106961. https://doi.org/10.1016/j.foodhyd.2021.106961.
(290) Uliniuc, A.; Popa, M.; Drockenmuller, E.; Boisson, F.; Leonard, D.; Hamaide, T. Toward Tunable Amphiphilic Copolymers via CuAAC Click Chemistry of Oligocaprolactones onto Starch Backbone. *Carbohydr. Polym.* **2013**, *96* (1), 259–269. https://doi.org/10.1016/j.carbpol.2013.03.047.
(291) Blanco, I.; Siracusa, V. The Use of Thermal Techniques in the Characterization of Bio-Sourced Polymers. *Materials (Basel)* **2021**, *14* (7), 1686. https://doi.org/10.3390/ma14071686.
(292) Tarasov, D.; Leitch, M.; Fatehi, P. Chemical and Thermal Properties of Precipitates Made from Hydrolysate of Spruce Wood Chips. *Wood Sci Technol* **2019**, *53* (4), 889–909. https://doi.org/10.1007/s00226-019-01101-3.
(293) Barana, D.; Ali, S. D.; Salanti, A.; Orlandi, M.; Castellani, L.; Hanel, T.; Zoia, L. Influence of Lignin Features on Thermal Stability and Mechanical Properties of Natural Rubber Compounds. *ACS Sustainable Chem. Eng.* **2016**, *4* (10), 5258–5267. https://doi.org/10.1021/acssuschemeng.6b00774.
(294) Vega, D.; Villar, M. A.; Failla, M. D.; Vallés, E. M. Thermogravimetric Analysis of Starch-Based Biodegradable Blends. *Polymer Bulletin* **1996**, *37* (2), 229–235. https://doi.org/10.1007/BF00294126.
(295) Ng, H. M.; Saidi, N. M.; Omar, F. S.; Ramesh, K.; Ramesh, S.; Bashir, S. Thermogravimetric Analysis of Polymers. In *Encyclopedia of Polymer Science and Technology*; John Wiley & Sons, Ltd, 2018; pp 1–29. https://doi.org/10.1002/0471440264.pst667.
(296) Yu, L.; Christie, G. Measurement of Starch Thermal Transitions Using Differential Scanning Calorimetry. *Carbohydrate Polymers* **2001**, *46* (2), 179–184. https://doi.org/10.1016/S0144-8617(00)00301-5.
(297) Amit, T. A.; Roy, R.; Raynie, D. E. Thermal and Structural Characterization of Two Commercially Available Technical Lignins for Potential Depolymerization via Hydrothermal Liquefaction. *Current Research in Green and Sustainable Chemistry* **2021**, *4*, 100106. https://doi.org/10.1016/j.crgsc.2021.100106.
(298) Amin, Md. R.; Chowdhury, M. A.; Kowser, Md. A. Characterization and Performance Analysis of Composite Bioplastics Synthesized Using Titanium Dioxide Nanoparticles with Corn Starch. *Heliyon* **2019**, *5* (8), e02009. https://doi.org/10.1016/j.heliyon.2019.e02009.
(299) Estrada-Monje, A.; Alonso-Romero, S.; Zitzumbo-Guzmán, R.; Estrada-Moreno, I. A.; Zaragoza-Contreras, E. A. Thermoplastic Starch-Based Blends with Improved Thermal and Thermomechanical Properties. *Polymers* **2021**, *13* (23), 4263. https://doi.org/10.3390/polym13234263.

(300) Barzegari, M. R.; Alemdar, A.; Zhang, Y.; Rodrigue, D. Thermal Analysis of Highly Filled Composites of Polystyrene with Lignin. *Polymers and Polymer Composites* **2013**, *21* (6), 357–366. https://doi.org/10.1177/096739111302100604.
(301) F. Bass, G.; H. Epps, T. Recent Developments towards Performance-Enhancing Lignin-Based Polymers. *Polymer Chemistry* **2021**, *12* (29), 4130–4158. https://doi.org/10.1039/D1PY00694K.
(302) Zong, E.; Liu, X.; Liu, L.; Wang, J.; Song, P.; Ma, Z.; Ding, J.; Fu, S. Graft Polymerization of Acrylic Monomers onto Lignin with CaCl2–H2O2 as Initiator: Preparation, Mechanism, Characterization, and Application in Poly(Lactic Acid). *ACS Sustainable Chem. Eng.* **2018**, *6* (1), 337–348. https://doi.org/10.1021/acssuschemeng.7b02599.
(303) Cui, C.; Sadeghifar, H.; Sen, S.; Argyropoulos, D. S. Toward Thermoplastic Lignin Polymers; Part II: Thermal & Polymer Characteristics of Kraft Lignin & Derivatives. *BioResources* **2013**, *8* (1), 864–886. https://doi.org/10.15376/biores.8.1.864-886.
(304) Ahvazi, B.; Cloutier, É.; Wojciechowicz, O.; Ngo, T.-D. Lignin Profiling: A Guide for Selecting Appropriate Lignins as Precursors in Biomaterials Development. *ACS Sustainable Chem. Eng.* **2016**, *4* (10), 5090–5105. https://doi.org/10.1021/acssuschemeng.6b00873.
(305) Schindler, A.; Doedt, M.; Gezgin, Ş.; Menzel, J.; Schmölzer, S. Identification of Polymers by Means of DSC, TG, STA and Computer-Assisted Database Search. *J Therm Anal Calorim* **2017**, *129* (2), 833–842. https://doi.org/10.1007/s10973-017-6208-5.
(306) Liu, P.; Yu, L.; Liu, H.; Chen, L.; Li, L. Glass Transition Temperature of Starch Studied by a High-Speed DSC. *Carbohydrate Polymers* **2009**, *77* (2), 250–253. https://doi.org/10.1016/j.carbpol.2008.12.027.
(307) Żołek-Tryznowska, Z.; Kałuża, A. The Influence of Starch Origin on the Properties of Starch Films: Packaging Performance. *Materials* **2021**, *14* (5), 1146. https://doi.org/10.3390/ma14051146.
(308) González, R. M.; Villanueva, M. P. Starch-Based Polymers for Food Packaging. In *Multifunctional and Nanoreinforced Polymers for Food Packaging*; Elsevier, 2011; pp 527–570. https://doi.org/10.1533/9780857092786.4.527.
(309) Peleg, M. A Note on the Tan ?(T) Peak as a Glass Transition Indicator in Biosolids. *Rheola Acta* **1995**, *34* (2), 215–220. https://doi.org/10.1007/BF00398441.
(310) Peng, H.; Nieuwendaal, R.; Soles, C. L. Polymer Dynamics in Constrained Geometries. In *Polymer Science: A Comprehensive Reference*; Elsevier, 2012; pp 345–376. https://doi.org/10.1016/B978-0-444-53349-4.00188-6.
(311) Bierwagen, G. P. *Surface coating*. Encyclopedia Britannica,. https://www.britannica.com/technology/surface-coating (accessed 2022-09-21).
(312) Lagarrigue, S.; Alvarez, G. The Rheology of Starch Dispersions at High Temperatures and High Shear Rates: A Review. *Journal of Food Engineering* **2001**, *50* (4), 189–202. https://doi.org/10.1016/S0260-8774(00)00239-9.
(313) Savitskaya, T.; Reznikov, I.; Grinshpan, D. Rheological Behavior of Lignin Based Dispersions Intended for Composite Fuel Production. *Appl. Rheol.* **2016**, *26*, 63476. https://doi.org/10.3933/APPLRHEOL-26-63476.
(314) Mezger, T. G. *The Rheology Handbook*, 3er ed.; European Coatings Tech Files; Vincentz Network: Hanover, Germany, 2011.
(315) Tanzi, M. C.; Farè, S.; Candiani, G. Mechanical Properties of Materials. In *Foundations of Biomaterials Engineering*; Elsevier, 2019; pp 105–136. https://doi.org/10.1016/B978-0-08-101034-1.00002-5.

(316) Yuan, T.; Zeng, J.; Wang, B.; Cheng, Z.; Chen, K. Lignin Containing Cellulose Nanofibers (LCNFs): Lignin Content-Morphology-Rheology Relationships. *Carbohydr. Polym.* **2021**, *254*, 117441. https://doi.org/10.1016/j.carbpol.2020.117441.
(317) Possari, L. T.; Bretas, R. E. S.; Rigolin, T. R.; Bettini, S. H. P. Dualistic Effect of Kraft Lignin on the Viscoelastic Behavior of Biodegradable Biobased PBSA. *Materials Today Communications* **2021**, *29*, 102847. https://doi.org/10.1016/j.mtcomm.2021.102847.
(318) Lin, J.-H.; Liang, C.-W.; Chang, Y.-H. Effect of Starch Source on Gel Properties of Kappa-Carrageenan-Starch Dispersions. *Food Hydrocolloids* **2016**, *60*, 509–515. https://doi.org/10.1016/j.foodhyd.2016.04.024.
(319) Sarker, M. Z. I.; Abd Elgadir, M.; Ferdosh, S.; Akanda, M. J. H.; Aditiawati, P.; Noda, T. Rheological Behavior of Starch-Based Biopolymer Mixtures in Selected Processed Foods. *Starch-Starke* **2013**, *65* (1–2), 73–81. https://doi.org/10.1002/star.201200072.
(320) Xie, F.; Xue, T.; Yu, L.; Chen, L.; Li, X.; Zhang, X. Rheological Properties of Starch-Based Materials and Starch/Poly(Lactic Acid) Blends. *Macromol. Symp.* **2007**, *249–250* (1), 529–534. https://doi.org/10.1002/masy.200750431.
(321) Reza Barzegari, M.; Alemdar, A.; Zhang, Y.; Rodrigue, D. Mechanical and Rheological Behavior of Highly Filled Polystyrene with Lignin. *Polym. Compos.* **2012**, *33* (3), 353–361. https://doi.org/10.1002/pc.22154.
(322) Rueda, M. M.; Auscher, M.-C.; Fulchiron, R.; Perie, T.; Martin, G.; Sonntag, P.; Cassagnau, P. Rheology and Applications of Highly Filled Polymers: A Review of Current Understanding. *Prog. Polym. Sci.* **2017**, *66*, 22–53. https://doi.org/10.1016/j.progpolymsci.2016.12.007.
(323) Petkova-Olsson, Y.; Ullsten, H.; Jarnstrom, L. Thermosensitive Silica-Pluronic-Starch Model Coating Dispersion-Part II: The Relationship between Rheology and Microstructure. *Colloid Surf. A-Physicochem. Eng. Asp.* **2016**, *509*, 415–426. https://doi.org/10.1016/j.colsurfa.2016.08.003.
(324) Temsiripong, T.; Pongsawatmanit, R.; Ikeda, S.; Nishinari, K. Influence of Xyloglucan on Gelatinization and Retrogradation of Tapioca Starch. *Food Hydrocolloids* **2005**, *19* (6), 1054–1063. https://doi.org/10.1016/j.foodhyd.2005.02.005.
(325) Liu, H. C.; Tuan, C.-C.; Bakhtiary Davijani, A. A.; Wang, P.-H.; Chang, H.; Wong, C.-P.; Kumar, S. Rheological Behavior of Polyacrylonitrile and Polyacrylonitrile/Lignin Blends. *Polymer* **2017**, *111*, 177–182. https://doi.org/10.1016/j.polymer.2017.01.043.
(326) Happs, R. M.; Addison, B.; Doeppke, C.; Donohoe, B. S.; Davis, M. F.; Harman-Ware, A. E. Comparison of Methodologies Used to Determine Aromatic Lignin Unit Ratios in Lignocellulosic Biomass. *Biotechnol Biofuels* **2021**, *14* (1), 58. https://doi.org/10.1186/s13068-021-01897-y.
(327) Lawrencia, D.; Wong, S. K.; Low, D. Y. S.; Goh, B. H.; Goh, J. K.; Ruktanonchai, U. R.; Soottitantawat, A.; Lee, L. H.; Tang, S. Y. Controlled Release Fertilizers: A Review on Coating Materials and Mechanism of Release. *Plants* **2021**, *10* (2), 238. https://doi.org/10.3390/plants10020238.
(328) Vega-Vásquez, P.; Mosier, N. S.; Irudayaraj, J. Nanoscale Drug Delivery Systems: From Medicine to Agriculture. *Front. Bioeng. Biotechnol.* **2020**, *8*, 79. https://doi.org/10.3389/fbioe.2020.00079.

Chapter 3: Process Development for Tall Oil Lignin Production

Adapted from: Jonathan A. Diaz-Baca and Pedram Fatehi *

Bioresour. Technol. **2021**, *329*, 124891. https://doi.org/10.1016/j.biortech.2021.124891

Green Processes Research Centre and Chemical Engineering Department,
Lakehead University, 955 Oliver Road,
Thunder Bay, ON, Canada, P7B5E1

* Corresponding author: email: pfatehi@lakeheadu.ca

The contribution of Jonathan A. Diaz-Baca to this work was the methodology design, formal analysis, writing and original drafting.

3.1. Abstract

The aim of this work was to study the production and characterization of tall oil lignin (TOL) from tall oil soap (TOS) of the kraft pulping process following a new process (i.e., LignoTall). Also, the properties of the TOL and kraft lignin (KL) produced via LignoForce technology were compared. Although TOL and KL were generated from the same black liquor and softwood species, they had remarkably different characteristics, confirming the impact of the production methods on the physicochemical properties of the isolated lignin. TOL had higher molecular weight, O/C elemental ratio, sulphur content, and carboxylate-OH content but lower methoxy group content than did KL. The high sulphur group content (7.3 %) of TOL can be very reactive in the vulcanization process. Moreover, the high carboxylate-OH content of TOL (0.56 mmol/g) is desirable for its utilization in epoxy resin production.

Keywords: Kraft pulping, Tall oil, biorefining, biomass fractionation

3.2. Introduction

Today, most of the industrially produced chemicals are fossil-derived. However, biomass has emerged as an alternate resource to reduce the environmental impact of oil-based products.[1] Analogous to a petroleum refinery, biorefinery utilizes biomass as a feedstock for the conversion of biomass to value-added products sustainably and has the potential to impulse the development of the circular economy.[2] Generally, the kraft pulping process is considered as a traditional biorefining operation, in which cellulose and hemicelluloses are utilized for paper production, and lignin and other aromatic materials are burned for supplying energy of the process. In the kraft process, tall oil can be recovered as a high-value product when softwood species are used as the biomass source of pulping.[2] In this case, the resin and fatty acids present in the wood are transformed into their sodium salt during kraft pulping operation, and later saponified and

separated from wood species as tall oil soap (TOS) in the tall oil production process.[3] When separated from black liquor, tall oil soap contains tall oil, lignin, water, and inorganic compounds.[4] Currently, TOS is acidulated to separate these components to generate tall oil with high purity for the market. After acidulation; the spent water, salt, and lignin are mixed with the black liquor of the pulping process and thus burned in the recovery section of the kraft process.[5] Currently, it is unclear if these by-products of the tall oil process, e.g., lignin, have any potential for valorization.

Recently, the LignoForce and LignoBoost methods were developed to isolate lignin from black liquor commercially.[6,7] In these two lignin production processes, lignin production is mainly optimized through acidification of black liquor with H_2SO_4 at the temperature range of 60-80 °C.[8] Interestingly, lignin in the tall oil production is also separated from black liquor via an acidification process at the temperature of 98 °C. However, acidulation is optimally used for generating tall oil soap, not lignin in the tall oil production process.[9] Moreover, the presence of fatty acids in the tall oil soap may have an impact on the isolation process of lignin of the TOS process. Therefore, it is unclear if the lignin generated in the kraft and tall oil production processes would have similar properties and thus similar potential applications. In the past, efforts were made to fractionate TOS,[4,5,10] but they mostly focused on the tall oil fraction, leaving the lignin fraction unexplored. To the authors' knowledge, there is no information available for the characterization of lignin present in TOS. The main objective of this work was to assess the extraction and properties of generated lignin in the LignoTall process. The successive use of lignin from TOS depends greatly on the fundamental studies of its physicochemical structure.[11] This study aimed to develop a process, i.e., the LignoTall process, for isolating lignin from the tall oil production process of the kraft pulping process. In this work, the fragmentation of TOS was conducted following a novel operation.

In the past, the generated lignin of LignoForce and LignoBoost processes was claimed to have potential uses in the production of phenols, flocculants, dispersants, carbon black, composite materials, and rubber fillers.[12] For instance, kraft lignin is an attractive replacement for carbon black in the production of green rubber composites.[13] Interestingly, solvent extraction was used as a strategy to improve the quality of lignin to be used as an additive in natural rubber production in the past.[14] In the current work, TOL was treated with organic solvents after its tall oil extraction to improve its purity.[14] To identify potential applications for the tall oil lignin, a series of physicochemical characterization, such as morphological, elemental, spectroscopic, molecular weight, and thermal analyses were carried out; and the results were compared with kraft lignin produced via the LignoForce system. The main novelty of this work was the introduction of the LignoTall process, and the physicochemical characterization of lignin generated in the LignoTall process from tall oil soap.

3.3. Material and methods

3.3.1. Raw materials

The tall oil soap (TOS) of softwood species generated in a kraft pulping process was received from a mill in northern Ontario, Canada, and used as a raw material for the development of the LignoTall process. Also, kraft lignin (KL), which was generated from the same wood species via the LignoForce technology, was obtained from the same mill. KL was ground in a mortar and used as a control sample. Sulphuric acid (H_2SO_4) (95.0-98.0 wt. %) was acquired from Fisher Scientific Company. Ethanol (95%), acetone (99.5%), hexanes (mixture of isomers) (≥98.5%), sodium hydroxide (NaOH) (≥97.0%), tetrahydrofuran (THF), (99%) dimethyl sulfoxide (DMSO)(≥99.9%), dimethyl sulphoxide-d_6 ([D_6]DMSO)(99.9 %), 3-(trimethylsilyl)propionic-2,2,3,3-d4 acid sodium salt (D, 98 %) (TSP), pyridine (99.8%), cyclohexanol (99%), chromium (III)

acetylacetonate (99.99%), and 2-chloro-4,4,5,5-tetramethyl-1,2,3 dioxaphospholane (TMDP, 95%), were all acquired from Millipore Sigma, Canada. Chloroform-D ($CDCL_3$) (D, 99.96%) was purchased from Cambridge Isotope Laboratories Inc. BOD nutrient buffered solutions (APHA formulation) were acquired from HACH Company, USA.

3.3.2. TOS fractionation and lignin extraction

The LignoTall process used for fractionating TOS is shown in Scheme 3.1. First, the solutions of 45 mL of H_2O and 9 mL of H_2SO_4 were added to 150 g of TOS at 70 °C and the mixtures were stirred for 20 min. Next, the mixture was heated in a separatory funnel (using a water bath, HAAKE S45, Thermo Scientific™) at 95 °C for 3 h. Afterward, the TOS was separated into 3 distinctive phases, which were collected and weighted. This standard process fractionated TOS into a tall oil phase (top), lignin-containing phase (middle), and spent water phase (bottom). The tall oil phase contains negligible amounts of lignin, and this tall oil is fairly lignin-free, as lignin remained emulsified in the lignin-containing phase.[4] The middle phase containing lignin was the interest of this work. After cooling to room temperature, the middle phase was treated with 150 mL of ethanol and left for gravitational settling overnight. The supernatant was collected, and the precipitates of this process were treated with 100 mL of ethanol three times every 6 h. This ethanol mixing process was repeated to ensure that all lignin of the middle phase was transferred to ethanol solution.

Lignin extraction from an ethanol solution was conducted by distilling ethanol in a rotary evaporator (Buchi, R210) at 40 °C. After the ethanol removal, a dark brown precipitate was obtained, which was placed into an oven at 60 °C for 24 h for remnant solvent evaporation. Lastly, the dried precipitate was treated with 20 mL of hexanes at room temperature to eliminate any tall oil remnant for producing pure lignin for further analysis. After mixing with hexane, purified tall oil lignin (TOL) particles were sedimented. TOL was collected by decantation and dried in an oven

at 60 °C for 24 h to complete the solvent evaporation. Then, the mass balance was developed for TOS and the collected middle layer containing lignin.

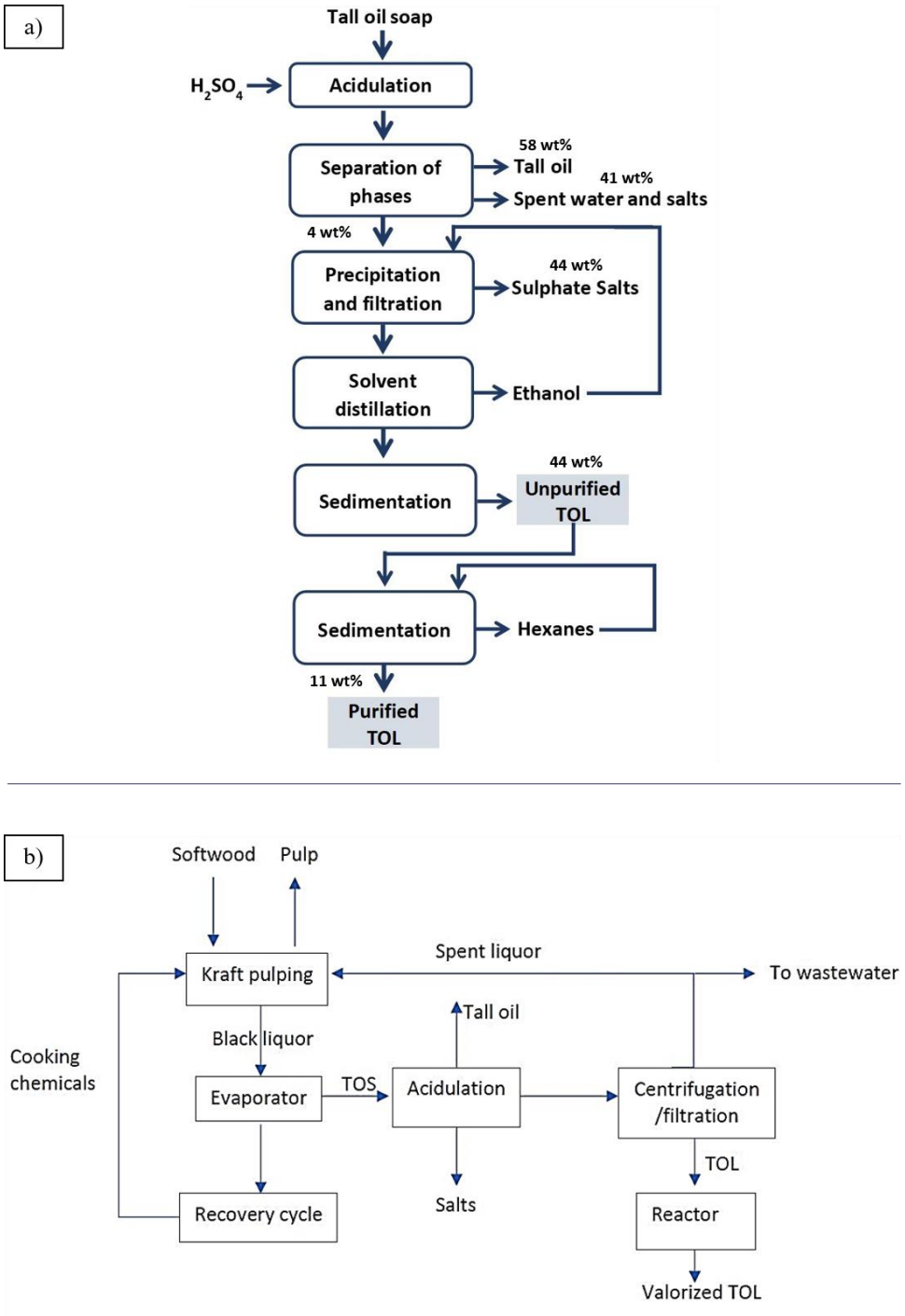

Scheme 3.1. a) Experimental procedure followed for extraction and production of pure TOL, b) process flow diagram of LignoTall process

3.3.3. Scanning electron microscopy

The morphology of KL and TOL was analyzed by a scanning electron microscope/energy dispersive spectrometer (SEM/EDX) (SU-70 Analytical Field Emission SEM, Hitachi) at 5 kV with different magnifications. The images were collected in a digital format. Samples were vacuum dried (Stable Temp® 282A, Cole-Palmer) at 50 °C for 12 h before gold coating and analysis. The contents of carbon and oxygen in the samples were detected and analyzed by an Oxford Aztec 80mm/124ev EDX detector attached to the SEM instrument.

3.3.4. Elemental analysis

Approximately, 2 mg of dried KL and TOL were combusted at 1200 °C for analyzing their carbon, hydrogen, nitrogen, and sulphur contents following the combustion method with an elemental analyzer (Vario EL cube, Elementar Analysensysteme GmbH). The oxygen content of the samples was determined by developing a mass balance for carbon, hydrogen, sulphur, nitrogen, on an inorganic-free basis. From the results, the atomic H/C and O/C ratios were calculated. The methoxy group (OCH_3) content of the lignin samples was estimated using the formula proposed previously.[15] The higher heating value (HHV) of the samples was estimated based on the equation (1):[16]

$$\mathrm{HHV} = 0.335C + 1.423H - 0.154O - 0.145N \quad (1)$$

where *C, H, O,* and *N* are the respective elemental contents.

3.3.5. Fourier transform infrared spectroscopy (FT-IR)

The FT-IR analysis of KL and TOL was carried out in the infrared region of 600–4000 cm^{-1} to understand the chemical bonds of the samples. The transmittance mode was acquired on a Fourier

transform Infrared spectrophotometer (Tensor 37, Bruker) with an attenuated total reflectance (ATR) accessory. The analysis was performed directly on 0.02 g of previously dried samples.

3.3.6. Carboxyl and sulphate group analysis

The carboxyl and sulphate group contents of KL and TOL were determined via titration. The titration was conducted using an automatic conductometer (856 Conductivity Module, Metrohm AG) according to the method discussed earlier.[17] First, 0.15 g of sample was mixed with 2 mL of NaCl (0.02 mol/L), second, 150 mL of deionized water was added, and last, samples were left overnight under stirring. Before the titration, the pH of the suspension was adjusted to 3.5 and then titrated with NaOH (0.01 mol/L).

3.3.7. Qualitative proton nuclear magnetic resonance (^{1}H-NMR) and methoxy group analysis

The ^{1}H-NMR analysis of KL and TOL was performed using 26-27 mg of previously dried samples (60 °C, 24 h) in 500 µL DMSO-d6. Also, 2-4 mg of TSP (internal standard) were added to each sample. The ^{1}H-NMR spectra were obtained using nuclear magnetic resonance spectroscopy (UNITY INOVA™-500 MHz, Varian, Inc.) with a total of 64 scans per sample at 25 °C and a 2.05 s acquisition time, a 90° pulse, and 1.00 s of relaxation delay time. The methoxy (OCH_3) group content of the samples was determined by the integration of the aromatic (6.0-7.7 ppm) and methoxy (3.50- 4.1) regions from ^{1}H-NMR spectra according to equation 2:[18]

$$\%OCH_3 = 28.28436 - 19.750047x \quad (2)$$

where x = (H-aromatic)/(H-methoxyl), and (H-aromatic) and (H-methoxyl) are integration values of the aromatic and methoxyl signals in the NMR spectra.

3.3.8. Quantitative phosphorus NMR (^{31}P-NMR) analysis

The ^{31}P-NMR analysis was performed to quantify the phenolic and aliphatic hydroxyl moieties of KL and TOL. The phosphitylation of the samples was performed as suggested earlier.[19] First, 35-38 mg of the sample were dissolved into chloroform-d ($CDCl_3$) and pyridine/$CDCl_3$ (1.6:1 v/v). For both samples, 53 µL of T1-relaxation agent was added. For KL, 200 µL of $CDCl_3$ and 400 µL of pyridine/$CDCl_3$, 36 µL of internal standard, and 100 µL TMDP were used. For TOL, 300 µL of $CDCl_3$ and 400 µL of pyridine/$CDCl_3$, 70 µL of internal standard, and 200 µL of TMDP were used. The ^{31}P-NMR spectra were obtained using a nuclear magnetic resonance spectrometer (UNITY INOVA™-500 MHz, Varian, Inc.) with a total of 256 scans per sample at 25 °C, a 1.6 s acquisition time, a 90° pulse, and 10 s of relaxation delay time.

3.3.9. Qualitative heteronuclear single quantum coherence (2D-HSQC) NMR analysis

The 2D-HSQC (heteronuclear single quantum coherence) NMR analysis of KL and TOL was carried out with 29-30 mg of samples dissolved in 500 µL DMSO-d6. Samples were agitated at 170 rpm overnight and 25 °C prior to the NMR analysis. The solutions were tested using nuclear magnetic resonance spectroscopy (AVANCE NEO-1.2 GHz, Bruker, Corporation). For the ^{1}H dimension, the matrices of 2048 data points were collected from 16 to 0 ppm, at 25 °C and 1.00 s recycling delay. For the ^{13}C dimension, the matrices of 1024 data points were collected from 160 to 0 ppm, with 256 increments of 64 scans at 25 °C and 1.00 s of recycling delay.[20]

3.3.10. Molecular weight and radius of gyration determination

The static light scattering (SLS) technique was performed to determine the absolute molecular weight (MW) and radius of gyration (R_g) of the samples in the solutions using a laser light scattering system that is attached to a goniometer (BI-200SM, Brookhaven Instruments Corporation). The maximum solid-state laser power used in the experiment was 35 mW at the

wavelength of 637 nm. The samples of KL and TOL were dissolved in 20 mL of DMSO (99.5%) overnight at 25 °C. The different aliquots of the lignin solutions were prepared with different concentrations (0.1 to 2.4 mg/mL), all the solutions were filtered with 0.22 μm Nylon membrane syringe filters before the SLS measurement. The absolute molecular weight and radius of gyration were calculated from the Berry plot analyzed by the instrument software (Brookhaven Instruments Corp). Results are the average of three independent measurements.

3.3.11. Solubility test

The solubility analysis of KL and TOL was performed in 5 different systems. The solutions (1 wt.%) of KL and TOL were prepared in H_2O (pH 3, 7, and 10), ethanol, acetone, ethanol-acetone mixture (70:30 v/v), DMSO, and THF. NaOH (0.5 mol/L) and H_2SO_4 (0.5 mol/L) were used to adjust the pH of the aqueous system. Afterward, the solutions were left overnight under agitation (100 rpm) at 25 °C and later centrifuged at 1000 rpm for 5 min. Then, 5 mL of the supernatants were dried in a vacuum oven (Stable Temp® Model 282A, Cole-Parmer) at 60 °C for 24 h and weighted for mass balance development.

3.3.12. Thermogravimetric analysis

Thermogravimetric analysis (TGA) was performed to investigate the thermal response of KL and TOL. Samples (7-8 mg) were dried in an oven at 60 °C for 24 h prior to the analysis. The analysis was performed under nitrogen atmosphere in a thermal analyzer (TGA i1000, Instrument Specialists Inc.) at a flow rate of 15 mL/min and heated from 25 °C to 800 °C at the rate of 5 °C/min. In addition, the ignition temperature (T_i) of samples was determined from the TGA results according to a method previously reported (Liu et al., 2018). The comprehensive combustion characteristic index (CCI) was used to evaluate the reactivity, combustion intensity, and burnout performance of KL and TOL. The CCI was estimated following equation (3):[21]

$$CCI = (DTG_{max} \times DTG_{mean}) / (T_i^2 \times T_b) \quad (3)$$

where CCI is the comprehensive combustion index, $\%^2/ (min^2 \cdot K^3)$; DTG_{max} is the maximum weight loss in DTG curve, %/min; DTG_{mean} is the average weight loss rate in DTG curve, %/min; T_i is the volatile ignition point, K, and T_b is the burnout temperature, K.

3.3.13. Ash determination

The ash content of KL and TOL was determined according to a method discussed earlier[22] using oxidative TGA at a 20 mL/min air flow rate. About 7 mg of each sample were heated from 20 °C to 105 °C at a rate of 30°C/min with 30 min of constant temperature, then heated at a rate of 15°C/min to reach 525°C and held for 120 min. Lastly, the temperature was decreased to 20°C and held for 30 min. This method is in accordance with ISO 1762 for ash analysis and was performed in a thermal analyzer (TGA i1000, Instrument Specialists Inc.).

3.3.14. Heat capacity determination

Differential scanning calorimetry (DSC) was used to determine the heat capacity (C_P) of the samples. Approximately, 7-10 mg of dried KL and TOL were placed in a Tzero® aluminum pan and placed into a differential scanning calorimeter (DSC Q2000, TA Instruments). The analysis was performed in N_2 atmosphere at 50 °C/min. In the DSC analysis, the temperature was raised from 20 °C to 150 °C, which was used to erase thermal history, then the temperature dropped to 20 °C at 5.0 °C/min to cool down the sample, and the second heating cycle was conducted from 20 °C to 150 °C at 10.0 °C/min. The maximum temperature of 150 °C was set based on the decomposition profile of the samples obtained from the TGA analysis of the samples. Three comparative points were taken as a reference at 50, 100, and 150 °C to compare how the C_P develops during the temperature increment for each sample.

3.3.15. XRD characterization

The middle phase salts (as shown in Scheme 3.1) were characterized by the X-ray diffraction (XRD) analysis to determine their chemical compositions. Samples were analyzed using an X-ray diffractometer (X'Pert PRO MPD, PANalytical B.V.) and the Cu-Kα radiation of 0.154 nm. The diffraction data was collected on a continuous scan over an angular range of $2\theta = 6 - 96°$ over 38 min with a generator voltage of 45 kV and a tube current of 40 mA. The phases of the spectrum were identified using the ICDD PDF-2 database.

3.3.16. BOD_5 and COD analysis

The biochemical oxygen demand (BOD) analysis of the spent water (shown in Scheme 3.1a) was carried out following the APHA 5210B, 5-Day BOD (BOD_5) test method.[23] The spent acid collected after tall oil production was centrifugated at 3000 rpm for 10 min to remove the majority of salts prior to the analysis. However, this sample still contained fine salt particles after centrifugation. The dissolved oxygen (DO) concentration in the solutions was measured with a DO portable meter attached to a luminescent/optical dissolved oxygen probe (HQd Portable Meter-LBDO101, HACH Company) before and after the incubation period. The BOD_5 was determined according to the DO concentration difference before and after the incubation. The chemical oxygen demand (COD) analysis of the spent water was carried out using a COD commercial kit (HR COD, CHEMetrics Inc.) according to the APHA 5220D standard procedure.[23] The COD was calculated according to the manufacturer's procedure.

3.4. Results and Discussion

3.4.1. TOS compositions

The TOS contained 57.8 ± 3.1 wt.% tall oil, 28.9 ± 1.1 wt.% water, 11.1 ± 1.2 wt.% salts, and 4.1 ± 0.4 wt.% lignin-containing middle phase. The compositions of the middle phase were 44.4 ± 6.4 wt.% of sulphate salts and fibers, 44.2 ± 5.3 wt.% tall oil, and 11.4 ± 1.7 wt.% TOL.

3.4.2. Morphological characterization of isolated lignin

The SEM images of KL and TOL were investigated. It was observed that the structure of these samples was noticeably different (Figure S3.1 in Supplementary material). The granular and uniform structure of KL with a particle size of 2 μm is observable. A completely different configuration is observed for the TOL with particle sizes of 50 to 75 μm. To generate TOL, different solvents, such as ethanol and hexane, were used; which formed precipitates with spherical particles. The self-assembly of lignin segments in the presence of the solvents could be induced by hydrogen bonding, van der Waals forces, electrostatic forces, and π-π interactions[24] resulting in the formation of spherical particles for TOL.

3.4.3. Elemental analysis

The elemental analysis was performed to obtain information about the chemical nature of KL and TOL. The organic elements of the materials are summarized in Table 3.1. The carbon of KL was higher, but its oxygen was lower, than those of TOL. Such results could be explained by the occurrence of the oxidative depolymerization of lignin during the acidulation of lignin in tall oil and TOL production, which may suggest the abundance of condensed C_5-substituted oxygen-containing units (e.g., 5-5 and/or β-5) in TOL.[25] As H_2SO_4 was heavily used in the production of TOL, its sulphur content was higher than that of KL.[26] These results revealed that the chemical

compositions of TOL differed from kraft lignin, which would imply that the structure of lignin that was associated with tall oil was different from KL even though they were originated from the same wood source and have gone through the same kraft pulping operation.

The O/C and H/C ratios were also calculated from the elemental compositions of KL and TOL. The O/C ratio was 0.30 and 0.47 for KL and TOL, respectively. The O/C ratio has been used as an indicator for the oxygenation degree of lignin.[27] Low O/C ratios in lignin are desirable for the production of carbon fibers,[27] however, the higher presence of oxidative species makes it more reactive.[28] Also, H/C ratios were 1.3 and 1.1 for KL and TOL, respectively. The H/C ratio has been used as an indicator of the relative proportion of saturated chains (i.e., cycles and aromatic rings) in comparison with unsaturated chains in lignin; in that the lower the H/C ratio, the more double bonds would be present in lignin.[25] Therefore, more double bonds and fewer side chains would probably be present in TOL than KL. The HHV is highly correlated with the carbon content of lignin. The estimated HHV for KL and TOL were 27.5 and 19.6 MJ/Kg, respectively (Table 3.1). The oxidative decomposition profile depicted that the samples contained less than 3 wt% ash (but TOL had more than KL).[26] It was found that large HHV values and low O/C ratio for lignocellulosic materials are preferred for energy-obtention applications.[28] The results suggest that probably the TOL is not suitable for energy-obtention applications.

Table 3.1. Elemental composition, O/C, H/C ratios, HHV values, and an ash content of KL and TOL.

Sample	C (%)	H (%)	N (%)	S (%)	O[a] (%)	Ratio O/C	Ratio H/C	HHV[b] (MJ/kg)	Ash[c] (%)
KL	64.4 ± 0.1	6.9 ± 0.1	0.0± 0.1	3.4 ± 0.1	25.3 ± 0.1	0.30	1.3	27.5	1.1

TOL	53.7 ± 0.9	4.8 ± 0.1	0.1 ± 0.1	7.3 ± 2.6	34.1 ± 3.4	0.47	1.1	19.6	2.6

[a] By difference
[b] Based on the formula proposed (Demirbas, 2017)
[c] Obtained based on method ISO-1762 (Aldaeus et al., 2017)
± Estimated standard deviation

3.4.4. Chemical structure analysis

FTIR characterization. The FT-IR spectra of KL and TOL were analyzed to establish structural differences and similarities among samples (Figure S3.2). The characteristic peaks for softwood kraft lignin were detected in the fingerprint region between 1800 cm^{-1} and 650 cm^{-1}.[29] The differences in the O-H stretch bands at 3030–3690 cm^{-1} observed for KL and TOL might be related to the different proportions of aliphatic and phenolic-OH contents of the samples.[29] Furthermore, the signal designated to the aromatic carboxyl stretching is observed in TOL at 1705 cm^{-1}, and its intensity is higher in KL than in TOL. In TOL, a band associated with the C-H bending in substituted aromatic structures is observed at 870 cm^{-1}, and this band is absent in KL. Lastly, a band associated with the aromatic C-H in-plane deformation in the guaiacyl ring appears at 1170 cm^{-1} in TOL, but it does not appear in KL. These results suggest the presence of phenyl propane units as the monomer blocks of all samples and confirm their softwood origin. The FT-IR signals also suggest the different content of phenolic, aliphatic, and carboxylic acid moieties in the two samples.

^{1}H-NMR characterization. The proton resonance peaks of KL and TOL were obtained from ^{1}H-NMR analysis (Figure S3.3a). In general, three important regions are identified in the spectrum of lignin: the regions of aromatic hydrogens, side chains, and aliphatic hydrogens, which correspond to the signals of 7.5-6.0 ppm, 6.0-4.0 ppm, 2.5-0.0 ppm, respectively.[30]

In the KL spectrum, a broad signal in the aromatic region is present with peaks distinguishable at 6.7-7.2 ppm relating to the G units of lignin. In the spectrum of TOL, a strong signal associated with condensed C_5-substituted units is observed, and there is a weaker signal in the aromatic region than the aliphatic region, which is mainly assigned to the G-units.[18] These results suggest that TOL has a polyphenolic structure and it can be presumed that the condensed C_5-substituted units are the predominant structural units. Additionally, a signal from 4.1 to 3.5 ppm was observed as indicative of the methoxy group for KL and TOL.[30] Considering the signal intensity of the peaks, the methoxy group content of KL and TOL was calculated to be 20.9 % and 11.5 %, respectively. These values are similar to those of methoxy (%) presented in Table 3.2.

^{31}P-NMR characterization. The OH groups of the KL and TOL samples were determined by ^{31}P-NMR (Figure S3.3b), and the results can be seen in Table 3.2. KL had the highest content of aliphatic-OH. In both samples, the phenolic hydroxy content was predominant. In addition, the phenolic-OH groups in TOL were mainly derived from C_5 substituted OH unit, whereas those in KL were mainly derived from the guaiacyl OH unit. The carboxylate group was higher for TOL, which was an indication of an intensified oxidation process than TOL.[31] In previous studies, the carboxylate groups in kraft lignin were originated from oxidation reactions during pulping or/and from associated fatty acids in lignin (Constant et al., 2016).[32] It has been reported that, at temperatures between 80 °C and 100 °C, minor oxidation would occur within kraft lignin, leading to a carboxylic acid formation and simultaneously to the guaiacyl units OH elimination (Asgari and Argyropoulos, 1998).[33] The above-mentioned range of temperature is what has been practiced in the TOS fractionation, which could facilitate the oxidation of guaiacyl-OH to carboxylate-OH for TOL (Table 3.2). For KL, the carboxylate content is most likely related to the oxidation during kraft pulping.

Table 3.2. Functional groups content of KL and TOL

Structure	KL	TOL
Aliphatic OH[a]	1.53	0.98
Phenolic OH[b]	3.25	2.25
C_5 substituted OH[a]	1.41	1.40
Guaiacyl OH[a]	1.63	0.70
P- hydroxyphenyl OH[a]	0.21	0.15
Carboxylate OH[a]	0.33	0.56
Methoxy (%)[c]	18.3	12.7
Carboxyl group[d]	0.02	0.05
Sulphate group[d]	0.11	0.23

[a] Hydroxy group content (mmol/g, measured via ^{31}P NMR analysis).
[b] Sum of C_5 substituted OH, Guaiacyl OH, and P- hydroxyphenyl OH content.
[c] Calculated from the elemental analysis values following the method of Jablonsky et al., 2015.[15]
[d] Surface carboxyl and sulphate group (mmol/g, measured via conductometric titration).

2D-HSQC-NMR characterization. The linkages and predominant units present in KL and TOL were assessed by 2D-HSQC-NMR analysis (data was shown in supplementary material in Figure S3.4). The main inter-unit linkages were the ether bonds (β-O-4'), phenylcoumaran (β-5'), p-hydroxyl types syringyl, guaiacyl, *p*-hydroxyphenyl, and *p*-hydroxybenzoate.[30] In general, the side chain region (δ_C/δ_H 50-90/2.5-6.0 ppm) and the aromatic region (δ_C/δ_H 90-130/6.0-7.5 ppm) were observable. These signals were similar to those reported for organosolv lignin.[28] In both KL and TOL, the common signals observed at δ_C/δ_H 55.1-56.3/3.7 ppm are assigned to C-H in the methoxyl group. In the KL spectrum, the signals observed at δ_C/δ_H 59.3/3.4 ppm are attributed to Cγ-Cγ in β-O-4' present in the major substructure A. In the aromatic region, the prevalent unit

observed for KL was guaiacyl (G) with signals at δ_C/δ_H 111.5/6.7 and 114.4/6.7 ppm. These results confirm that the G-units were the main structural units of KL and the β-O-4' was the main linkage. In the TOL spectrum, the signals observed at δ_C/δ_H 60.4/3.4 ppm and δ_C/δ_H 63.1/3.5 ppm were attributed to Cγ-Cγ in β-O-4' (substructure A) and Cγ-Cγ in β-5' (substructure B), respectively. Contrary to the prevalent G unit found in KL, the signals were associated with the *p*-hydroxyphenyl (H) and *p*-hydroxybenzoate (PB) units and were also found at δ_C/δ_H 124.4/7.1-6.9 ppm and δ_C/δ_H 129.5/7.3 ppm in TOL. Interestingly, the presence of *p*-hydroxybenzoate units confirmed the prevalence of the carboxyl group in TOL.

Carboxyl and sulphate group contents. The carboxyl and sulphate group contents of KL and TOL were obtained by conductometric titration and the results are shown in Table 3.2. In general, the titration and NMR analysis show the same trend for the carboxyl group content of the samples, however, the titration method showed smaller values, as conductimetric titration facilitated the surface analysis of the samples due to limited solubility of the samples in the aqueous system. Similarly, the sulphate group content is estimated to originate from the surface of TOL particles, but it confirms the sulphur content results determined by elemental analysis (Table 3.1). TOL had the highest concentration of sulphate group (Table 3.2) and the highest sulphur content (Table 3.1).

3.4.5. Molecular weight determination of isolated lignin

The MW and R_g of the samples are summarized in Table 3.3. It is evident that the MW of TOL was higher than that of KL. The R_g and MW of the molecule are highly correlated to the degree of polymerization of lignin.[34] It was also reported that the degree of branching is a determining factor for the R_g,[35] which would reveal the compactness of lignin segments in the solution. It is seen that TOL had a larger R_g, therefore, TOL had possibly a larger size and a looser structure than KL in solution.

Table 3.3. Molecular weight and R_g, heat capacity at temperatures of 50, 100, and 150 ˚C, ignition temperature, and comprehensive combustion characteristic index of KL and TOL.

Sample	MW × 10^5 (g/mol)	Rg (nm)	Signal change [a] (J/g˚C)	C_p (J/g˚C)			T_i (˚C)	CCI (%²/min²K³)
				50˚C	100˚C	150˚C		
KL	1.509 ± 0.013	11.3 ± 5.5	0.17	0.89	0.99	1.04	398	1.11×10^{-11}
TOL	2.905 ± 0.064	17.8 ± 3.6	1.11	1.52	1.77	2.45	327	3.11×10^{-12}

[a] Signal from the initial onset point (21 °C) to the final temperature

3.4.6. Solubility analysis

To have a better understanding of the behavior of the samples in aqueous and non-aqueous systems and its correlation with their functional groups, the solubility of the lignin products was assessed. Generally, the samples were more soluble in non-aqueous systems (e.g., ethanol, acetone, DMSO, THF) than in aqueous systems (Table 3.4). The highest solubility was seen in THF, 14.5 g/L, and 26.7 g/L for KL and TOL, respectively. The solubility of both samples was lower in other solvents and significantly lower in aqueous systems.

The solubility of lignin in organic solvents is governed by the intrinsic parameters of the solvent, such as hydrogen bonding and polar interactions, and the lignin's structural properties, such as molecular weight and functional group content.[36] Probably, the higher amount of saturated chains and the lower amount of OH content (Table 3.2) of TOL would promote its hydrophobicity and thus improved affinity to organic solvents, particularly to non-polar solvents, such as THF (polarity of solvents is related to its dielectric constant ε, and it is DMSO > Ethanol > Acetone > THF).[37] Interestingly, the solubility of all samples was higher in the mixture of ethanol-acetone (70:30 v/v)

than each solvent individually. When mixed, the intermolecular forces, such as hydrogen bonding that is developed between the molecules of ethanol and acetone, are less than the ones present in each solvent in the pure form,[38] leading to a more intensive interaction in the solubility of all samples. As expected, both samples were more soluble in alkaline aqueous systems than other aqueous environments, as a result of the ionization of the phenolic OH-group in both samples.

Table 3.4. Solubility (1 wt.%) of KL and TOL in H_2O (pH 3, 7, and 10), ethanol, acetone, ethanol-acetone, DMSO, and THF.

Solvent	KL	TOL
	Solubility (g/L)	
H_2O- pH 3	1.1 ± 0.1	1.6 ± 0.3
H_2O- pH 7	2.3 ± 0.3	2.6 ± 0.2
H_2O- pH 10	5.4 ± 0.1	3.5 ± 0.1
Ethanol	5.5 ± 0.2	6.9 ± 0.3
Acetone	6.2 ± 0.5	7.1 ± 0.4
Ethanol-acetone (70/30 v/v)	11.6 ± 0.3	12.5 ± 0.1
DMSO	11.8 ± 0.4	12.1 ± 0.1
THF	14.5 ± 0.6	26.7 ± 1.2

± Estimated standard deviation

3.4.7. Thermal analysis of isolated lignin

Thermal decomposition profiles. The thermal decomposition profiles of KL and TOL were analyzed (data was shown in Figure S3.5). It is seen that TOL had a weight loss in the range of 140 °C and 300 °C, and this major weight loss was not seen in KL. This trend might be attributed to the higher carboxylate groups of TOL, which is similar to the results reported in the past.[40] Also,

it is seen that both KL and TOL lost 50% of their weight at different temperatures of 511 °C and 444 °C, respectively. It was reported[26] that the decomposition of KL with 50% weight loss was between 450 °C and 500 °C mainly due to the cleavage of ether-type and C-C bonds.

Moreover, a wide decomposition temperature range (175 °C to 580 °C) for the samples suggests that the decomposition of different groups occurred at different temperatures. The decomposition occurred from 280 °C to 580 °C (with the highest rate between 400 °C and 550 °C) was promoted by the intensive evolution of volatile compounds, such as methane, methanol, and carbonyl groups.[41] The energetic exothermic step in the temperature range of 320 °C and 450 °C is most probably associated with the fragmentation of the side chains from the aromatic rings as a result of the cleavage of β-O-4 and β-5 linkages.[42] In this range, the decomposition rate is higher for KL than for TOL. The last observable step appeared at 570 °C, and this step is related to the decomposition of the aromatic rings due to the cleavage of C-C bonds of lignin,[42] which is more significant for KL than TOL. Additionally, the ignition temperature (T_i) (Table 3.3), an important fuel property, was calculated from the TGA analysis. TOL showed a T_i of 327 °C, which was much lower than that of KL (398 °C) and was related to the lower aromatic contents of TOL than KL.[26] Furthermore, the maximum CCI values of KL and TOL were 1.11×10^{-11} $\%^2/min^2K^3$ and 3.11×10^{-12} $\%^2/min^2K^3$ respectively (Table 3.3). The larger the CCI value, the better the combustion performance of the sample, KL had a higher CCI value, however, both KL and TOL had a CCI value lower than the reported for biofuel (4.97×10^{-5} $\%^2/min^2K^3$).[43]

Heat capacity. Heat capacity (C_p) is a fundamental thermodynamic property that is essential for the evaluation and standardization of the transformation process of lignin involving heat exchange. The stability of C_p can be related to the molecular rigidity of the polymeric chains.[44] Previously, fewer aliphatic-OH group content and more aliphatic carbon content of lignin were related to a

less stable C_p, presenting a C_p change at a lower temperature as a result of less rigid lignin chains.[45] KL shows higher stability of C_p, which is probably related to its higher aliphatic-OH groups (Table 3.2) allowing for more hydrogen-bonding development. On the contrary, TOL with lower aliphatic-OH groups (Table 3.2) had a more significant increment in C_p with the temperature and the highest C_p change (Table 3.3). In both samples, there are different increments in the C_p from the initial onset point to the final temperature (raw data is available in Figure S3.5). Generally, the C_p was higher at a higher temperature (Table 3.3). Additionally, the trend of the C_p change observed in KL and TOL is different, indicating more rigidity for KL chains due to a more compact structure and hydrogen bonding development (Table 3.3). The large variation in the C_p value of TOL could be attributed to the higher molecular weight and looser structure of TOL (Table 3.3).

Fractionation and isolation process of TOL. The fractionation of TOS yielded three valuable materials: tall oil, TOL, and sulphate salts. Although the total mass of TOL was small, the burning of the tall oil-free fraction for heat recovery, as is currently carried out in the pulp industry, may not be economically feasible as it contains a significant amount of water and salts. The energy balance of tall oil-free fraction includes the heat generation via burning TOL (HHV of 19.6 MJ/Kg, Table 3.1) and heat consumption required for the evaporation of water (2.26 MJ/kg).[46] Considering the water and TOL contents of the tall oil-free spent liquor, the net energy gained via mixing the tall oil-free fraction with black liquor would be 0.5 MJ/kg, which is marginal. However, such mixing would increase the load to the evaporator and recovery boiler of the kraft process and underutilize the generated lignin and salts. In this case, by eliminating such mixing, the unnecessary load to the recovery process of the kraft pulping may drop, if the recovery boiler is the bottleneck of the process, as this liquor does not contribute to the energy recovery of the process. As shown in Scheme 3.1b, Tall oil can be generated via the acidulation process. The

fractionation process of this tall oil depleted fraction would generate sodium sulphate decahydrate, i.e., Glauber's salt (data was shown in Figure S3.2a), to be used, for example, as a phase-change material in the solar energy and for thermal energy storage in the building and textile industry.[47,48] Salt can be separated via sedimentation or filtration in the LignoTall process (Scheme 3.1b). The lignin-containing solution can go to another step of the process to extract TOL. In the current work, we used solvents to generate pure TOL for analytical purposes. Solvents may be used to produce pure lignin if needed.[14] Alternatively, centrifugation and ultrafiltration can promote TOL extraction. The generated TOL can go to another reactor, in which its properties will be further adjusted for rubber production or epoxy resins, for example (via chemical reactions). Furthermore, the spent water generated after the removal of salts and lignin could be sent to the pulping digester as a source of water supply for the pulping. Alternatively, it can be sent to the wastewater treatment system of the mill. The BOD_5/COD ratio of the spent water was measured to be 0.25 (4830 mg/L /19708 mg/L). As our sample liquor contained some fine salts, and the salts contributed to the slightly lower BOD_5/COD ratio. To increase this ratio to be >0.3 for better biological degradation, the spent liquor can be more intensely centrifuged/filtered/ion-exchanged or further treated with microorganisms (e.g., *Micrococcus* and *Staphylococcus, Kurthia Sophie, Alcaligenes faecalis,* and *Pseudomonas aeruginosa*) prior to recycling to the pulping digester or wastewater treatment systems.[49]

3.5. Conclusions

A new process, LignoTall, for producing lignin derivatives in the kraft pulping operation was introduced. For the first time, a comprehensive characterization of the lignin derivative generated from the fractionation of TOS was performed. The isolated lignin had different properties from KL. In comparison with KL, TOL had higher sulphur content, a larger number of carboxylate-OH

groups, and higher molecular weight, which would promote its potential application as a rubber additive or reinforcer of epoxy resins. The results confirmed the possibility of generating a new lignin derivative in the kraft pulping process following the LignoTall process.

3.6. References

(1). Takkellapati, S., Li, T., Gonzalez, M.A., **2018**. An overview of biorefinery-derived platform chemicals from a cellulose and hemicellulose biorefinery. Clean Technol. Environ. Policy 20, 1615–1630. https://doi.org/10.1007/s10098-018-1568-5

(2). Galbe, M., Wallberg, O., **2019.** Pretreatment for biorefineries: a review of common methods for efficient utilisation of lignocellulosic materials. Biotechnol. Biofuels 12, 2–26. https://doi.org/10.1186/s13068-019-1634-1

(3). Evdokimov, A.N., Kurzin, A.V., Trifonova, A.D., Popova, L.M., Buisman, G.J.H., **2017**. Desulfurization of black liquor soap for production of crude tall oil with lower sulfur content. Wood Sci. Technol. 51, 1353–1363. https://doi.org/10.1007/s00226-017-0912-y

(4). Aro, T., Fatehi, P., **2017**. Tall oil production from black liquor: Challenges and opportunities. Sep. Purif. Technol. 175, 469–480. https://doi.org/10.1016/j.seppur.2016.10.027

(5). Niemeläinen, M., **2018**. Tall oil depitching in kraft pulp mill. Aalto University, Espoo, Finland.

(6). Kouisni, L., Gagné, A., Maki, K., Holt-Hindle, P., Paleologou, M., **2016.** LignoForce System for the Recovery of Lignin from Black Liquor: Feedstock Options, Odor Profile, and Product Characterization. ACS Sustain. Chem. Eng. 4, 5152–5159. https://doi.org/10.1021/acssuschemeng.6b00907

(7). Öhman, F., Theliander, H., Tomani, P., Axegard, P., **2013**. Method for separating lignin from black liquor. US8486224B2.

(8). Hubbe, M.A., Alén, R., Paleologou, M., Kannangara, M., Kihlman, J., **2019**. Lignin Recovery from Spent Alkaline Pulping Liquors Using Acidification, Membrane Separation, and Related Processing Steps: A Review. Bioresources 14, 2300–2351.

(9). Foran, C.D., **2006**. Tall oil soap recovery., in: TAPPI Kraft Recovery Operation Short Course. TAPPI Press, Savannah, GA, p. 3.7-1-3.7-23.

(10). Aro, T.D., **2017**. Tall Oil Production Process and Characterization. Lakehead University, Thunder Bay, ON., Canada.

(11). Ragauskas, A.J., Beckham, G.T., Biddy, M.J., Chandra, R., Chen, F., Davis, M.F., Davison, B.H., Dixon, R.A., Gilna, P., Keller, M., Langan, P., Naskar, A.K., Saddler, J.N., Tschaplinski, T.J., Tuskan, G.A., Wyman, C.E., **2014.** Lignin Valorization: Improving Lignin Processing in the Biorefinery. Science 344, 1246843–1246843. https://doi.org/10.1126/science.1246843

(12). Dessbesell, L., Paleologou, M., Leitch, M., Pulkki, R., Xu, C., **2020**. Global lignin supply overview and kraft lignin potential as an alternative for petroleum-based polymers. Renew. Sustain. Energy Rev. 123, 109768. https://doi.org/10.1016/j.rser.2020.109768

(13). Mohamad Aini, N.A., Othman, N., Hussin, M.H., Sahakaro, K., Hayeemasae, N., **2020**. Lignin as Alternative Reinforcing Filler in the Rubber Industry: A Review. Front. Mater. 6, 1–18. https://doi.org/10.3389/fmats.2019.00329

(14). Barana, D., Orlandi, M., Zoia, L., Castellani, L., Hanel, T., Bolck, C., Gosselink, R., **2018**. Lignin Based Functional Additives for Natural Rubber. ACS Sustain. Chem. Eng. 6, 11843–11852. https://doi.org/10.1021/acssuschemeng.8b02145
(15). Jablonsky, M., Botkova, M., Adamovska, J., **2015**. Prediction of methoxyl groups content in lignin based on ultimate analysis. Cellulose Chem. Technol. 49, 165–168.
(16). Demirbas, A., **2017**. Higher heating values of lignin types from wood and non-wood lignocellulosic biomasses. Energy Sources Part Recovery Util. Environ. Eff. 39, 592–598. https://doi.org/10.1080/15567036.2016.1248798
(17). Hosseinpour Feizi, Z., Fatehi, P., **2020**. Carboxymethylated cellulose nanocrystals as clay suspension dispersants: effect of size and surface functional groups. Cellulose 27, 3759–3772. https://doi.org/10.1007/s10570-020-03024-w
(18). Tana, T., Zhang, Z., Moghaddam, L., Rackemann, D.W., Rencoret, J., Gutiérrez, A., del Río, J.C., Doherty, W.O.S., **2016**. Structural Changes of Sugar Cane Bagasse Lignin during Cellulosic Ethanol Production Process. ACS Sustain. Chem. Eng. 4, 5483–5494. https://doi.org/10.1021/acssuschemeng.6b01093
(19). Meng, X., Crestini, C., Ben, H., Hao, N., Pu, Y., Ragauskas, A.J., Argyropoulos, D.S., **2019**. Determination of hydroxyl groups in biorefinery resources via quantitative 31P NMR spectroscopy. Nat. Protoc. 14, 2627–2647. https://doi.org/10.1038/s41596-019-0191-1
(20). Singh, D., Dhepe, P.L., **2019**. Altering the O/C Ratio of Lignin Derived Monomers without Sacrificing Atom Efficiency. ChemistrySelect 4, 14050–14055. https://doi.org/10.1002/slct.201903320
(21). Liu, Y., Cao, X., Duan, X., Wang, Y., Che, D., **2018.** Thermal analysis on combustion characteristics of predried dyeing sludge. Appl. Therm. Eng. 140, 158–165. https://doi.org/10.1016/j.applthermaleng.2018.05.055
(22). Aldaeus, F., Olsson, A.M., Stevanic, J.S., **2017**. Miniaturized determination of ash content in kraft lignin samples using oxidative thermogravimetric analysis. Nord. Pulp Pap. Res. J. 32, 280–282. https://doi.org/10.3183/npprj-2017-32-02-p280-282
(23). American Public Health Association, **2017**. Standard Methods for the Examination of Water and Wastewater, 23rd ed. American Public Health Association, American Water Works Association, Water Environment Federation.
(24). Zhang, Z., Yang, R., Gao, W., Yao, X., **2017.** Investigation of [Emim][OAc] as a mild pretreatment solvent for enhancing the sulfonation efficiency of alkali lignin. RSC Adv. 7, 31009–31017. https://doi.org/10.1039/C7RA03877A
(25). Pérez, E., Tuck, C.O., **2018.** Quantitative analysis of products from lignin depolymerisation in high-temperature water. Eur. Polym. J. 99, 38–48. https://doi.org/10.1016/j.eurpolymj.2017.11.053
(26). Ház, A., Jablonský, M., Šurina, I., Kačík, F., Bubeníková, T., Ďurkovič, J., **2019.** Chemical composition and thermal behavior of kraft lignins. Forests 10, 483. https://doi.org/10.3390/f10060483
(27). Rossberg, C., Janzon, R., Saake, B., Leschinsky, M., **2019.** Effect of Process Parameters in Pilot Scale Operation on Properties of Organosolv Lignin. BioResources 14, 4543–4559. https://doi.org/DOI: 10.15376/biores.14.2.4543-4559
(28). Li, X., Wu, S., **2014.** Chemical Structure and Pyrolysis Characteristics of the Soda-Alkali Lignin Fractions. Bioresources 9, 6277-6289. https://doi.org/10.15376/biores.9.4.6277-6289

(29). Singh, S.K., Dhepe, P.L., **2016.** Isolation of lignin by organosolv process from different varieties of rice husk: Understanding their physical and chemical properties. Bioresour. Technol. 221, 310–317. https://doi.org/10.1016/j.biortech.2016.09.042
(30). Rashid, T., Kait, C.F., Murugesan, T., **2016.** A "Fourier Transformed Infrared" Compound Study of Lignin Recovered from a Formic Acid Process. Procedia Eng. 148, 1312–1319. https://doi.org/10.1016/j.proeng.2016.06.547
(31). Liu, X., Li, T., Wu, S., Ma, H., Yin, Y., **2020.** Structural characterization and comparison of enzymatic and deep eutectic solvents isolated lignin from various green processes: Toward lignin valorization. Bioresour. Technol. 310, 123460. https://doi.org/10.1016/j.biortech.2020.123460
(32). Jiang, B., Zhang, Y., Guo, T., Zhao, H., Jin, Y., **2018**. Structural Characterization of Lignin and Lignin-Carbohydrate Complex (LCC) from Ginkgo Shells (Ginkgo biloba L.) by Comprehensive NMR Spectroscopy. Polymers 10, 736. https://doi.org/10.3390/polym10070736
(33). Constant, S., Wienk, H.L.J., Frissen, A.E., Peinder, P. de, Boelens, R., van Es, D.S., Grisel, R.J.H., Weckhuysen, B.M., Huijgen, W.J.J., Gosselink, R.J.A., Bruijnincx, P.C.A., **2016.** New insights into the structure and composition of technical lignins: a comparative characterisation study. Green Chem. 18, 2651–2665. https://doi.org/10.1039/C5GC03043A
(34). Asgari, F., Argyropoulos, D.S., **1998.** Fundamentals of oxygen delignification. Part II, Functional group formation/elimination in residual Kraft lignin. Can. J. Chem. 76, 1606–1615.
(35). Petridis, L., Smith, J.C., **2016.** Conformations of Low-Molecular-Weight Lignin Polymers in Water. ChemSusChem 9, 289–295. https://doi.org/10.1002/cssc.201501350
(36). Clauss, M.M., Weldin, D.L., Frank, E., Giebel, E., Buchmeiser, M.R., **2015.** Size-Exclusion Chromatography and Aggregation Studies of Acetylated Lignins in *N,N*-Dimethylacetamide in the Presence of Salts. Macromol. Chem. Phys. 216, 2012–2019. https://doi.org/10.1002/macp.201500222
(37). Dastpak, A., Lourençon, T.V., Balakshin, M., Farhan Hashmi, S., Lundström, M., Wilson, B.P., **2020.** Solubility study of lignin in industrial organic solvents and investigation of electrochemical properties of spray-coated solutions. Ind. Crops Prod. 148, 112310. https://doi.org/10.1016/j.indcrop.2020.112310
(38). Loudon, M., Parise, J., **2016.** Solvents in organic chemistry, in: Organic Chemistry. W. H. Freeman, pp. 339–346.
(39). Jadhav, D.L., Karthick, N.K., Kannan, P.P., Shanmugam, R., Elangovan, A., Arivazhagan, G., **2017**. Molecular interaction forces in acetone + ethanol binary liquid solutions: FTIR and theoretical studies. J. Mol. Struct. 1130, 497–502. https://doi.org/10.1016/j.molstruc.2016.10.055
(40). Mousavioun, P., Doherty, W.O.S., **2010.** Chemical and thermal properties of fractionated bagasse soda lignin. Ind. Crops Prod. 31, 52–58. https://doi.org/10.1016/j.indcrop.2009.09.001
(41). Hua, W., Liu, C., Wu, S., Li, X., **2016.** Analysis of Structural Units and Their Influence on Thermal Degradation of Alkali Lignins. Bioresources 11,1959-1970. https://doi.org/10.15376/biores.11.1.1959-1970
(42). de Carvalho Oliveira, F., Srinivas, K., Helms, G.L., Isern, N.G., Cort, J.R., Gonçalves, A.R., Ahring, B.K., **2018.** Characterization of coffee (Coffea arabica) husk lignin and

degradation products obtained after oxygen and alkali addition. Bioresour. Technol. 257, 172–180. https://doi.org/10.1016/j.biortech.2018.01.041
(43). Lai, Y., Wang, B., Chen, X., Yuan, Y., Zhong, L., Qiao, X., Zhang, Y., Yuan, M., Shu, 44. J., Wang, P., **2014.** Thermogravimetric Analysis of Combustion Characteristics of Palm Oil and Rapeseed Oil Biodiesel. Biotechnology 14, 9–15. https://doi.org/10.3923/biotech.2015.9.15
(44). Wang, R.-M., Zheng, S.R., Zheng, Y.P., **2011**. Matrix materials, in: Polymer Matrix Composites and Technology. Elsevier, pp. 101–548. https://doi.org/10.1533/9780857092229.1.101
(45). Saito, T., Perkins, J.H., Vautard, F., Meyer, H.M., Messman, J.M., Tolnai, B., Naskar, A.K., **2014.** Methanol Fractionation of Softwood Kraft Lignin: Impact on the Lignin Properties. ChemSusChem 7, 221–228. https://doi.org/10.1002/cssc.201300509
(46). Wallace, J.M., Hobbs, P.V., **2006.** Atmospheric Thermodynamics, in: Wallace, J.M., Hobbs, P.V. (Eds.), Atmospheric Science (Second Edition). Academic Press, San Diego, pp. 63–111. https://doi.org/10.1016/B978-0-12-732951-2.50008-9
(47). De Paola, M., Arcuri, N., Calabrò, V., De Simone, M., **2017.** Thermal and Stability Investigation of Phase Change Material Dispersions for Thermal Energy Storage by T-History and Optical Methods. Energies 10, 354. https://doi.org/10.3390/en10030354
(48). Iqbal, K., Sun, D., **2018.** Synthesis of nanoencapsulated Glauber's salt using PMMA shell and its application on cotton for thermoregulating effect. Cellulose 25, 2103–2113. https://doi.org/10.1007/s10570-018-1692-8
(49). Kumar, A., Dhall, P., Kumar, R., **2010**. Redefining BOD:COD ratio of pulp mill industrial wastewaters in BOD analysis by formulating a specific microbial seed. Int. Biodeterior. Biodegrad. 64, 197–202. https://doi.org/10.1016/j.ibiod.2010.01.005

3.7. Appendix A. Supporting information

Process Development for Tall Oil Lignin Production

Jonathan A. Diaz-Baca, Pedram Fatehi*

Chemical Engineering Department, Lakehead University, 955 Oliver Road, Thunder Bay, ON P7B SE1, Canada

*Corresponding author: E-mail: pfatehi@lakeheadu.ca;

Number of pages 6 (S3.1-S3.6)

Number of Figures 5 (S3.1-S3.5)

Number of Tables 0

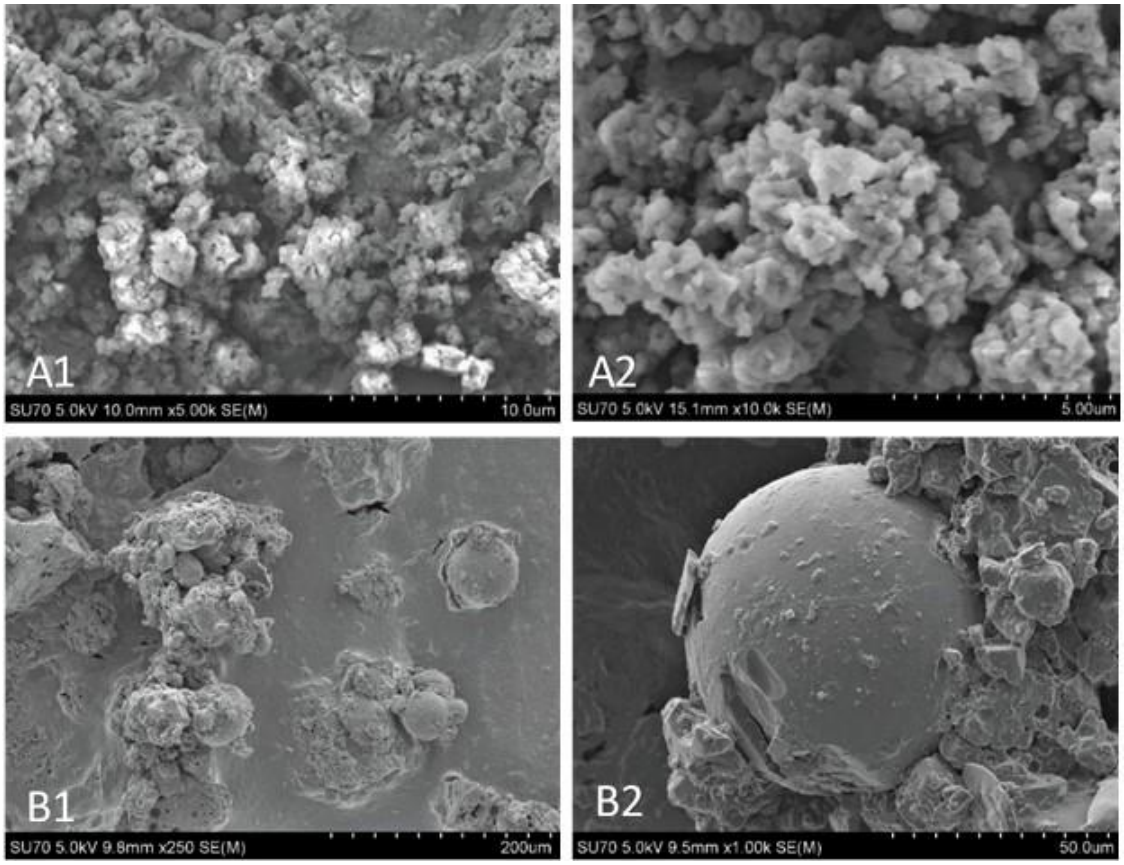

Figure S3.1. SEM images from KL(A1-2) and TOL (B1-2).

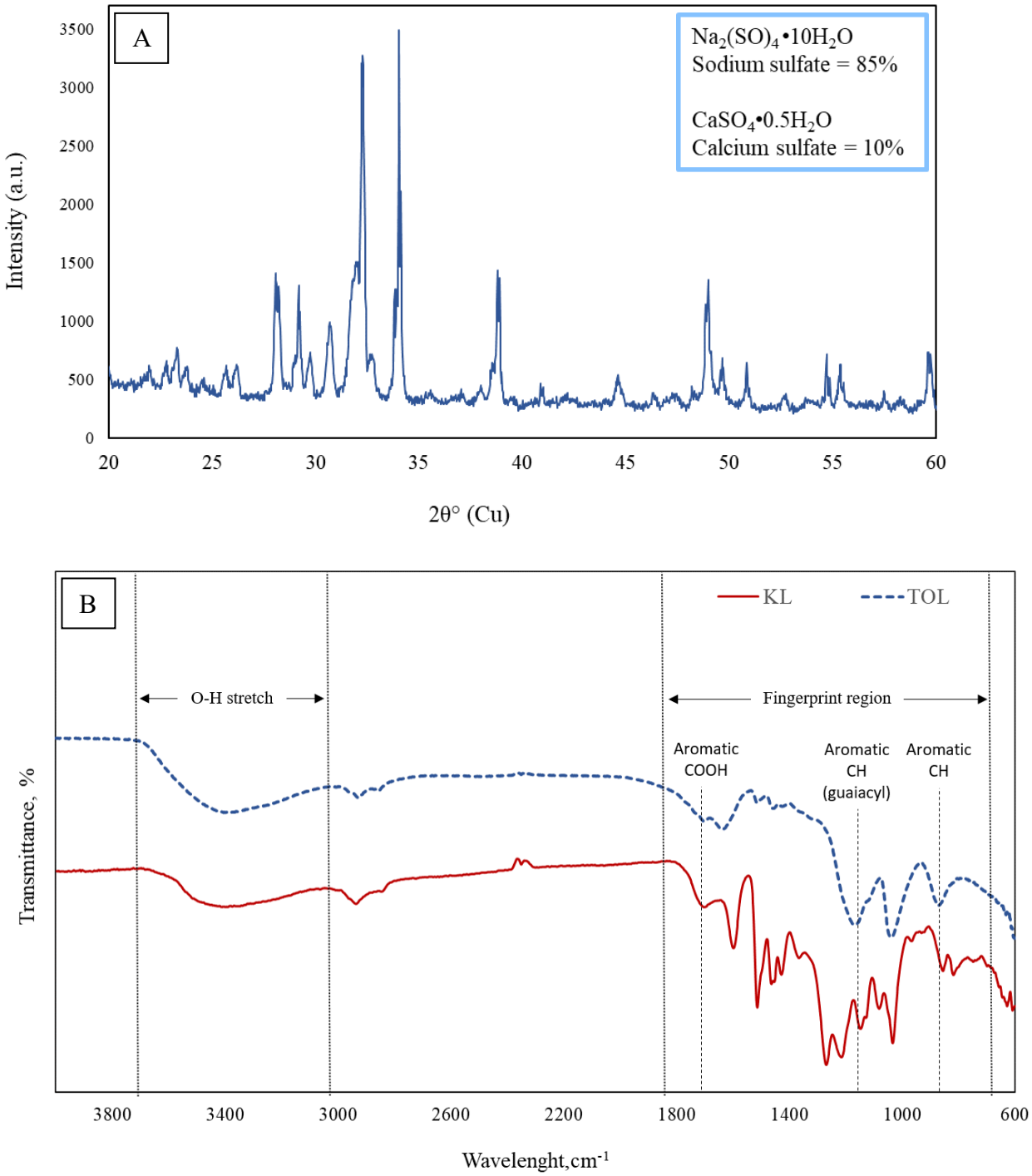

Figure S3.2. (A) XRD pattern of the salts separated from the middle layer (lignin-containing layer). (B) FT-IR spectra of KL and TOL.

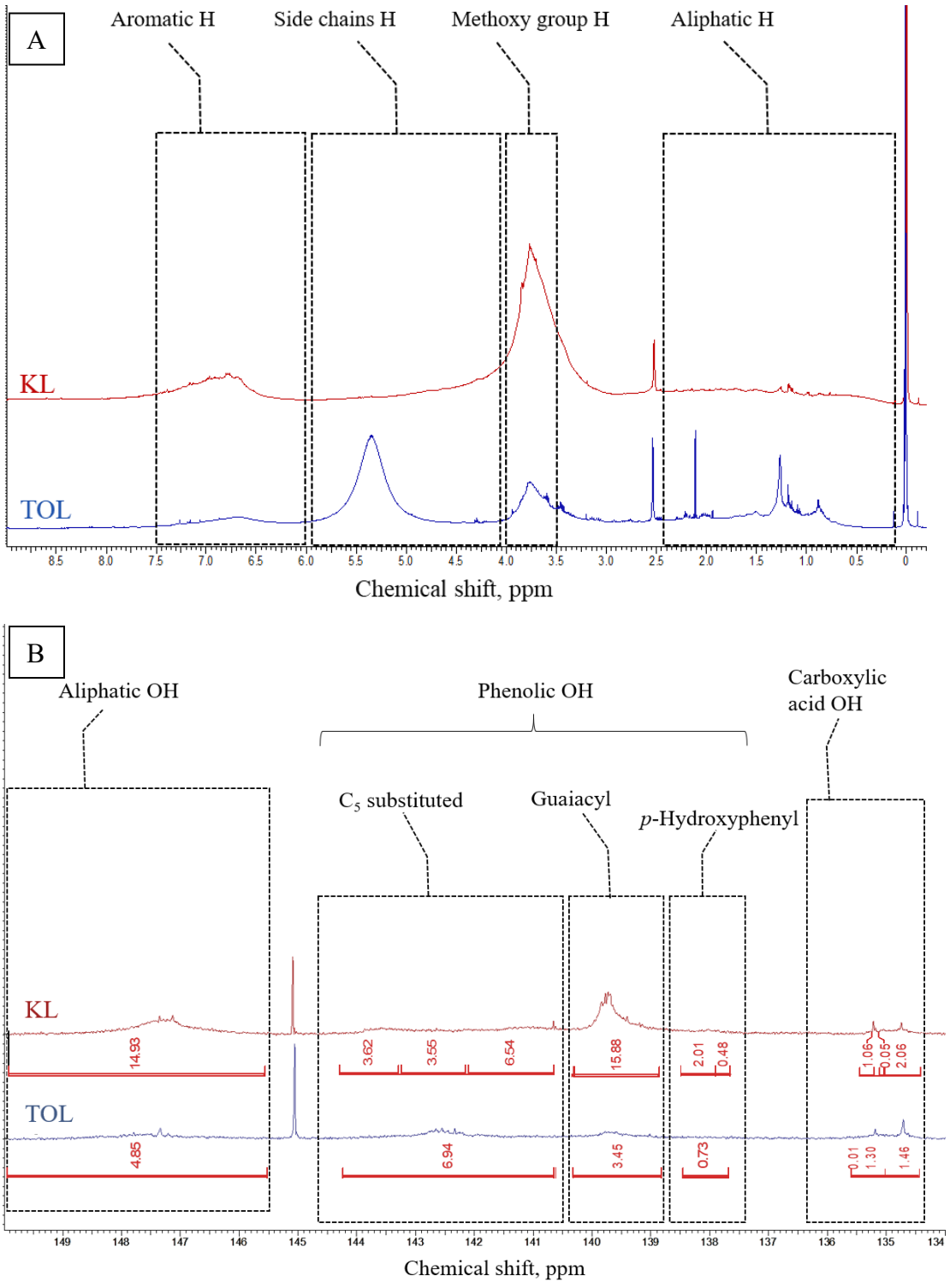

Figure S3.3. (A) ^{1}H NMR spectra of KL and TOL. (B) Quantitative ^{31}P NMR spectra of phosphitylated KL and TOL.

A

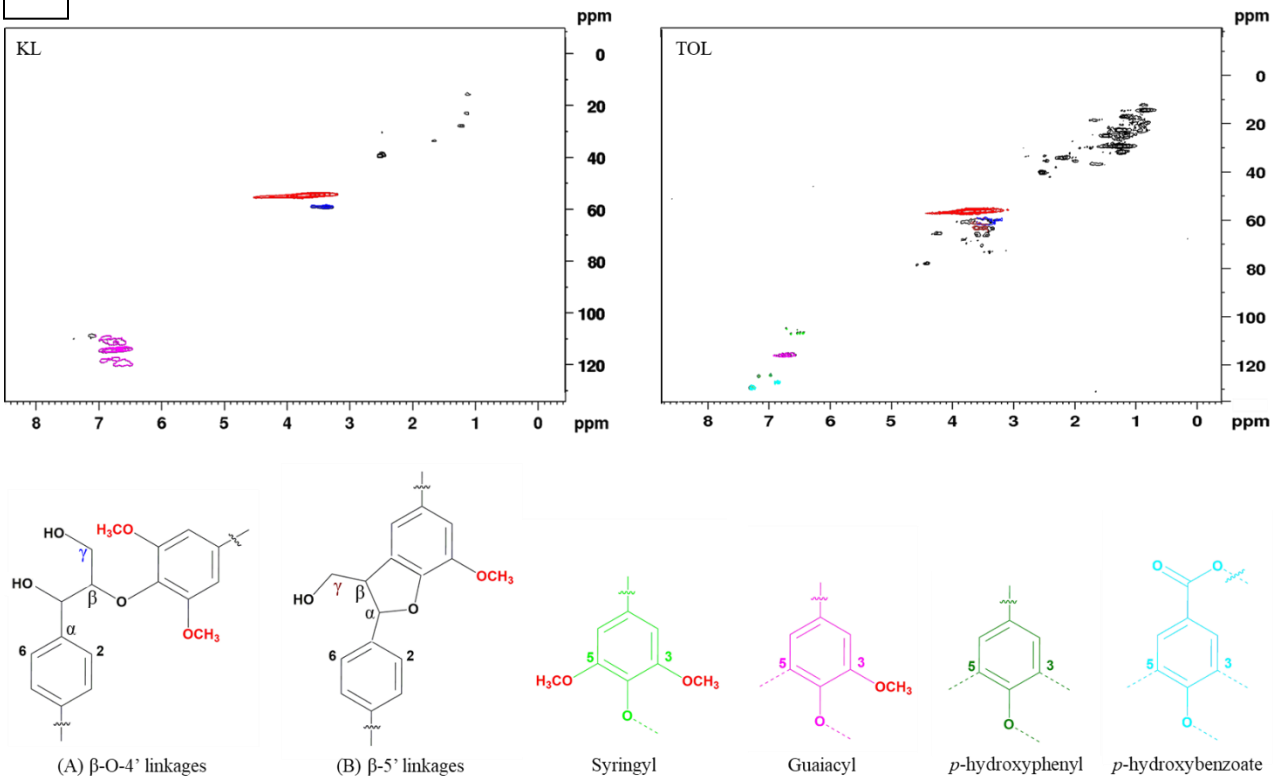

B

Assignment	KL	TOL
	δ_C/δ_H	δ_C/δ_H
C-H in $-OCH_3$ (Methoxy)	55.1/3.7	56.3/3.7
Cγ-Cγ in β-O-4' substructures (A)	59.3/3.4	60.4/3.4
Cγ-Cγ in β-5' substructures (B)	-	63.1/3.5
$C_{2,6}$-$H_{2,6}$ (syringyl)	-	106.7/6.5
C_2-H_2 (guaiacyl)	111.5/6.7	-
C_5-H_5 (guaiacyl)	114.4/6.7	115.5/6.7
$C_{2,6}$-$H_{2,6}$ (*p*-hydroxyphenyl)	-	124.4/7.1-6.9
$C_{2,6}$-$H_{2,6}$ (*p*-hydroxybenzoate)	-	129.5/7.3

Figure S3.4. (A) 2D-HSQC-NMR and main substructures present in KL and TOL. (B) Assignments of $^{13}C/^{1}H$ heteronuclear single quantum coherence spectra (HSQC) of KL and TOL.

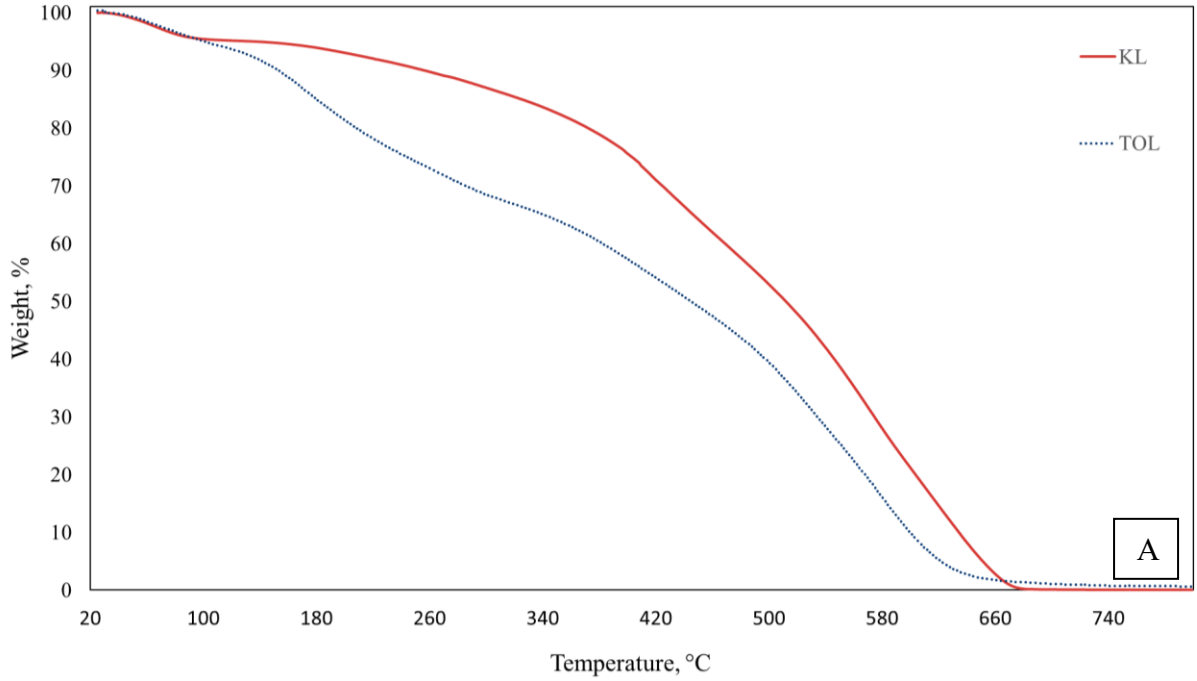
100
90
80
70
60
50
40
30
20
10
0
Weight, %
20
100
180
260
340
420
500
580
660
740
Temperature, °C
KL
TOL
A

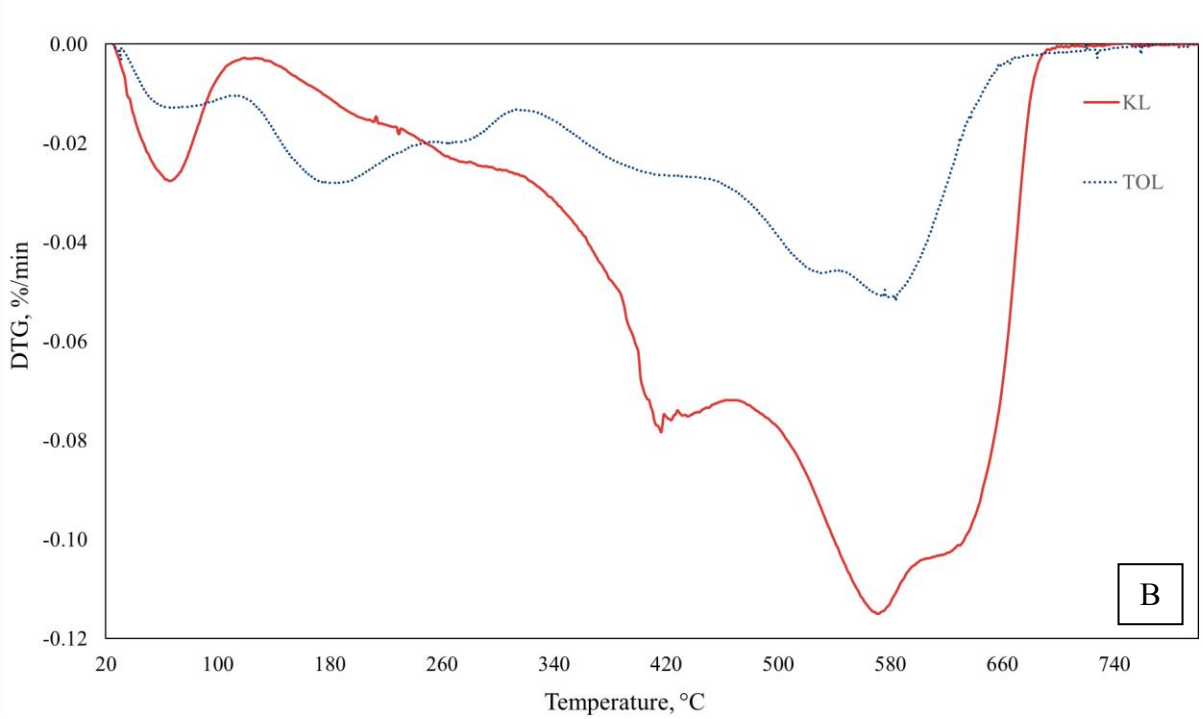
0.00
-0.02
-0.04
-0.06
-0.08
-0.10
-0.12
DTG, %/min
20
100
180
260
340
420
500
580
660
740
Temperature, °C
KL
TOL
B

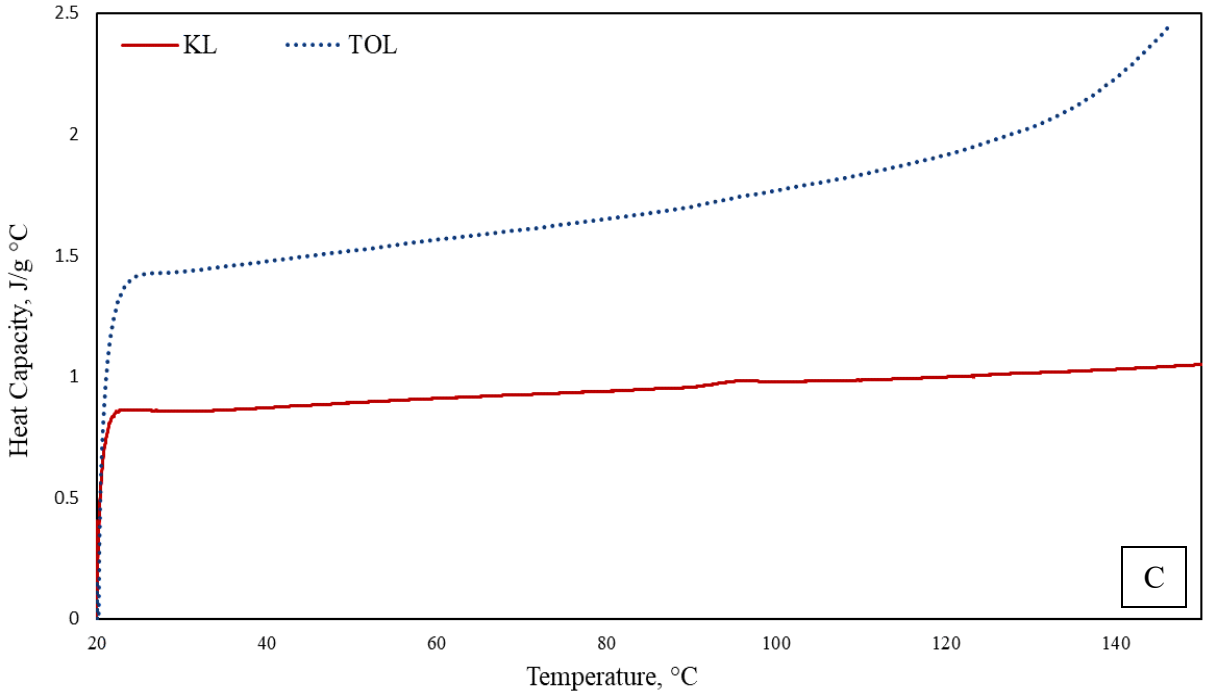

Figure S3.5. (A), Thermogravimetric curves of KL and TOL. (B), DTG curves of KL and TOL. (C) Heat capacity thermogram from DSC of samples KL and TOL from 20 °C to 150 °C.

Chapter 4: Generation of Sulphonated Lignin-Starch Polymer and its Use as a Flocculant

Jonathan A. Diaz-Baca, Ayyoub Salaghi, Pedram Fatehi*

Submitted to Biomacromolecules. 2022

Biorefining Research Institute and Chemical Engineering Department,

Lakehead University, 955 Oliver Road,

Thunder Bay, ON P7B SE1, Canada

*Corresponding author: email: pfatehi@lakeheadu.ca

The contribution of Jonathan A. Diaz-Baca to this work was performing experiments, formal analysis, writing and original drafting

4.1. Abstract

This paper reports the polymerization of tall oil lignin (TOL) and potato starch with 2-methyl-2-propene-1-sulphonic acid sodium salt (MPSA), a sulphonate-containing monomer, in a three-component system to generate flocculants for colloidal systems. By utilizing the advanced ^{1}H, COSY, HSQC, HSQC-TOCSY, and HMBC NMR techniques, it was confirmed that the phenolic substructures of TOL and the anhydroglucose unit of starch were covalently polymerized by the monomer to generate the three-block copolymer. The molecular weight, radius of gyration, and shape factor of the copolymers were fundamentally correlated to the structure of lignin and starch, as well as the polymerization outcomes. The deposition behavior of the copolymer, studied by a quartz crystal microbalance with dissipation (QCM-D) analysis, revealed that the copolymer with a larger molecular weight (ALS-5) deposited more and generated more compact adlayer than the copolymer with a smaller molecular weight on a solid surface. Owing to its higher charge density, molecular weight, and extended coil-like structure, ALS-5 produced larger flocs with faster sedimentation in the colloidal systems, regardless of the extent of agitation and gravitational force. The results of this work provide a new approach to preparing a lignin-starch polymer, i.e., a sustainable biomacromolecule, with excellent flocculation performance in colloidal systems.

Keywords: Lignin, Starch, Polymerization, Sulphonation, Flocculation

4.2. Introduction

Lignin is a non-cellulosic component of the woody material. Structurally, lignin is an amorphous and complex biopolymer composed of polyphenolic units.[1] A diversity of functional groups, such as hydroxyl, phenoxyl, carbonyl, carboxyl, and methoxy, make lignin a reactive material for various applications. Traditionally, lignin has been obtained as a by-product of pulp and paper

production. The LignoForce and LignoBoost processes were developed to commercially isolate lignin from the black liquor of kraft pulping processes.[2,3] LignoForce and LignoBoost kraft lignin (KL) has potential uses in producing bioproducts, such as flocculants, dispersants, carbon black, composite materials, and rubber reinforcers.[4,5] In addition to these processes, a new method named LignoTall was introduced and investigated for generating tall oil lignin (TOL) from the tall oil soap of softwood-based kraft pulping operation.[6] However, the potential applications of TOL have yet to be explored.

Since TOL has low solubility in water, modifying it with a highly hydrophilic polymer is a logical option for increasing its water solubility.[6,7] Starch is a natural and abundant polymer available at a relatively low production cost and is the primary form of polysaccharides found in various plant species.[8,9] Starch has an exceptionally high molecular weight and many hydroxyl groups, thus it is an excellent candidate for modifying TOL.[10,11] However, past studies primarily focused on the physical blending of starch and lignin,[12–16] and the generation of covalently bound starch-lignin macromolecule was rarely studied. Therefore, the first objective of this work was to make water-soluble TOL-starch copolymers with a high molecular weight.

To improve their inherent properties, distinct approaches have been followed to functionalize lignin and starch. In the past, the free radical polymerization of various monomers, such as acrylic acid, methacrylic acid, acrylamide, styrene, and methacryloyloxyethyl trimethylammonium chloride, has been successfully carried out on lignin and starch.[17–19] For instance, when anionically polymerized chains (i.e., polyacrylic acid) were introduced to the backbones of lignin or starch, it significantly increased its water solubility and flocculation efficiency.[20,21] For this purpose, most studies used lignin or starch in a binary polymerization system of synthetic and natural materials. In this work, lignin and starch were polymerized with a sulphonate-containing monomer via the

free radical polymerization technique in a three-component system to generate a sustainable product containing lignin and starch.

Several studies have focused on applying lignin-based or starch-based polymers as biobased flocculants in colloidal systems.[22–24] The introduction of different functional groups, such as amino, imino, ammonium, amide, carboxyl, and sulphonate, in the backbone of lignin or starch would render it a cationic or anionic polymer. Generally, these ionic biobased polymers can interact with the oppositely charged particles in colloidal systems, such as wastewaters, and act as flocculants.[25,26] Lignin-based flocculants have been extensively evaluated for flocculating cationic and anionic simulated wastewater, such as dyes, kaolin, aluminum oxide, and municipal wastewater.[27–29] Starch-based flocculants have also been used to flocculate dyes, kaolin, sodium humate, heavy metals, and industrial wastewaters.[30–32] However, the assessment of the flocculation performance of ternary anionic copolymers of TOL-starch, as a sustainable bioflocculant, has not been reported yet. Therefore, the current work aimed to identify the potential use of the TOL-starch copolymers as a flocculant of aluminum oxide particles in colloidal systems. In this work, the aluminum oxide colloidal system was selected as a representative system of the wastewater effluents generated in the refining process of mineral processes.[33]

Understanding the chemical structure of the copolymers is essential for discovering the flocculation mechanisms of polymers in colloidal systems.[23] Flocculants form flocs through charge neutralization, bridging, or patching mechanisms.[26] These mechanisms rely on the physicochemical interactions between the flocculant and the suspended particles, which are affected by the type of functional groups (e.g., sulphonate), charge density, shape, and molecular weight of the flocculant.[34-36] For synthetic polymers, the higher the molecular weight, the lower

the solubility.[22] Another objective of this work was to understand the chemical structure of the copolymers and their possible correlation with their interactions with particles in colloidal systems. In the past, 1D and 2D NMR spectroscopic methods were used to comprehensively characterize the chemical structure of complicated copolymers.[37–39] Learning from these studies, various 1D and 2D nuclear magnetic resonance (NMR) methods were used to elucidate the chemical structure of the anionic TOL-starch copolymers in this work. In addition, the solubility, molecular weight, shape factor, and thermogravimetric properties of anionic TOL-starch copolymers were determined. Moreover, the flocculation mechanism and performance of the produced polymer were evaluated with quartz crystal microbalance with dissipation (QCM-D), focused beam reflectance measurement (FBRM), Turbiscan and LUMiSizer instruments.

4.3. Materials and methods

4.3.1. Materials

Tall oil soap (TOS) was received from a mill in northern Ontario, Canada, which used softwood species to produce tall oil soap in a kraft pulping operation. TOS was subjected to an acidification process followed by solvent extraction to obtain tall oil lignin (TOL) as the primary raw material of this study.[6] Potato starch, ACS grade soluble (99.9 %, CAS 9005-84-9, amylose content 30.9 ± 0.2 %), 2-methyl-2-propene-1-sulphonic acid sodium salt (MPSA), sodium persulphate ($K_2S_4O_8$), sodium bisulphite ($NaHSO_3$), poly(diallyl dimethylammonium chloride) (PDADMAC) (100–200 kg/mol), sodium hydroxide (NaOH, 97%), sulphuric acid (H_2SO_4, 98%), potassium hydroxide (KOH) (8 g/mol), hydrochloric acid reagent grade (HCl) (37%), ρ-hydroxybenzoic acid, ethanol (95%), acetone (99.5%), hexane (mixture of isomers) (≥98.5%), sodium hydroxide (NaOH) (≥97.0%), lithium bromide (LiBr), tetrahydrofuran (THF) (99%), dimethyl sulfoxide (DMSO) (≥99.9%), dimethyl sulphoxide-d_6 (DMSO-d6) (99.9 %), and 3-(Trimethylsilyl)propionic-2,2,3,3-

d4 acid sodium salt tetramethylsilane (TSP) (≥98.5%) were all acquired from Sigma, Canada. Also, 0.45 μm Nylon and polypropylene membrane syringe filters were received from Fisher Scientific, Canada. Aluminum oxide (Al_2O_3) was purchased from Beta Diamond Products Inc., Yorba Linda, CA, USA. Lithium chloride (LiCl) was purchased from VWR, Canada. Potassium polyvinyl sulphate (PVSK) (100,000–200,000 g/mol, 97.7 wt.% esterified) was obtained from Wako Pure Chem. Ltd., Osaka, Japan. A dialysis membrane (1,000 g/mol cut off) was provided by Spectrum Labs.

4.3.2. TOL-starch-MPSA copolymerization reactions

The copolymerization of TOL, starch, and MPSA were carried out following a free radical polymerization mechanism in an aqueous environment under a nitrogen atmosphere in a 250 mL three-neck round bottom flask equipped with a magnetic stirrer. In this set of experiments, 1 g of TOL, 1 g of starch, and 0.7 or 3.6 g of MPSA were used in the reactions. The quantities of MPSA were selected as an MPSA/ (TOL + starch) average molar ratio of 1 and 5. The ratio of 1 was selected since the low monomer content of the monomer would produce a product with the maximum natural polymer (i.e., TOL + starch) content (75 wt.%). In contrast, the ratio of 5 was used since the high monomer content would produce a bioproducts with a lower content of biopolymers (35 wt.%). During the reactions, a blend of potassium persulphate and sodium bisulphite ($K_2S_2O_8$ and $NaHSO_3$, 1:1 weight ratio) was used as the initiator at 1.5 wt.% with respect to the total weight of lignin and starch. The copolymerization reactions were carried out at 80 °C and pH 11 for 3 h. Upon completion of the reactions, the reaction mixtures were cooled to room temperature, neutralized with HCl (0.5 mol/g), and kept in dialysis membrane tubes for 72 h to remove any inorganic salts and unreacted reagents. Subsequently, the purified products were dried in a vacuum oven at 50°C and used in this study. To facilitate the discussion in the following

sections, the copolymers generated with an MPSA to TOL molar ratio of 1 and 5 were named ALS-1 and ALS-5, respectively.

4.3.3. Elemental analysis

The elemental analysis was carried out following the combustion method for TOL, starch, and anionic TOL-starch copolymers.[40] The samples were oven-dried at 102 °C before examination. Approximately 2 mg of dried sample was combusted at 1200 °C to determine their carbon, hydrogen, nitrogen, and sulphur elements using an elemental analyzer (Vario EL cube, Elementar Analysensysteme GmbH, Germany). The oxygen content of the samples was determined via a mass balance from carbon, hydrogen, sulphur, and nitrogen on an inorganic-free basis.[40]

4.3.4. Solubility, charge density, and phenolic group analyses

The solubility of TOL, starch and anionic TOL-starch copolymers was determined, and the charge density and phenolic group were quantified for TOL-starch copolymers.[41]. The solubility of TOL, starch, and anionic TOL-starch copolymers was determined by adding 0.2 g of the polymers to 19.8 g of distilled water, while stirring for 12 h at 500 rpm at 25 °C in a stirring plate. Next, the suspensions were centrifuged at 1000 rpm for 5 min. The supernatants were gathered to analyze the charge density and solubility of the samples. The concentration of the samples in the supernatants was determined by drying the supernatants at 102 °C. The solubility was calculated based on the concentration of the samples in the supernatants and their initial concentrations in the solutions.

The charge density of the samples was determined by a Particle Charge Detector, Mütek PCD 04 titrator (BTG Instruments GmbH, Germany) via titrating against PDADMAC (0.005 M) or PVSK (0.005 M) solutions. In addition, the phenolic contents of the samples were measured using an automatic potentiometric titrator (785 DMP Titrino, Metrohm, Switzerland). About 0.06 g of

dried samples was added to 100 mL of deionized water containing 1 mL of 0.8 mol/L potassium hydroxide in a 250 mL beaker. After stirring at 200 rpm for 5 min, 4 mL of 0.5% para-hydroxybenzoic acid solution was added as an internal standard. Then, the solution was titrated against 0.1 mol/L HCl. The volume of HCl consumed to decrease the pH of the sample solution to specific endpoints is noted as V1′ (pH 10), V2′ (pH 7) and V3′ (pH 3), and their corresponding endpoints for blank solutions (without sample) are noted as V1, V2 and V3, respectively. The phenolic hydroxyl group content of the samples was calculated according to Eq. (1). Results are the average of three independent measurements.

$$\text{Phenolic hydroxyl group content}\left(\text{mmol}/\text{g}\right) = \frac{C_{\text{HCL}}\ [(\text{V2}' - \text{V1}') - (\text{V2} - \text{V1})]}{m} \quad (1)$$

In this equation, C_{HCL} is the concentration of HCl solution as the titrant, 0.1 mmol/L, and m is the mass (g) of the samples.

4.3.5. NMR experiments

In this analysis, 70 mg of previously dried TOL (60 °C, 24 h) were added to 1000 µL of DMSO-d_6, and 70 mg of starch and TOL-starch polymers were added to 1000 µL of 0.5 wt.% LiBr in DMSO-d_6.[42] All samples were stirred for 18 h at 25 °C. Proton nuclear magnetic resonance (^{1}H-NMR), two-dimensional homonuclear correlation spectroscopy (^{1}H–^{1}H COSY), multidimensional NMR spectra, heteronuclear single quantum coherence (^{1}H-^{13}C HSQC), HSQC total correlation spectroscopy (^{1}H-^{13}C HSQC-TOCSY) and heteronuclear multiple bond correlation (^{1}H-^{13}C HMBC) experiments were performed for these samples. The NMR experiments were obtained using nuclear magnetic resonance spectroscopy (AVANCE NEO-1.2 GHz, Bruker Corporation, USA). Adjustments for ^{1}H-NMR and ^{1}H–^{1}H COSY were as follows: ^{1}H-NMR: 64 number scans and a 90° pulse with a relaxation delay of 1.00 s. The multidimensional NMR spectra were obtained by the Bruker pulse programs "hsqcetgpsisp2.3, "hsqcdietgpsisp.2", and "hmbcgplpndqf"

for ^{1}H-^{13}C HSQC, ^{1}H-^{13}C HSQC-TOCSY, and ^{1}H-^{13}C HMBC, respectively. The following Bruker pulse sequences were implemented: 13 ppm spectra width in the F2 (^{1}H) dimension with 2048 data points (155 ms acquisition time), 165 ppm spectra width in the F1 (^{13}C) dimension with 256 data points (6.1 ms acquisition time), a 1.5 s pulse delay, $^{1}J_{C\text{-}H}$ of 145 Hz and 48 scans.[43] All NMR experiments were carried out at 70 °C.[44] TSP was used as the internal standard for all samples and calibration of the correlation peaks (δ_C/δ_H 0.0/0.0 ppm). The NMR data points were processed using the TopSpin 4.0.9 software (2020 Bruker BioSpin GmbH).

4.3.6. Molecular weight, radius of gyration, and hydrodynamic radius determination

The static light scattering (SLS) technique was performed to determine the absolute molecular weight (MW) and radius of gyration (R_g) of TOL, starch, and anionic TOL-starch polymers. The dynamic light scattering (DLS) technique was used to determine the samples' hydrodynamic radius (R_h). A laser light scattering system attached to a goniometer (BI-200SM, Brookhaven Instruments Corporation, USA) was used for analyzing the samples. The maximum solid-state laser power used in the experiment was 35 mW at 637 nm. Measurements were performed at 25 °C and different scattering angles within the range of 20° and 155° for SLS while using a fixed scattering angle of 90° for DLS. Samples of TOL, starch, and anionic TOL-starch polymers were dissolved in 20 mL of 8% w/v DMSO/LiCl solution and stirred overnight at 25 °C. The different aliquots of the polymer solutions were prepared at different concentrations (0.1 to 2.4 mg/mL) for SLS, whereas aliquots of 1 g/mL were used for DLS.[45] Before the measurements, all the solutions were filtered twice with 0.45 μm polypropylene membrane syringe filters. The absolute molecular weight and radius of gyration were calculated from the SLS results, and the Berry plot was analyzed by the instrument software (Brookhaven Instruments Corp). The R_g and R_h values were

combined to obtain the shape factor, ρ, by calculating the R_g/R_h ratio.[46] Reported results are the average of three independent measurements.

4.3.7. Thermal stability analysis

Differential scanning calorimetry (DSC) was used to determine the samples' glass transition temperatures (T_g). Approximately 10-12 mg of dried TOL, starch, and anionic TOL-starch polymers were placed in a Tzero® aluminum pan and tested by a differential scanning calorimeter (DSC Q2000, TA Instruments, USA). The analysis was performed under a nitrogen atmosphere at 50 °C/min. In the DSC analysis, the temperature was raised from 20 °C to 230 °C, which was used to erase thermal history, then the temperature dropped to 20 °C at 5.0 °C/min to cool down the samples, and the second heating cycle was conducted from 20 °C to 230 °C at 10.0 °C/min. The evaluated results were generated in the second heating cycle. In addition, thermogravimetric analysis (TGA) was performed to investigate the thermal response of TOL, starch, and anionic TOL-starch copolymers. Samples (7-8 mg) were dried in an oven at 60 °C for 24 h prior to the analysis. The analysis was performed under a nitrogen atmosphere in a thermal analyzer (TGA i1000, Instrument Specialists Inc., USA) at a 15 mL/min flow rate and heated from 25 °C to 800 °C at the rate of 5 °C/min.

4.3.8. Adsorption analysis onto a model surface

The adsorption mechanism of TOL, starch, and anionic TOL-starch polymers onto aluminum oxide surfaces was conducted using a Quartz crystal microbalance with dissipation (QCM-D 401, E1, Q-Sense Inc., Sweden).[47,48] This work used aluminum oxide-coated crystal sensors (5 MHz, RenLux Crystal LTD) as a model surface for the adsorption analysis. Samples were prepared (0.1 wt.% solutions) with Milli-Q grade water at pH 7 and stirred for 18 h. The designed solutions were injected through the chamber of the QCM instrument using a peristaltic pump at a flow rate of

0.15 mL/min and 25 ± 2 °C.[49] Milli-Q grade water was used as a buffer solution to establish a constant baseline for all samples. Two minutes after the baseline was steady using the buffer solution, the sample solutions were introduced to the sensor for analysis. Once the adsorption on the sensor was achieved, the buffer solution was introduced to remove any loose or non-adsorbed polymer from the sensor's surface. The shifts in frequency (F) and dissipation (D) of the sensors were monitored. Data from the 3rd overtone was used for the analysis and data modeling. To describe the QCM-D data, viscoelastic modeling and data fitting were carried out. The Voigt model representation was used as the shift in $D > 0$, and the harmonics of overtones were sufficiently separated.[50] The data analysis and time monitoring were conducted using the Q-Tools software (Q-Sense, Sweden).

4.3.9. Flocculation performance

Flocculation analysis under dynamic conditions. The flocculation performance of the polymers in the aluminum oxide suspension was assessed using a focused beam reflectance measurement (FBRM, Particle Track E25, Mettler-Toledo, USA). The instrument determined the chord length (i.e., the distance between the two edges of a particle or a floc) and the number of flocs (counts).[51] The data was acquired using 90 log channels over 1–1000 μm by the iC-FBRM software (version 4.4.29).[52,53] In this set of experiments, a laser probe having a diameter of 25 mm was placed in 200 mL of aluminum oxide suspensions (20 g/L) and stirred at 250 rpm. The beam was rotated around the axis of the probe at the scanning speed of 2 m/s with a scan diameter of 5 mm. The focal point was set to − 20 μm (as default), and the scan duration was set at 3 s. After reaching steady-state conditions, desired volumes (100–2000 μL) of polymer solutions (0.2 wt.%) were successfully added to the aluminum oxide suspensions until the optimal dosage was reached. The optimal dosage was defined as the one that produced the largest mean chord length before deflocculation

occurred due to overdosing.[54] The software evaluated and defined the number-weighted mean chord length (mean chord length).

Sedimentation analysis. The sedimentation behavior of aluminum oxide suspensions in the absence and presence of the polymers was assessed using a vertical scan analyzer, Turbiscan Lab Expert (Formulation, France). In this set of experiments, the optimum dosages of TOL, starch, ALS-1, and ALS-5 (2, 80, 18, and 16 mg/g, respectively) were added to aluminum oxide suspensions (5 g/L concentration) and stirred at 150 rpm for 30 min. The analysis was conducted as explained in previous studies.[55,56] The samples were vertically scanned at 880 nm wavelength every 2 s at 25 °C for 60 min. The efficiency of the studied polymers in flocculating particles was analyzed from the destabilization index (TSI) of the suspensions, which provides evidence for settling particles. The larger the TSI, the more unstable the suspension system would be, indicating more settling of particles.[56]

Sedimentation velocity analysis. A dispersion stability analyzer, LUMiSizer (LUM GmbH, Germany), was used for monitoring the settling velocity of aluminum oxide particles at 25 °C.[57] The aluminum oxide suspensions were exposed to various centrifugal forces, facilitating the sedimentation of the particles at different relative centrifugal force (RCF), which is the centrifugal force ratio to the earth's gravitation force applied to a particle.[58] Aluminum oxide suspensions were prepared at a 5 g/L concentration and pH 7. The optimum dosages of TOL, starch, ALS-1 and ALS-5 (2, 80, 18, and 16 mg/g, respectively) solutions were added to the aluminum oxide suspensions. All samples were placed into the LUMiSizer cells to be subjected to different gravitational forces. In the instrument, the light source was emitted through the samples at λ=865 nm, and the local transmission was recorded every 2 s over the entire cell length.[59]

4.4. Results and discussion

4.4.1. NMR characterization

H^1 and ^1H–^1H COSY NMR analysis. The ^{1}H-NMR (1D) spectra of TOL, starch, and anionic TOL-starch copolymers are depicted in Figure 4.1. Typically, there are three important identified regions in the spectrum of lignin; the signals at the 6.00-7.50 ppm region attributing to the aromatic H, 4.00-6.00 ppm region attributing to the H of interunit carbon of the lignin's side chain (particularly β position), and at the 0.00-2.50 ppm region attributing to the aliphatic H.[60] In addition to the mentioned three major regions, the signal from 3.50 to 4.10 ppm is attributed to the methoxy group of lignin.[61]

In the 1D spectrum of starch, the signal at the 5.40-5.50 ppm region is attributed to the -OH of C2 and C3 in the anhydroglucose unit (AGU) of the starch structure. Moreover, the signals attributing to H_1-(1→4 linkage) and H_1'-(1→6 linkage) appear at 4.90 and 5.10 ppm, respectively.[7,62] Regarding the anionic TOL-starch copolymers, the detected signals of the 4.50-5.80 ppm region are consistent with the signals for starch in the 1D spectra, which proves the presence of starch in the chemical structure of these copolymers (Figures 4.2 and 4.3).[42] At the same time, the signals of the 6.00-7.50 ppm region prove the presence of TOL in the anionic TOL-starch copolymers. No signs of structural differences were found between the spectra of ALS-1 and ALS-5.

With the aid of 2D-COSY, the overlapped signals from 1D and the signals of adjacent ^{1}H resonances were identified, as depicted in Figure 4.2. The contour cluster signals appearing in diagonal (diagonal-peak) correspond to the ^{1}H shift. The symmetrical off-diagonal contour signals (cross-peaks) are found from coupling H shifts on the horizontal (F_1) and vertical axes (F_2). The connection between diagonal and cross peaks establishes their vicinity among the carbon chain in the chemical structure.[63] The cross-peak found at 6.80 and 7.80 ppm (Figure 4.2a) is attributed to

the H in its phenolic hydroxyl group of the TOL.[64] It is worth mentioning that this signal is not found intensely in the spectra of the copolymers (Figure S4.1, Supporting Information), indicating the involvement of the phenolic hydroxyl group of TOL in the copolymerization reactions. As seen in Figures 4.2 (c and d), the diagonal peak detected at 3.60 ppm is assigned to the H of C_1 in the propene unit of MPSA, which confirms its presence in the structure of the anionic TOL-starch copolymers. No visible differences were found between ALS-1 and ALS-5, as only the length of the polymerized MPSA chain would have changed in the polymerization reaction, which will be discussed later.

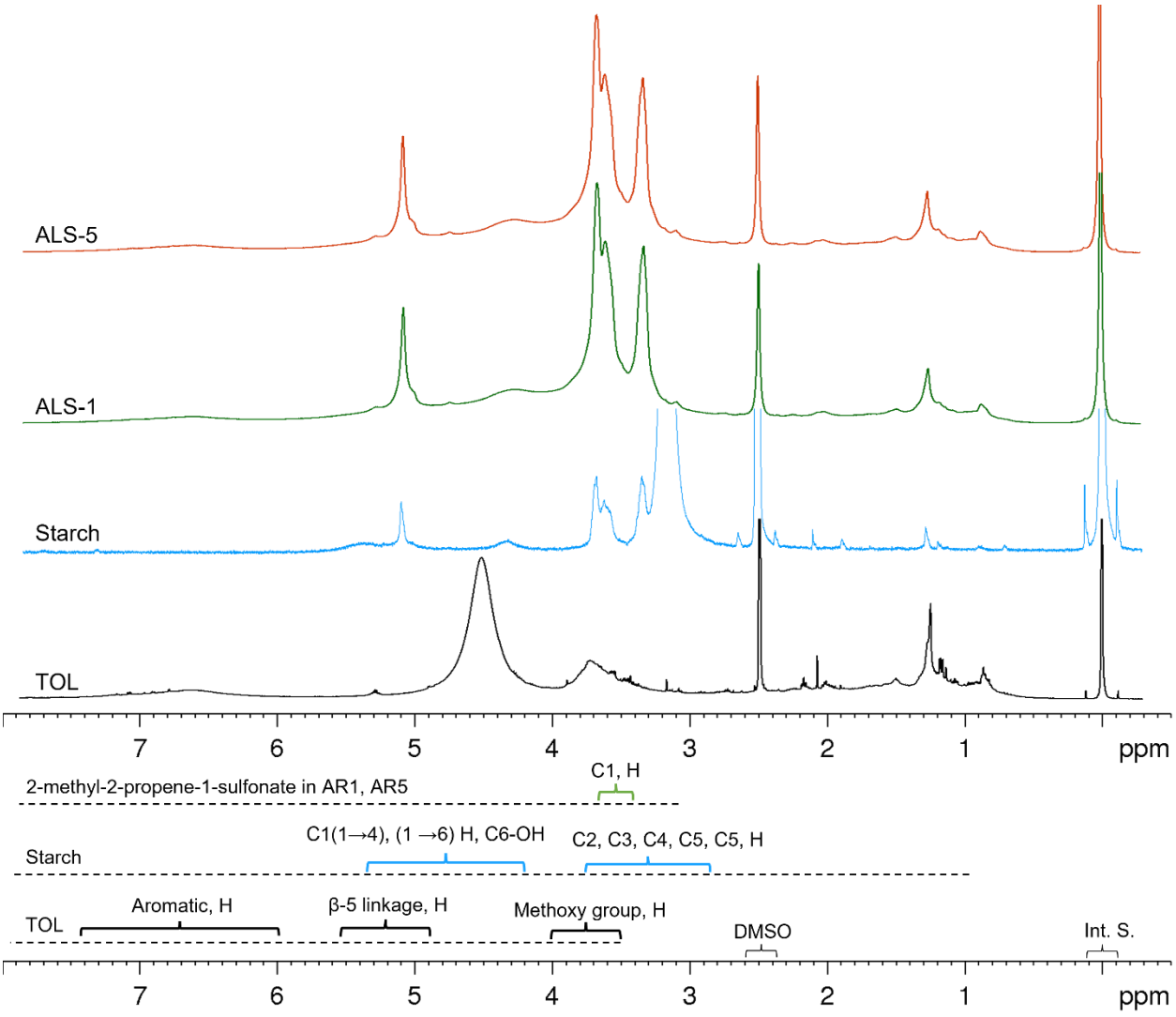

Figure 4.1. ^{1}H-NMR spectra of TOL, starch, ALS-1, and ALS-5. DMSO-d6 was used as solvent, and TSP as internal standard.

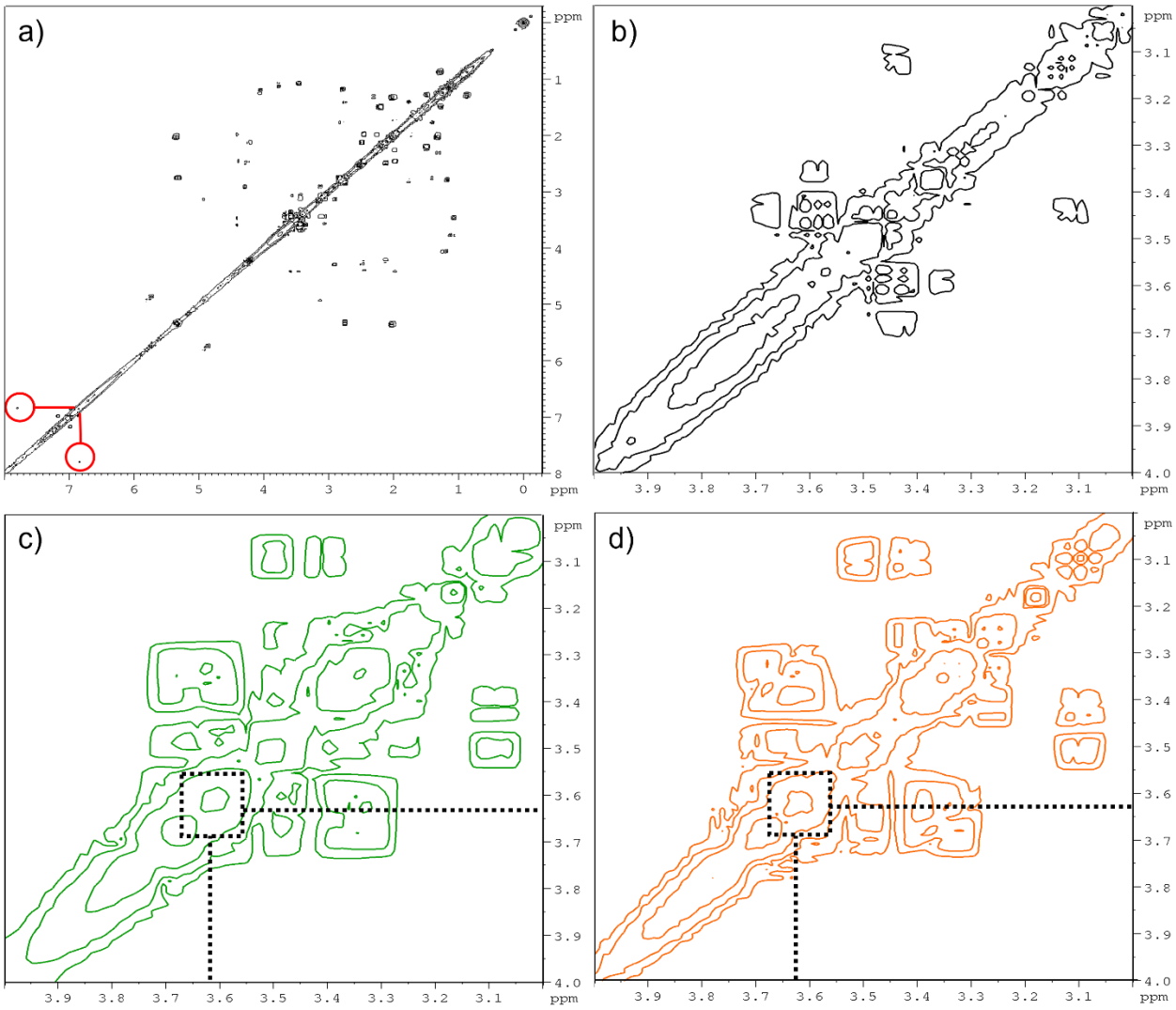

Figure 4.2. ^{1}H–^{1}H COSY spectra of TOL (a and b), ALS-1 (c), and ALS-5 (d). Red circles in a) indicate the cross-peak of the H from phenolic hydroxyl of TOL. Doted square in c) and d) indicates the diagonal peak of the H from the propene unit of MPSA.

^{1}H-^{13}C HSQC, ^{1}H-^{13}C HSQC-TOCSY and ^{1}H-^{13}C HMBC analysis. The ^{1}H-^{13}C HSQC spectra of TOL, starch, and anionic TOL-starch copolymers are displayed in Figure 4.3, where the signal from C is observed in the Y-axis (F1), and H is observed in the X-axis (F2). This analysis made it possible to determine the H-C single-bond correlations of polymers (Table 4.1). The cross-peaks

of TOL substructures (Figure 4.3a) are visible at the δ_C/δ_H of 58.10/3.70, 108.30/6.50, and 117.30/6.70 ppm for the methoxy groups, syringyl groups, and guaiacyl aromatic subunits, respectively.[65] A main particularity of TOL is the predominance of phenylcoumaran units with β-5' linkages in its structure, as is observed in the cross-peak of δ_C/δ_H 64.80/3.50 ppm.[6,66] Regarding the starch structure (Figure 4.3b), the cross-peak of δ_C/δ_H at 101.60/5.20 ppm is identified for the C1; and the cross-peaks at 62.20-80.60/3.40-3.70 ppm are associated with the C2 to C6 of the anhydroglucose unit (AGU).[62] The assignments related to the aromatic subunits, methoxy groups, and the AGU are in the anionic TOL-starch copolymers. There is a weaker signal from the aromatic subunits of the anionic ALS copolymers than that of TOL, indicating a structural change in these substructures due to the polymerization reactions that occurred in the phenolic OH group of TOL. Additionally, the cross-peaks at 80.55/3.65 and 80.55/3.70 ppm are assigned to the propene unit of MPSA. Therefore, these observations confirm that ALS-1 and ALS-5 contain TOL, starch, and MPSA as part of their structure (Scheme 4.1 1) resulting from the radical copolymerization reactions. No significant differences were observed between ALS-1 and ALS-5 in Figures 4.3 (c and d), indicating that the chemical structure and linkages are alike between the two copolymers. The extended HSQC NMR spectra can be found in the Supporting Information (Figure S4.2).

Table 4.1. NMR signal assignments of TOL, starch, and MPSA from $^{1}H–^{13}C$ HSQC NMR spectroscopy.

Assignment	TOL	Starch	MPSA
	δ_C/δ_H (ppm)	**δ_C/δ_H (ppm)**	**δ_C/δ_H (ppm)**
C-H in -OCH_3 (methoxy)	58.10/3.70	-	-
Cγ-Cγ in β-5' substructures	64.80/3.50	-	-

$C_{2,6}$-$H_{2,6}$ (syringyl)	108.30/6.50	-	-
$C_{5,6}$-$H_{5,6}$ (guaiacyl)	117.30/6.70	-	-
$C_{2,6}$-$H_{2,6}$ (*p*-hydroxyphenyl)	125.65/7.15, 6.95	-	-
$C_{2,6}$-$H_{2,6}$ (*p*-hydroxybenzoate)	130.1/7.30		-
C6 (AGU)	-	62.25/3.72, 3.63	-
C5 (AGU)	-	73.17/3.65	-
C2 (AGU)	-	73.65/3.35	-
C3 (AGU)	-	74.72/3.71	-
C4 (AGU)	-	80.60/3.39	-
C1' (AGU)	-	96.74/4.92	-
C1 (AGU)	-	101.60/5.15	-
H of C_1 (propene)	-	-	80.55/3.65

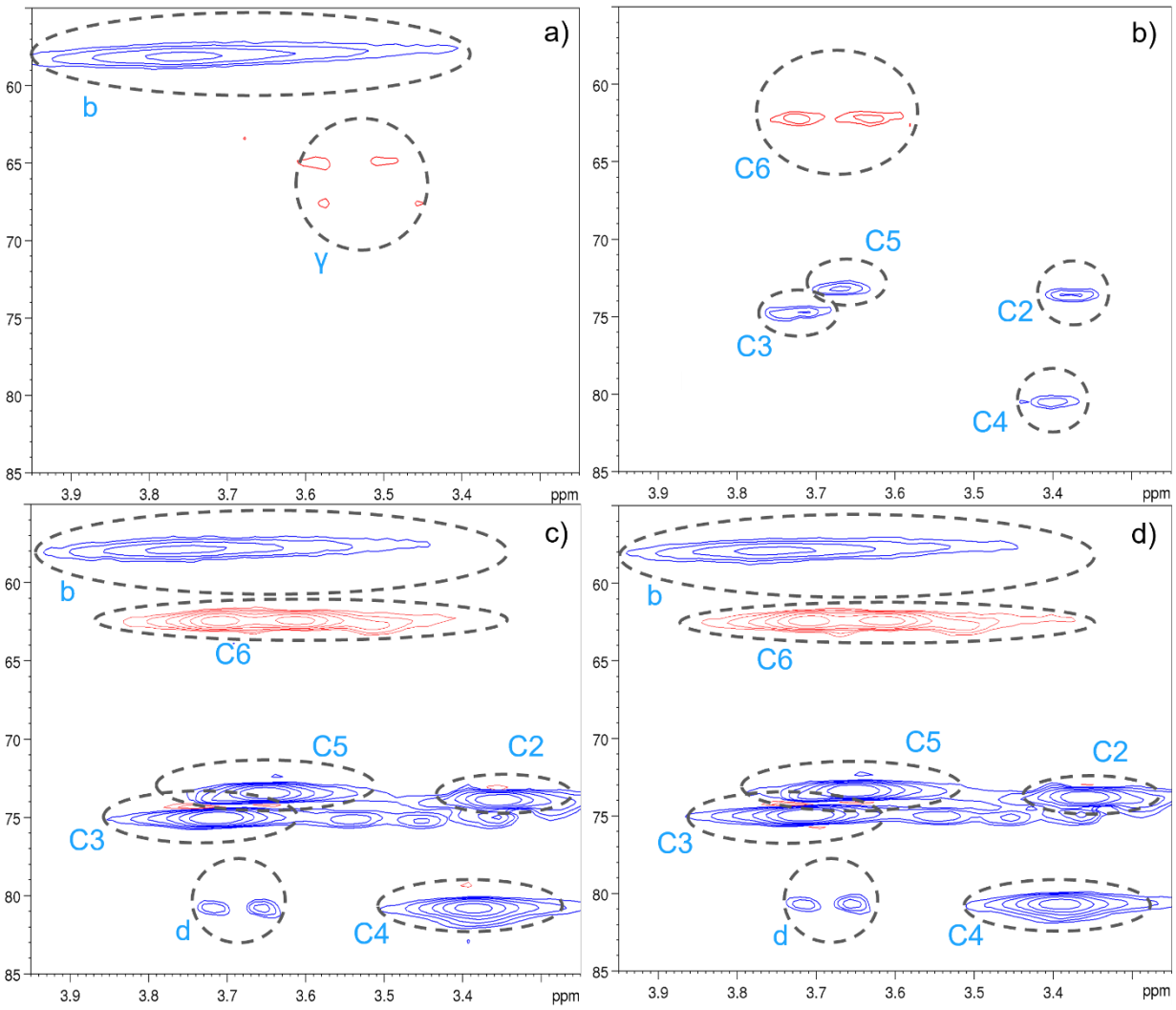

Figure 4.3. ^{1}H-^{13}C HSQC NMR spectra of TOL (a), starch (b), ALS-1 (c), and ALS-5 (d). Cross-peaks corresponding to CH_1 or CH_3 groups appears in blue (positive region), while cross-peaks of CH_2 appear in red (negative region). The labels are assigned as described in the chemical structure shown in Scheme 4.1e.

The ^{1}H-^{13}C HSQC-TOCSY experiment identified coupling networks in the anionic TOL-starch copolymers (Figure 4.4). The HSQC-TOCSY is a useful tool to elucidate the structure of molecules with overlapping ^{1}H and ^{13}C signals that HSQC or homonuclear experiments cannot assign.[67] In the TOCSY experiments, a proton or carbon can correlate with all other protons in its coupling network.[68] No TOCSY correlations were identified for TOL in the analyzed AGU (anhydroglucose unit) region (3.1 ppm-5.2 ppm, 60.0 ppm-105.0 ppm).[69] Only the signal

corresponding to the Cγ of the β-5 linkage was observed (Figure 4.4a). The corresponding spectrum for the aromatic region of TOL can be found in the Supporting Information (Figure S4.3). For starch (Figure 4.4b), the TOCSY correlations were only observed between C1 and C2 at the δ_C of 73.75 ppm because of the lack of resolution related to the low solubility of the pristine starch. Interestingly, the solubility enhancement of the anionic copolymers facilitates a better resolution in the HSQC-TOCSY experiments compared to that of starch, which indicates the rupture of the starch's granules and loss of its native structure. The TOCSY correlations between C1 and the AGU's carbons of C4, C3, and C5 were observed at δ_C = 80.60, 74.72, and 73.17 ppm, respectively.[69] Furthermore, TOCSY correlations between the C1 and the protons in C6 and C2 in the AGU were observed at δ_H = 3.63 ppm and 3.35 ppm. These correlations were identified for ALS-1 and ALS-5 (Figures 4.4c and 4.4d). These observations indicate that the pyranose ring of the AGU was not cleaved by the conditions of the polymerization reactions, which is linked to the propene unit of MPSA, as displayed in Scheme 4.1.

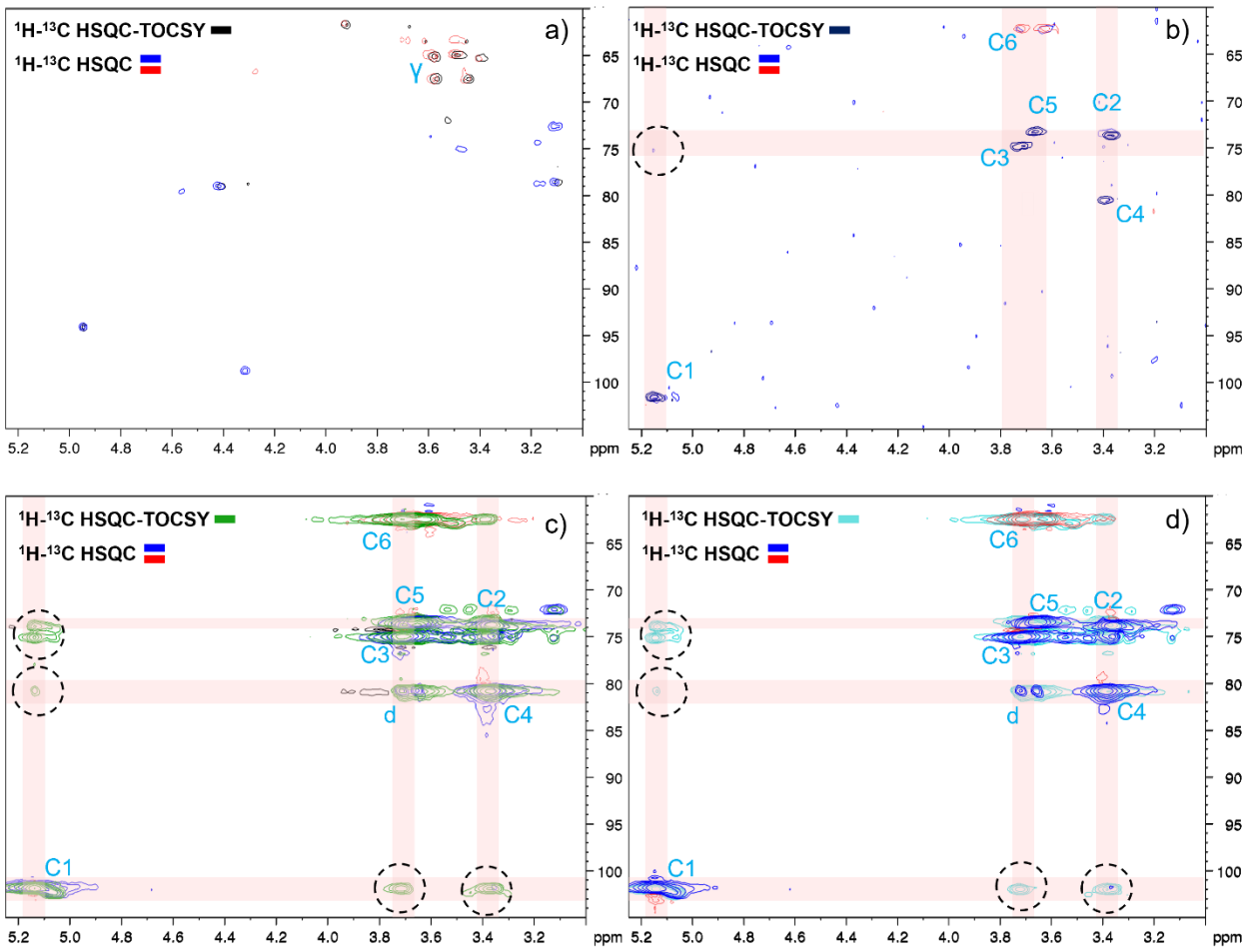

Figure 4.4. ^{1}H-^{13}C HSQC-TOCSY and ^{1}H-^{13}C HSQC overlaid NMR spectra of TOL (a), starch (b), ALS-1 (c), and ALS-5 (d). Dotted circles indicate TOCSY correlations of carbons (horizontal) and protons (vertical). The labels are assigned as described in the chemical structure shown in Scheme 4.1e.

To further analyze the chemical structures and linkages present in the anionic TOL-starch copolymers, the ^{1}H-^{13}C HMBC NMR experiment was performed (Figure 4.5). With the aid of ^{1}H-^{13}C HMBC experiments, it was possible to correlate the H and C related or separated by two, three, or four bonds, even over non-carbon bonds, such as ether bonds.[68,70] The overlaid HMBC and HSQC spectra for ALS-1 and ALS-5 are observed in Figures 4.5a and 4.5b, respectively. The overlaid NMR spectra showed the correlations of C1 in the AGU (anhydroglucose unit) at the δ_C /δ_H of 101.60/5.15 ppm and C2, C4, and C5 observed at the δ_C of 73.65, 80.60, and 73.17 ppm,

correspondingly. The correlations from C1 to C5 confirm that the anionic copolymers contain the pyranose ring from starch after the polymerization reactions. The HMBC analysis also revealed that the C of (δ_C = 80.55 ppm) the propene unit on MPSA in the anionic polymers was presented and coupled with the H of C5 and C6 of the AGU as is schematized in Scheme 4.1e. These NMR results confirmed the presence of a covalent linkage between the AGU of starch and the polymerized MPSA chain. They demonstrated the phenolic substructure's involvement in this copolymerization, resulting in the ALS-1 and ALS-5 ternary structures.

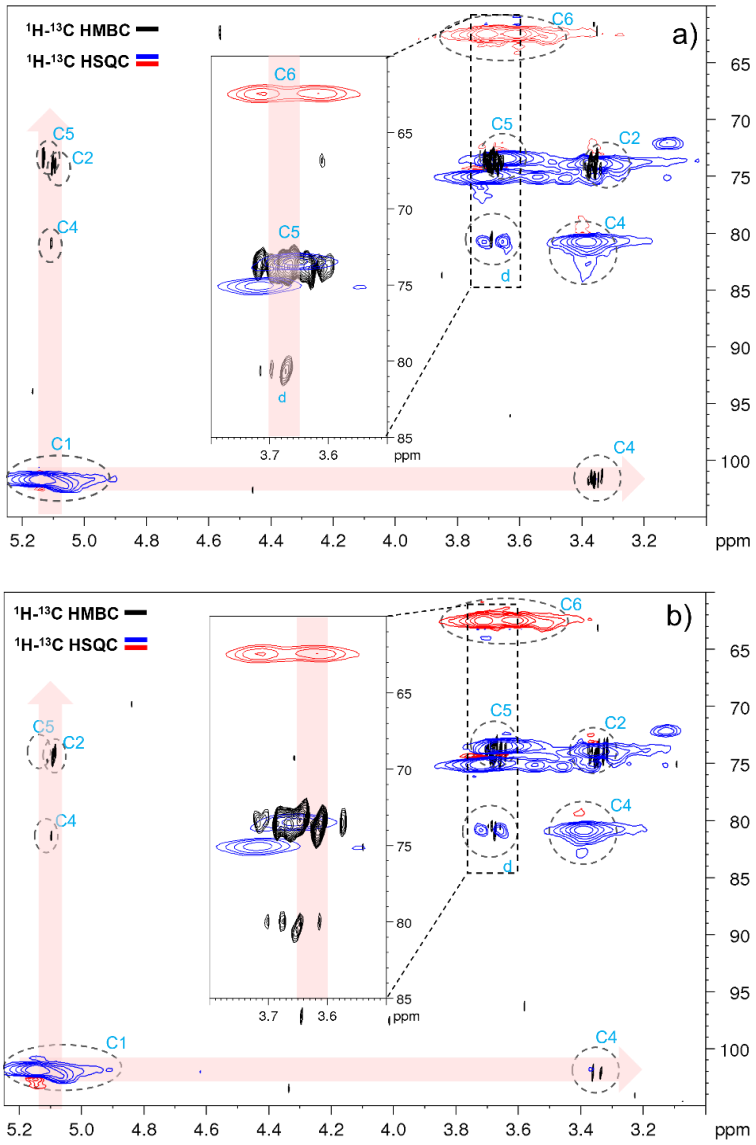

Figure 4.5. Partial ^{1}H-^{13}C HSQC (blue/red) and ^{1}H-^{13}C HMBC (black) overlaid NMR spectra of ALS-1 (a) and ALS-5 (b).

4.4.2. TOL-starch-MPSA copolymerization reaction

The proposed copolymerization reaction pathway and the chemical structures of the anionic TOL-starch copolymers are displayed in Scheme 4.1. The pH of the reaction medium was adjusted to 11 to allow the solubilization of TOL and starch by disrupting the interchain hydrogen bonding.[71] The copolymerization reactions of TOL, starch, and MPSA were carried out following a free radical polymerization mechanism. First, the initiator ($K_2S_2O_8$ and $NaHSO_3$) was activated by heat, producing sulphate and sulphite radicals (Scheme 4.1a), which reacted with TOL (Scheme 4.1b), MPSA (Scheme 4.1c), and starch (Scheme 4.1d), to generate their radical forms. The formation of phenoxy radicals in TOL and C6-hydroxy radicals in starch developed very reactive sites in both biopolymers, which would facilitate the polymerization of MPSA bridging TOL and starch to create ternary anionic TOL-starch copolymers (Scheme 4.1f).[72,73] Amylopectin is a highly branched and compact structure, and its steric hindrance makes it less susceptible to undergoing chemical reactions.[74,75] Hence, the polymerization reactions between starch and MPSA monomer would prefer the more accessible and linear amylose chains, as shown in Scheme 4.1e.[76] Overall, the NMR results discussed in this work confirmed the success of the copolymerization reactions, producing ternary anionic TOL-starch copolymers. No chemical differences were found between ALS-1 and ALS-5, which suggests that both ternary anionic copolymers had similar chemical structures.

a)

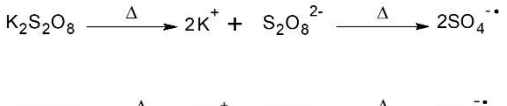

b)

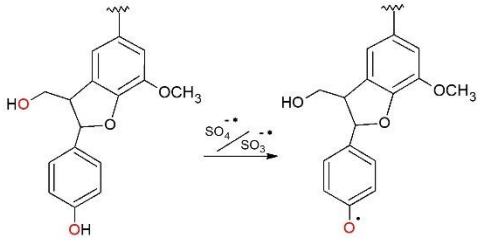

c)

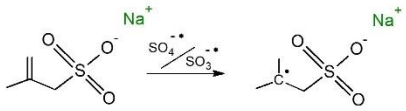

d)

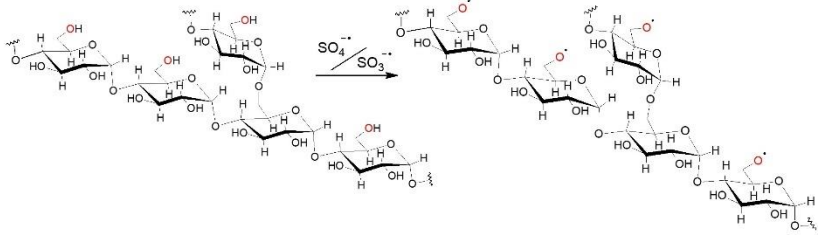

e)

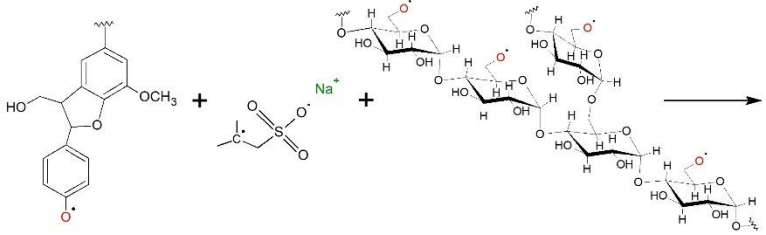

f)

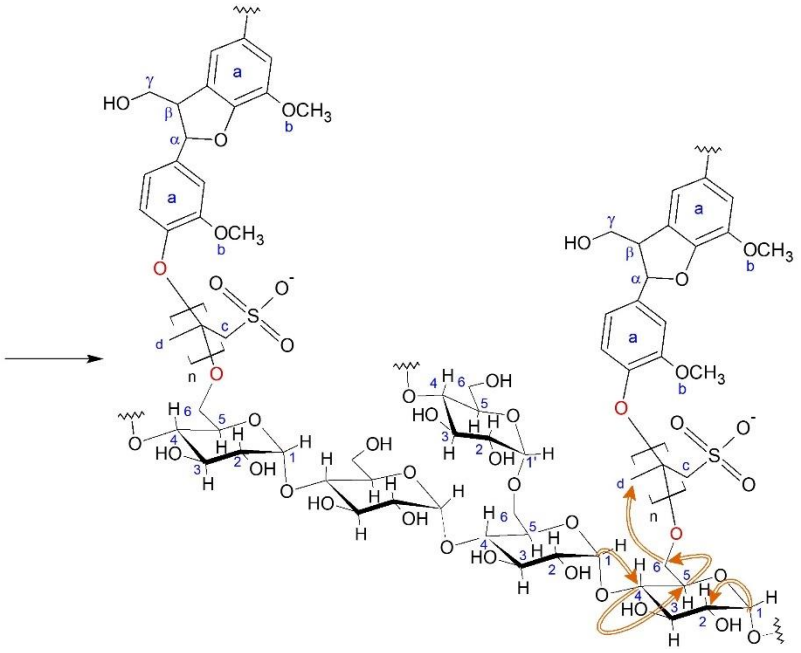

Scheme 4.1. Proposed reaction mechanism of copolymerization of TOL-starch with MPSA (a-f). Chemical structure of the anionic TOL-starch ternary copolymers revealed by 1D and 2D NMR analysis (e).

4.4.3. Solubility, charge density, and elemental composition

The results for water solubility and charge density of TOL, starch, and anionic TOL-starch copolymers are depicted in Table 4.2. As detailed in previous work,[6] the solubility of TOL in water was low (13%). The low water solubility of TOL impeded the accurate determination of its charge density, and hence, it is not reported. However, after the copolymerization reactions, the water solubility of anionic TOL-starch copolymers increased to about 37-40%. Interestingly, the charge density and solubility of the anionic copolymers depend on the MPSA ratio, as the charge density is associated with the presence of the sulphonate group in MPSA (Table 4.2).

The carbon, hydrogen, nitrogen, sulphur, and oxygen contents of TOL, starch, and anionic TOL-starch copolymers are also summarized in Table 4.2. In general, the generated anionic copolymers are expected to contain more H and O elements than TOL since starch and MPSA with a higher H and O were attached to TOL via the polymerization reaction.[77] Additionally, the sulphur content of the anionic copolymers originating from the sulphonate groups of MPSA was significantly lower than that of TOL. The grafting of starch can explain this decrement, as attaching a sulphur-free polysaccharide to lignin decreases the sulphur content of the sample. Moreover, during the purification of the polymers, the sulphur salts, which were naturally present in the TOL, were removed, contributing to the lower sulphur content of the product.

Table 4.2. Solubility, charge density and elemental composition of TOL, starch and anionic TOL-starch copolymers.

Sample	Solubility (%)	Charge density (mmol/g)	C (%)	H (%)	N (%)	S (%)	O (%)[a]
TOL	13	ND	53.7 ± 0.9	4.8 ± 0.1	0.1 ± 0.0	7.3 ± 2.5	34.1 ± 3.4
Starch	10	ND	42.6 ± 0.2	6.7 ± 0.1	0.0 ± 0.0	0.0 ± 0.0	50.6 ± 0.3
ALS-1	37	0.7	47.1 ± 0.1	8.1 ± 0.1	0.1 ± 0.0	0.4 ± 0.1	43.6 ± 0.1
ALS-5	40	0.9	47.5 ± 0.8	7.8 ± 0.5	0.0 ± 0.0	0.6 ± 0.2	44.0 ± 1.2

ND, not determined

± standard deviation

[a] calculated by the difference

Phenolic group content, molecular weight, and radius of gyration determination. The phenolic hydroxyl group content of TOL, starch, and anionic TOL-starch copolymers are presented in Table 4.3. The presence of phenolic hydroxyl groups in the anionic copolymers is attributed to the presence of TOL in their chemical structures. Based on the results, the concentration of the phenolic hydroxyl group of anionic TOL-starch copolymers was lower than that of TOL. As shown in Table 4.3, ALS-5 possesses the lowest amount of phenolic hydroxyl group (0.90 mmol/g) among the polymers. A lower concentration of phenolic hydroxyl groups in the copolymers is associated with a higher grafting ratio of MPSA to TOL, as more active phenolic sites are occupied after the reaction.[78]

The MW and R_g of TOL, starch, and anionic TOL-starch copolymers are also summarized in Table 4.3. As expected, starch showed a significantly larger MW and R_g than TOL did. As discussed in previous studies, the association between MW and R_g is closely related to the degree of polymerization and branching of polymers.[79–81] As tabulated in Table 4.3, the anionic copolymers presented a higher MW and R_g than TOL but lower than starch did. The lower MW of the ALS1

than that of starch can be attributed to the loss of the native structure of starch macromolecules. During the polymerization reactions at a high temperature, the starch macromolecule would undergo a series of random hydrolysis and peeling reactions, producing hydrolyzed starch, which would then react with MPSA to yield the final anionic product. The procedure for corroborating the hydrolysis and peeling reactions of starch is described in the Supporting Information. When starch was treated under the same reaction conditions of the polymerization in the absence of other chemicals, the light scattering analysis confirmed the MW of 690×10^3 g/mol and R_h of 28 nm for hydrolyzed starch in this work. These reactions would mainly occur on the linear amylose chain of starch in an alkaline environment, as reported earlier.[82–84] Among the anionic TOL-starch copolymers, the higher MW and R_g (11000 $\times10^3$ g/mol and 71 nm, respectively) were observed for ALS-5 than for ALS-1 (1800 $\times10^3$ g/mol and 23 nm, respectively). From these results, it is evident that the molar ratio of chemicals in the polymerization reaction caused the formation of a bulkier copolymer by generating more and larger polymeric chains of MPSA, TOL and starch. However, as the sulphur content of the copolymer was not significant in the ALS copolymer (Table 4.2), but the copolymer had a higher MW, R_h, and R_g than TOL and starch (Table 4.3), it can be stated that MPSA facilitated the linkage of TOL and starch, and the copolymers had perhaps higher starch and TOL contents even though it was not possible to quantify their actual proportions in the copolymers in this work.

The shape factor was obtained from the data of R_g/R_h. Combining these two size determinations made it possible to get the polymer shape, which depends on the polymer architecture and spatial in-solution distribution.[46] Typically, when R_g is smaller than R_h ($R_g/R_h \leq 0.775$), the polymer shows a globular structure, whereas when R_g is larger than R_h ($R_g/R_h \geq 1.5$), the polymer would be arranged as a random coil.[85,86] As tabulated in Table 4.3, starch and ALS-1 presented a shape factor

corresponding to globular structure, while the TOL and ALS-5 displayed a random coil structure. The differences between starch and TOL are due to the natural spherical shape of the unmodified starch compared to the smaller but coiled shape of TOL. Among the anionic TOL-starch copolymers, the higher ratio of MPSA resulted in a larger MW and more extended coil-like structure for ALS-5, which might be related to the longer polymerized chains within its polymeric structure.[87] Oppositely, ALS-1, with a lower MPSA ratio and smaller MW, presented a smaller and more compacted globular-like form.[88]

Table 4.3. Phenolic hydroxyl group content, MW, R_g, and R_h of TOL, starch, and anionic TOL-starch copolymers.

Sample	Phenolic group content (mmol/g)	MW × 10^3 (g/mol)	R_g (nm)	R_h (nm)	R_g/R_h
TOL	2.80	30 ± 10	18 ± 4	12 ± 3	1.50
Starch	0.00	5880 ± 500	29 ± 13	44 ± 9	0.66
ALS-1	1.12	1800 ± 490	23 ± 4	43 ± 6	0.53
ALS-5	0.90	11000 ± 1200	71 ± 6	47 ± 7	1.51

± in MW and R_g, standard deviation

± in R_h, relative variance

4.4.4. Thermal analysis

The glass transition temperature (T_g) obtained from the differential scanning calorimetry (DSC) analysis (Figure 4.6a) of TOL, starch, and anionic TOL-starch copolymers are summarized in Table 4.4. The T_g is related to the molecular mobility of the polymeric molecules, triggered by heat, and it depends on several factors, such as MW and branching degree.[7,89] As is seen in Table

4.4, the T_g of TOL was found to be 179 °C, which was higher than that of the anionic copolymers, where the T_g of 174 °C and 178 °C were observed for ALS-1 and ALS-5, respectively. After the copolymerization reaction of lignin, both the intermolecular H-bonding among the OH groups of the copolymer and the relaxation of the phenolic moieties were reduced, causing the decrement in the T_g.[89] The lower T_g of the anionic copolymers is caused by the presence of starch and polymerized chain of MPSA.[90,91] Starch exhibited a low T_g because its highly branched amylopectin portion possesses short chains that are more mobile and flexible than the stiff TOL chains.[89,92] Between the anionic copolymers, ALS-5 has a higher T_g than ALS-1, including a more extended structure with a larger molecular weight ALS-5 that needs a higher temperature to reach the glass transition temperature.

Table 4.4. T_g, T_{50}, and DTG_{max}, of TOL, starch, and anionic TOL-starch copolymers.

Sample	T_g (°C)	T_{50} (°C)	DTG_{max} (°C)
TOL	179	460	585
Starch	85	337	328
ALS-1	174	366	357
ALS-5	178	367	358

The thermal decomposition profiles of TOL, starch, and anionic TOL-starch copolymers were analyzed to discuss their thermal behavior. The typical TG and DTG curves for all samples are presented in Figures 4.7b and 4.7c, respectively. During the initial thermal decomposition step, the thermal stability of the anionic copolymers was higher than the decomposition rate of TOL. During the intermediate decomposition step, the T_{50} (the temperature at which 50% weight loss occurred) for TOL is 460 °C, which is higher than that of other samples. Adding starch and MPSA to the

backbone of TOL delayed its initial thermal decomposition compared to that of pure TOL, which can be explained by the larger MW of the anionic copolymers (Table 4.2).[93,94] When the temperature was higher than 400 °C, the anionic copolymers were less resistant to thermal decomposition than TOL was, as observed in Figure 4.6b, which is mainly due to the decay of the glycosidic linkages of its starch chains. However, at temperatures above 350 °C, the anionic copolymers were more resistant to weight loss than starch, owing to the presence of TOL and MPSA.

Moreover, the DTG curves for TOL, starch, and anionic TOL-starch copolymers are shown in Figure 4.6c. The thermal decomposition of TOL can be divided into three stages. The first weight loss, related to moisture loss, occurred in the range of 80 °C and120 °C. The second weight loss is observed in the range of 360 °C and 580 °C, which is attributed to the cleavage of the β-O-4 linkages. Lastly, the third weight loss is observed in the range of 580 °C and 680 °C, which is prompted by the breakup of the C-C bonds.[95] In the DTG curves for the anionic copolymers, one more weight loss step is observed in the temperature range of 260 to 380 °C, which is associated with the cleavage of the α-1-4 glycosidic linkage found in the chemical structure of starch.[96] Furthermore, the DTG_{max} (the temperature when the maximum rate of weight loss occurs) for the anionic copolymers was caused by the thermal decomposition of the α-1-4 glycosidic linkages.

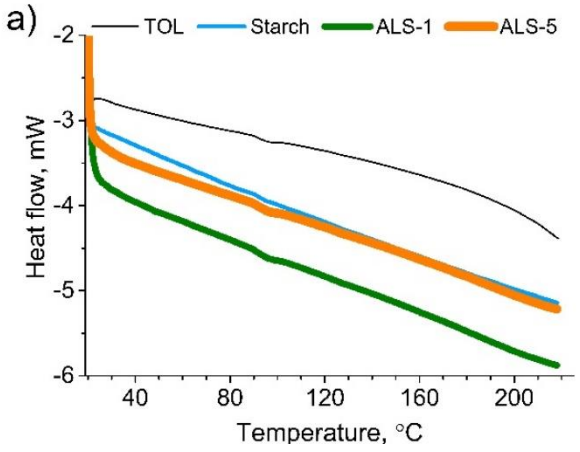

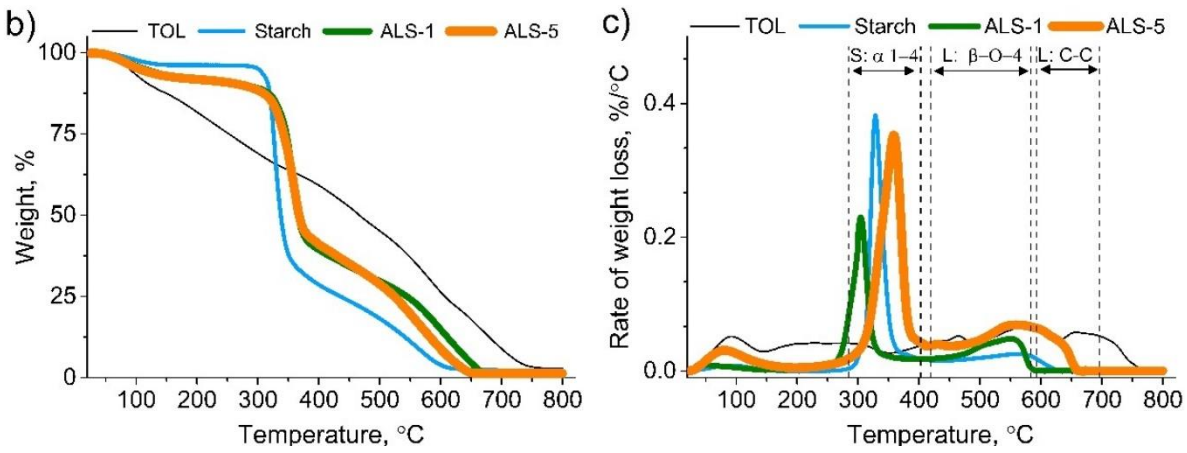

Figure 4.6. DSC (a) thermogravimetric (b) and DTG (c) curves of TOL, starch, and anionic TOL-starch copolymers. Dotted vertical lines in (c) delimit the decomposition stages associated with the predominant linkages.

4.4.5. Adsorption and surface interaction analysis

The adsorption analysis of TOL, starch, and anionic TOL-starch copolymers was performed using a QCM-D. In this system, as the polymer is deposited on the aluminum oxide sensor, the frequency (F) of the sensor starts to decrease, and the dissipation (D) of the sensor starts to increase in proportion to the adsorbed mass.[97] As observed in Figure 4.7, the anionic copolymers adsorbed more than TOL on the sensor's surface. This behavior resulted from their more significant negative charge density, allowing electrostatic interactions between the anionic polymeric chains and the aluminum oxide surface. Starch with a higher molecular weight adsorbed more and generated a more compact adlayer than other biopolymers inferring its more reconfigurational changes upon adsorption on the solid surface.

As seen, TOL showed the lowest D/F ratio (2.3×10^{-6}/-13 Hz), suggesting the adsorption of a rigid and compact adlayer. Among all samples, the highest D/F ratio (4.8×10^{-6}/-26 Hz) was observed when ALS-1 was introduced to the sensor's surface. This D/F ratio indicates a slightly denser polymeric adlayer on the aluminum oxide sensor. The lower molecular weight and its TOL content

probably made it so rigid that it made a thick adlayer upon adsorption. The higher molecular weight and starch content of ALS-5 likely contributed to its higher adsorption and more compact adlayer structure than ALS-1.

Once the buffer was introduced to the system, it rinsed the loosely attached polymers, which was observed as an increment of F by approximately 3 Hz, indicating that the adsorbed layer was weakly attached to the sensor. Contrarily, after the buffer rinsing, the D/F ratio of starch increased because of the water uptake (i.e., swelling) of the starch granule.[98,99] As discussed earlier, starch has undergone hydrolysis during the polymerization reaction, and hydrophobic TOL was part of the copolymer, limiting the swelling performance of ASL copolymers.

After introducing the buffer to the systems, a minor F increment was observed for the anionic copolymers. For this system, the anionic copolymers' interaction with the sensor's positive surface was sufficiently strong to resist the buffer rinsing and maintained the adsorbed layer mostly unaltered, with no shift in D or F (Figure S4.4, Supporting Information).

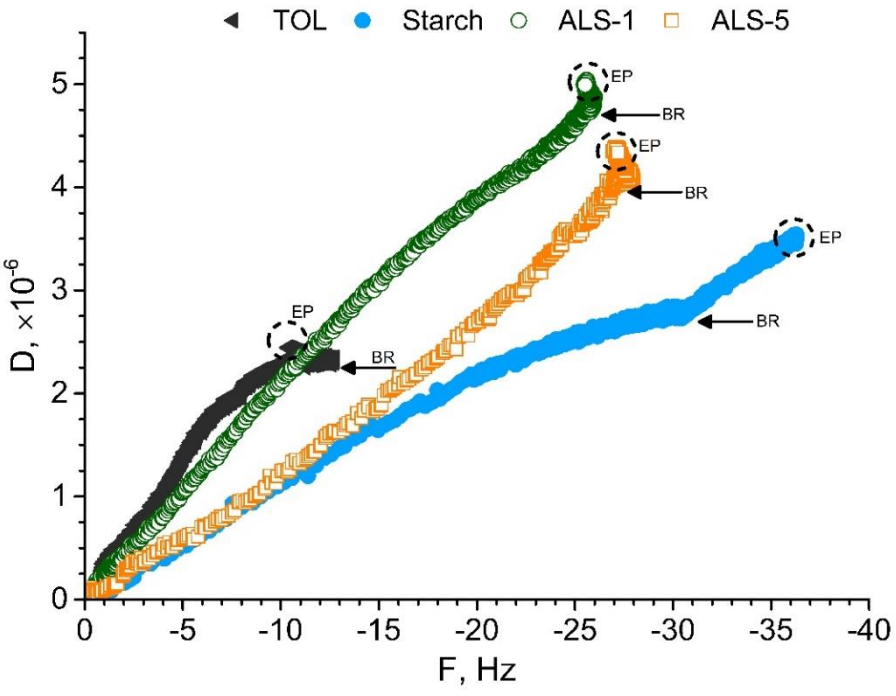

Figure 4.7. Adsorption of TOL, starch, and anionic TOL-starch copolymers on the aluminum oxide sensor from QCM-D. Arrows indicate the moment of buffer rinsing (BR). Dashed circles denote the endpoint of the experiment (EP).

4.4.6. Flocculation analysis

Focused beam reflectance measurements. Focused beam reflectance measurements (FBRM) were performed to observe the aluminum oxide particle size before and after adding TOL, starch, and anionic TOL-starch copolymers. The chord length distribution (CLD) of the produced flocs is shown as the function of counts in aluminum oxide suspensions before and after adding the polymers, as displayed in Figure 4.8. The CLD versus counts represent the flocculation efficiency of each polymer in aluminum oxide suspensions. The assessment of the optimum dosages for each polymer is available in the Supporting Information (Figure S5). In this system, the less efficient flocculants require higher doses to affect the CLD and counts of particles effectively.[100,101] Generally, increasing the dosages of the anionic copolymers in the aluminum oxide suspensions decreased the number of particle counts and widened the CDL peaks. In the aluminum oxide suspension, adding anionic copolymers shifted the CDL to the direction of larger flocs (>10 μm) and decreased the particle counts (Figure 4.8). Overall, adding 18 mg/g of ALS-1 or 16 mg/g of ALS-5 to aluminum oxide suspension showed better flocculation performance compared to TOL and starch. Starch can form complexes with the ionic forms of metal oxides, such as aluminum oxide. There are two types of interactions that explain the formation of these flocs. One is the formation of Werner-type coordination complexes, where the hydroxyl groups of the AGU will ligate the aluminum cores.[102] The other one is the formation of capillary complexes, where the capillaries of the swollen starch granules hold the aluminum ions.[99] These types of interaction are more susceptible to breakage and less ineffective in forming stable flocs. Thus, the performance

of starch is inferior to the anionic copolymers that involve a combination of bridging and electrostatic interactions in the flocculation of aluminum oxide.[74,103]

Notably, ALS-5 widened the CDL and reduced the counts of flocs in aluminum oxide suspension more considerably than other polymers did (Figure 4.8). Expectedly, AL5-5 with a higher MW, R_h, and charge density (Tables 4.2 and 4.3) showed a better flocculation performance in aluminum oxide suspension than ALS-1. Based on these results, it is presumed that by increasing the MW, bulkiness, and charge density of the TOL-starch copolymers, their performance as the flocculants of aluminum oxide particles will increase. Moreover, it is observed from the optimization assessments that some oversized and unstable flocs were generated by adding the anionic copolymers (Figure S4.5, Supporting Information). The large flocs produced immediately after adding the anionic copolymers were not sufficiently resistant against the applied agitation force (250 rpm) during the FBRM test. However, after the breakage, the rearrangement of the flocs produced more stable flocs as seen in Figure S4.5.

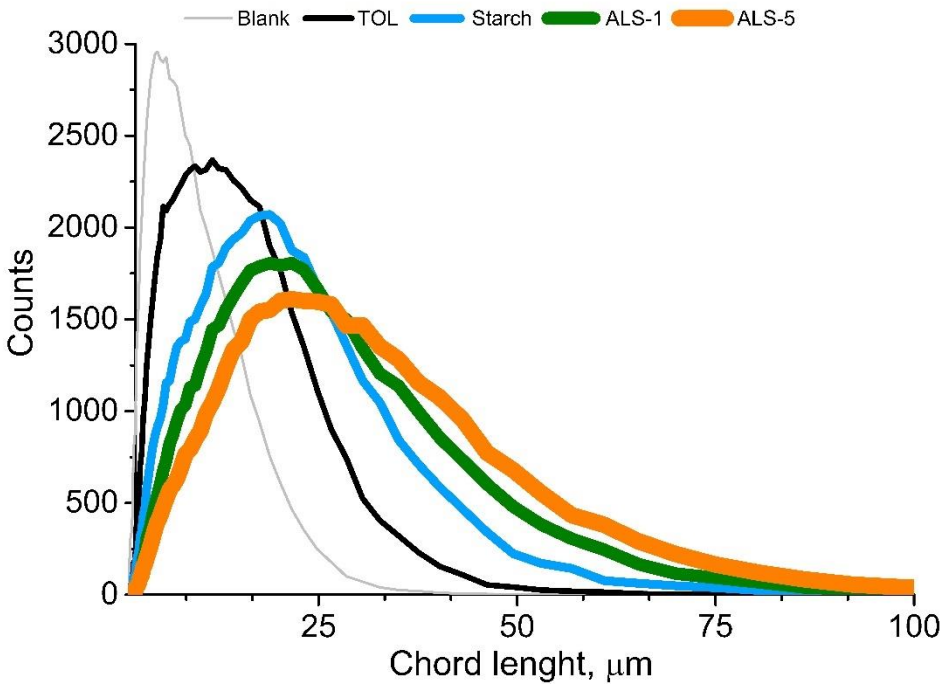

Figure 4.8. Chord length distribution (CLD) of the flocs produced after treating aluminum oxide particles (blank) with TOL, starch, and anionic TOL-starch copolymers.

Gravitational and centrifugal sedimentation analyses. The sedimentation analysis of the aluminum oxide suspensions under gravitational and centrifugal forces after adding optimum dosages of TOL, starch, and anionic TOL-starch copolymers was studied. A vertical scan analyzer measured the gravitational sedimentation under stagnant conditions. In this study (Figure 4.9a), the sedimentation efficiency for the suspensions was determined considering the TSI (Turbiscan stability index) factor as a function of time,[104] where the higher the TSI, the lower the stability of the suspension (i.e., more efficient flocculation) would be achieved.[105] Previous findings discussed the MW of the flocculants and their gravitational settling efficiency in aluminum oxide suspensions.[103,106]

In this shear-free test, the addition of TOL and starch showed no significant effect on the destabilization of aluminum oxide suspensions. Such lack of development is mainly due to a negligible charge density of TOL and starch. At the same time, the addition of anionic TOL-starch copolymers showed a synergistic effect of the MW and charge density on the destabilization of aluminum oxide, evidenced by the increment in the TSI. As shown in Figure 4.9a, it is noticeable that with the addition of ALS-1 and ALS-5 to the aluminum oxide suspension, the settlement rate of the aluminum oxide particles changed from a gradual progression observed in the blank sample to more rapid and sudden sedimentation during the first 180 seconds. A high MW associated with a moderate charge density in a shear-free environment made the anionic copolymers destabilize the aluminum oxide suspensions effectively.

Among the anionic TOL-starch copolymers, the product with a higher MW and charge density (ALS-5) showed the highest TSI after 60 minutes; and the TSI increased from 20 to 34, representing an increment of 70% in the TSI (Figure 4.9a). When ALS-5 was added, the final

settling steadiness was reached after 50 minutes, whereas a plateau was reached for ALS-1 after 10 min of dosing. These findings indicated that the interaction between the anionic TOL-starch copolymers and the aluminum oxide particles resulted from the combination of electrostatic forces and bridging originating from the negatively charged sulphonate groups and the long polymeric chains.[100]

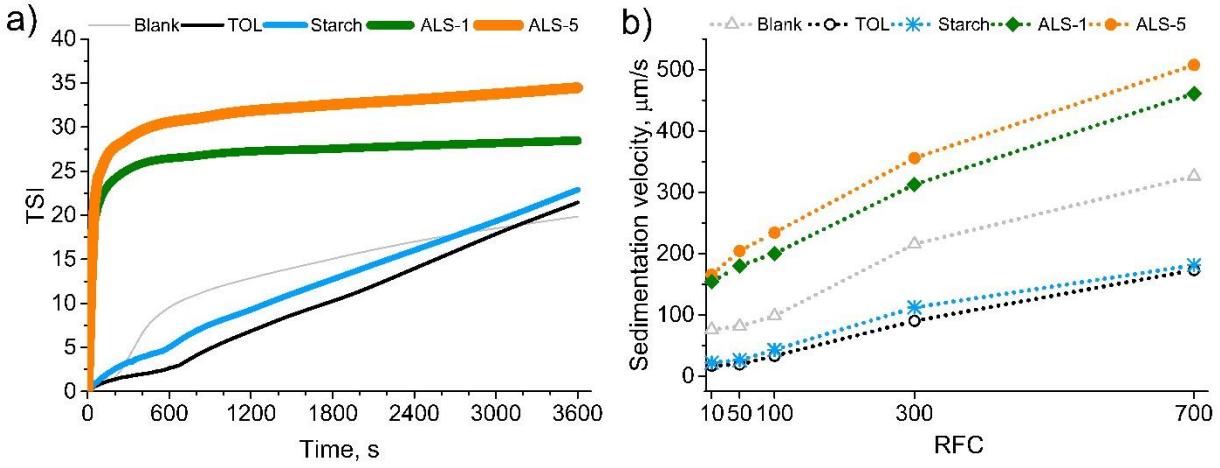

Figure 4.9. The gravitational sedimentation behavior (a) and centrifugal sedimentation velocity (b) of aluminum oxide particles without (blank) or with the presence of TOL, starch, and anionic TOL-starch copolymers.

Under different gravitational forces, the stability of aluminum oxide suspensions was measured after adding optimum dosages of TOL, starch, and anionic TOL-starch copolymers. Figure 4.9b summarizes the resultant sedimentation velocities at different RCFs (ratio of centrifugal to earth acceleration).[107] As expected, the sedimentation velocity of aluminum oxide particles increased noticeably after adding anionic TOL-starch copolymers. Interestingly, when TOL or starch was added to the aluminum oxide suspensions, a slight stabilization of the suspensions was observed under the tested RCFs. This effect can also be seen during the first 30 minutes of the gravitational sedimentation assays (Figure 4.9a). During the flocculation under shear forces (Figure 4.8), the floc formation is a dynamic process driven by hydrodynamic forces originating from the

stirring/mixing.[108] Under these forces, the stabilizing effect of TOL and starch on the aluminum oxide particles is disrupted. The stabilizing effect of TOL and starch is due to the electrostatic interaction and steric stabilization between their hydroxyl groups and the positive surface of the aluminum oxide particles, causing a delay of the self-aggregation in a shear-free environment.[109,110]. Hence, the sedimentation velocities decreased in comparison with the blank aluminum oxide. The sedimentation velocity of the particles under various RCFs mainly depends on their size and shape.[106,111] However, the density and porosity of the built-up flocs are also important factors for the floc settling behavior.[112] Based on the obtained results (Figure 4.9b), the highest sedimentation velocity was observed from the addition of ALS-5, with a larger MW and R_h (Table 4.3) among the anionic TOL-starch copolymers. ALS-5 produced bulkier and more porous flocs among all samples (Figure S4.6, Supporting Information), resulting in heavier flocs and higher sedimentation velocities. On the contrary, ALS-1 produced slighter smaller, and more rigid flocs.

4.5. Conclusion

Ternary anionic TOL-starch copolymers were successfully produced, and their structures were investigated by comprehensive NMR analysis. The phenylcoumaran units with β-5' linkages from TOL, the anhydroglucose units and the glycosidic linkages from starch, and the propene unit from MPSA were presented in the structure of the anionic TOL-starch copolymers as observed by 1D (H-NMR) and 2D (COSY, HSQC, HSQC-TOCSY, and HMBC) NMR analyses. Moreover, NMR results confirmed the involvement of the phenolic substructures and the existence of an ether bond between the anhydroglucose unit and MPSA chains in the TOL-starch copolymers. The MW of ALS-1 and ALS-5 was 1800×10^3 and 11000×10^3 g/mol, respectively. The larger MW of ALS-5 was ascribed to the insertion of longer MPSA chains and the presence of starch and TOL in the

copolymer, which produced a more extended and coil-like structure (shape factor =1.5), which also increased the T_g and T_{50} (178 and 367 °C, respectively), demonstrating higher thermal stability of the sample. The opposite was observed for ALS-1, as its lower MPSA ratio in the polymerization reaction generated a smaller and more compacted globular-like structure of the copolymer with a shape factor of 0.5 and a T_g of 174 °C.

ALS-1 and ALS-5 adsorbed more and stronger on the aluminum oxide surface than TOL or starch did, owing to the sulphate groups originating from MPSA in the copolymer. In general, TOL and starch showed poor flocculation efficiency for aluminum oxide particles in a suspension system. The large MW, tridimensional structure, and negative charge density observed in ALS-1 and ALS-5 are desirable characteristics for the flocculation of aluminum oxide-suspended particles. Furthermore, the flocculation efficiency of ALS-1 and ALS-5 in the aluminum oxide suspension was higher than that of TOL and starch. Under agitations, the smaller MW and more condensed structure of ALS-1 produced more compacted and resistant flocs. However, in both gravitational and centrifugal sedimentation experiments, the larger and expanded structure of ALS-5 permitted the formation of larger flocs with faster sedimentation. In a shear-free environment, ALS-5 exhibited the best flocculation performance among all samples. These results are promising as they indicate the viability of producing ternary ionic sustainable biomacromolecules from TOL and starch and using the product for removing inorganic suspended particles from colloidal systems.

4.6. References

(1). Dessbesell, L.; Paleologou, M.; Leitch, M.; Pulkki, R.; Xu, C. (Charles). Global Lignin Supply Overview and Kraft Lignin Potential as an Alternative for Petroleum-Based Polymers. *Renewable Sustainable Energy Rev.* **2020**, *123*, 109768. https://doi.org/10.1016/j.rser.2020.109768

(2). Kouisni, L.; Gagné, A.; Maki, K.; Holt-Hindle, P.; Paleologou, M. LignoForce System for the Recovery of Lignin from Black Liquor: Feedstock Options, Odor Profile, and Product Characterization. *ACS Sustainable Chem. Eng.* **2016**, *4* (10), 5152–5159. https://doi.org/10.1021/acssuschemeng.6b00907

(3). Öhman, F.; Theliander, H.; Tomani, P.; Axegard, P. Method for Separating Lignin from Black Liquor. US8486224B2, July 16, 2013
(4). Suota, M. J.; Kochepka, D. M.; Ganter Moura, M. G.; Pirich, C. L.; Matos, M.; Magalhães, W. L. E.; Ramos, L. P. Lignin Functionalization Strategies and the Potential Applications of Its Derivatives – A Review. *BioRes* **2021**, *16* (3), 6471–6511. https://doi.org/10.15376/biores.16.3.Suota
(5). Li, T.; Takkellapati, S. The Current and Emerging Sources of Technical Lignins and Their Applications. *Biofuel. Bioprod. Biorefin.* **2018**, *0*, 1–32. https://doi.org/10.1002/bbb.1913
(6). Diaz-Baca, J. A.; Fatehi, P. Process Development for Tall Oil Lignin Production. *Bioresour. Technol.* **2021**, *329*, 124891. https://doi.org/10.1016/j.biortech.2021.124891
(7). Wang, L.; Shen, J.; Men, Y.; Wu, Y.; Peng, Q.; Wang, X.; Yang, R.; Mahmood, K.; Liu, Z. Corn Starch-Based Graft Copolymers Prepared via ATRP at the Molecular Level. *Polym. Chem*. **2015**, *6* (18), 3480–3488. https://doi.org/10.1039/C5PY00184F
(8). Smith, A. M. The Biosynthesis of Starch Granules. *Biomacromolecules* **2001**, *2* (2), 335–341. https://doi.org/10.1021/bm000133c
(9). Le Corre, D.; Bras, J.; Dufresne, A. Starch Nanoparticles: A Review. *Biomacromolecules* **2010**, *11* (5), 1139–1153. https://doi.org/10.1021/bm901428y
(10). Li, M.-C.; Wu, Q.; Song, K.; French, A. D.; Mei, C.; Lei, T. PH-Responsive Water-Based Drilling Fluids Containing Bentonite and Chitin Nanocrystals. *ACS Sustainable Chem. Eng.* **2018**, *6* (3), 3783–3795. https://doi.org/10.1021/acssuschemeng.7b04156
(11). Singh, G. P.; Bangar, S. P.; Yang, T.; Trif, M.; Kumar, V.; Kumar, D. Effect on the Properties of Edible Starch-Based Films by the Incorporation of Additives: A Review. *Polymers* **2022**, *14* (10), 1987. https://doi.org/10.3390/polym14101987
(12). Majeed, Z.; Mansor, N.; Ajab, Z.; Man, Z.; Sarwono, A. Kraft Lignin Ameliorates Degradation Resistance of Starch in Urea Delivery Biocomposites. *Polym. Test.* **2018**, *65*, 398–406. https://doi.org/10.1016/j.polymertesting.2017.12.011
(13). Li, M.; Jia, Y.; Shen, X.; Shen, T.; Tan, Z.; Zhuang, W.; Zhao, G.; Zhu, C.; Ying, H. Investigation into Lignin Modified PBAT/Thermoplastic Starch Composites: Thermal, Mechanical, Rheological and Water Absorption Properties. *Ind. Crops. Prod.* **2021**, *171*, 113916. https://doi.org/10.1016/j.indcrop.2021.113916
(14). Lepifre, S.; Froment, M.; Cazaux, F.; Houot, S.; Lourdin, D.; Coqueret, X.; Lapierre, C.; Baumberger, S. Lignin Incorporation Combined with Electron-Beam Irradiation Improves the Surface Water Resistance of Starch Films. *Biomacromolecules* **2004**, *5* (5), 1678–1686. https://doi.org/10.1021/bm040005e
(15). Ni, S.; Bian, H.; Zhang, Y.; Fu, Y.; Liu, W.; Qin, M.; Xiao, H. Starch-Based Composite Films with Enhanced Hydrophobicity, Thermal Stability, and UV-Shielding Efficacy Induced by Lignin Nanoparticles. *Biomacromolecules* **2022**, *23* (3), 829–838. https://doi.org/10.1021/acs.biomac.1c01288
(16). Wu, Q.; Shao, W.; Xia, N.; Wang, P.; Kong, F. A Separable Paper Adhesive Based on the Starch—lignin Composite. *Carbohydr. Polym* **2020**, *229*, 115488. https://doi.org/10.1016/j.carbpol.2019.115488
(17). Kaewtatip, K.; Tanrattanakul, V. Preparation of Cassava Starch Grafted with Polystyrene by Suspension Polymerization. *Carbohydr. Polym* **2008**, *73* (4), 647–655. https://doi.org/10.1016/j.carbpol.2008.01.006

(18). Gupta, C.; Sverdlove, M. J.; Washburn, N. R. Molecular Architecture Requirements for Polymer-Grafted Lignin Superplasticizers. *Soft Matter* **2015**, *11* (13), 2691–2699. https://doi.org/10.1039/C4SM02675F
(19). Liu, Z.; Chao, G.; Chen, L.; Dong, X.; Kong, F.; Wang, S.; Gibrill, M. E.; Lucia, L.; Fatehi, P. Preparation of an Amphoteric Lignin Copolymer and Its Value in the Papermaking Industry. *BioResources* **2020**, *15* (4), 9625–9641. https://doi.org/10.15376/biores.15.4.9625-9641
(20). Sarkar, A. K.; Ghorai, S.; Patra, A. S.; Mishra, B. K.; Mandre, N. R.; Pal, S. Modified Amylopectin Based Flocculant for the Treatment of Synthetic Effluent and Industrial Wastewaters. *Int. J. Biol. Macromol.* **2015**, *72*, 356–363. https://doi.org/10.1016/j.ijbiomac.2014.08.019
(21). Ataie, M.; Sutherland, K.; Pakzad, L.; Fatehi, P. Assembly of Aluminum Oxide Particles with Lignin-Acrylic Acid Polymer in Saline Systems. *Colloid Surf. A-Physicochem. Eng. Asp.* **2022**, *648*, 129322. https://doi.org/10.1016/j.colsurfa.2022.129322
(22). Wang, B.; Wang, S.-F.; Lam, S. S.; Sonne, C.; Yuan, T.-Q.; Song, G.-Y.; Sun, R.-C. A Review on Production of Lignin-Based FLocculants: Sustainable Feedstock and Low Carbon Footprint Applications. *Renewable Sustainable Energy Rev.* **2020**, *134*, 110384. https://doi.org/10.1016/j.rser.2020.110384
(23). Jiang, X.; Li, Y.; Tang, X.; Jiang, J.; He, Q.; Xiong, Z.; Zheng, H. Biopolymer-Based Flocculants: A Review of Recent Technologies. *Environ. Sci. Pollut. Res.* **2021**, *28* (34), 46934–46963. https://doi.org/10.1007/s11356-021-15299-y
(24). Sabaghi, S.; Fatehi, P. Phenomenological Changes in Lignin Following Polymerization and Its Effects on Flocculating Clay Particles. *Biomacromolecules* **2019**, *20* (10), 3940–3951. https://doi.org/10.1021/acs.biomac.9b01016
(25). Ten, E.; Vermerris, W. Recent Developments in Polymers Derived from Industrial Lignin. *J. Appl. Polym. Sci.* **2015**, *132* (24), app.42069. https://doi.org/10.1002/app.42069.
(26). Salehizadeh, H.; Yan, N.; Farnood, R. Recent Advances in Polysaccharide Bio-Based Flocculants. *Biotechnol. Adv.* **2018**, *36* (1), 92–119. https://doi.org/10.1016/j.biotechadv.2017.10.002
(27). Guo, K.; Gao, B.; Yue, Q.; Xu, X.; Li, R.; Shen, X. Characterization and Performance of a Novel Lignin-Based Flocculant for the Treatment of Dye Wastewater. *Int. Biodeterior. Biodegrad.* **2018**, *133*, 99–107. https://doi.org/10.1016/j.ibiod.2018.06.015
(28). Md Noor, A. M.; Mohtar, S. S.; Saman, N.; Tengku Malim Busu, T. N. Z.; Shaari, N.; Yusoff, N. A.; Mat, H. Preparation of Quaternized Lignin Derived from Oil Palm Empty Fruit Bunches and Its Flocculation Properties. *J. Wood Chem. Technol.* **2019**, *39* (6), 399–420. https://doi.org/10.1080/02773813.2019.1636823
(29). Moore, C.; Gao, W.; Fatehi, P. Cationic Lignin Polymers as Flocculant for Municipal Wastewater. *Polymers* **2021**, *13* (22), 3871. https://doi.org/10.3390/polym13223871
(30). Wu, L.; Zhang, X.; Chen, L.; Zhang, H.; Li, C.; Lv, Y.; Xu, Y.; Jia, X.; Shi, Y.; Guo, X. Amphoteric Starch Derivatives as Reusable Flocculant for Heavy-Metal Removal. *RSC Adv.* **2018**, *8* (3), 1274–1280. https://doi.org/10.1039/C7RA12798G
(31). Liu, Z.; Wei, H.; Li, A.; Yang, H. Evaluation of Structural Effects on the Flocculation Performance of a Co-Graft Starch-Based Flocculant. *Water Research* **2017**, *118*, 160–166. https://doi.org/10.1016/j.watres.2017.04.032
(32). Das, S.; Patra, P.; Singha, K.; Biswas, P.; Sarkar, S.; Pal, S. Graft Copolymeric Flocculant Using Functionalized Starch towards Treatment of Blast Furnace Effluent. *Int. J. Biol. Macromol.* **2019**, *125*, 35–40. https://doi.org/10.1016/j.ijbiomac.2018.12.026

(33). Perumal, P.; Piekkari, K.; Sreenivasan, H.; Kinnunen, P.; Illikainen, M. One-Part Geopolymers from Mining Residues – Effect of Thermal Treatment on Three Different Tailings. *Miner. Eng.* **2019**, *144*, 106026. https://doi.org/10.1016/j.mineng.2019.106026
(34). Lee, C. S.; Robinson, J.; Chong, M. F. A Review on Application of Flocculants in Wastewater Treatment. *Process Saf. Environ. Prot.* **2014**, *92* (6), 489–508. https://doi.org/10.1016/j.psep.2014.04.010
(35). Saravanan, A.; Thamarai, P.; Kumar, P. S.; Rangasamy, G. Recent Advances in Polymer Composite, Extraction, and Their Application for Wastewater Treatment: A Review. *Chemosphere* **2022**, *308*, 136368. https://doi.org/10.1016/j.chemosphere.2022.136368
(36). Evstigneev, E. I. Factors Affecting Lignin Solubility. *Russ J Appl Chem* **2011**, *84* (6), 1040–1045. https://doi.org/10.1134/S1070427211060243
(37). Giummarella, N.; Balakshin, M.; Koutaniemi, S.; Karkonen, A.; Lawoko, M. Nativity of Lignin Carbohydrate Bonds Substantiated by Biomimetic Synthesis. *J. Exp. Bot.* **2019**, *70* (20), 5591–5601. https://doi.org/10.1093/jxb/erz324
(38). Teramura, H.; Sasaki, K.; Oshima, T.; Aikawa, S.; Matsuda, F.; Okamoto, M.; Shirai, T.; Kawaguchi, H.; Ogino, C.; Yamasaki, M.; Kikuchi, J.; Kondo, A. Changes in Lignin and Polysaccharide Components in 13 Cultivars of Rice Straw Following Dilute Acid Pretreatment as Studied by Solution-State 2D H-1-C-13 NMR. *PLoS One* **2015**, *10* (6), e0128417. https://doi.org/10.1371/journal.pone.0128417
(39). Takasaki, M.; Kimura, K.; Nakagawa, Y.; Sato, N.; Bae, B.; Miyatake, K.; Watanabe, M. Complete NMR Assignment of a Sulfonated Aromatic Block Copolymer via Heteronuclear Single-Quantum Correlation, Heteronuclear Multiple-Bond Correlation and Heteronuclear Single-Quantum Correlation Total Correlation Spectroscopy. *Polym. J.* **2012**, *44* (8), 845–849. https://doi.org/10.1038/pj.2012.125
(40). Sameni, J.; Krigstin, S.; Sain, M. Characterization of Lignins Isolated from Industrial Residues and Their Beneficial Uses. *BioResources* **2016**, *11* (4), 8435–8456
(41). Konduri, M. K. R.; Fatehi, P. Designing Anionic Lignin Based Dispersant for Kaolin Suspensions. *Colloids Surf., A* **2018**, *538*, 639–650. https://doi.org/10.1016/j.colsurfa.2017.11.011
(42). Tizzotti, M. J.; Sweedman, M. C.; Tang, D.; Schaefer, C.; Gilbert, R. G. New ^{1}H NMR Procedure for the Characterization of Native and Modified Food-Grade Starches. *J. Agric. Food Chem.* **2011**, *59* (13), 6913–6919. https://doi.org/10.1021/jf201209z
(43). Ghavidel, N.; Konduri, M. K. R.; Fatehi, P. Chemical Reactivity and Sulfo-Functionalization Response of Enzymatically Produced Lignin. *Ind. Crops. Prod.* **2021**, *172*, 113950. https://doi.org/10.1016/j.indcrop.2021.113950
(44). Schmitz, S.; Dona, A. C.; Castignolles, P.; Gilbert, R. G.; Gaborieau, M. Assessment of the Extent of Starch Dissolution in Dimethyl Sulfoxide by ^{1}H NMR Spectroscopy. *Macromol. Biosci.* **2009**, *9* (5), 506–514. https://doi.org/10.1002/mabi.200800244
(45). Kong, F.; Wang, S.; Gao, W.; Fatehi, P. Novel Pathway to Produce High Molecular Weight Kraft Lignin–Acrylic Acid Polymers in Acidic Suspension Systems. *RSC Adv.* **2018**, *8* (22), 12322–12336. https://doi.org/10.1039/C7RA12971H
(46). Baalousha, M.; Kammer, F. V. D.; Motelica-Heino, M.; Hilal, H. S.; Le Coustumer, P. Size Fractionation and Characterization of Natural Colloids by Flow-Field Flow Fractionation Coupled to Multi-Angle Laser Light Scattering. *J. Chromatogr. A* **2006**, *1104* (1–2), 272–281. https://doi.org/10.1016/j.chroma.2005.11.095

(47). Eita, M. In Situ Study of the Adsorption of Humic Acid on the Surface of Aluminium Oxide by QCM-D Reveals Novel Features. *Soft Matter* **2011**, *7* (2), 709–715. https://doi.org/10.1039/C0SM00648C
(48). Chen, Q.; Xu, S.; Liu, Q.; Masliyah, J.; Xu, Z. QCM-D Study of Nanoparticle Interactions. *Adv. Colloid Interface Sci.* **2016**, *233*, 94–114. https://doi.org/10.1016/j.cis.2015.10.004
(49). Alipoormazandarani, N.; Fatehi, P. Adsorption Characteristics of Carboxymethylated Lignin on Rigid and Soft Surfaces Probed by Quartz Crystal Microbalance. *Langmuir* **2018**, *34* (50), 15293–15303. https://doi.org/10.1021/acs.langmuir.8b02694
(50). Dunér, G.; Thormann, E.; Dėdinaitė, A. Quartz Crystal Microbalance with Dissipation (QCM-D) Studies of the Viscoelastic Response from a Continuously Growing Grafted Polyelectrolyte Layer. *J. Colloid Interface Sci.* **2013**, *408*, 229–234. https://doi.org/10.1016/j.jcis.2013.07.008
(51). Wu, M. R.; van de Ven, T. G. M. Flocculation and Reflocculation: Interplay between the Adsorption Behavior of the Components of a Dual Flocculant. *Colloids Surf. A Physicochem. Eng. Asp.* **2009**, *341* (1–3), 40–45. https://doi.org/10.1016/j.colsurfa.2009.03.034
(52). Blanco, A.; Fuente, E.; Negro, C.; Tijero, J. Flocculation Monitoring: Focused Beam Reflectance Measurement as a Measurement Tool. *Can. J. Chem. Eng.* **2008**, *80* (4), 1–7. https://doi.org/10.1002/cjce.5450800403
(53). Thapa, K. B.; Qi, Y.; Hoadley, A. F. Using FBRM to Investigate the Sewage Sludge Flocculation Efficiency of Cationic Polyelectrolytes. *Water Sci. Technol.* **2009**, *59* (3), 583–593. https://doi.org/10.2166/wst.2009.006
(54). Miranda, R.; Negro, C.; Blanco, A. Internal Treatment of Process Waters in Paper Production by Dissolved Air Flotation with Newly Developed Chemicals. 1. Laboratory Tests. *Ind. Eng. Chem. Res.* **2009**, *48* (4), 2199–2205. https://doi.org/10.1021/ie801047h
(55). Konduri, M. K. R.; Fatehi, P. Influence of PH and Ionic Strength on Flocculation of Clay Suspensions with Cationic Xylan Copolymer. *Colloids Surf., A* **2017**, *530*, 20–32. https://doi.org/10.1016/j.colsurfa.2017.07.045
(56). Mengual, O. TURBISCAN MA 2000: Multiple Light Scattering Measurement for Concentrated Emulsion and Suspension Instability Analysis. *Talanta* **1999**, *50* (2), 445–456. https://doi.org/10.1016/S0039-9140(99)00129-0
(57). Lamas, B.; Abreu, B.; Fonseca, A.; Martins, N.; Oliveira, M. Assessing Colloidal Stability of Long Term MWCNT Based Nanofluids. *J. Colloid Interface Sci.* **2012**, *381* (1), 17–23. https://doi.org/10.1016/j.jcis.2012.05.014
(58). Erramreddy, V. V.; Tu, S.; Ghosh, S. Rheological Reversibility and Long-Term Stability of Repulsive and Attractive Nanoemulsion Gels. *RSC Adv.* **2017**, *7* (75), 47818–47832. https://doi.org/10.1039/C7RA09605D
(59). Tehrani-Bagha, A. R. Cationic Gemini Surfactant with Cleavable Spacer: Emulsion Stability. *Colloids Surf., A* **2016**, *508*, 79–84. https://doi.org/10.1016/j.colsurfa.2016.08.020
(60). Fernández-Costas, C.; Gouveia, S.; Sanromán, M. A.; Moldes, D. Structural Characterization of Kraft Lignins from Different Spent Cooking Liquors by 1D and 2D Nuclear Magnetic Resonance Spectroscopy. *Biomass and Bioenergy* **2014**, *63*, 156–166. https://doi.org/10.1016/j.biombioe.2014.02.020
(61). Tana, T.; Zhang, Z.; Moghaddam, L.; Rackemann, D. W.; Rencoret, J.; Gutiérrez, A.; del Río, J. C.; Doherty, W. O. S. Structural Changes of Sugar Cane Bagasse Lignin during Cellulosic Ethanol Production Process. *ACS Sustain. Chem. Eng* **2016**, *4* (10), 5483–5494. https://doi.org/10.1021/acssuschemeng.6b01093

(62). Falk, H.; Stanek, M. Two-Dimensional1H And13C NMR Spectroscopy and the Structural Aspects of Amylose and Amylopectin. *Monatsh. Chem.* **1997**, *128* (8–9), 777–784. https://doi.org/10.1007/BF00807088
(63). Sachinvala, N. D.; Hamed, O. A.; Winsor, D. L.; Niemczura, W. P.; Maskos, K.; Parikh, D. V.; Glasser, W.; Becker, U.; Blanchard, E. J.; Bertoniere, N. R. Characterization of Tri-o-Methylcellulose by One- and Two-Dimensional NMR Methods. *J. Polym. Sci. A Polym. Chem.* **1999**, *37* (21), 4019–4032. https://doi.org/10.1002/(SICI)1099-0518(19991101)37:21<4019::AID-POLA16>3.0.CO;2-Z
(64). Moon, S.; Lee, Y.; Choi, S.; Hong, S.; Lee, S.; Park, A.-H. A.; Park, Y. Spectroscopic Investigation of Thermochemical Depolymerization of Lignin Model Compounds in the Presence of Novel Liquidlike Nanoparticle Organic Hybrid Solvents for Efficient Biomass Valorization. *Org. Process Res. Dev.* **2018**, *22* (12), 1723–1732. https://doi.org/10.1021/acs.oprd.8b00282
(65). Iu, X.; Li, T.; Wu, S.; Ma, H.; Yin, Y. Structural Characterization and Comparison of Enzymatic and Deep Eutectic Solvents Isolated Lignin from Various Green Processes: Toward Lignin Valorization. *Bioresour. Technol.* **2020**, *310*, 123460. https://doi.org/10.1016/j.biortech.2020.123460
(66). Lahive, C. W.; Lancefield, C. S.; Codina, A.; Kamer, P. C. J.; Westwood, N. J. Revealing the Fate of the Phenylcoumaran Linkage during Lignin Oxidation Reactions. *Org. Biomol. Chem.* **2018**, *16* (11), 1976–1982. https://doi.org/10.1039/C7OB03087H
(67). Buedenbender, L.; Habener, L. J.; Grkovic, T.; Kurtböke, D. İ.; Duffy, S.; Avery, V. M.; Carroll, A. R. HSQC–TOCSY Fingerprinting for Prioritization of Polyketide- and Peptide-Producing Microbial Isolates. *J. Nat. Prod.* **2018**, *81* (4), 957–965. https://doi.org/10.1021/acs.jnatprod.7b01063
(68). Nishimura, H.; Kamiya, A.; Nagata, T.; Katahira, M.; Watanabe, T. Direct Evidence for α Ether Linkage between Lignin and Carbohydrates in Wood Cell Walls. *Sci. Rep.* **2018**, *8* (1), 6538. https://doi.org/10.1038/s41598-018-24328-9
(69). Petersen, B. O.; Motawie, M. S.; Møller, B. L.; Hindsgaul, O.; Meier, S. NMR Characterization of Chemically Synthesized Branched α-Dextrin Model Compounds. *Carbohydr. Res.* **2015**, *403*, 149–156. https://doi.org/10.1016/j.carres.2014.05.011
(70). Miles-Barrett, D. M.; Neal, A. R.; Hand, C.; Montgomery, J. R. D.; Panovic, I.; Ojo, O. S.; Lancefield, C. S.; Cordes, D. B.; Slawin, A. M. Z.; Lebl, T.; Westwood, N. J. The Synthesis and Analysis of Lignin-Bound Hibbert Ketone Structures in Technical Lignins. *Org. Biomol. Chem.* **2016**, *14* (42), 10023–10030. https://doi.org/10.1039/C6OB01915C
(71). Lee, J. H.; Han, J.-A.; Lim, S.-T. Effect of PH on Aqueous Structure of Maize Starches Analyzed by HPSEC-MALLS-RI System. *Food Hydrocolloids* **2009**, *23* (7), 1935–1939. https://doi.org/10.1016/j.foodhyd.2008.12.007
(72). Cui, G.; Wang, X.; Xun, J.; Lou, T. Microwave Assisted Synthesis and Characterization of a Ternary Flocculant from Chitosan, Acrylamide and Lignin. *Int. Biodeterior. Biodegrad.* **2017**, *123*, 269–275. https://doi.org/10.1016/j.ibiod.2017.07.011
(73). Constantin, M.; Mihalcea, I.; Oanea, I.; Harabagiu, V.; Fundueanu, G. Studies on Graft Copolymerization of 3-Acrylamidopropyl Trimethylammonium Chloride on Pullulan. *Carbohydr. Polym.* **2011**, *84* (3), 926–932. https://doi.org/10.1016/j.carbpol.2010.12.043
(74). Bratskaya, S.; Schwarz, S.; Liebert, T.; Heinze, T. Starch Derivatives of High Degree of Functionalization. *Colloids Surf., A* **2005**, *254* (1–3), 75–80. https://doi.org/10.1016/j.colsurfa.2004.11.030

(75). Witt, T.; Gilbert, R. G. Causal Relations between Structural Features of Amylopectin, a Semicrystalline Hyperbranched Polymer. *Biomacromolecules* **2014**, *15* (7), 2501–2511. https://doi.org/10.1021/bm500353e
(76). Qiao, D.; Yu, L.; Bao, X.; Zhang, B.; Jiang, F. Understanding the Microstructure and Absorption Rate of Starch-Based Superabsorbent Polymers Prepared under High Starch Concentration. *Carbohydr. Polym.* **2017**, *175*, 141–148. https://doi.org/10.1016/j.carbpol.2017.07.071
(77). Wang, S.; Xu, J.; Wang, Q.; Fan, X.; Yu, Y.; Wang, P.; Zhang, Y.; Yuan, J.; Cavaco-Paulo, A. Preparation and Rheological Properties of Starch- g -Poly(Butyl Acrylate) Catalyzed by Horseradish Peroxidase. *Process Biochem.* **2017**, *59*, 104–110. https://doi.org/10.1016/j.procbio.2017.01.014
(78). Sabaghi, S.; Alipoormazandarani, N.; Fatehi, P. Production and Application of Triblock Hydrolysis Lignin-Based Anionic Copolymers in Aqueous Systems. *ACS Omega* **2021**, acsomega.0c06344. https://doi.org/10.1021/acsomega.0c06344
(79). Aberle, Th.; Burchard, W.; Vorwerg, W.; Radosta, S. Conformational Contributions of Amylose and Amylopectin to the Structural Properties of Starches from Various Sources. *Starch/Stärke* **1994**, *46* (9), 329–335. https://doi.org/10.1002/star.19940460903
(80). Clauss, M. M.; Weldin, D. L.; Frank, E.; Giebel, E.; Buchmeiser, M. R. Size-Exclusion Chromatography and Aggregation Studies of Acetylated Lignins in *N,N* -Dimethylacetamide in the Presence of Salts. *Macromol. Chem. Phys.* **2015**, *216* (20), 2012–2019. https://doi.org/10.1002/macp.201500222
(81). Petridis, L.; Smith, J. C. Conformations of Low-Molecular-Weight Lignin Polymers in Water. *ChemSusChem* **2016**, *9* (3), 289–295. https://doi.org/10.1002/cssc.201501350
(82). Holló, J.; László, E. Kinetical Comparison of the Acidic, Alkaline and Enzymatic Hydrolysis of Starch. *Period. Polytech. Chem. Eng.* **1970**, *14* (1), 33–46
(83). Iuga, M.; Mironeasa, S. A Review of the Hydrothermal Treatments Impact on Starch Based Systems Properties. *Crit. Rev. Food Sci. Nutr.* **2020**, *60* (22), 3890–3915. https://doi.org/10.1080/10408398.2019.1664978
(84). Shogren, R. L. Flocculation of Kaolin by Waxy Maize Starch Phosphates. *Carbohydr. Polym.* **2009**, *76* (4), 639–644. https://doi.org/10.1016/j.carbpol.2008.11.027
(85). Williams, R. J.; Pitto-Barry, A.; Kirby, N.; Dove, A. P.; O'Reilly, R. K. Cyclic Graft Copolymer Unimolecular Micelles: Effects of Cyclization on Particle Morphology and Thermoresponsive Behavior. *Macromolecules* **2016**, *49* (7), 2802–2813. https://doi.org/10.1021/acs.macromol.5b02710
(86). Haydukivska, K.; Blavatska, V.; Paturej, J. Universal Size Ratios of Gaussian Polymers with Complex Architecture: Radius of Gyration vs Hydrodynamic Radius. *Sci. Rep.* **2020**, *10* (1), 14127. https://doi.org/10.1038/s41598-020-70649-z
(87). Trzebicka, B.; Szweda, D.; Rangelov, S.; Kowalczuk, A.; Mendrek, B.; Utrata-Wesołek, A.; Dworak, A. (Co)Polymers of Oligo(Ethylene Glycol) Methacrylates—Temperature-Induced Aggregation in Aqueous Solution. *J. Polym. Sci., Part A: Polym. Chem.* **2013**, *51* (3), 614–623. https://doi.org/10.1002/pola.26410
(88). Bresseleers, J.; Bagheri, M.; Lebleu, C.; Lecommandoux, S.; Sandre, O.; Pijpers, I. A. B.; Mason, A. F.; Meeuwissen, S.; Nostrum, C. F. van; Hennink, W. E.; Hest, J. C. M. van. Tuning Size and Morphology of MPEG-b-p(HPMA-Bz) Copolymer Self-Assemblies Using Microfluidics. *Polymers* **2020**, *12* (11), 2572. https://doi.org/10.3390/polym12112572

(89). Liu, P.; Yu, L.; Wang, X.; Li, D.; Chen, L.; Li, X. Glass Transition Temperature of Starches with Different Amylose/Amylopectin Ratios. *J. Cereal Sci.* **2010**, *51* (3), 388–391. https://doi.org/10.1016/j.jcs.2010.02.007
(90). Silva, M. E. S. R. e; Dutra, E. R.; Mano, V.; Machado, J. C. Preparation and Thermal Study of Polymers Derived from Acrylamide. *Polym. Degrad. Stab.* **2000**, *67* (3), 491–495. https://doi.org/10.1016/S0141-3910(99)00149-4
(91). Siyamak, S.; Laycock, B.; Luckman, P. Synthesis of Starch Graft-Copolymers via Reactive Extrusion: Process Development and Structural Analysis. *Carbohydr. Polym.* **2020**, *227*, 115066. https://doi.org/10.1016/j.carbpol.2019.115066
(92). Thiewes, H. J.; Steeneken, P. A. M. The Glass Transition and the Sub-Tg Endotherm of Amorphous and Native Potato Starch at Low Moisture Content. *Carbohydr. Polym.* **1997**, *32* (2), 123–130. https://doi.org/10.1016/S0144-8617(96)00133-6
(93). Zhang, X.; Golding, J.; Burgar, I. Thermal Decomposition Chemistry of Starch Studied by 13C High-Resolution Solid-State NMR Spectroscopy. *Polymer* **2002**, *43* (22), 5791–5796. https://doi.org/10.1016/S0032-3861(02)00546-3
(94). Zhao, J.; Xiuwen, W.; Hu, J.; Liu, Q.; Shen, D.; Xiao, R. Thermal Degradation of Softwood Lignin and Hardwood Lignin by TG-FTIR and Py-GC/MS. *Polym. Degrad. Stab.* **2014**, *108*, 133–138. https://doi.org/10.1016/j.polymdegradstab.2014.06.006
(95). Singh, S. K.; Dhepe, P. L. Isolation of Lignin by Organosolv Process from Different Varieties of Rice Husk: Understanding Their Physical and Chemical Properties. *Bioresour. Technol.* **2016**, *221*, 310–317. https://doi.org/10.1016/j.biortech.2016.09.042
(96). Kaczmarska, K.; Żymankowska-Kumon, S.; Byczyński, Ł.; Grabowska, B.; Bobrowski, A.; Cukrowicz, S. Thermoanalytical Studies (TG–DTG–DSC, Py–GC/MS) of Sodium Carboxymethyl Starch with Different Degrees of Substitution. *Journal of Thermal Analysis and Calorimetry* **2019**, *138* (6), 4417–4425. https://doi.org/10.1007/s10973-019-08892-4
(97). Alves, N. M.; Picart, C.; Mano, J. F. Self Assembling and Crosslinking of Polyelectrolyte Multilayer Films of Chitosan and Alginate Studied by QCM and IR Spectroscopy. *Macromol. Biosci.* **2009**, *9* (8), 776–785. https://doi.org/10.1002/mabi.200800336
(98). Eaton, M. D.; Domene-López, D.; Wang, Q.; G. Montalbán, M.; Martin-Gullon, I.; Shull, K. R. Exploring the Effect of Humidity on Thermoplastic Starch Films Using the Quartz Crystal Microbalance. *Carbohydr. Polym.* **2021**, *261*, 117727. https://doi.org/10.1016/j.carbpol.2021.117727
(99). Staroszczyk, H.; Ciesielski, W.; Tomasik, P. Starch-Metal Complexes and Metal Compounds: Starch-Metal Compounds. *J. Sci. Food Agric* **2018**. https://doi.org/10.1002/jsfa.8820
(100). Ghimici, L.; Nichifor, M. Novel Biodegradable Flocculanting Agents Based on Cationic Amphiphilic Polysaccharides. *Bioresour. Technol.* **2010**, *101* (22), 8549–8554. https://doi.org/10.1016/j.biortech.2010.06.049
(101). Guo, Y.; Kong, F.; Fatehi, P. Generation and Use of Lignin- *g* -AMPS in Extended DLVO Theory for Evaluating the Flocculation of Colloidal Particles. *ACS Omega* **2020**, *5* (33), 21032–21041. https://doi.org/10.1021/acsomega.0c02598
(102). Ciesielski, W.; Tomasik, P. Complexes of Amylose and Amylopectins with Multivalent Metal Salts. *J. Inorg. Biochem.* **2004**, *98* (12), 2039–2051. https://doi.org/10.1016/j.jinorgbio.2004.09.010.
(103). Zhang, Y.; Gao, W.; Fatehi, P. Structure and Settling Performance of Aluminum Oxide and Poly(Acrylic Acid) Flocs in Suspension Systems. *Sep. Purif. Technol.* **2019**, *215*, 115–124. https://doi.org/10.1016/j.seppur.2019.01.012

(104). Czaikoski, A.; Gomes, A.; Kaufmann, K. C.; Liszbinski, R. B.; de Jesus, M. B.; Cunha, R. L. da. Lignin Derivatives Stabilizing Oil-in-Water Emulsions: Technological Aspects, Interfacial Rheology and Cytotoxicity. *Ind. Crops. Prod.* **2020**, *154*, 112762. https://doi.org/10.1016/j.indcrop.2020.112762.
(105). Wiśniewska, M.; Chibowski, S.; Urban, T.; Sternik, D.; Terpiłowski, K. Impact of Anionic Polyacrylamide on Stability and Surface Properties of the Al2O3–Polymer Solution System at Different Temperatures. *Colloid Polym. Sci.* **2016**, *294* (9), 1511–1517. https://doi.org/10.1007/s00396-016-3906-7.
(106). Hasan, A.; Fatehi, P. Flocculation of Kaolin Particles with Cationic Lignin Polymers. *Sci. Rep.* **2019**, *9* (1). https://doi.org/10.1038/s41598-019-39135-z.
(107). Petzold, G.; Goltzsche, C.; Mende, M.; Schwarz, S.; Jaeger, W. Monitoring the Stability of Nanosized Silica Dispersions in Presence of Polycations by a Novel Centrifugal Sedimentation Method. *J. Appl. Polym. Sci.* **2009**, *114* (2), 696–704. https://doi.org/10.1002/app.30608
(108). Ataie, M.; Sutherland, K.; Pakzad, L.; Fatehi, P. Experimental and Modeling Analysis of Lignin Derived Polymer in Flocculating Aluminium Oxide Particles. *Sep. Purif. Technol.* **2020**, *247*, 116944. https://doi.org/10.1016/j.seppur.2020.116944
(109). Zamiri, R.; Zakaria, A.; Ahangar, H. A.; Darroudi, M.; Zak, A. K.; Drummen, G. P. C. Aqueous Starch as a Stabilizer in Zinc Oxide Nanoparticle Synthesis via Laser Ablation. *J. Alloys Compd.* **2012**, *516*, 41–48. https://doi.org/10.1016/j.jallcom.2011.11.118
(110). Mo, S.; Shao, X.; Chen, Y.; Cheng, Z. Increasing Entropy for Colloidal Stabilization. *Sci. Rep.* **2016**, *6* (1), 36836. https://doi.org/10.1038/srep36836
(111). Kazzaz, A. E.; Feizi, Z. H.; Kong, F.; Fatehi, P. Interaction of Poly(Acrylic Acid) and Aluminum Oxide Particles in Suspension: Particle Size Effect. *Colloids Surf. A Physicochem. Eng. Asp.* **2018**, *556*, 218–226. https://doi.org/10.1016/j.colsurfa.2018.08.013
(112). Jarvis, P.; Jefferson, B.; Parsons, S. A. Measuring Floc Structural Characteristics. *Rev Environ Sci Biotechnol* **2005**, *4* (1–2), 1–18. https://doi.org/10.1007/s11157-005-7092-1

4.7. Appendix A. Supporting information

Generation of Sulphonated Lignin-Starch Polymer and its Use as a Flocculant

Jonathan A. Diaz-Baca, Pedram Fatehi*

Biorefining Research Institute and Chemical Engineering Department, Lakehead University, 955 Oliver Road, Thunder Bay, ON P7B SE1, Canada

*Corresponding author: email: pfatehi@lakeheadu.ca, tel:807-343-8010-8697

Number of pages 9 (S4.1-S4.9)

Number of Figures 6 (S4.1-S4.6)

Number of Tables 0

Methods

Starch random hydrolysis and peeling reaction

The corroboration of random hydrolysis and peeling reactions of starch was carried out following the same experimental conditions, the free radical polymerization stated in the main text. In this set of experiments, 1 g of starch in 20 mL of water adjusted to pH 11 with NaOH (1 mol/g) was used for the reaction. After purification, the product was dried in a vacuum oven at 50°C and used in this study.

Scanning electron microscopy

The surface morphology of the aluminum oxide and the flocs of aluminum oxide/TOL, aluminum oxide/starch, and aluminum oxide/anionic products was studied via scanning electron microscopy (SEM) analysis using a Hitachi SU-70 (Hitachi Ltd., Chiyoda, Tokyo, Japan) microscope at 10 kV. In this analysis, the aluminum oxide was mixed with water and hydrated at pH 7 overnight to be used as a blank sample. In addition, the optimum dose of the polymers was added with 100 mL of aluminum oxide suspension (5 g/L concentration) in Erlenmeyer flasks at 150 rpm for one hour to allow the flocculation. The samples were then collected without filtration, vacuum oven-dried at 50 °C, and then were gold-coated for the SEM analysis.

Results

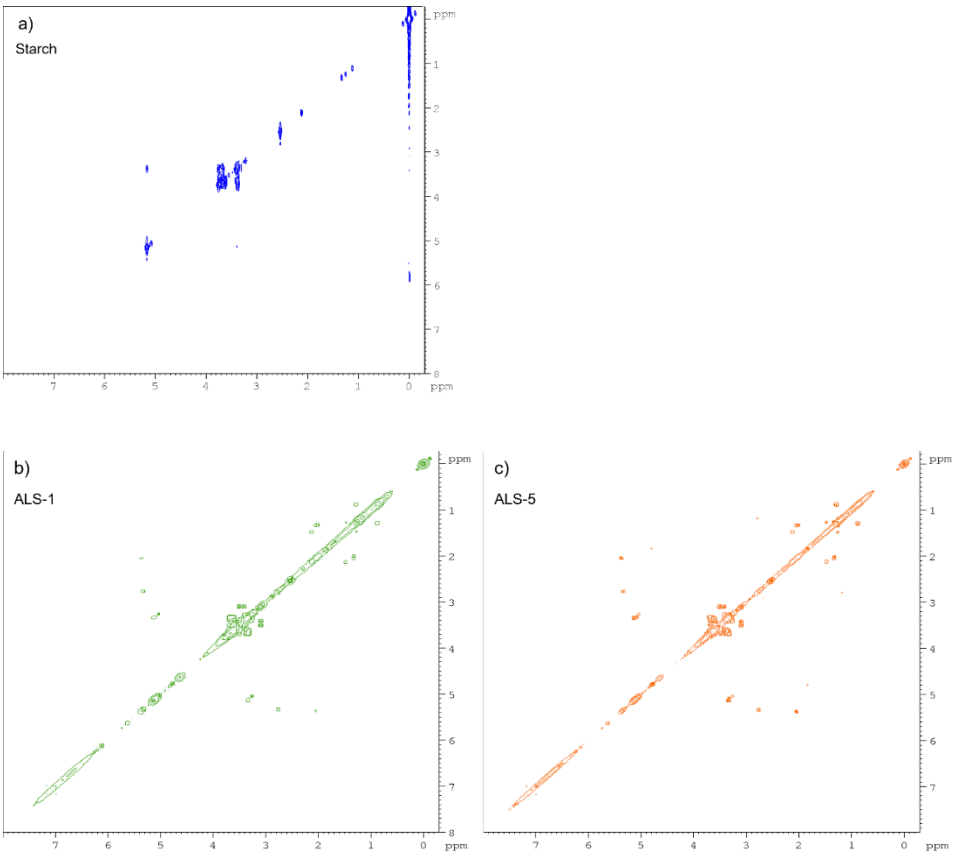

Figure S4.1. ^{1}H-^{1}H COSY NMR spectra of starch (a), ALS-1 (b), and ALS-5 (c).

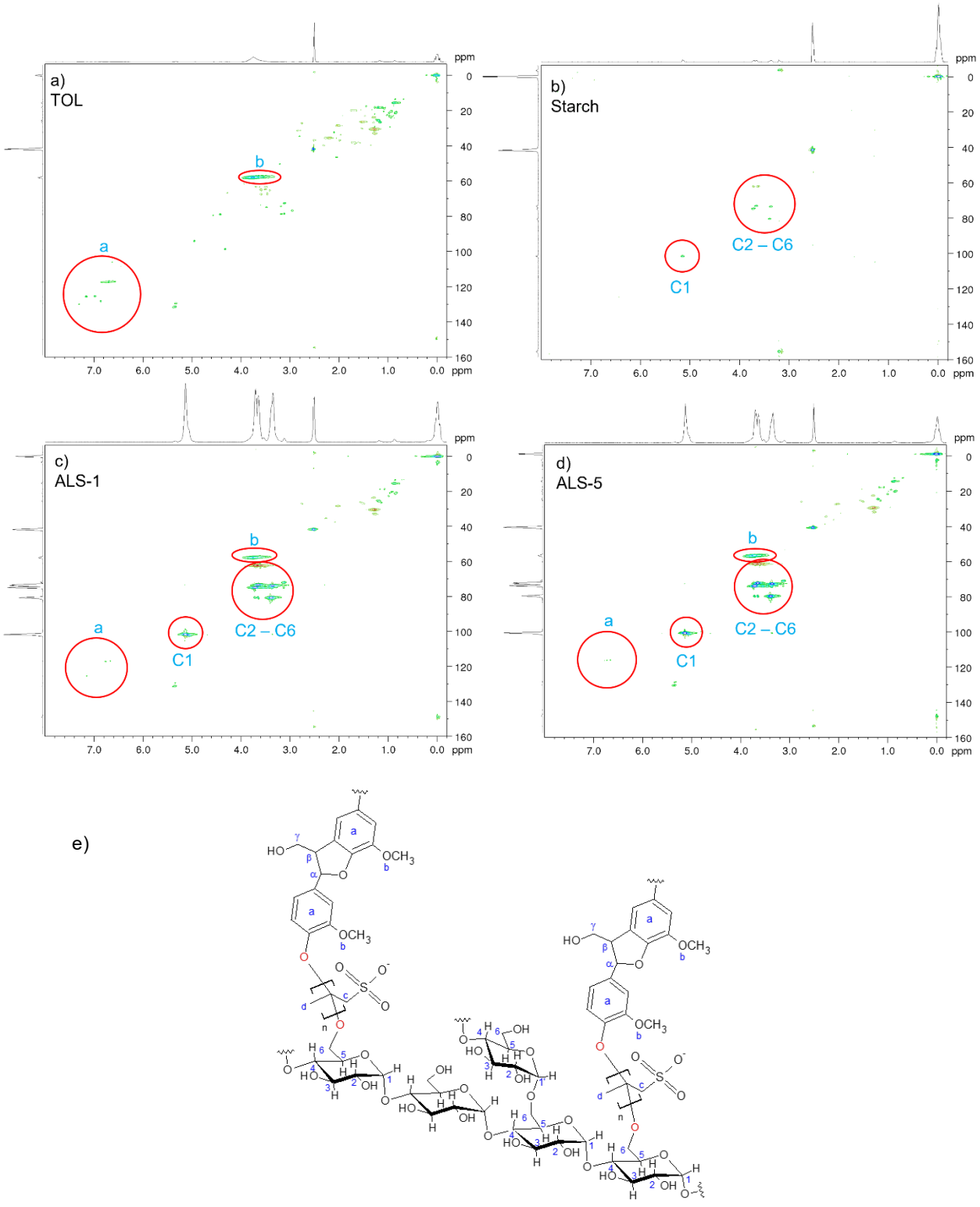

Figure S4.2. ^{1}H-^{13}C HSQC spectra of TOL (a), starch (b), ALS-1 (c), and ALS-5 (d). Red circles indicate the corresponding cross-peaks of the aromatic region, methoxy and AGU, as described in the proposed structure of the anionic TOL-starch ternary copolymers (e).

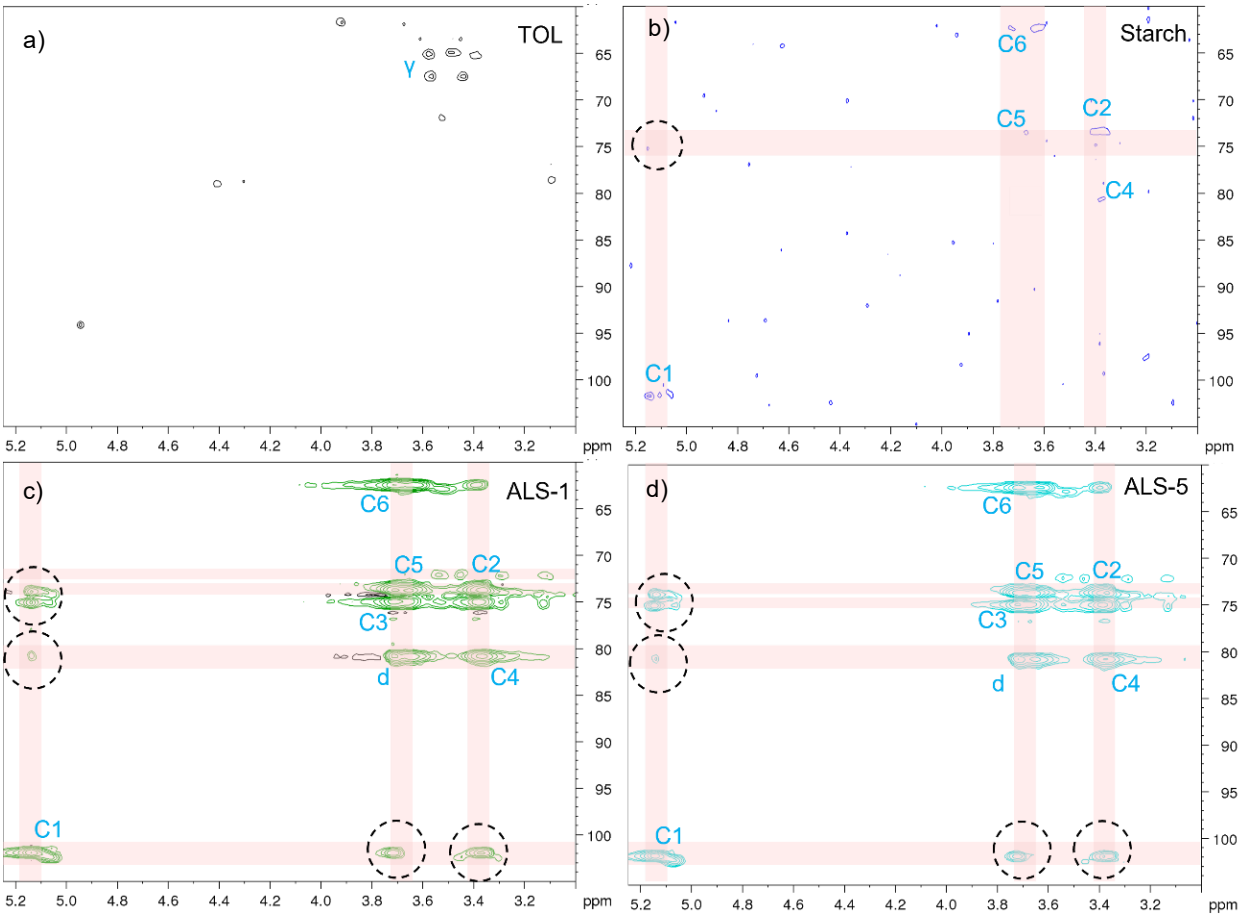

Figure S4.3. ^{1}H-^{13}C HSQC-TOCSY spectra of TOL (a), starch (b), ALS-1 (c), and ALS-5 (d). Doted circles indicate TOCSY correlations of carbons (vertical) and protons (horizontal). The labels are assigned as described in the chemical structure shown in Figure S4.2e.

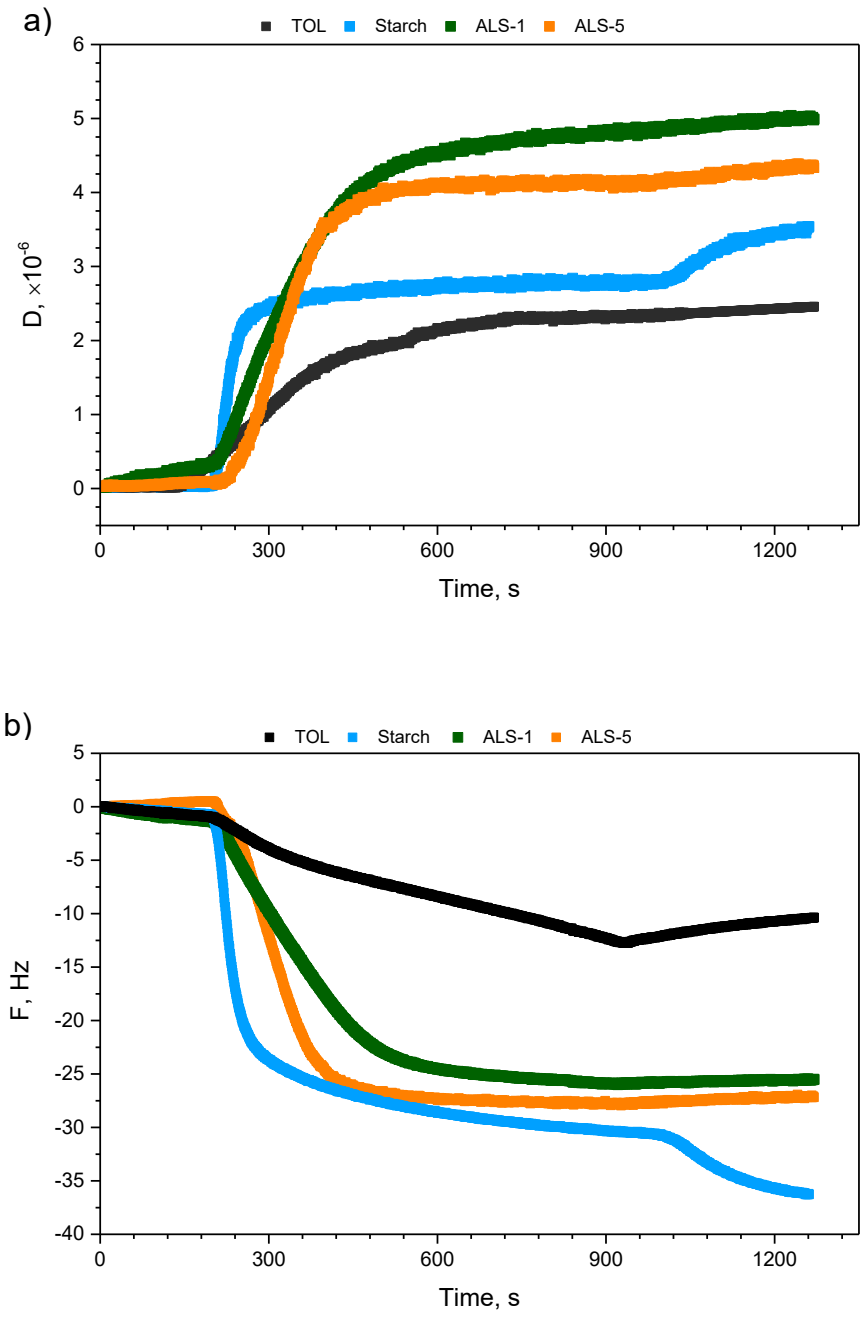

Figure S4.4. Adsorption of TOL, starch, ALS-1, and ALS-5 on the aluminum oxide sensor displayed by the shift in D (a) and the shift in F (b).

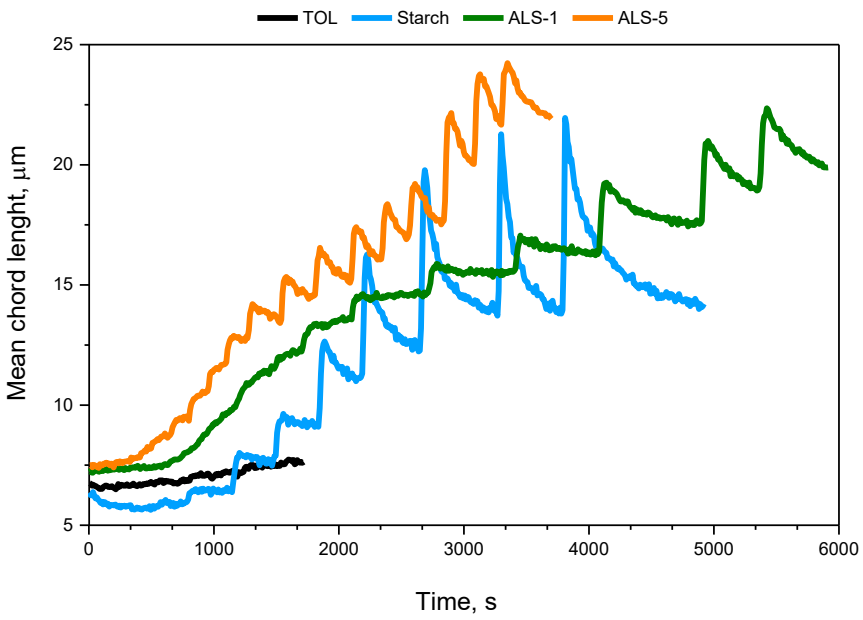

Figure S4.5. Mean chord length profiles of aluminum oxide suspensions after the addition of TOL, starch, ALS-1, and ALS-5 with dose increment until the observation of deflocculation

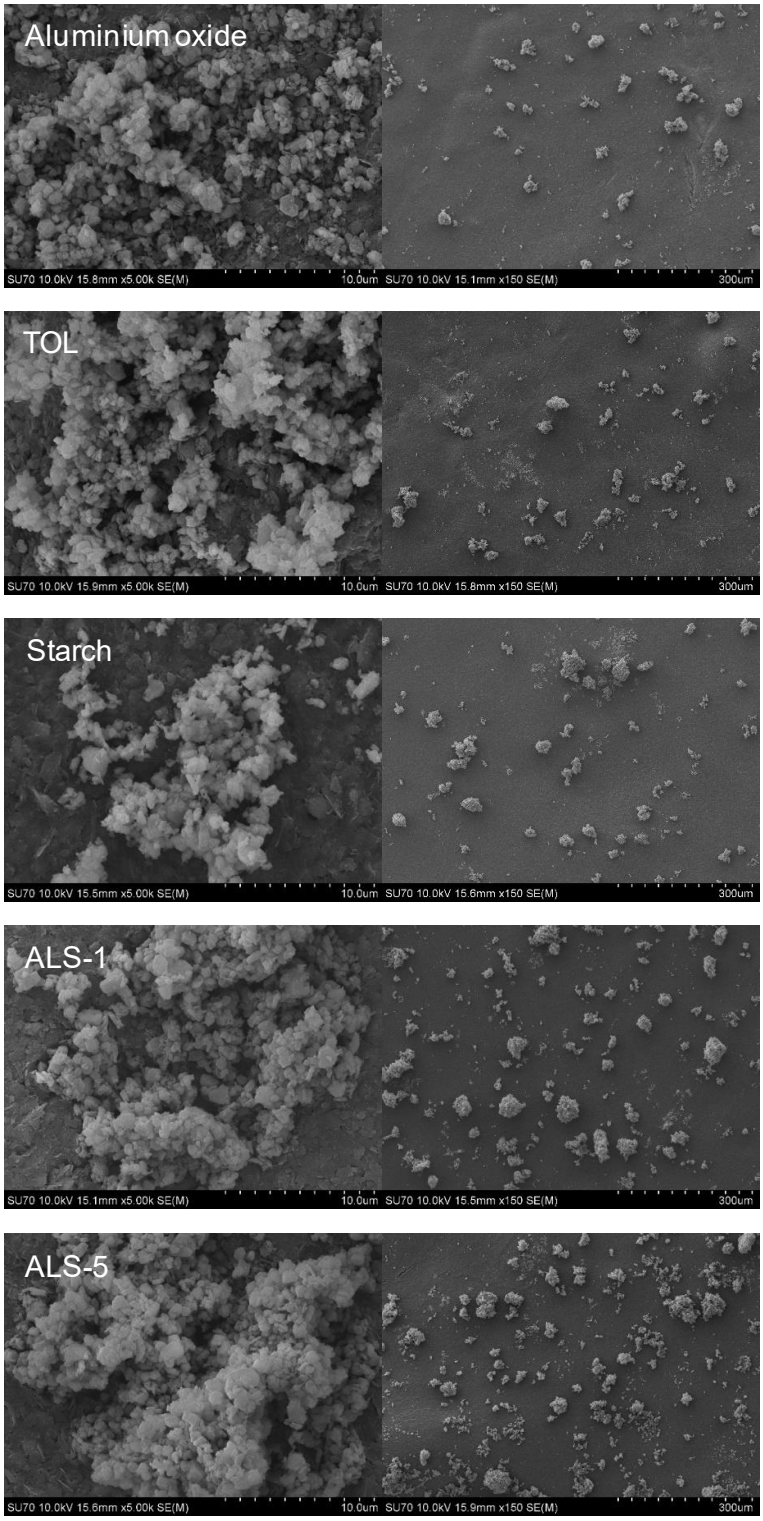

Figure S4.6. SEM images of aluminum oxide particles and the flocs formed by TOL, starch, ALS-1, and ALS-5 (with a magnification of ×5000 and 150).

Chapter 5: Temperature Responsive Crosslinked Lignin-Starch Macromolecule

Jonathan A. Diaz-Baca, Pedram Fatehi*

Submitted to ACS Sustainable Chem. Eng. 2022

Green Processes Research Centre and Chemical Engineering Department,

Lakehead University, 955 Oliver Road,

Thunder Bay, ON P7B5E1, Canada

*Corresponding author: email: pfatehi@lakeheadu.ca, tel:807-343-8010-8697

The contribution of Jonathan A. Diaz-Baca to this work was performing the experiments, validating, and drafting the manuscript.

5.1. Abstract

Kraft lignin (KL) is a complex biopolymer obtained as a by-product from the delignification of wood and grasses. Starch is also a natural polymer with a relatively simple structure and relatively limited solubility in water. The preset work reports developing a temperature-responsive high molecular weight macromolecule from crosslinking of KL and potato starch (KLS). The NMR and XPS analyses quantified the changes in the aromatic and anhydroglucose units of KL and starch, observing a higher content of C–O–C bonds, which confirms the presence of glycerol ether cross-linkages between starch and KL in KLS. The temperature-dependent water solubility and rheological characteristics of KLS were related to the insertion of hydrophilic starch chains, crosslinking degree and physicochemical characteristics of KL. The incorporation of KL and ether crosslinks increased the thermal stability of KLS. The rheological analysis of KLS dispersions revealed the formation of a thermo-responsive structured network. Because of its multiple functional groups and large molecular weight ($3.6 – 4.2 \times 10^5$ g/mol) arranged in an extended globular shape, KLS formed a gel-like structure in a heating-cooling treatment.

Keywords: lignin, starch, temperature-responsive, crosslinking, physicochemical characterization

5.2. Introduction

Lignin is a complex polymer of phenyl propanol units and is the earth's second most abundant natural polymer. Lignin is primarily obtained as a by-product from the delignification of lignocelluloses in the pulp and paper industry. The kraft pulping process is currently the most dominant delignification method, in which kraft lignin (KL) is generated, and the production of KL has the fastest-growing market among technical lignins.[1,2] KL has a highly heterogenous structure with a three-dimensional amorphous arrangement. Despite its complexity, KL is a non-

toxic and biodegradable polymer with desirable properties for producing bio-based value-added materials.[3] Different approaches have been undertaken to widen the use of KL in industry, and the crosslinking of KL with other natural polymers is a strategy that has gained attention in recent years.[4–8] Generally, the low molecular weight of KL is a characteristic that is often targeted for increasing its performance in different polymeric applications such as dispersants, adhesives or hydrogels.[9–11]

Starch is a biodegradable natural polymer that is inexpensive and available in large quantities. Unlike KL, starch has a relatively simple structure, consisting of repetitive units of anhydroglucose (AGU) arranged in linear (amylose) and branched (amylopectin) fractions.[12] Starch is often chemically modified to alter its native physicochemical and mechanical properties by targeting the several hydroxyl groups available in its structure.[13] Most modifications are carried out by using small synthetic compounds or via grafting, etherification, and graft polymerization.[14–16]

The incorporation of lignin in starch-based composites has recently received significant attention. Lignin is preferred because it aids in overcoming the difficult processability, retrogradation and syneresis (i.e., gel contraction causing liquid exudation), and low mechanical and thermal resistance of the starch-based composites.[17] These starch-lignin materials have been investigated for applications such as slow-release fertilizers, films/coatings, adhesives, and bio-composites. For instance, KL was used as a filler in crosslinked starch composites to reduce the biodegradability of fertilizer films.[18] It was also investigated in starch-based coating for packaging materials.[19] KL was mixed with starch to produce water-resistant adhesives.[20] However, lignin had only a minor role in the explored applications since it contained a small fraction (5 to 20 wt.%) of the composite. Moreover, those composites were incorporated into different synthetic polymers

(e.g., poly(butylene-adipate-co-terephthalate)–PBAT),[21] which reduces the sustainable character of the material.

Previous work reported primarily physical blending and non-covalent interactions of KL and starch. The physical blends of polymers frequently display multiphase and miscibility challenges and are less stable against temperature or pH shifts.[22,23] To this date, only a reduced number of reports are available regarding the production, characterization, or application of covalently linked starch-lignin copolymers. The existing literature is limited to studying the copolymerization of starch with sodium lignosulphonates to produce biobased paper adhesives.[24] Also, most applications of lignin-starch composites were reported for solid-state materials, such as films, coatings, or adhesives. In contrast, the assessment of water-based applications has not been investigated yet since generating such materials with the physical blending of KL and starch is impossible. Water-dispersible polymers display specific behavior in aqueous systems, including dissolving, dispersing, or swelling, which are desirable properties for such applications as stabilizers, flocculants, dispersants, thickeners, and gel-formers.

Remarkably, information about the chemical characterization, physicochemical and rheological properties of the covalently bound starch-lignin macromolecules is scarce. The chemical structure of the macromolecules has not been detailed yet. However, understanding the properties of starch-lignin macromolecules is essential for accurately selecting their appropriate applications.[25–27] Structural analysis of starch-lignin macromolecules helps identify the major substructures and interunit linkages presented in the macromolecules.[28] Also, the relationship between physicochemical properties and their applicability in aqueous media can be established by determining the size, conformation, thermal response, and viscoelastic behavior of the

macromolecules.[29–32] In this work, we comprehensively studied the chemical structure, physicochemical characteristics, and thermal properties of KL-starch macromolecules.

This work aimed to develop a high molecular weight macromolecule of crosslinked KL and starch (KLS). For this purpose, it was decided to use epichlorohydrin, as the crosslinking reagent, since it has been proven to be an effective crosslinker for KL and starch in different systems.[33,34] The primary novelty of this work was the fabrication of covalently crosslinked KL-starch macromolecules with temperature-responsive features. The chemical structure, physicochemical characteristics, thermal properties, and rheological behaviour of the macromolecules were comprehensively studied using advanced tools, such as H-NMR, P-NMR, HSQC-NMR, XPS, SLS, TGA, DSC and dynamic oscillatory rheology.

5.3. Experimental Section

5.3.1. Materials

Kraft lignin (KL) of softwood species generated via the LignoForce^{TM} system was received from a mill in northern Ontario, Canada. Potato starch, ACS grade soluble (99.9 %, CAS 9005-84-9, amylose content 30.9 ± 0.2 %), dimethyl sulfoxide (DMSO) (≥99.9%), boron trifluoride etherate (^{+}H $^{-}BF_3OH$), tetrabutylammonium bromide (TBAB) (≥98.0%), poly(diallyldimetylammonium chloride) (PDADMAC) (100–200 kg/mol), sodium hydroxide (NaOH) (≥ 97%), sulphuric acid (H_2SO_4), hydrochloric acid reagent grade (HCl) (37%), ρ-hydroxybenzoic acid, ethanol (95%), acetone (≥99.5%), lithium bromide (LiBr), dimethyl sulphoxide-d_6 (DMSO-d_6) (99.9 %), 3- 2-Chloro-4,4,5,5-tetramethyl-1,3,2-dioxaphospholane (CDP) (95 %), (Trimethylsilyl)propionic-2,2,3,3-d4 acid sodium salt tetramethylsilane (TSP) (≥98.5 %), cyclohexanol (99 %), and chromium(III) acetylacetonate (97%) were all acquired from Millipore Sigma, Oakville, Canada. Epichlorohydrin (ECH) (99%) and the 0.45 µm Nylon membrane syringe filters were acquired

from Fisher Scientific, Ottawa, Canada. Lithium chloride (LiCl) was purchased from VWR, Canada. Potassium polyvinyl sulphate (PVSK) (100,000–200,000 g/mol, 97.7 wt.% esterified) was obtained from Wako Pure Chem. Ltd., Osaka, Japan. Also, a dialysis membrane (1,000 g/mol cut off) was provided by Spectrum Labs. N,N-Dimethylformamide (DMF) ACS reagent was acquired from ACP chemicals, Montreal, Canada.

5.3.2. Experimental Design

The analysis of the reaction conditions and their interaction was performed using the 2^3 factorial design, as detailed in Table 5.1. This experiment analyzed three factors: KL to starch mass ratio, epichlorohydrin (ECH) concentration, and the solvent of the reaction medium (qualitative). Each qualitative factor contained two levels and center points for a total of 12 experimental runs to investigate the effect of the studied factors on the response (i.e., solubility) of the produced lignin-starch macromolecule (KLS). The Design-Expert® software (MN, USA) was used to build the factorial design and provide a graphical illustration of the data and interaction results.

Table 5.1. The 2^3 factorial design performed with three factors (one qualitative factor), each containing two levels and center points

Factor	Low level, −	High level, +	Center level, 0
KL to starch, mass ratio	25/75	75/25	50/50
ECH mass, g/g	0.5	2.5	1.25
Solvent type	DMF	DMSO	NA

NA, not applicable for qualitative factor

5.3.3. Starch characterization

Elemental analysis of starch. The elemental determination (carbon, hydrogen, nitrogen, and sulfur) of starch was performed using the combustion method (CHNS).[35] 2 mg of previously dried (60 °C, vacuum oven) starch was combusted at 1200 °C to determine their elements using an elemental analyzer (Vario EL cube, Elementar Analysensysteme GmbH, Germany). The oxygen content of starch was determined through the mass balance from the subtraction of carbon, hydrogen, nitrogen, and sulfur content on an inorganic-free basis.

Analysis of the amylose content of starch. The amylose content of starch was analyzed using the standardized iodine-binding colorimetry method ISO 6647-1:2020as reported earlier.[36,37] The absorbance of the solutions of the starch-iodine complex was analyzed at 720 nm with a UV/Vis spectrophotometer (Genesys 10S UV/vis, Thermo Scientific, USA).[38] The amylose content was estimated from the average ± standard error of three independent measurements.

Polarized light microscopy of starch granules. The microscopy analysis of the starch granules was carried out using a starch dispersion in water (0.25 mg/mL). As reported previously (Xiao et al., 2020), 100 µL of the starch suspension were placed in between a glass slide and a coverslip to performed the microscopy analysis.[39] The analysis was carried out in a polarizing light microscope (OLYMPUS BX51-P, Olympus corporation, Japan). The morphology and hilum position of starch granules was observed under plain-polarized transmitted light and cross-polarized transmitted light, respectively. The images were obtained using the 10X and 20X objectives and a color digital microscope camera (OLYMPUS SC190, Olympus corporation, Japan).

5.3.4. KL-Starch crosslinking reaction

The crosslinking of KL and starch was carried out in a two-step reaction process. A total mass of 2 g of KL and starch was used in the reaction, as depicted in Table 4.2. In the 1st step, KL was solubilized in two different aprotic solvents of DMSO and DMF to have a solution of 5 w/v %. Afterward, the KL solution was added to a three-neck round-bottom flask equipped with a reflux condenser and stirred at 250 rpm. Then, 1 g of $BF_3.Et_2O$ was slowly added to the system, which was followed by the addition of ECH dropwise. In this experiment, very-low, medium-low and low (1, 2.5 and 5 g, respectively) amounts of crosslinker were used, but higher ratios of epichlorohydrin to lignin (20:1 to 10:1) were used in other studies.[40,41] The reaction was carried out for 3 h at 60 °C.[34,42] Next, the mixture was placed in a rotary evaporator (60 °C, 33 bar) (R210, Büchi®, DE, USA) to remove the unreacted ECH from the reaction.[43] The produced material of this process, denoted as KL-CI, was kept for further use and analysis, as KL-CI-1DMSO, KL-CI-1DMF, KL-CI-5DMSO, KL-CI-5DMF generated with 1 or 5g of ECH and DMSO or DMF solvent.

In the 2nd step, starch was dispersed in NaOH (1 mol/g) to obtain a 5 w/v % slurry after 12 h under stirring and 25 °C. Afterward, the starch slurry was added to a round flask with a reflux condenser. Then, 250 mg of TBAB was added to the slurry and kept under stirring (450 rpm) for 5 min at 60 °C. Next, the KL-CI solution was added dropwise to the flask. The temperature was increased to 70 °C, and the reaction was carried out for 5 h.[44,45] Upon completion, the reaction mixture was cooled to room temperature, neutralized with HCl (0.5 mol/g), and then kept in dialysis membrane tubes for 72 h to remove inorganic salts and unreacted reagents. Then, dialyzed products were dried in a vacuum oven (Model 282A, Fisherbrand™ Isotemp™, ON, Canada) at 50°C and used for calculating the mass recovery yield (Equation 1). Subsequently, the obtained

KL-starch products (KLS) were purified with ethanol/acetone (70/30 v/v) mixture to remove unreacted lignin and then with warm water (60 °C) to remove unreacted starch. The purified KLS was dried in a vacuum oven at 60 °C and collected for the mass recovery yield calculation (Equation 2). Different KLS products were generated under different conditions, as stated in Table 5.2.

$$\text{Yield after dialysis } (\%) = \frac{dry\ mass\ of\ dialized\ product}{mass\ of\ KL + mass\ of\ Starch} \times 100 \quad (1)$$

$$\text{Yield after purification } (\%) = \frac{dry\ mass\ of\ purified\ product}{dry\ mass\ of\ dialized\ product} \times 100 \quad (2)$$

Table 5.2. Summary of experimental runs and controlled variables for each KLS sample.

Sample	KL/Starch, mass ratio	ECH, g	KL solvent
KLS-5	25/75	1	DMSO
KLS-1	25/75	1	DMF
KLS-7	25/75	5	DMSO
KLS-3	25/75	5	DMF
KLS-6	75/25	1	DMSO
KLS-2	75/25	1	DMF
KLS-8	75/25	5	DMSO
KLS-4	75/25	5	DMF
KLS-9	50/50	2.5	DMSO

KLS-11	50/50	2.5	DMF
KLS-10	50/50	2.5	DMSO
KLS-12	50/50	2.5	DMF

5.3.5. ^{1}H and HSQC NMR

The Proton nuclear magnetic resonance (^{1}H NMR) and two-dimensional heteronuclear single quantum coherence NMR (2D-HSQC) analyses of KL, starch, KL-CI and KLS were performed to understand the chemical structures of the materials. For ^{1}H and HSQC NMR analyses, 50–60 mg of KL or KL-CI were dissolved in 1 mL of DMSO-d_6, whereas 50–60 mg of starch or KLS were dissolved in 1 mL of 0.5 wt.% LiBr/DMSO-d_6 solution.[46] Also, 5-6 mg of TSP (internal standard) were added to each sample. All samples were stirred for 24 h at 25 °C before the analysis. The ^{1}H NMR and 2D-HSQC spectra were obtained using nuclear magnetic resonance spectroscopy (AVANCE NEO-1.2 GHz, Bruker Corporation, USA). The analysis temperature was 25 °C for KL, KL-CI and 70 °C for starch and KLS macromolecule (Schmitz et al., 2009).

Adjustments for ^{1}H NMR were set as follows: a total of 16 scans per sample, a 3.28 s acquisition time, a 30° pulse, and 1.00 s of relaxation delay time. For the acquisition of HSQC NMR spectra, the Bruker pulse program "hsqcetgpsisp2.3 was used, 13 ppm spectra width in the F2 (^{1}H) dimension with 2048 data points (155 ms acquisition time), 165 ppm spectra width in the F1 (^{13}C) dimension with 256 data points (6.2 ms acquisition time), a 1.5 s pulse delay, and 16 scans were applied. The NMR data points and spectra were processed using the TopSpin 4.0.9 software (2020 Bruker BioSpin GmbH).

5.3.6. ^{31}P NMR

The quantification of the phenolic and aliphatic hydroxyl groups of KL, KL-CI, and selected KLS macromolecule was carried out via phosphitylation reaction followed by ^{31}P nuclear magnetic resonance (^{31}P NMR) analysis.[47] First, 30-70 mg of the samples were dissolved in 1 mL of the solvent mixture of chloroform-d ($CDCl_3$) and pyridine (1:1.6 v/v). The solutions of relaxation agent (chromium (III) acetylacetonate) (2.5 mg/mL) and internal standard (TSP) (20 mg/mL) in $CDCl_3$/pyridine were also prepared. For all samples, 200 µL of phosphitylation reagent CDP, 100 µL of relaxation agent (chromium (III) acetylacetonate) and 70 µL of cyclohexanol (0.23 mmol/mL in $CDCl_3$/pyridine) were mixed. The ^{31}P NMR spectra were obtained using a nuclear magnetic resonance spectroscopy (AVANCE NEO-1.2 GHz, Bruker Corporation, USA) with a total of 1024 scans per sample at 25 °C, a 0.6 s acquisition time, a 90° pulse, and 5 s of relaxation delay time. The NMR data points and spectra were processed using the TopSpin 4.0.9 software (2020 Bruker BioSpin GmbH).

5.3.7. XPS

The surface chemical compositions of KL, starch, and KLS were analyzed using an X-ray photoelectron spectroscopy (XPS) analyzer (Kratos AXIS Supra, Shimadzu Group Company, Japan) with a dual anode Al/Ag monochromatic X-ray source (1486.7 eV). Samples were mortar ground and dried in a vacuum oven (50 °C). After that, the samples were placed onto a double-sided carbon tape and submitted to the XPS machine. The operating conditions were set at 15 kV (90 W) in a FAT mode (fixed analyzer transmission) with a pass energy of 40 eV for the region of interest and 80 eV for the survey region. The obtained XPS spectra and the quantification of the chemical bonds were determined using ESCApe™ 1.4.0.1149 software (Kratos Analytical, Japan).[48]

5.3.8. Potentiometric Titration of Phenolic Groups

The phenolic group contents of KL and KLS were determined by potentiometric titration using an automatic titrator (785 DMP Titrino, Metrohm, Switzerland). Approximately 0.06 g of dried samples were added to 100 mL of deionized water containing 1 mL of 0.8 mol/L KOH. Next, 0.5% of *p*-hydroxybenzoic acid solution was added as an internal standard. Then, the solution was titrated against 0.1 mol/L HCl. The phenolic hydroxyl group content of the samples was calculated according to (Equation 3).[49] Results are the average of three independent measurements.

$$\text{Phenolic hydroxyl group content}\left(\text{mmol}/\text{g}\right) = \frac{C_{\text{HCL}}\ [(\text{V2}' - \text{V1}') - (\text{V2} - \text{V1})]}{m} \qquad (3)$$

5.3.9. Charge Density

The charge density of KL, starch and KLS was determined by a Particle Charge Detector (PCD-04+Titrator, Mütek, Germany) as previously described.[50] The 1 wt.% suspension of the samples was shaken at 200 rpm and 25 °C for 12 h in a water bath (Innova 3100, Brunswick Scientific, Edison, NJ, USA). Afterward, the suspensions were centrifuged at 1000 rpm for 5 min. Then, 1 mL of the solution portion of the samples was titrated against PVSK (0.005 mol/g) to determine the charge density of the soluble samples. To determine the surface charge density of the insoluble fraction, 0.05 g of the precipitated samples (on a dried basis) were suspended in 50 mL of PDADMAC (0.025 mol/g) solution and titrated against PVSK (0.005 mol/g) solution.

5.3.10. Solubility Measurements

The solubility of KL, starch and KLS was measured by adding 0.2 g of the materials to 19.8 mL of deionized water. In one set of experiments, the test was performed at a constant temperature of 25 °C. The suspensions were shaken at 200 rpm and 25 °C for 12 h in a water bath (Innova 3100, Brunswick Scientific, Edison, NJ, USA). In another set of experiments, the test was performed at

five different temperatures from 10 to 70 °C. The suspensions were in constant stirring at 500 rpm on a stirring plate inside a low-temperature incubator (Fisher Scientific, OH, USA) at 10, 25, 40, 55 and 70 °C for 24 h. Next, the suspensions were centrifuged at 1000 rpm for 5 min. The supernatants were collected and weighted after drying at 105 °C in a conventional oven. The solubility of the samples from both set of experiments was calculated considering the collected, dried weight of the insoluble samples.

5.3.11. Light Scattering Analysis

Molecular weight and radius of gyration. The absolute molecular weight (MW) and radius of gyration (R_g) of KL, starch, and KLS macromolecule were determined via the static light scattering (SLS) technique.[51] A laser light scattering system attached to a goniometer (BI-200SM, Brookhaven Instruments Corporation, NY, USA) was used in this analysis. A maximum solid-state laser power of 35 mW and a wavelength of 637 nm were applied. Different concentrations (0.2 to 2.0 mg/mL) of the samples were prepared in DMSO/LiCl solution (8 w/v %) and stirred for 24 h at 25 °C. All solutions were filtered twice with 0.45 μm Nylon membrane syringe filters before the SLS analysis. The assessment was made in duplicate at multiple scattering angles from 20° to 155° and 25 °C. The MW and R_g were automatically obtained from the Berry plot,[52] which was constructed by the BI-200SM software (Brookhaven Instruments Corp).

Hydrodynamic diameter analysis. The hydrodynamic radius (R_h) of KL, starch, and KLS macromolecule was determined via the dynamic light scattering (DLS) technique. In this experiment, a laser light scattering system attached to a goniometer (BI-200SM, Brookhaven Instruments Corporation, NY, USA) was used. The maximum solid-state laser power used in the experiment was 35 mW at the wavelength of 637 nm. The analysis was made at 25 °C and at a fixed scattering angle of 90°.[53] First, 1 mg/mL of each sample in DMSO/LiCl (8 w/v %) was

prepared and stirred for 24 h at 25 °C. Before the DLS analysis, all the solutions were filtered twice with 0.45 μm Nylon membrane syringe filters. The analyses were conducted in triplicate, and the average values were reported. The R_g/R_h ratio was also calculated by considering R_g and R_h to obtain the shape factor, ρ.[54]

5.3.12. Thermal Analysis

The thermogravimetric analysis (TGA) was performed to determine the thermal stability of KL, starch and KLS macromolecule.[55] Samples were dried in a vacuum oven at 50 °C for 24 h prior to the analysis. The thermal analysis was performed by a thermal analyzer (TGA i1000, Instrument Specialists Inc., WI, USA) for 7-8 mg of the samples in a nitrogen atmosphere at a 15 mL/min flow rate and monitoring the weight change over the temperature range of 25 °C to 800 °C at the rate of 10 °C/min. The analyses were conducted in duplicate, and the average and standard deviation values were reported.

The glass transition temperature (T_g) of KL, starch and KLS macromolecule was also estimated by a differential scanning calorimetry (DSC).[56] In this experiment, 10 to 12 mg of dried samples were placed in hermetic Tzero® aluminum pans and loaded into a differential scanning calorimeter (DSC Q2000, TA Instruments, DE, USA). The analysis was carried out in a nitrogen atmosphere at a flow rate of 50 °C/min. In this experiment, two heating and one cooling cycle were performed. First, the temperature was raised from 20 °C to 230 °C, which was used to erase thermal history, then a cooling ramp from 230 °C to 20 °C at 5.0 °C/min was applied. Afterward, a second heating cycle from 20 °C to 230 °C at 10.0 °C/min was performed for the T_g determination. The analyses were conducted in duplicate, and the average and standard deviation values were reported.

5.3.13. Rheological Characterization

The viscoelastic properties of the water containing disperse systems of KL, starch, and KLS macromolecule were determined by dynamic oscillatory measurements. A hybrid rotational rheometer (Discovery HR-2, TA Instruments, DE, USA) was used for this analysis. For the measurements, a Peltier concentric cylinder and a starch impeller geometry (rad=18.5 mm), specifically designed for the characterization of starch slurries (TA Instruments, DE, USA), were used.[57] First, samples were prepared at 2 wt.% to be above the entanglement concentration of starch and between a semi-dilute unentangled and a semi-dilute entangled regime.[58,59] The samples were kept under stirring for 12 h before transferring to the rheometer cup.[60] The analysis was carried out while the rotor was lowered in the cup, leaving a gap of 5 mm between the impeller and the bottom of the cup. Each sample was preconditioned at 25 °C, 30 rad/s for 120 s to set uniform conditions before every experiment.

For the rheological characterization, four different test procedures were carried out: a shear sweep, strain/amplitude sweep, frequency sweep, and heating-cooling temperature ramp.[61,62] Each test was completed in triplicate, and the averaged trend was used. The shear sweep experiments were conducted to determine the apparent viscosity. The shear rate was set from 0.1 to 100.0 1/s with 5 s of equilibrium time and 25 °C, following a decreasing shear rate from 100 to 0.1 1/s. The strain amplitude sweep experiments were conducted to determine the viscoelastic linear region of the samples. The strain sweep was set from 0.01 to 100.00 % at a constant frequency mode of 1.0 Hz and 25 °C. After that, the frequency sweep experiments were conducted at 25 °C and an angular frequency ranging from 0.01 to 10.00 Hz with a continuous oscillating strain of 0.3 %. The temperature ramp experiments were performed with heating-cooling curves and an oscillating strain of 0.3 % with a frequency of 1.0 Hz. The heating ramp was carried out from 10 to 70 °C

with a heating rate of 2 °C/min and 10 s of soaking time. After reaching 70 °C, the cooling ramp was set to a rate of 5 °C/min and 10 s of soaking time.

5.4. Results and Discussion

5.4.1. Starch Characterization

Starch granules presented an oval and spherical morphology, and the hilum was positioned at one end of the granules, which is characteristic of potato starch, as observed in Figure S5.1. The elemental composition analysis showed high purity, and no nitrogen nor sulphur impurities were detected, C 42.6 ± 0.2 %, H 6.7±0.1 %, N 0.0±0.0 %, S 0.0±0.0 %, and O 50.6±0.3 %.

5.4.2. Solubility Optimization

To identify the effect of reaction conditions (KL to starch ratio, ECH concentration, and the solvent) on the water-solubility of the KLS macromolecule, experiments were carried out following a factorial analysis of a 2^3 design, and the results are shown in Table S5.1 of Supporting Information. The solubility of KL was 2.36 g/L, which was similar to that reported previously.[53] The solubility of starch in water was found to be the lowest among all samples (0.96 g/L) at room temperature (22 °C). Concerning the KLS macromolecule, the solubility values ranged from 1.50 (KLS-4) to 6.37 g/L (KLS-7). The interaction plots between the studied factors can be found in Figures S5.2-S5.4 in Supporting Information. The solubility of the KLS macromolecule increased when the KL content was lower (25/75), and ECH concentration was the highest (2.5 g/g). Likewise, a lower ratio of starch and lower ECH concentration (0.5 g/g) resulted in lower solubility of KLS. The higher starch/lignin ratio resulted in the highest solubility because of the higher proportion of starch as the more hydrophilic component in the structure of KLS. In this case, the starch granules were opened during the reactions under basic conditions and 80 °C, and the

hydrophilic starch chains were released and crosslinked with KL-CI chains.[63,64] The highest content of ECH also promoted more attachment points between KL-CI and the starch chains, resulting in a higher solubility. It should be stated that the concentration of ECH used in this work was lower than that used for producing highly crosslinked products, such as lignin-based epoxy resins, which are mostly insoluble.[40,41]

When comparing the solvents, DMSO was the preferred solvent for producing KLS with higher solubility. DMSO possesses a larger dielectric constant and dipole moment than DMF, which promotes a more efficient stabilization of the charged species during the reaction, thus favoring the crosslinking between KL and starch. The best conditions for producing KLS macromolecules with the highest solubility were 25/75 KL/starch ratio, 2.5 g/g of ECH, and DMSO as the solvent. These optimum parameters were used for generating KLS-7. Based on their solubility differences (Table S5.1 in Supporting Information), three KLS macromolecules, KLS-4, KLS-5, and KLS-7, were selected to further analysis.

5.4.3. Charge Density and Phenolic Hydroxyl Content

The charge density and the phenolic hydroxyl (Ph−OH) content of the samples are displayed in Table S5.1. The charge density of KL and starch was -0.5 mmol/g, owing to the ionization of the −COOH groups of KL and the residues of phosphate monoester groups naturally attached to the AGU in starch.[65−68] After the crosslinking reaction and purification, the KLS macromolecule had a limited charge density. Likewise, an evident decrease in the Ph−OH group concentration is seen when KL was compared with the KLS macromolecule. The Ph−OH content decreased at different percentages of the KL content, from 50% (KLS-6) as the lowest to 85% (KLS-10) as the highest. These results are attributed to the crosslinking between the Ph−OH groups of KL and starch, which caused the decrement in the free Ph−OH groups. However, a small decrement in the charge density

was observed, resulting from side reactions happening at the –COOH groups of KL as described previously.[69–71]

5.4.4. NMR Characterization

^{1}H-NMR analysis. The chemical structure of KL, starch and KLS macromolecule was analyzed by ^{1}H-NMR (Figure 5.1). The signal corresponding to the internal standard and DMSO-d_6 are observed for all samples at 1.0 and 2.5 ppm, respectively. In the ^{1}H spectrum of KL, the protons belonging to the aliphatic moieties of KL are observed in the region of 0.50-2.40 ppm, and the protons from the –OCH_3 groups are observable in the region of 3.50-4.10 ppm. The peaks observed at the region of 6.00-7.50 ppm are attributed to the aromatic protons.[72] For starch, the peaks observed at 4.90-5.10 ppm region are attributed to the protons of the 1→4 and 1→6 inter-unit linkage between the anhydroglucose units (AGU) of the starch chains, respectively. The protons of the AGU structure (C_2- C_6) are detectable in the region of 3.20-3.90 ppm. Moreover, the signal of the protons belonging to –OH of C_2 and C_3 carbons of the AGU is detected in the region of 5.40-5.50 ppm, respectively.[46] To corroborate the structure of the intermediate product and establish the effect of ECH concentration and the solvent, KL-CI was also analyzed by ^{1}H-NMR. KL-CI-1DMSO, KL-CI-1DMF, KL-CI-5DMSO, KL-CI-5DMF intermediates were generated in the 1st step of the reaction. In Figure S5.5 (Supporting Information), the new peaks are observed in the structure of KL-CI with respect to that of KL. A new peak at 2.1 ppm corresponds to the H in –OH group of the chloro-propyl chain in all KL-CI, but this peak was absent in KL.[73] The intensity of the new peaks is slightly distinct in different samples, which might indicate the efficacy of DMSO as a better solvent medium for the reaction due to a larger dielectric constant and dipole moment, increasing the reaction rate.[74]

Generally, the peaks related to the $-CH_2$ and $-CH$ chloro-propyl chain of the intermediate are observable in the region of 3.60-3.90 ppm.[75,76] However, in the KL-CI spectra, these peaks overlapped with the protons from the $-OCH_3$ groups. The peaks in the region of 0.5-1.0 ppm correspond to the alkyl region of KL.[77] In addition, the corresponding peaks observed for KL and starch are recognizable on the spectrum of KLS. The peak assigned to the H in $-OH$ group of the chloro-propyl chain was observed at 2.2 ppm in the KLS macromolecule. In addition, the distinctive peak signal between 3.9 to 6.30 ppm in all KLS macromolecules is attributed to the glycerol ether crosslinks generated between KL and starch.[75,78–80] However, it was impossible to distinguish the detailed structure of the macromolecules due to overlapping peaks of the AGU and the glycosidic linkages of starch. We conducted ^{1}H-^{13}C HSQC NMR spectrometry to understand the detailed structure of the generated macromolecules.

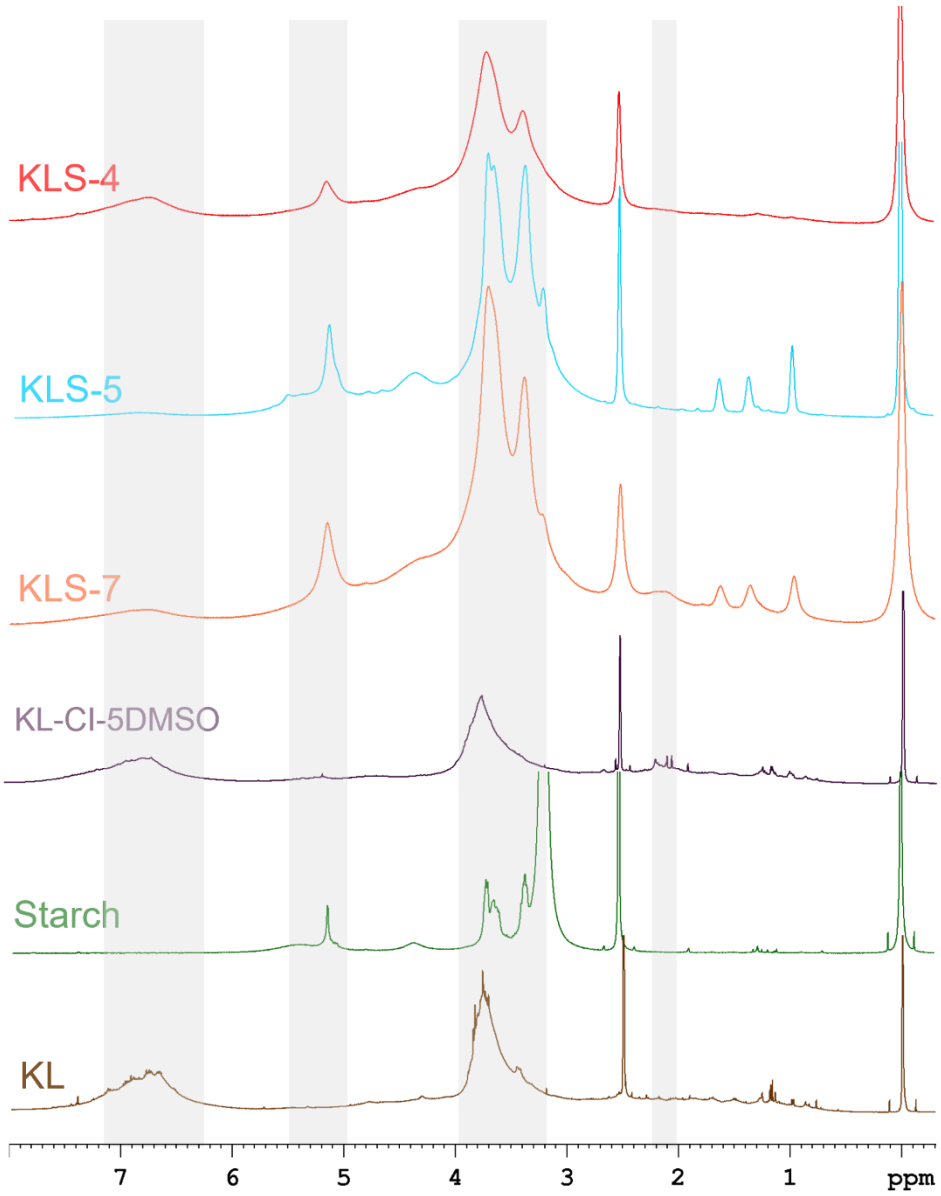

Figure 5.1. ^{1}H-NMR spectra of KL, starch, KL-CI, and KLS products. Shaded peaks are identified as described in the text. Peaks for the internal standard of TSP and the solvent of DMSO-d6 are observed at 1.0 and 2.5 ppm, respectively.

HSQC NMR analysis. The ^{1}H-^{13}C HSQC NMR spectra of the macromolecules are shown in Figure 5.2. The cross-peaks are noticeable at the δ_C/δ_H of 45.7/3.7 and 48.8/3.6 ppm for $-CH_2$ (A and B, respectively) of the chloro-propyl chain on the KL-CI sample, as depicted in Figure S5.7

in Supporting Information. The cross-peaks of the –CH (D) were identified at the δ_C/δ_H of 70.9/3.8 ppm (Figure S5.8 in supplementary information). As depicted in Figure S5.8, the cross-peaks of the glycerol ether crosslinks were identified at the δ_C/δ_H of 50.5/3.2, 47.9/3.6 and 69.9/3.9 ppm for the $-CH_2$ (B), $-CH_2$ (A), and -CH (D) on the KLS macromolecule, respectively, which are the key signals relating the glycerol ether crosslinks between KL and starch. Such peaks were absent in the spectra of KL and starch. Moreover, the assignments related to the aromatic subunits, $-OCH_3$ groups, and the AGU are present and distinguishable in all KLS macromolecules as is detailed in Figure 5.2.[76,81–83] Therefore, HSQC spectra observations showed the existence of a chemical bond between KL and starch confirming the crosslinking of KL and starch.

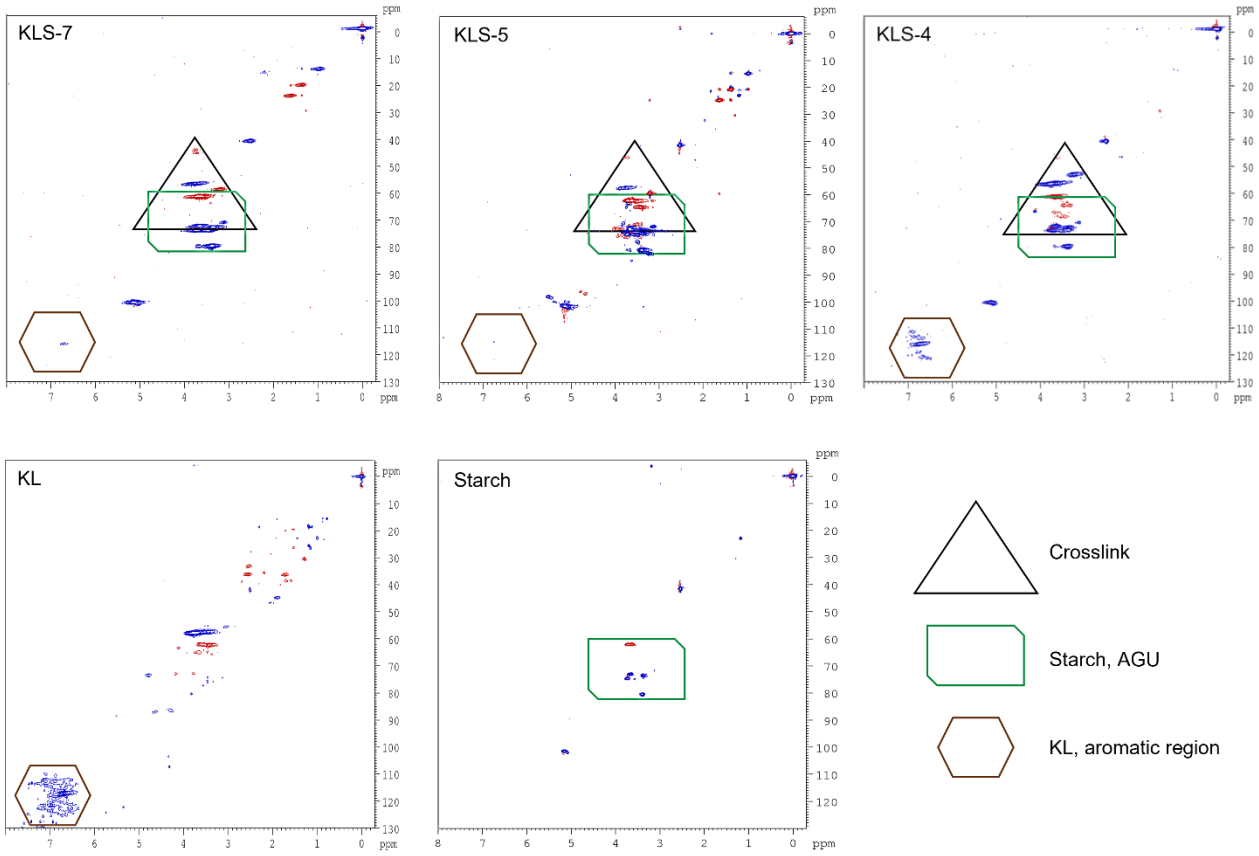

Figure 5.2. ^{1}H-^{13}C HSQC NMR spectra of KL, starch, and KLS products. The identified cross-peaks are brown hexagon (Guaiacyl, Syringyl), green rectangle (starch's AGU), black triangle

(crosslink). The cross-peaks corresponding to CH_1 or CH_3 groups appear in blue (positive region), while cross-peaks from CH_2 appear in red (negative region).

Quantitative P-NMR analysis. The ^{31}P-NMR spectra of KL, KL-CI, and KLS-7 (as the most soluble sample) displayed in Figure 5.3 were analyzed to attest to the aliphatic, phenolic (C5-substituted, guaiacyl, and *p*-hydroxyphenyl), and carboxylate –OH content of the samples after phosphitylation. As is observed in Figure 5.3, the content of aliphatic, total phenolic, and carboxylate –OH of KL-CI were lower than those in KL. The highest decrement was observed for the total phenolic OH, confirming that the etherification of KL happened mainly in this group. Nevertheless, the minor changes in the aliphatic and carboxylate –OH show that the etherification was not selective to only the phenolic OH group.

Interestingly, the total concentration of –OH groups in KLS-7 was 2.6 mmol/g less than that of the –OH group in KL-CI (Figure 5.3). This difference can be indicative of interchain crosslinking occurring between the chloropropyl groups of KL-CI and the free phenolic or carboxylate –OH groups remaining in KL-CI in addition to the predominant crosslinking between KL-CI and starch. These results proved that the phenolic OH groups were the main reactive groups for the etherification of KL, but some aliphatic and carboxylate –OH participated in the reaction with the chlorohydrin molecules.

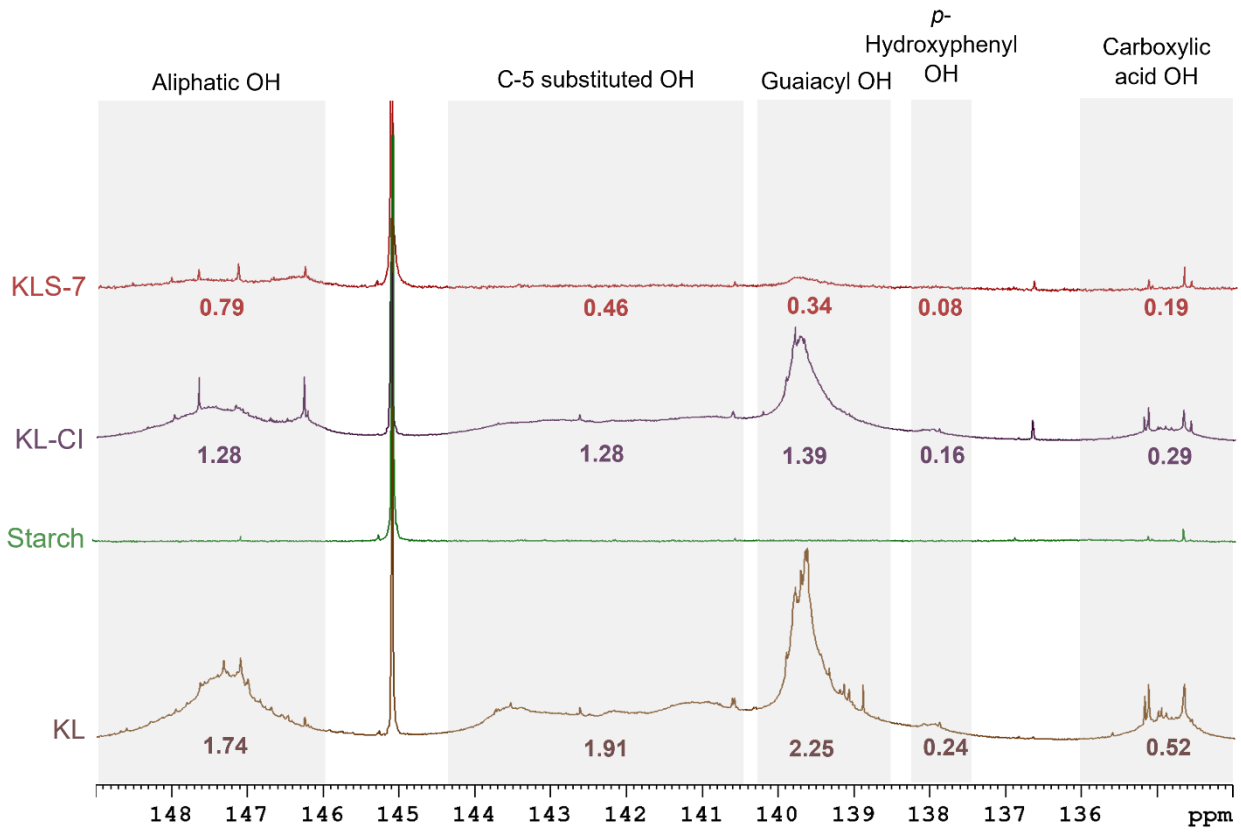

Figure 5.3. ^{31}P-NMR of KL, starch, KL-CI, and KLS-7. Numbers under the curve indicate the OH functional group content (mmol/g) obtained via quantitative ^{31}P-NMR analysis. Internal standard cyclohexanol peak is identified at 145.15 ppm.

5.4.5. XPS Analysis

The structural compositions of KL, starch, and KLS macromolecule were also studied by XPS. The core level spectra of C 1s with the fitting analysis for the peaks related to carbon linkages are observed in Figure 5.4. After the deconvolution of the peaks, the C–C (C1) linkage was observed at a binding energy of 284.8 eV. The carbon peaks at binding energies of 286.4, 287.7, and 289.0 eV are related to the C–O/C–O–C (C2) and O–C–O (C3), O–C=O (C4) linkages, respectively.[84,85]

As is detailed in Table S5.2 in Supporting Information, The C–C linkage represents the most prevalent linkage in KL (59.1 %), while the C–O (C2 and C3) linkages represent more than 60 % of the mass of starch.[86] In general, KLS showed a higher concentration of C-O and C-O-C linkages

than KL and starch. The increment in the C-O and C-O-C linkages resulted from the presence of the glycerol ether crosslinks between KL and starch in KLS.[71,87] For KLS macromolecule, the content of O−C−O linkages was more than that of KL. When the amount of KL was low in KLS (i.e., 25/75 ratio), the concentration of O−C−O linkages was higher (5 to 11 %). In addition, the content of O−C=O in KLS was associated with the presence of the carboxylic acid groups of KL, because those groups are absent in starch naturally, as observed in Figure 5.4.[88] These findings supported the NMR results confirming the crosslinking reaction between KL and starch via glycerol ether linkages by evidencing a higher concentration of C−O−C in KLS.

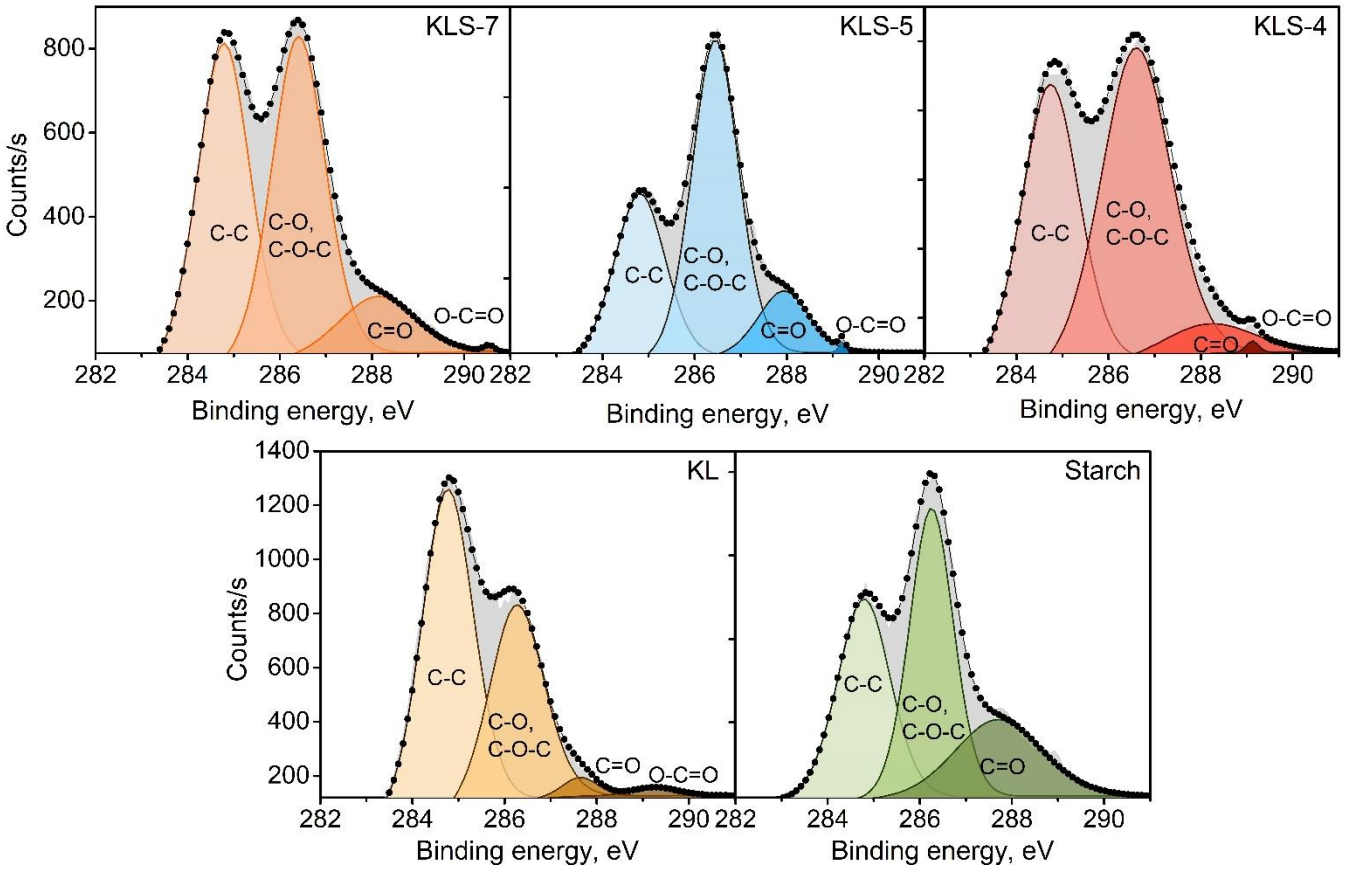

Figure 5.4. XPS spectra of C1s for KL, starch, and KLS macromolecules. Dotted line represents the fitted curve and shaded peaks represent the envelope.

5.4.6. KL-Starch Crosslinking Reaction

Scheme 5.1 shows the possible reaction mechanism for the generation of crosslinked lignin-starch macromolecules. In this study, KL and starch were crosslinked by epichlorohydrin (ECH). Three different mass ratios (75/25, 50/50 and 25/75) of KL to starch were used. In this system, the ECH was added at three different concentrations of 2.5, 1.25, and 0.5 g/g of total content, and the solvent was DMSO or DMF for solubilizing KL and providing an aprotic medium, while NaOH was used for solubilizing starch. In the first step of this reaction, the KL-epichlorohydrin (KL-CI) intermediate was generated. Initially, ECH was protonated in the presence of boron trifluoride etherate participating as the Lewis acid catalyst.[34,89] Once protonated, ECH reacted with the OH groups of KL by a ring-opening reaction to form a chlorohydrin ether group (Figure S5.5). After removing the unreacted ECH, the only available chlorohydrin groups were the ones present in the KL-CI. In the second step, the presence of TBAB in the alkaline environment, as the phase transfer catalyst, facilitates the ionization of starch OH groups at the interface between the KL-CI and starch medium.[44] The reaction of the chlorohydrin groups of KL-CI with the C_6 in the ionized starch led to the formation of glycerol ethers linkages (Scheme 5.1 and Figure S5.8) between KL-CI and starch to form the KL-starch crosslinked macromolecule (KLS) as depicted in Scheme 5.1.[90–92] The yield of the KLS after dialysis was between 83 % and 99 %. After the purification and removal of unreacted materials (corroborated by FT-IR, Figure S5.9), the mass recovery yield was from 47 to 92 % (Table S5.1), which reflects the highest efficiency of the crosslinking reaction obtained from the experimental parameters used for producing KLS-7.

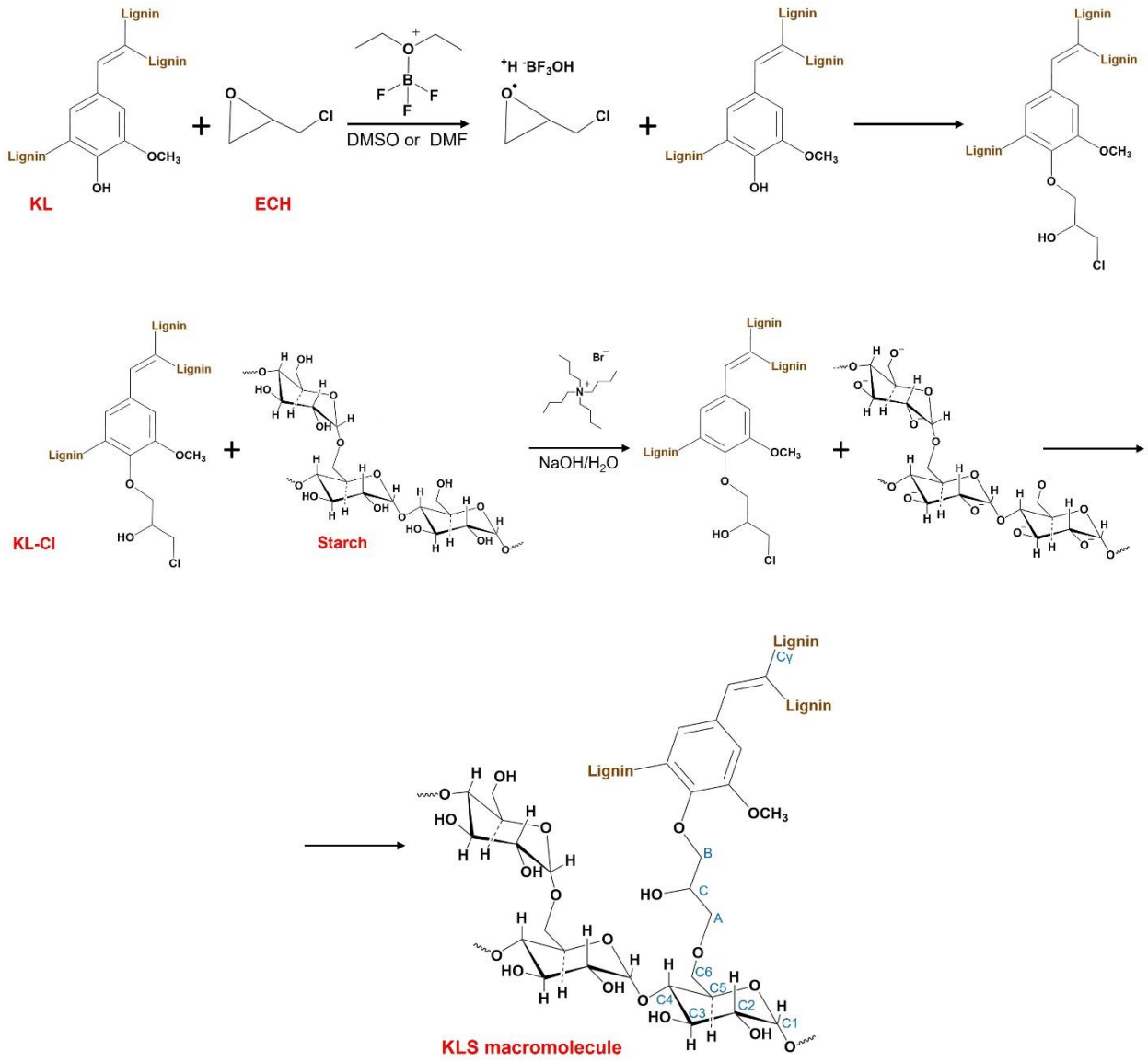

Scheme 5.1. Proposed reaction mechanism of the crosslinking reaction between KL and starch

5.4.7. Molecular Weight and Shape Factor

The MW, R_g, R_h, and the shape factor of KL, starch, and the selected KLS macromolecule in DMSO/LiCl at 25 °C are presented in Table 5.3. The MW, R_g, and R_h of starch and KLS were significantly larger than those of KL. In general, the attachment of the starch chains to the KL structure increased the size of the KLS macromolecule. However, compared to starch in solution,

all KLS had smaller R_g. Among the KLS macromolecule, KLS-5 had the highest MW and R_h, owing to the greater starch content in the sample (25/75 mass ratio). This behavior is attributed to the size of the starch, which reacted with KL-CI to produce KLS and was smaller than that of granular starch. Previous to the crosslinking reaction, granular starch was solubilized in NaOH (1 mol/g), promoting the random hydrolysis and peeling reactions, which caused the scission and debranching of starch, producing smaller polymeric portions.[93,94] The crosslinking of KL-CI and the debranched starch produced tridimensional macromolecules with higher MW than KL but smaller than granular starch.

The shape factor (R_g/R_h) was also calculated to determine the spatial conformation of the samples in the solution.[95] As observed in Table 5.3, the shape factor of KL (0.7) is representative of the tridimensional conformation, analogous to the typical globular conformation reported for the shape factor of 0.78.[96] For granular starch, the solvent media forced the disruption of the hydrogen bonds, which stabilized the helical conformation of starch (amylose chains), making it to adopt a prolate ellipsoidal conformation as depicted by the shape factor of 1.4.[97] On the other hand, the conformation of KLS was closer to that of KL (0.5 to 0.7), representing more of a globular shape given by their tridimensional structure rather than a coil or ellipsoid conformation as shown in Figure 5.5.[96,98] Among the KLS, an expanded structure with a denser core can be described for KLS-5 (Figure 5.5). The lower content of ECH generated fewer interchain crosslinks between starch and KL-CI, which allowed the high content of crosslinked starch chains to be more extended in the macromolecule. In comparison to KLS-4, KLS-7 was produced with the same KL/starch ratio but with higher ECH, which promoted interchain crosslinks maintaining the mass more evenly distributed throughout the structure. For KLS-4, the conformational shape is closer

to that of KL, by having a higher KL content and higher crosslinks due to higher ECH concentration, the conformation resulted in a compact globular shape.

Table 5.3. MW, R_g and R_h of KL, starch and selected KLS co-polymers.

Sample	MW × 10^5, g/mol	R_g, nm	R_h, nm	R_g/R_h
KL	1.18 ± 0.06	34 ± 5	49 ± 0.1	0.7
Starch	58.8 ± 6.50	96 ± 6	70 ± 1.2	1.4
KLS-7	3.71 ± 0.37	53 ± 7	87 ± 0.1	0.6
KLS-5	4.16 ± 0.14	46 ± 3	103 ± 0.1	0.5
KLS-4	3.59 ± 0.33	55 ± 6	75 ± 0.2	0.7

± standard deviation (in MW and R_g), relative variance (in R_h)

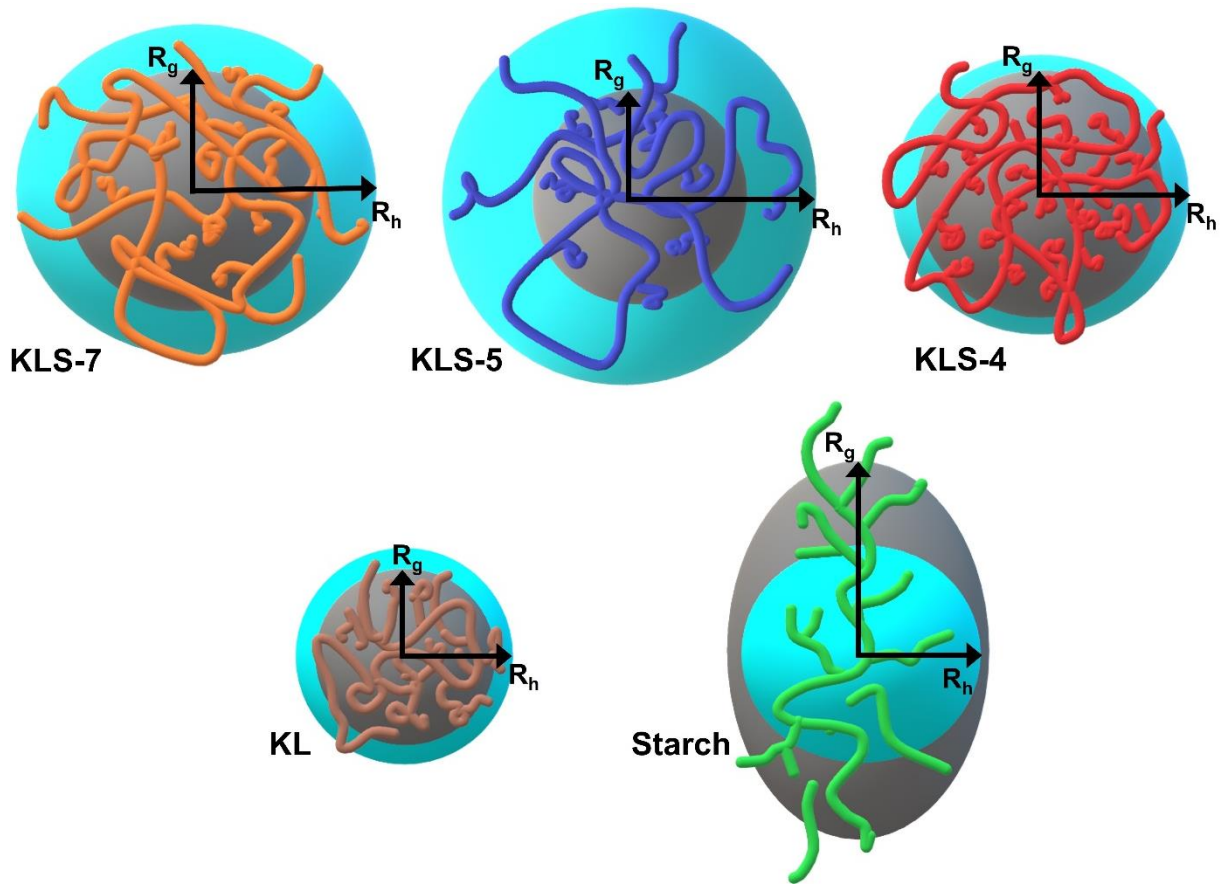

Figure 5.5. Schematic illustration of the shapes of KL, starch, and KLS macromolecules according to their R_g/R_h shape factor. R_g is indicated by the gray figure and R_h is indicated by the light blue sphere.

5.4.8. Temperature Responsive Properties

The water-solubility of KL, starch, and the selected KLS macromolecule was measured at different temperatures (10, 25, 40, 55, and 70 °C). As observed in Figure 5.6, the solubility of KL was not temperature dependent, showing only a slight decrement from 2.57 g/L at 10 °C to 2.15 g/L at 70 °C. Oppositely, the solubility of starch increased significantly as the temperature rose above 25 °C. As the temperature rose, the hydrogen bonds were disrupted, and the semi-crystalline state of the starch granules changed to a rubbery state.[99] The amylose fractions migrated out of the granules, leading to a higher solubilization and gelatinization process.[100] In this case, the KLS macromolecule, all samples were more soluble than starch at cold temperatures and more than KL at >55 °C. The more starch in the KLS, the more response to water solubility was observed for the samples. In this regard, the higher content of starch in their structure provides greater dependence on temperature. During the reaction, the starch granules are cracked, and the hydrophilic chains of starch crosslink to KL-CI. The resulting macromolecule has the hydrophilic chains from the starch and the hydrophobic chains from KL. The macromolecule stabilizes by hydrogen bonding at temperatures <25 °C. But as the temperature increases, these bonds are disrupted, leading to higher solubility.[101,102] These results show the synergetic effect of the crosslinking between KL and starch on the solubility of the macromolecule by having a solubility that was between that of KL and starch at different temperatures.

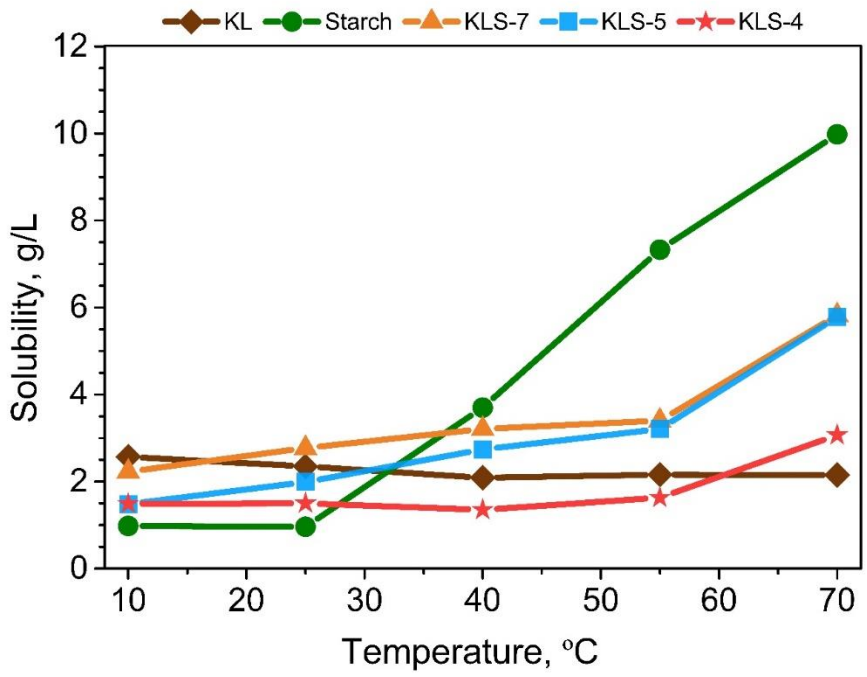

Figure 5.6. Water-solubility at 10, 25, 40, 55 and 70 °C of KL, Starch and selected KLS macromolecule.

5.4.9. Thermal Stability Performance

The thermal stability of KL, starch, and the selected KLS macromolecule was investigated by TGA and DSC, as depicted in Figure 5.7. The TGA and DTG curves are displayed in Figures 5.7a and 5.7c, respectively. The onset temperature ($T_{o,\ the}$ temperature at which the first change in the slope of the curve occurs), temperature of 50 weight loss percentage (T_{50}), as well as the maximum thermal decomposition temperature (DTG_{max}), were used to describe the thermal stability of the samples. The T_o was taken as the reference for the initial decomposition temperature. This temperature was 378±4 °C for KL and 306±4 °C for starch.[103,104] The initial decomposition temperature for KL is due to the breakup of the phenyl propane side chains. At the same time, that for starch is ascribed to the thermal condensation of -OH groups and the formation of ether fragments.[105] Similar trend was observed for the T_{50} and the DTG_{max}. Both temperatures were

higher for KL, 509±1 °C and 573±1 °C, respectively. The higher thermal stability of KL is because the cleavage of ether-type inter-unit and C–C bonds of KL occurred at a higher temperature than the cleavage of the glycosidic bonds and AGU in starch.

Among the KLS macromolecules, all samples showed a lower T_o than starch because of the loss of crystallinity resulting from disrupting the starch granules.[104] However, the T_{50} of KLS was higher than that of starch. This demonstrates the positive effect of crosslinking KL and starch on the thermal stability of the products. In this case, the crosslinked structure of the macromolecule is more thermally stable than starch and KL as can also be observed for KLS-4 possessing the highest thermal stability among all samples (T_{50} = 551±4 °C). The KLS macromolecule also had distinctive DTG_{max} peaks (Figure 5.7c) corresponding to the decomposition of the α-1-4 glycosidic and the β-O-4 linkages. The DTG_{max} of KLS-7 and KLS-5 was 320±2 °C and 331±1 °C, respectively, which is similar to the DTG_{max} of starch. Whereas KLS-4 presented a DTG_{max} closer to that of KL. These results showed how the ratio of KL/starch and concentration of crosslinker has a significant impact on the thermal stability of the macromolecule. Higher content of KL and higher crosslinking degree led to higher thermal stability.

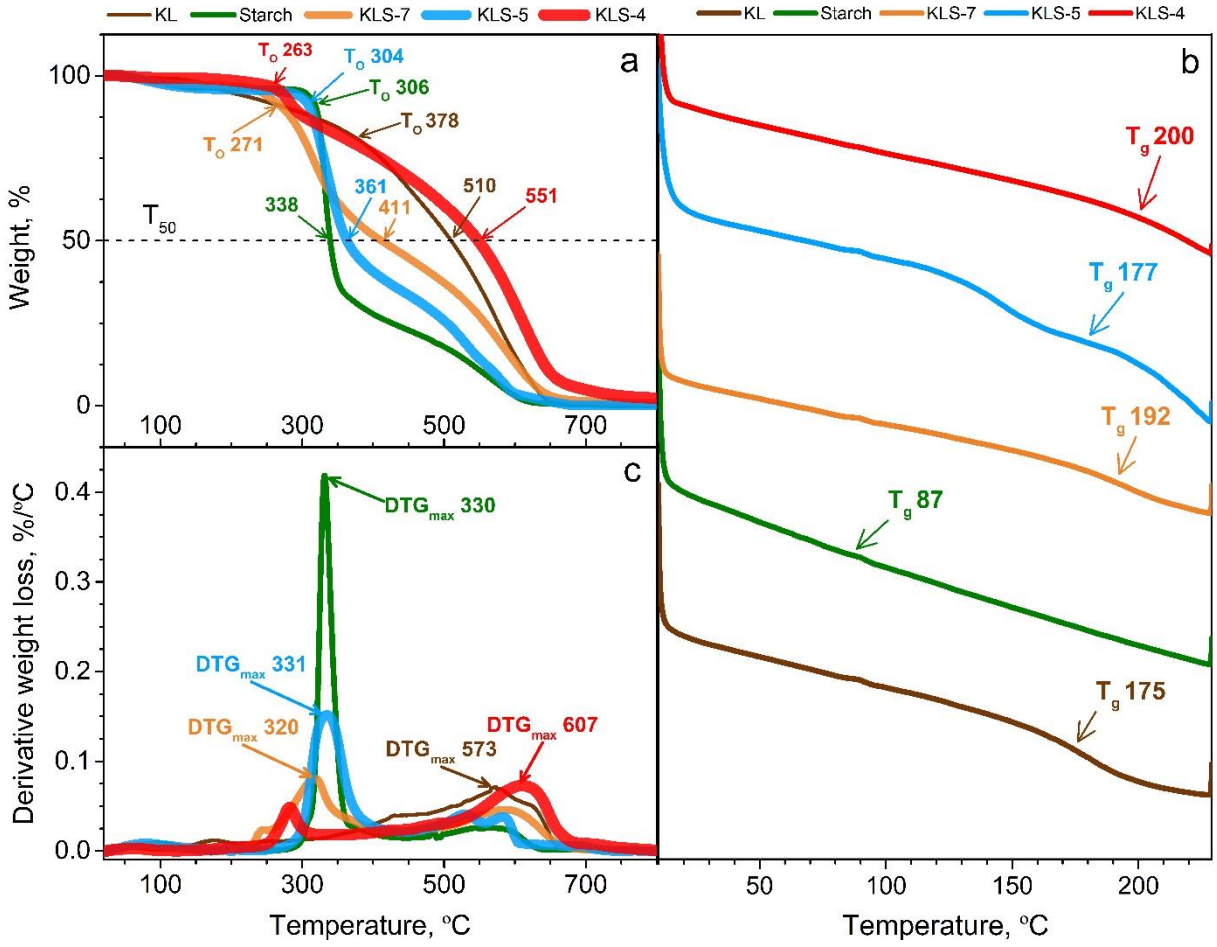

Figure 5.7. Thermal analysis of KL, starch and KLS macromolecules. (a) TGA curves with arrow indicating T_o and T_{50}. (b) DSC curves showing the T_g. (c) DTG curves with arrows pointing to the DTG_{max}.

The glass transition temperatures (T_g) of KL, starch, and the KLS macromolecule are shown in Figure 5.7b. The T_g generally depends on the MW, geometric configuration, crosslinking degree, crystallinity, and chain flexibility.[106] The T_g of KL and starch was 175 °C and 87 °C, respectively. As KL contains different functional groups and intermolecular interactions, such as hydrogen bonding and hydrophobic interactions, which significantly restrict chain mobility and increase T_g.[107] On the other hand, having only hydrogen bonding as intermolecular forces and multiple branching points provides starch with more flexibility to the chains resulting in a lower T_g.[108] Typically, the decrement in the free volume in a polymer (i.e., gaps formed between entangled

polymer chains in a polymer matrix) will increase the T_g.[109,110] For the KLS macromolecule, the crosslinking would reduce the free volume of the chains, as observed from the R_g/R_h (Figure 5.5 and Table 5.3), which elevated the T_g (up to 200 °C). As KLS-4 contained more lignin molecules, more hydrogen bonding and hydrophobic interactions were expected. Because KLS-4 possessed a higher MW than KL, its chain mobility was restricted to a greater extent causing a higher T_g, whose trend was similar to that of T_{50}. However, the contrary is seen for KLS-5, with less KL content and less crosslinking leading to fewer intermolecular interactions and hence a lower T_g.

5.4.10. Rheological Properties

Flow behavior. The viscosity of the KL, starch, and selected KLS dispersions is presented in Figure 5.8. As observed, all samples showed a non-Newtonian flow behavior exhibiting two phenomena: shear thinning and shear thickening.[111] At low shear rates (<1 1/s), the shear thinning behavior is observed since the viscosity η decreased when the shear rate increases to 1/s, which is attributed to their molecular disentanglement caused by shear increment. At high shear rates (>5 1/s), the shear thickening is seen as the viscosity η increases by increasing the shear rate. The high shear rates cause a significant stretching of the polymeric chains inducing elastic stress, which results in flow instability known as elastic turbulence.[112–114]

For KL and starch, the critical transition point (from shear thinning to shear thickening) appeared below 1 1/s with low viscosity (10^{-3} Pa·s). However, after the shear rate increment, KL showed hysteresis resulting from the irreversible network rupture, as seen from the gap between ramp-up and down experiments (Figure 5.8).[115] Starch dispersion showed reversibility, conserving the network generated mainly by the soluble amylose chains.

For the KLS macromolecules, the critical transition point appeared at a higher shear rate and viscosity than KL and starch. The viscosity curves of KLS-7 and KLS-4 showed hysteresis

between the up and down ramp curves in the shear thinning region, while KLS-5 showed complete reversibility of the flow behavior at high shear rates. This reversibility might be related to the expanded and less crosslinked structure of KLS-5 as described by its shape factor (Figure 5.5), resulting in a flexible structure to form more stable elastic networks compared to the more compacted shapes of KLS-7 and KLS-4.[116,117] These results exhibited shear-induced transitions in the flow properties of the KLS macromolecule dispersions, forming complex and multiphase systems in water.

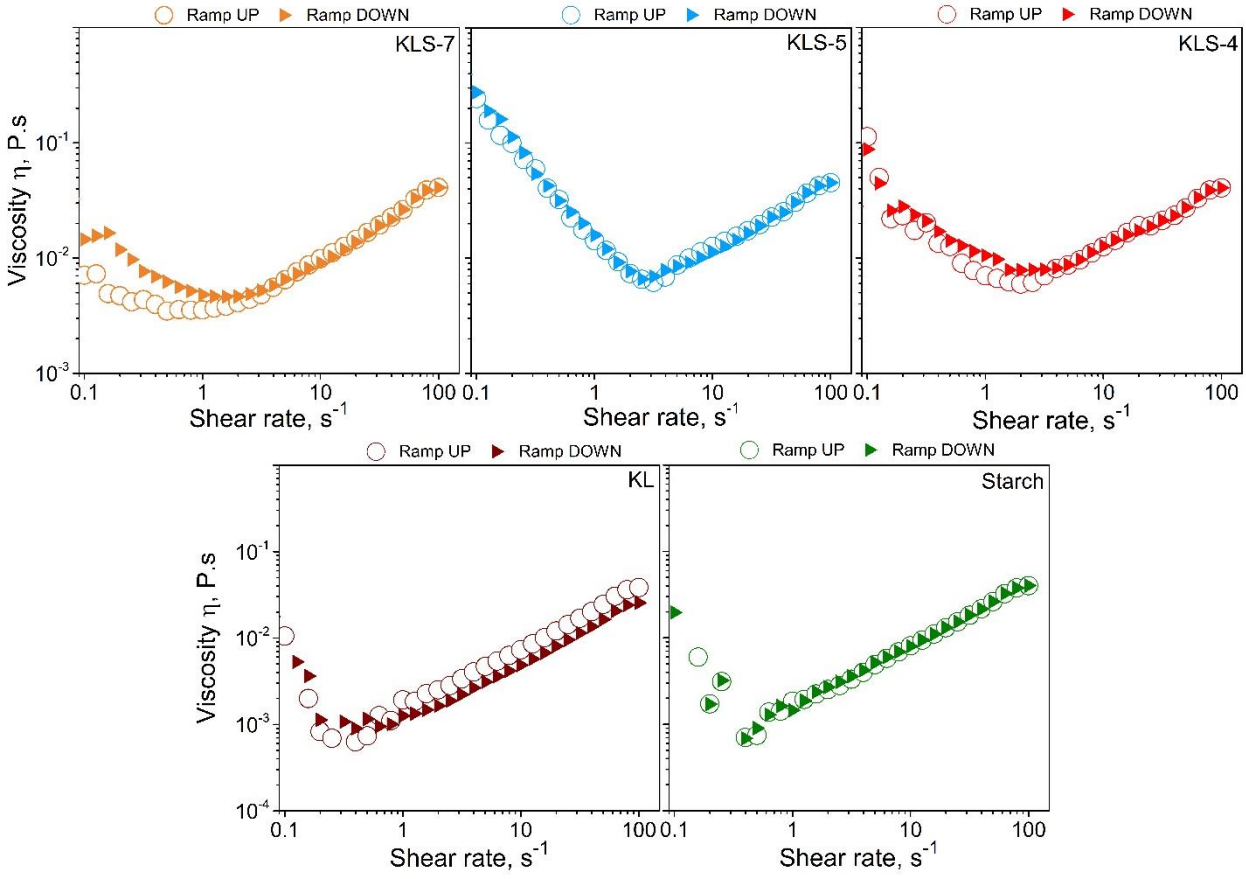

Figure 5.8. Ramp-up (0.1 to 100 s^{-1}) and ramp-down (100 to 0.1 s^{-1}) flow curves of 2 wt.% water dispersions of KL, starch and selected KLS macromolecules at 25 °C.

Strain and frequency sweeps. The viscoelastic properties of the KL, starch, and selected KLS macromolecule dispersions are shown in Figure 5.9 as a function of angular frequency. The viscoelasticity is described by the storage modulus G' (elastic behavior) and loss modulus G" (viscous behavior), respectively. In order to work on a non-destructive deformation range, the linear viscoelastic region (i.e., G' and G" values have horizontal linearity) of KL, starch and selected KLS macromolecules was found at 0.3 % oscillation strain determined from the strain sweep curves displayed in Figure S5.12 of the Supporting Information. It is observed from the frequency sweep curves (Figure 5.9) that all samples showed the dependency of G' and G" towards angular frequency. In particular, the loss modulus of KL was much greater than the storage modulus at any given angular frequency, showing a primarily liquid-state behavior.[118] For starch, at low angular frequencies (<1 rad/s), G' was higher than G", resembling a gel-like behavior, transitioning to liquid-like (G"> G') behavior at frequencies above 1 rad/s.[119] Unlike KL and starch, KLS macromolecules showed a more structured network. Because of the crosslinked structure and a polymeric network supported by hydrophobic and hydrogen bonding interactions, KLS displaced a gel-like behavior at much higher angular frequencies (5 to 10 rad/s) than starch, and higher frequencies transitioned the KLS suspension to a liquid-like state. Interestingly, KLS-4 revealed higher G' values and transitioning frequency among KLS. The highly crosslinked and tridimensional structure, and the occurrence of more hydrogen bonding and hydrophobic interactions, owing to the higher lignin content of KLS-4, helped develop a more robust polymeric network.

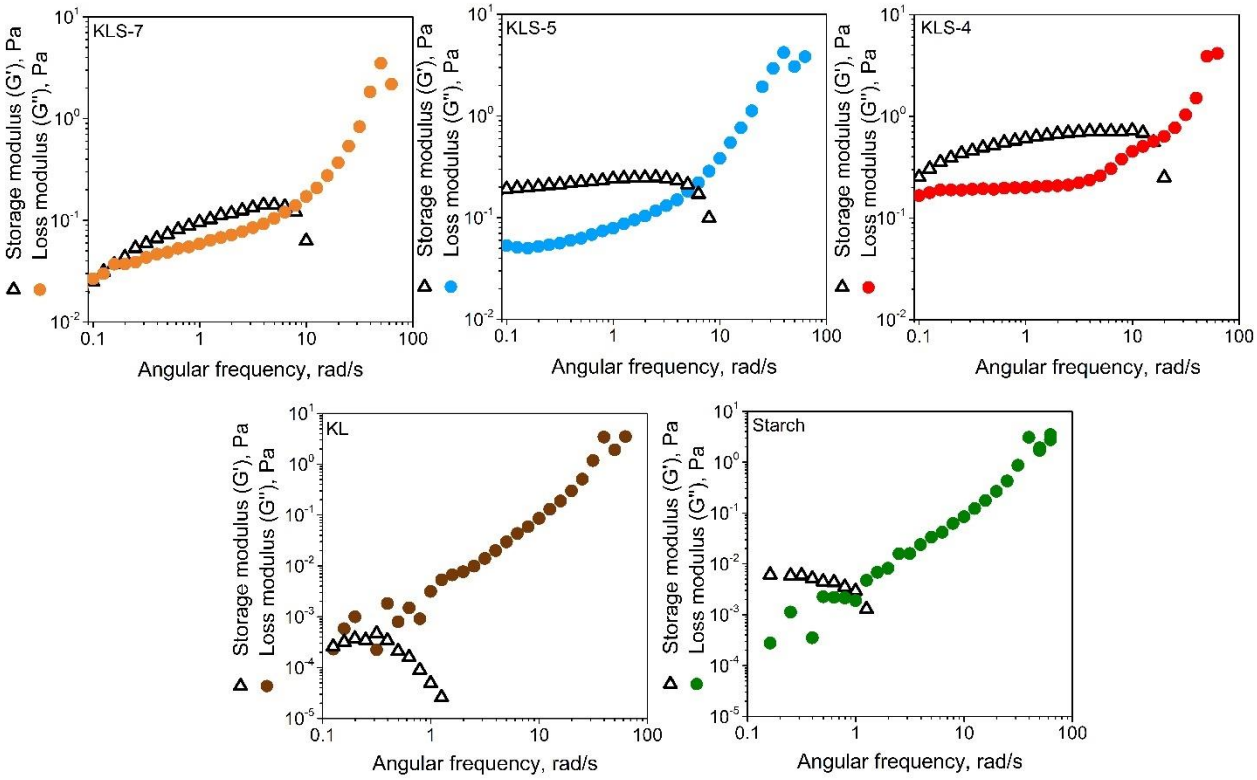

Figure 5.9. Oscillatory frequency sweep (0.1 to 100 rad/s) of 2 wt.% water dispersions of KL, starch and KLS at 25 °C.

Temperature sweep. The temperature dependence of KL, starch, and selected KLS macromolecule dispersions was determined via temperature sweep with a heat-cool cycle, as depicted in Figure 5.10. As observed from the temperature ramps, KL behaved as a liquid-like material and showed no clear temperature dependence of G' and G". Unlike KL, the change of G' and G" of starch was evident at a temperature higher than 60 °C, both elastic and viscous moduli were increased, and the transitioning to a gel-like behavior was notable. During the cooling-down, starch dispersion changed to be temperature independent with G' and G" remaining constant. This change resulted from the swelling and irreversible rupture of the starch's granules while developing hydrogen bonding with water.[61] For the KLS macromolecules, the three samples were

temperature-responsive (Figure 5.10). KLS-7 and KLS-3 behaved as gel-like materials during the heating-up ramp at low temperatures. Both macromolecules transitioned to a liquid-like material above 50 °C (10 degrees lower than starch) due to solubilization (Figure 5.6) and macromolecule-water hydrogen bonding and intermolecular interactions disruption. However, KLS-5 remained liquid-like throughout the heating ramp with a slight decrease of G' due to the disruption of the network aggregates and intramolecular hydrogen bonds by the constant shear rate. As this process is temperature and time dependant, the bulkier structure of KLS-5 took longer time to rearrange and develop the new interactions network leading to G' > G''.[120] During the cooling-down ramp, KLS-5 behaved as gel-like material, indicating that new interaction networks were formed after heating.[119] Unlike those of KLS-7 and KLS-4, in the cooling-down ramp, the G' and G" of KLS-5 increased as the temperature decreased from 70 to 10 °C. The fewer crosslinks in KLS-5 permitted chain motion for the re-formation of hydrogen bonds and hydrophobic intermolecular interactions.[121] The higher MW, extended shape, loose structure, and more flexible chains of KLS-5 (Table 5.3, Figures 5.5 and 5.7) allowed the rearrangement of the polymeric network and formation of the gel-like structure after a heating-cooling treatment exhibiting a thermo-responsive performance.

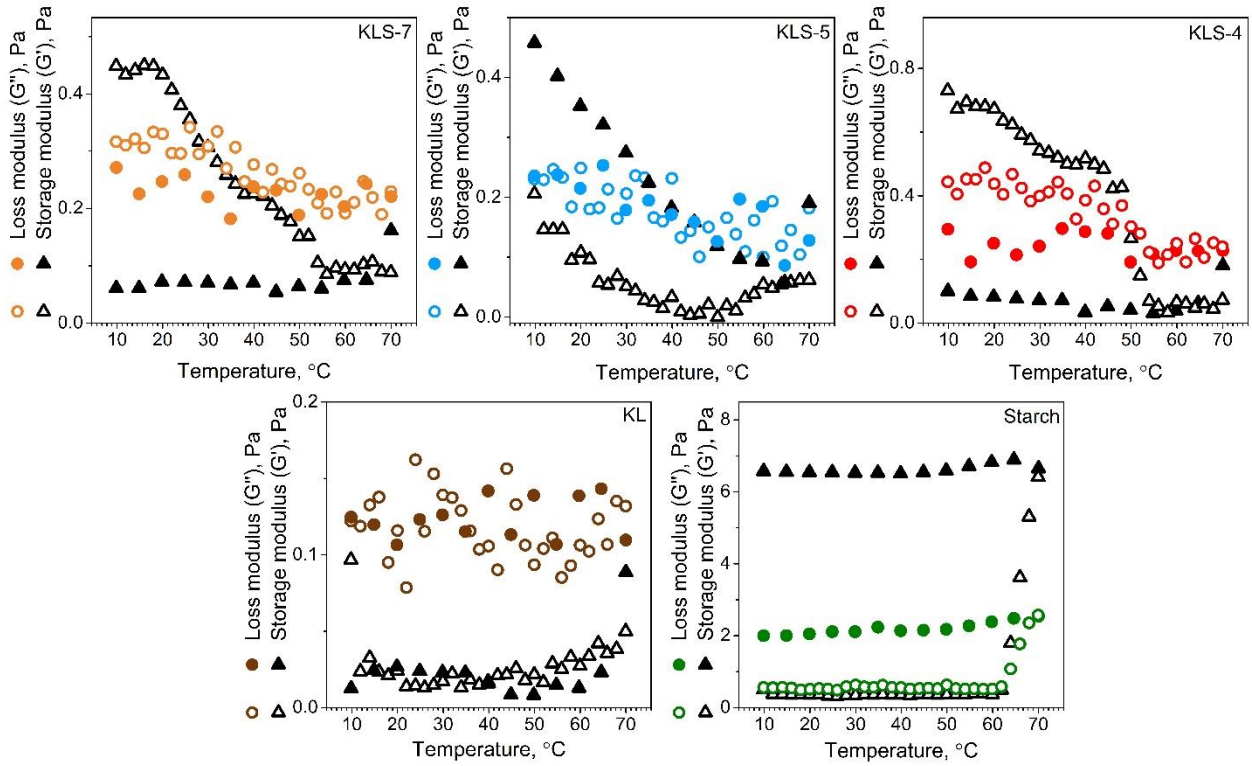

Figure 5.10. Oscillatory temperature sweep of 2 wt.% water dispersions of KL, starch, and selected KLS macromolecules. Open symbol shows the heating-up ramp (10 to 70 °C) and the closed symbol the cooling-down ramp (70 to 10 °C).

5.5. Conclusions

In this work, KL-starch copolymers covalently crosslinked with epichlorohydrin (KLS) were successfully generated with high (75 wt.%), medium (50 wt.%) and low (25% wt.%) KL content. The NMR and XPS results confirmed the presence of the glycerol ether linkages between KL and starch, proving the success of the crosslinking reaction. Via crosslinking KL and starch, temperature-responsive KLS macromolecules were generated. The crosslinking of starch with KL provided the KLS macromolecule with a large number of hydroxyl groups capable of forming hydrogen bonds. These bonds are stable at low temperatures but easily disrupted at high temperatures, leading to higher solubility in water. The KLS macromolecule showed a non-linear structure with the MW increased up to 4.16 $\times 10^5$ g/mol because of the attachment of the starch

chains to KL-CI as observed by NMR and XPS results. The KLS macromolecule showed a globular conformation with different degrees of compactness given by the R_g/R_h shape factor. The higher the KL and crosslinking content, the more compact the polymeric conformation was. Additionally, the incorporation of ether crosslinks, ether interunit, and C–C bonds derived from KL provoke higher thermal stability in KLS than starch. The flow and viscoelastic properties of KLS demonstrated the formation of a more structured network than KL and starch. The generated network was stabilized by hydrophobic and hydrogen bond interactions developed among the multiple hydroxy, carboxy, methoxy, and aromatic groups in KLS. Unlike KL, the viscoelastic properties of the KLS were temperature responsive. Notably, KLS-5 formed a gel-like structure after a heating-cooling treatment because of its higher MW and extended shape, the re-formation of intermolecular interactions and rearrangement of the polymeric network occurred.

5.6. References

(1). Demuner, I. F.; Colodette, J. L.; Demuner, A. J.; Jardim, C. M. Biorefinery Review: Wide-Reaching Products Through Kraft Lignin. *BioResources* **2019**, *14* (3), 7543–7581.

(2). Dessbesell, L.; Paleologou, M.; Leitch, M.; Pulkki, R.; Xu, C. (Charles). Global Lignin Supply Overview and Kraft Lignin Potential as an Alternative for Petroleum-Based Polymers. *Renewable Sustainable Energy Rev.* **2020**, *123*, 109768. https://doi.org/10.1016/j.rser.2020.109768.

(3). Key, R. E.; Bozell, J. J. Progress toward Lignin Valorization via Selective Catalytic Technologies and the Tailoring of Biosynthetic Pathways. *ACS Sustainable Chem. Eng.* **2016**, *4* (10), 5123–5135. https://doi.org/10.1021/acssuschemeng.6b01319.

(4). Jiang, C.; He, H.; Yao, X.; Yu, P.; Zhou, L.; Jia, D. Self-Crosslinkable Lignin/Epoxidized Natural Rubber Composites. *J. Appl. Polym. Sci.* **2014**, *131* (23), n/a-n/a. https://doi.org/10.1002/app.41166.

(5). Liu, H.; Chung, H. Lignin-Based Polymers via Graft Copolymerization. *J. Polym. Sci., Part A: Polym. Chem.* **2017**, *55* (21), 3515–3528. https://doi.org/10.1002/pola.28744.

(6). Lizundia, E.; Sipponen, M. H.; Greca, L. G.; Balakshin, M.; Tardy, B. L.; Rojas, O. J.; Puglia, D. Multifunctional Lignin-Based Nanocomposites and Nanohybrids. *Green Chem.* **2021**, *23* (18), 6698–6760. https://doi.org/10.1039/d1gc01684a.

(7). Ma, C.; Kim, T.-H.; Liu, K.; Ma, M.-G.; Choi, S.-E.; Si, C. Multifunctional Lignin-Based Composite Materials for Emerging Applications. *Front. Bioeng. Biotechnol.* **2021**, *9*, 708976. https://doi.org/10.3389/fbioe.2021.708976.

(8). Shiyan, H.; Fang, G.; Li, S.; Liu, G.; Jiang, G. Cu(II) Ion Adsorption onto Hydroxymethylated Lignin-Chitosan Crosslinked Membrane. *BioResources* **2014**, *9* (3), 4971–4980. https://doi.org/10.15376/biores.9.3.4971-4980.
(9). Culebras, M.; Pishnamazi, M.; Walker, G. M.; Collins, M. N. Facile Tailoring of Structures for Controlled Release of Paracetamol from Sustainable Lignin Derived Platforms. *Molecules* **2021**, *26* (6), 1593. https://doi.org/10.3390/molecules26061593.
(10). Jiang, X.; Tian, Z.; Ji, X.; Ma, H.; Yang, G.; He, M.; Dai, L.; Xu, T.; Si, C. Alkylation Modification for Lignin Color Reduction and Molecular Weight Adjustment. *Int. J. Biol. Macromol.* **2022**, *201*, 400–410. https://doi.org/10.1016/j.ijbiomac.2021.12.162.
(11). Wells, T.; Kosa, M.; Ragauskas, A. J. Polymerization of Kraft Lignin via Ultrasonication for High-Molecular-Weight Applications. *Ultrason. Sonochem.* **2013**, *20* (6), 1463–1469. https://doi.org/10.1016/j.ultsonch.2013.05.001.
(12). Nasrollahzadeh, M.; Sajjadi, M.; Sajadi, S. M.; Issaabadi, Z. Green Nanotechnology. In *Interface Science and Technology*; Elsevier, 2019; Vol. 28, pp 145–198. https://doi.org/10.1016/B978-0-12-813586-0.00005-5.
(13). Fan, Y.; Picchioni, F. Modification of Starch: A Review on the Application of "Green" Solvents and Controlled Functionalization. *Carbohydr. Polym.* **2020**, *241*, 116350. https://doi.org/10.1016/j.carbpol.2020.116350.
(14). Gilet, A.; Quettier, C.; Wiatz, V.; Bricout, H.; Ferreira, M.; Rousseau, C.; Monflier, E.; Tilloy, S. Unconventional Media and Technologies for Starch Etherification and Esterification. *Green Chem.* **2018**, *20* (6), 1152–1168. https://doi.org/10.1039/C7GC03135A.
(15). Meimoun, J.; Wiatz, V.; Saint-Loup, R.; Parcq, J.; Favrelle, A.; Bonnet, F.; Zinck, P. Modification of Starch by Graft Copolymerization: Starch Graft Copolymerization. *Starch/Staerke* **2018**, *70* (1–2), 1600351. https://doi.org/10.1002/star.201600351.
(16). Wang, X.; Huang, L.; Zhang, C.; Deng, Y.; Xie, P.; Liu, L.; Cheng, J. Research Advances in Chemical Modifications of Starch for Hydrophobicity and Its Applications: A Review. *Carbohydr. Polym.* **2020**, *240*, 116292. https://doi.org/10.1016/j.carbpol.2020.116292.
(17). de S. M. de Freitas, A.; Rodrigues, J. S.; Maciel, C. C.; Pires, A. A. F.; Lemes, A. P.; Ferreira, M.; Botaro, V. R. Improvements in Thermal and Mechanical Properties of Composites Based on Thermoplastic Starch and Kraft Lignin. *Int. J. Biol. Macromol.* **2021**, *184*, 863–873. https://doi.org/10.1016/j.ijbiomac.2021.06.153.
(18). Majeed, Z.; Ajab, Z.; Guan, Q.; Abbasi, A. Z.; Mahmood, Q.; Mahnashi, M. H.; Alyami, B. A. A.; Alqarni, A. O.; Alqahtani, Y. S.; Mansor, N. Reduction in Lignin Peroxidase Activity Revealed by Effects of Lignin Content in Urea Crosslinked Starch under Aerobic Biodegradation in Soil. *BioResources* **2021**, *16* (1), 1940–1948.
(19). Javed, A.; Ullsten, H.; Rättö, P.; Järnström, L. Lignin-Containing Coatings for Packaging Materials. *Nord. Pulp Pap. Res. J.* **2018**, *33* (3), 548–556. https://doi.org/10.1515/npprj-2018-3042.
(20). Nasiri, A.; Wearing, J.; Dubé, M. A. Using Lignin to Modify Starch-Based Adhesive Performance. *ChemEngineering* **2020**, *4* (1), 3. https://doi.org/10.3390/chemengineering4010003.
(21). Li, M.; Jia, Y.; Shen, X.; Shen, T.; Tan, Z.; Zhuang, W.; Zhao, G.; Zhu, C.; Ying, H. Investigation into Lignin Modified PBAT/Thermoplastic Starch Composites: Thermal, Mechanical, Rheological and Water Absorption Properties. *Ind. Crops. Prod.* **2021**, *171*, 113916. https://doi.org/10.1016/j.indcrop.2021.113916.

(22). Boufflet, P.; Wood, S.; Wade, J.; Fei, Z.; Kim, J.-S.; Heeney, M. Comparing Blends and Blocks: Synthesis of Partially Fluorinated Diblock Polythiophene Copolymers to Investigate the Thermal Stability of Optical and Morphological Properties. *Beilstein J. Org. Chem*. **2016**, *12*, 2150–2163. https://doi.org/10.3762/bjoc.12.205.
(23). Gao, D.; Hollinger, J.; Seferos, D. S. Selenophene–Thiophene Block Copolymer Solar Cells with Thermostable Nanostructures. *ACS Nano* **2012**, *6* (8), 7114–7121. https://doi.org/10.1021/nn3021844.
(24). Wu, Q.; Shao, W.; Xia, N.; Wang, P.; Kong, F. A Separable Paper Adhesive Based on the Starch—lignin Composite. *Carbohydr. Polym* **2020**, *229*, 115488. https://doi.org/10.1016/j.carbpol.2019.115488.
(25). Cheng, H.; Chen, L.; McClements, D. J.; Yang, T.; Zhang, Z.; Ren, F.; Miao, M.; Tian, Y.; Jin, Z. Starch-Based Biodegradable Packaging Materials: A Review of Their Preparation, Characterization and Diverse Applications in the Food Industry. *Trends Food Sci. Technol.* **2021**, *114*, 70–82. https://doi.org/10.1016/j.tifs.2021.05.017.
(26). Stark, N. M.; Yelle, D. J.; Agarwal, U. P. Techniques for Characterizing Lignin. In *Lignin in Polymer Composites*; Elsevier, 2016; pp 49–66. https://doi.org/10.1016/B978-0-323-35565-0.00004-7.
(27). Zhu, F. NMR Spectroscopy of Starch Systems. *Food Hydrocolloids* **2017**, *63*, 611–624. https://doi.org/10.1016/j.foodhyd.2016.10.015.
(28). Faleva, A. V.; Kozhevnikov, A. Yu.; Pokryshkin, S. A.; Falev, D. I.; Shestakov, S. L.; Popova, J. A. Structural Characteristics of Different Softwood Lignins According to 1D and 2D NMR Spectroscopy. *J. Wood Chem. Technol.* **2020**, *40* (3), 178–189. https://doi.org/10.1080/02773813.2020.1722702.
(29). Domene-López, D.; García-Quesada, J. C.; Martin-Gullon, I.; Montalbán, M. G. Influence of Starch Composition and Molecular Weight on Physicochemical Properties of Biodegradable Films. *Polymers* **2019**, *11* (7), 1084. https://doi.org/10.3390/polym11071084.
(30). Ni, S.; Bian, H.; Zhang, Y.; Fu, Y.; Liu, W.; Qin, M.; Xiao, H. Starch-Based Composite Films with Enhanced Hydrophobicity, Thermal Stability, and UV-Shielding Efficacy Induced by Lignin Nanoparticles. *Biomacromolecules* **2022**, *23* (3), 829–838. https://doi.org/10.1021/acs.biomac.1c01288.
(31). Reza Barzegari, M.; Alemdar, A.; Zhang, Y.; Rodrigue, D. Mechanical and Rheological Behavior of Highly Filled Polystyrene with Lignin. *Polym. Compos.* **2012**, *33* (3), 353–361. https://doi.org/10.1002/pc.22154.
(32). Xie, F.; Xue, T.; Yu, L.; Chen, L.; Li, X.; Zhang, X. Rheological Properties of Starch-Based Materials and Starch/Poly(Lactic Acid) Blends. *Macromol. Symp.* **2007**, *249–250* (1), 529–534. https://doi.org/10.1002/masy.200750431.
(33). Tratnik, N.; Kuo, P.-Y.; Tanguy, N. R.; Gnanasekar, P.; Yan, N. Biobased Epoxidized Starch Wood Adhesives: Effect of Amylopectin and Amylose Content on Adhesion Properties. *ACS Sustainable Chem. Eng.* **2020**, *8* (49), 17997–18005. https://doi.org/10.1021/acssuschemeng.0c05716.
(34). Lin, X.; Zhou, M.; Wang, S.; Lou, H.; Yang, D.; Qiu, X. Synthesis, Structure, and Dispersion Property of a Novel Lignin-Based Polyoxyethylene Ether from Kraft Lignin and Poly(Ethylene Glycol). *ACS Sustainable Chem. Eng.* **2014**, *2* (7), 1902–1909. https://doi.org/10.1021/sc500241g.
(35). Sameni, J.; Krigstin, S.; Sain, M. Characterization of Lignins Isolated from Industrial Residues and Their Beneficial Uses. *BioResources* **2016**, *11* (4), 8435–8456.

(36). International Standardization Organization. ISO 6647-1:2020, Rice — Determination of Amylose Content — Part 1, 2020. https://www.iso.org/obp/ui/#iso:std:iso:6647:-1:ed-3:v1:en (accessed 2023-01-04).
(37). Vilaplana, F.; Hasjim, J.; Gilbert, R. G. Amylose Content in Starches: Toward Optimal Definition and Validating Experimental Methods. *Carbohydrate Polymers* **2012**, *88* (1), 103–111. https://doi.org/10.1016/j.carbpol.2011.11.072.
(38). Fitzgerald, M. A.; Bergman, C. J.; Resurreccion, A. P.; Möller, J.; Jimenez, R.; Reinke, R. F.; Martin, M.; Blanco, P.; Molina, F.; Chen, M.-H.; Kuri, V.; Romero, M. V.; Habibi, F.; Umemoto, T.; Jongdee, S.; Graterol, E.; Reddy, K. R.; Bassinello, P. Z.; Sivakami, R.; Rani, N. S.; Das, S.; Wang, Y. J.; Indrasari, S. D.; Ramli, A.; Ahmad, R.; Dipti, S. S.; Xie, L.; Lang, N. T.; Singh, P.; Toro, D. C.; Tavasoli, F.; Mestres, C. Addressing the Dilemmas of Measuring Amylose in Rice. Cereal Chemistry Journal 2009, 86 (5), 492–498. https://doi.org/10.1094/CCHEM-86-5-0492.
(39). Xiao, H.; Wang, S.; Xu, W.; Yin, Y.; Xu, D.; Zhang, L.; Liu, G.-Q.; Luo, F.; Sun, S.; Lin, Q.; Xu, B. The Study on Starch Granules by Using Darkfield and Polarized Light Microscopy. *Journal of Food Composition and Analysis* **2020**, *92*, 103576. https://doi.org/10.1016/j.jfca.2020.103576.
(40). Chen, C.; Zhu, M.; Li, M.; Fan, Y.; Sun, R.-C. Epoxidation and Etherification of Alkaline Lignin to Prepare Water-Soluble Derivatives and Its Performance in Improvement of Enzymatic Hydrolysis Efficiency. *Biotechnol. Biofuels* **2016**, *9* (1), 87. https://doi.org/10.1186/s13068-016-0499-9.
(41). Jung, J. Y.; Park, C.-H.; Lee, E. Y. Epoxidation of Methanol-Soluble Kraft Lignin for Lignin-Derived Epoxy Resin and Its Usage in the Preparation of Biopolyester. *J. Wood Chem. Technol.* **2017**, *37* (6), 433–442. https://doi.org/10.1080/02773813.2017.1310901.
(42). Salanti, A.; Zoia, L.; Orlandi, M. Chemical Modifications of Lignin for the Preparation of Macromers Containing Cyclic Carbonates. *Green Chem.* **2016**, *18* (14), 4063–4072. https://doi.org/10.1039/C6GC01028H.
(43). Rowell, R. M.; Chen, G. C. Epichlorohydrin Coupling Reactions with Wood: Part 1. Reaction with Biologically Active Alcohols. *Wood Sci.Technol.* **1994**, *28* (5). https://doi.org/10.1007/BF00195285.
(44). Jyothi, A. N.; Moorthy, S. N.; Rajasekharan, K. N. Effect of Cross-Linking with Epichlorohydrin on the Properties of Cassava (Manihot Esculenta Crantz) Starch. *Starch/Staerke* **2006**, *58* (6), 292–299. https://doi.org/10.1002/star.200500468.
(45). Salanti, A.; Zoia, L.; Simonutti, R.; Orlandi, M. Epoxidized Lignin Derivatives as Bio-Based Cross-Linkers Used in the Preparation of Epoxy Resins. *BioResources* **2018**, *13* (2), 2374–2396.
(46). Tizzotti, M. J.; Sweedman, M. C.; Tang, D.; Schaefer, C.; Gilbert, R. G. New ^{1}H NMR Procedure for the Characterization of Native and Modified Food-Grade Starches. *J. Agric. Food Chem.* **2011**, *59* (13), 6913–6919. https://doi.org/10.1021/jf201209z.
(47). Meng, X.; Crestini, C.; Ben, H.; Hao, N.; Pu, Y.; Ragauskas, A. J.; Argyropoulos, D. S. Determination of Hydroxyl Groups in Biorefinery Resources via Quantitative 31P NMR Spectroscopy. *Nat. Protoc.* **2019**, *14* (9), 2627–2647. https://doi.org/10.1038/s41596-019-0191-1.
(48). Lange, H.; Schiffels, P.; Sette, M.; Sevastyanova, O.; Crestini, C. Fractional Precipitation of Wheat Straw Organosolv Lignin: Macroscopic Properties and Structural Insights. *ACS*

Sustainable Chem. Eng. **2016**, *4* (10), 5136–5151. https://doi.org/10.1021/acssuschemeng.6b01475.
(49). El Mansouri, N.-E.; Salvadó, J. Analytical Methods for Determining Functional Groups in Various Technical Lignins. *Ind. Crops. Prod.* **2007**, *26* (2), 116–124. https://doi.org/10.1016/j.indcrop.2007.02.006.
(50). Konduri, M. K. R.; Fatehi, P. Designing Anionic Lignin Based Dispersant for Kaolin Suspensions. *Colloids Surf., A* **2018**, *538*, 639–650. https://doi.org/10.1016/j.colsurfa.2017.11.011.
(51). Tolbert, A.; Akinosho, H.; Khunsupat, R.; Naskar, A. K.; Ragauskas, A. J. Characterization and Analysis of the Molecular Weight of Lignin for Biorefining Studies. *Biofuels, Bioprod. Biorefin.* **2014**, *8* (6), 836–856. https://doi.org/10.1002/bbb.1500.
(52). Contreras, S.; Gaspar, A. R.; Guerra, A.; Lucia, L. A.; Argyropoulos, D. S. Propensity of Lignin to Associate: Light Scattering Photometry Study with Native Lignins. *Biomacromolecules* **2008**, *9* (12), 3362–3369. https://doi.org/10.1021/bm800673a.
(53). Kong, F.; Wang, S.; Gao, W.; Fatehi, P. Novel Pathway to Produce High Molecular Weight Kraft Lignin–Acrylic Acid Polymers in Acidic Suspension Systems. *RSC Adv.* **2018**, *8* (22), 12322–12336. https://doi.org/10.1039/C7RA12971H.
(54). Baalousha, M.; Kammer, F. V. D.; Motelica-Heino, M.; Hilal, H. S.; Le Coustumer, P. Size Fractionation and Characterization of Natural Colloids by Flow-Field Flow Fractionation Coupled to Multi-Angle Laser Light Scattering. *J. Chromatogr. A* **2006**, *1104* (1–2), 272–281. https://doi.org/10.1016/j.chroma.2005.11.095.
(55). Wang, D.; Wang, Y.; Li, T.; Zhang, S.; Ma, P.; Shi, D.; Chen, M.; Dong, W. A Bio-Based Flame-Retardant Starch Based On Phytic Acid. *ACS Sustainable Chem. Eng.* **2020**, *8* (27), 10265–10274. https://doi.org/10.1021/acssuschemeng.0c03277.
(56). Kun, D.; Pukánszky, B. Polymer/Lignin Blends: Interactions, Properties, Applications. *Eur. Polym. J.* **2017**, *93*, 618–641. https://doi.org/10.1016/j.eurpolymj.2017.04.035.
(57). Byars, J. A.; Singh, M. Rheological and Textural Properties of Pulse Starch Gels: Rheological and Textural Properties of Pulse Starch. *Starch/Staerke* **2016**, *68* (7–8), 778–784. https://doi.org/10.1002/star.201500271.
(58). Guo, L.; Cui, B. The Relationship between Entanglement Concentration and Physicochemical Properties of Potato and Sweet Potato Starch Dispersions. *Int. J. Food Sci. Technol.* **2018**, *53* (2), 337–346. https://doi.org/10.1111/ijfs.13590.
(59). Kong, L.; Ziegler, G. R. Role of Molecular Entanglements in Starch Fiber Formation by Electrospinning. *Biomacromolecules* **2012**, *13* (8), 2247–2253. https://doi.org/10.1021/bm300396j.
(60). Savitskaya, T.; Reznikov, I.; Grinshpan, D. Rheological Behavior of Lignin Based Dispersions Intended for Composite Fuel Production. *Appl. Rheol.* **2016**, *26*, 63476. https://doi.org/10.3933/APPLRHEOL-26-63476.
(61). Ahuja, A.; Lee, R.; Latshaw, A.; Foster, P. Rheology of Starch Dispersions at High Temperatures. *J. Texture Stud.* **2020**, *51* (4), 575–584. https://doi.org/10.1111/jtxs.12517.
(62). Chile, L.; Kaser, S.; Hatzikiriakos, S.; Mehrkhodavandi, P. Synthesis and Thermorheological Analysis of Biobased Lignin-Graft-Poly(Lactide) Copolymers and Their Blends. *ACS Sustainable Chemistry & Engineering* **2018**, *6* (2), 1650–1661. https://doi.org/10.1021/acssuschemeng.7b02866.

(63). Qin, Y.; Zhang, H.; Dai, Y.; Hou, H.; Dong, H. Effect of Alkali Treatment on Structure and Properties of High Amylose Corn Starch Film. *Materials* **2019**, *12* (10), 1705. https://doi.org/10.3390/ma12101705.
(64). Roberts, S. A.; Cameron, R. E. The Effects of Concentration and Sodium Hydroxide on the Rheological Properties of Potato Starch Gelatinisation. *Carbohydr. Polym.* **2002**, *50* (2), 133–143. https://doi.org/10.1016/S0144-8617(02)00007-3.
(65). Jacobsen, H. B.; Madsen, M. H.; Christiansen, J.; Nielsen, T. H. The Degree of Starch Phosphorylation as Influenced by Phosphate Deprivation of Potato (Solanum Tuberosum L.) Plants. *Potato Res.* **1998**, *41* (2), 109–116. https://doi.org/10.1007/BF02358433.
(66). Lim, S.; Seib, P. A. Location of Phosphate Esters in a Wheat Starch Phosphate by 3"P-Nuclear Magnetic Resonance Spectroscopy'. *Cereal Chem.* **1993**, *70* (2), 145–142.
(67). Oveissi, F.; Fatehi, P. Characterization of Four Different Lignins as a First Step toward the Identification of Suitable End-Use Applications. *J. Appl. Polym. Sci.* **2015**, *132* (32), n/a-n/a. https://doi.org/10.1002/app.42336.
(68). Xu, X.; Huang, X.-F.; Visser, R. G. F.; Trindade, L. M. Engineering Potato Starch with a Higher Phosphate Content. *PLoS ONE* **2017**, *12* (1), e0169610. https://doi.org/10.1371/journal.pone.0169610.
(69). Aouf, C.; Le Guernevé, C.; Caillol, S.; Fulcrand, H. Study of the O-Glycidylation of Natural Phenolic Compounds. The Relationship between the Phenolic Structure and the Reaction Mechanism. *Tetrahedron* **2013**, *69* (4), 1345–1353. https://doi.org/10.1016/j.tet.2012.11.079.
(70). Gioia, C.; Colonna, M.; Tagami, A.; Medina, L.; Sevastyanova, O.; Berglund, L. A.; Lawoko, M. Lignin-Based Epoxy Resins: Unravelling the Relationship between Structure and Material Properties. *Biomacromolecules* **2020**, *21* (5), 1920–1928. https://doi.org/10.1021/acs.biomac.0c00057.
(71). Karaaslan, M. A.; Lin, L.-T.; Ko, F.; Renneckar, S. Carbon Aerogels From Softwood Kraft Lignin for High Performance Supercapacitor Electrodes. *Front. Mater.* **2022**, *9*, 894061. https://doi.org/10.3389/fmats.2022.894061.
(72). Nagy, M.; Kosa, M.; Theliander, H.; Ragauskas, A. J. Characterization of CO_2 Precipitated Kraft Lignin to Promote Its Utilization. *Green Chem.* **2010**, *12* (1), 31–34. https://doi.org/10.1039/B913602A.
(73). Truscello, A. M.; Gambarotti, C.; Lauria, M.; Auricchio, S.; Leonardi, G.; Shisodia, S. U.; Citterio, A. One-Pot Synthesis of Aryloxypropanediols from Glycerol: Towards Valuable Chemicals from Renewable Sources. *Green Chem.* **2013**, *15* (3), 625. https://doi.org/10.1039/c2gc36793a.
(74). Duereh, A.; Sato, Y.; Smith, R. L.; Inomata, H. Methodology for Replacing Dipolar Aprotic Solvents Used in API Processing with Safe Hydrogen-Bond Donor and Acceptor Solvent-Pair Mixtures. *Org. Process Res. Dev.* **2017**, *21* (1), 114–124. https://doi.org/10.1021/acs.oprd.6b00401.
(75). Aydin, H. M.; Salimi, K.; Rzayev, Z. M. O.; Pişkin, E. Microwave-Assisted Rapid Synthesis of Poly(Glycerol-Sebacate) Elastomers. *Biomater. Sci.* **2013**, *1* (5), 503. https://doi.org/10.1039/c3bm00157a.
(76). Giroto, A. S.; do Valle, S. F.; Ribeiro, T.; Ribeiro, C.; Mattoso, L. H. C. Towards Urea and Glycerol Utilization as "Building Blocks" for Polyurethane Production: A Detailed Study about Reactivity and Structure for Environmentally Friendly Polymer Synthesis. *React. Funct. Polym.* **2020**, *153*, 104629. https://doi.org/10.1016/j.reactfunctpolym.2020.104629.

(77). Lancefield, C. S.; Wienk, H. L. J.; Boelens, R.; Weckhuysen, B. M.; Bruijnincx, P. C. A. Identification of a Diagnostic Structural Motif Reveals a New Reaction Intermediate and Condensation Pathway in Kraft Lignin Formation. *Chem. Sci.* **2018**, *9* (30), 6348–6360. https://doi.org/10.1039/C8SC02000K.
(78). Feketefoldi, B.; Cermenek, B. Chitosan-Based Anion Exchange Membranes for Direct Ethanol Fuel Cells. *J. Membra. Sci. Technol.* **2016**, *06* (01). https://doi.org/10.4172/2155-9589.1000145.
(79). Nikafshar, S.; Wang, J.; Dunne, K.; Sangthonganotai, P.; Nejad, M. Choosing the Right Lignin to Fully Replace Bisphenol A in Epoxy Resin Formulation. *ChemSusChem* **2021**, *14* (4), 1184–1195. https://doi.org/10.1002/cssc.202002729.
(80). Simanaviciute, D.; Liudvinaviciute, D.; Klimaviciute, R.; Rutkaite, R. Cross-Linked Cationic Starch Derivatives for Immobilization of Chlorogenic Acid. *Eur. Polym. J.* **2017**, *93*, 833–842. https://doi.org/10.1016/j.eurpolymj.2017.02.022.
(81). Crestini, C.; Lange, H.; Sette, M.; Argyropoulos, D. S. On the Structure of Softwood Kraft Lignin. *Green Chem.* **2017**, *19* (17), 4104–4121. https://doi.org/10.1039/C7GC01812F.
(82). Jordan, T.; Schmidt, S.; Liebert, T.; Heinze, T. Molten Imidazole – a Starch Solvent. *Green Chem.* **2014**, *16* (4), 1967. https://doi.org/10.1039/c3gc41818a.
(83). Kono, H. Characterization and Properties of Carboxymethyl Cellulose Hydrogels Crosslinked by Polyethylene Glycol. *Carbohydr. Polym.* **2014**, *106*, 84–93. https://doi.org/10.1016/j.carbpol.2014.02.020.
(84). Ghavidel, N.; Konduri, M. K. R.; Fatehi, P. Chemical Reactivity and Sulfo-Functionalization Response of Enzymatically Produced Lignin. *Ind. Crops. Prod.* **2021**, *172*, 113950. https://doi.org/10.1016/j.indcrop.2021.113950.
(85). Sirviö, J. A.; Heiskanen, J. P. Carbamation of Starch with Amine Using Dimethyl Carbonate as Coupling Agent. *ACS Omega* **2019**, *4* (13), 15702–15710. https://doi.org/10.1021/acsomega.9b02350.
(86). Saad, M.; Gaiani, C.; Mullet, M.; Scher, J.; Cuq, B. X-Ray Photoelectron Spectroscopy for Wheat Powders: Measurement of Surface Chemical Composition. *J. Agric. Food Chem.* **2011**, *59* (5), 1527–1540. https://doi.org/10.1021/jf102315h.
(87). Pang, Y.; Sun, Y.; Luo, Y.; Zhou, M.; Qiu, X.; Yi, C.; Lou, H. Preparation of Novel All-Lignin Microcapsules via Interfacial Cross-Linking of Pickering Emulsion. *Ind. Crops. Prod.* **2021**, *167*, 113468. https://doi.org/10.1016/j.indcrop.2021.113468.
(88). Chirila, O.; Totolin, M.; Cazacu, G.; Dobromir, M.; Vasile, C. Lignin Modification with Carboxylic Acids and Butyrolactone under Cold Plasma Conditions. *Ind. Eng. Chem. Res.* **2013**, *52* (37), 13264–13271. https://doi.org/10.1021/ie4015183.
(89). Liu, Y.; Huang, X.; Han, K.; Dai, Y.; Zhang, X.; Zhao, Y. High-Performance Lignin-Based Water-Soluble Macromolecular Photoinitiator for the Fabrication of Hybrid Hydrogel. *ACS Sustainable Chem. Eng.* **2019**, *7* (4), 4004–4011. https://doi.org/10.1021/acssuschemeng.8b05357.
(90). Bendoraitiene, J.; Lekniute-Kyzike, E.; Rutkaite, R. Biodegradation of Cross-Linked and Cationic Starches. *Int. J. Biol. Macromol.* **2018**, *119*, 345–351. https://doi.org/10.1016/j.ijbiomac.2018.07.155.
(91). Malik, M. K.; Kumar, V.; Sharma, P. P.; Singh, J.; Fuloria, S.; Subrimanyan, V.; Fuloria, N. K.; Kumar, P. Improvement in Digestion Resistibility of Mandua Starch (*Eleusine Coracana*) after Cross-Linking with Epichlorohydrin. *ACS Omega* **2022**, acsomega.2c02327. https://doi.org/10.1021/acsomega.2c02327.

(92). Saidane, D.; Barbe, J.-C.; Birot, M.; Deleuze, H. Preparation of Functionalized Kraft Lignin Beads. *J. Appl. Polym. Sci.* **2009**, n/a-n/a. https://doi.org/10.1002/app.31659.
(93). Aberle, Th.; Burchard, W.; Vorwerg, W.; Radosta, S. Conformational Contributions of Amylose and Amylopectin to the Structural Properties of Starches from Various Sources. *Starch/Staerke* **1994**, *46* (9), 329–335. https://doi.org/10.1002/star.19940460903.
(94). Han, J. Structural Changes in Corn Starches during Alkaline Dissolution by Vortexing. *Carbohydr. Polym.* **2004**, *55* (2), 193–199. https://doi.org/10.1016/j.carbpol.2003.09.006.
(95). Patterson, J. P.; Robin, M. P.; Chassenieux, C.; Colombani, O.; O'Reilly, R. K. The Analysis of Solution Self-Assembled Polymeric Nanomaterials. *Chem. Soc. Rev.* **2014**, *43* (8), 2412–2425. https://doi.org/10.1039/C3CS60454C.
(96). Lohrke, J.; Briel, A.; Mäder, K. Characterization of Superparamagnetic Iron Oxide Nanoparticles by Asymmetrical Flow-Field-Flow-Fractionation. *Nanomedicine* **2008**, *3* (4), 437–452. https://doi.org/10.2217/17435889.3.4.437.
(97). Brewer, A. K.; Striegel, A. M. Characterizing the Size, Shape, and Compactness of a Polydisperse Prolate Ellipsoidal Particle via Quadruple-Detector Hydrodynamic Chromatography. *Analyst* **2011**, *136* (3), 515–519. https://doi.org/10.1039/C0AN00738B.
(98). Haydukivska, K.; Blavatska, V.; Paturej, J. Universal Size Ratios of Gaussian Polymers with Complex Architecture: Radius of Gyration vs Hydrodynamic Radius. *Sci. Rep.* **2020**, *10* (1), 14127. https://doi.org/10.1038/s41598-020-70649-z.
(99). Kumoro, A. C.; Retnowati, D. S.; Ratnawati, R.; Widiyanti, M. Estimation of Aqueous Solubility of Starch from Various Botanical Sources Using Flory Huggins Theory Approach. *Chem. Eng. Commun.* **2021**, *208* (5), 624–635. https://doi.org/10.1080/00986445.2019.1691539.
(100). Lin, L.; Cai, C.; Gilbert, R. G.; Li, E.; Wang, J.; Wei, C. Relationships between Amylopectin Molecular Structures and Functional Properties of Different-Sized Fractions of Normal and High-Amylose Maize Starches. *Food Hydrocolloids* **2016**, *52*, 359–368. https://doi.org/10.1016/j.foodhyd.2015.07.019.
(101). Olayinka, O. O.; Adebowale, K. O.; Olu-Owolabi, I. B. Physicochemical Properties, Morphological and X-Ray Pattern of Chemically Modified White Sorghum Starch. (Bicolor-Moench). *J. Food Sci. Technol.* **2013**, *50* (1), 70–77. https://doi.org/10.1007/s13197-011-0233-3.
(102). Zhiguang, C.; Junrong, H.; Huayin, P.; Keipper, W. The Effects of Temperature on Starch Molecular Conformation and Hydrogen Bonding. *Starch/Staerke* **2022**, *74* (7–8), 2100288. https://doi.org/10.1002/star.202100288.
(103). Aldaeus, F.; Olsson, A.-M.; Stevanic, J. S. Miniaturized Determination of Ash Content in Kraft Lignin Samples Using Oxidative Thermogravimetric Analysis. *Nord. Pulp Pap. Res. J.* **2017**, *32* (2), 280–282. https://doi.org/10.3183/npprj-2017-32-02-p280-282.
(104). Shuzhen, N.; Liang, J.; Hui, Z.; Yongchao, Z.; Guigan, F.; Huining, X.; Hongqi, D. Enhancing Hydrophobicity, Strength and UV Shielding Capacity of Starch Film via Novel Co-Cross-Linking in Neutral Conditions. *Royal Soc. Open Sci.* **2018**, *5* (11), 181206. https://doi.org/10.1098/rsos.181206.
(105). Liu, X.; Wang, Y.; Yu, L.; Tong, Z.; Chen, L.; Liu, H.; Li, X. Thermal Degradation and Stability of Starch under Different Processing Conditions. *Starch/Staerke* **2013**, *65* (1–2), 48–60. https://doi.org/10.1002/star.201200198.
(106). Shrivastava, A. Introduction to Plastics Engineering. In *Introduction to Plastics Engineering*; Elsevier, 2018; pp 1–16. https://doi.org/10.1016/B978-0-323-39500-7.00001-0.

(107). Li, H.; McDonald, A. G. Fractionation and Characterization of Industrial Lignins. *Ind. Crops. Prod.* **2014**, *62*, 67–76. https://doi.org/10.1016/j.indcrop.2014.08.013.
(108). Liu, P.; Yu, L.; Wang, X.; Li, D.; Chen, L.; Li, X. Glass Transition Temperature of Starches with Different Amylose/Amylopectin Ratios. *J. Cereal Sci.* **2010**, *51* (3), 388–391. https://doi.org/10.1016/j.jcs.2010.02.007.
(109). Auras, R. A. Solubility of Gases and Vapors in Polylactide Polymers. In *Thermodynamics, Solubility and Environmental Issues*; Elsevier, 2007; pp 343–368. https://doi.org/10.1016/B978-044452707-3/50021-5.
(110). Chung, H.-J.; Woo, K.-S.; Lim, S.-T. Glass Transition and Enthalpy Relaxation of Cross-Linked Corn Starches. *Carbohydr. Polym.* **2004**, *55* (1), 9–15. https://doi.org/10.1016/j.carbpol.2003.04.002.
(111). Zarei, M.; Aalaie, J. Application of Shear Thickening Fluids in Material Development. *J. Mater. Res. Technol.* **2020**, *9* (5), 10411–10433. https://doi.org/10.1016/j.jmrt.2020.07.049.
(112). Avila-de la Rosa, G.; Carrillo-Navas, H.; Echeverría, J. C.; Bello-Pérez, L. A.; Vernon-Carter, E. J.; Alvarez-Ramirez, J. Mechanisms of Elastic Turbulence in Gelatinized Starch Dispersions. *Chaos, Solitons & Fractals* **2015**, *77*, 29–38. https://doi.org/10.1016/j.chaos.2015.04.013.
(113). Groisman, A.; Steinberg, V. Elastic Turbulence in a Polymer Solution Flow. *Nature* **2000**, *405* (6782), 53–55. https://doi.org/10.1038/35011019.
(114). Rock, A.; Hincapie, R. E.; Tahir, M.; Langanke, N.; Ganzer, L. On the Role of Polymer Viscoelasticity in Enhanced Oil Recovery: Extensive Laboratory Data and Review. *Polymers* **2020**, *12* (10), 2276. https://doi.org/10.3390/polym12102276.
(115). Li, M.; Wu, Q.; Moon, R. J.; Hubbe, M. A.; Bortner, M. J. Rheological Aspects of Cellulose Nanomaterials: Governing Factors and Emerging Applications. *Adv. Mater.* **2021**, *33* (21), 2006052. https://doi.org/10.1002/adma.202006052.
(116). Barnes, H. A. Shear-Thickening ("Dilatancy") in Suspensions of Nonaggregating Solid Particles Dispersed in Newtonian Liquids. *J. Rheol.* **1989**, *33* (2), 329–366. https://doi.org/10.1122/1.550017.
(117). Wagner, N. J.; Brady, J. F. Shear Thickening in Colloidal Dispersions. *Phys. Today* **2009**, *62* (10), 27–32. https://doi.org/10.1063/1.3248476.
(118). Gharehkhani, S.; Gao, W.; Fatehi, P. In-Situ Rheological Studies of Cationic Lignin Polymerization in an Acidic Aqueous System. *Polymers (Basel)* **2020**, *12* (12), 2982. https://doi.org/10.3390/polym12122982.
(119). Dong, H.; Zhang, Q.; Gao, J.; Chen, L.; Vasanthan, T. Comparison of Morphology and Rheology of Starch Nanoparticles Prepared from Pulse and Cereal Starches by Rapid Antisolvent Nanoprecipitation. *Food Hydrocolloids* **2021**, *119*, 106828. https://doi.org/10.1016/j.foodhyd.2021.106828.
(120). Torres, M. D.; Chenlo, F.; Moreira, R. Rheological Effect of Gelatinisation Using Different Temperature-Time Conditions on Potato Starch Dispersions: Mechanical Characterisation of the Obtained Gels. *Food Bioprocess Technol.* **2018**, *11* (1), 132–140. https://doi.org/10.1007/s11947-017-2000-6.
(121). Zhang, H.; Wehrman, M. D.; Schultz, K. M. Structural Changes in Polymeric Gel Scaffolds Around the Overlap Concentration. *Front. Chem.* **2019**, *7*, 317. https://doi.org/10.3389/fchem.2019.00317.

5.7. Appendix A. Supporting information

Temperature Responsive Crosslinked Lignin-Starch Macromolecule

Jonathan A. Diaz-Baca, Pedram Fatehi*

Chemical Engineering Department, Lakehead University, 955 Oliver Road, Thunder Bay, ON P7B SE1, Canada

*Corresponding author: E-mail: pfatehi@lakeheadu.ca; Tel.: +1-807-343-8010-8697; Fax: +1-807-346-7943

Number of pages 14 (S5.1-S5.14)

Number of Figures 11 (S5.1-S5.11)

Number of Tables 2 (S5.1-S5.2)

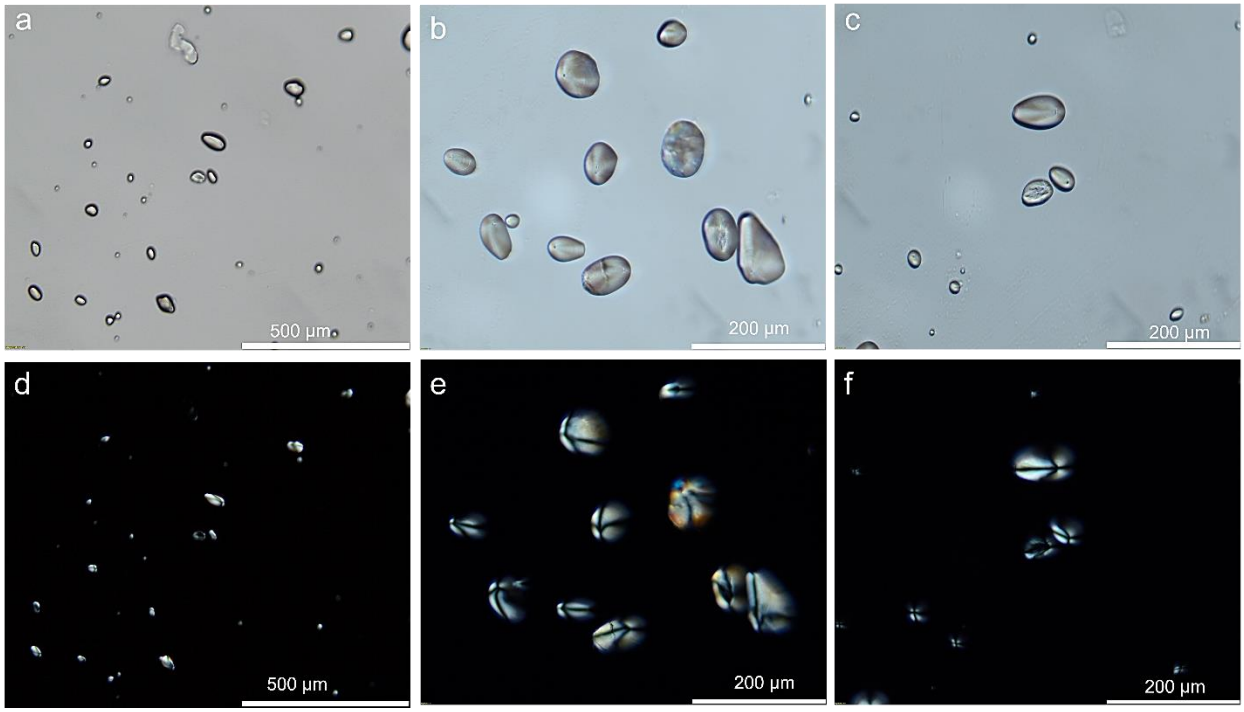

Figure S5.1. Morphology of starch under plain-polarized transmitted light microscope (a, b, and c). Morphology of starch granules under cross-polarized transmitted light microscope (d, e, and f).

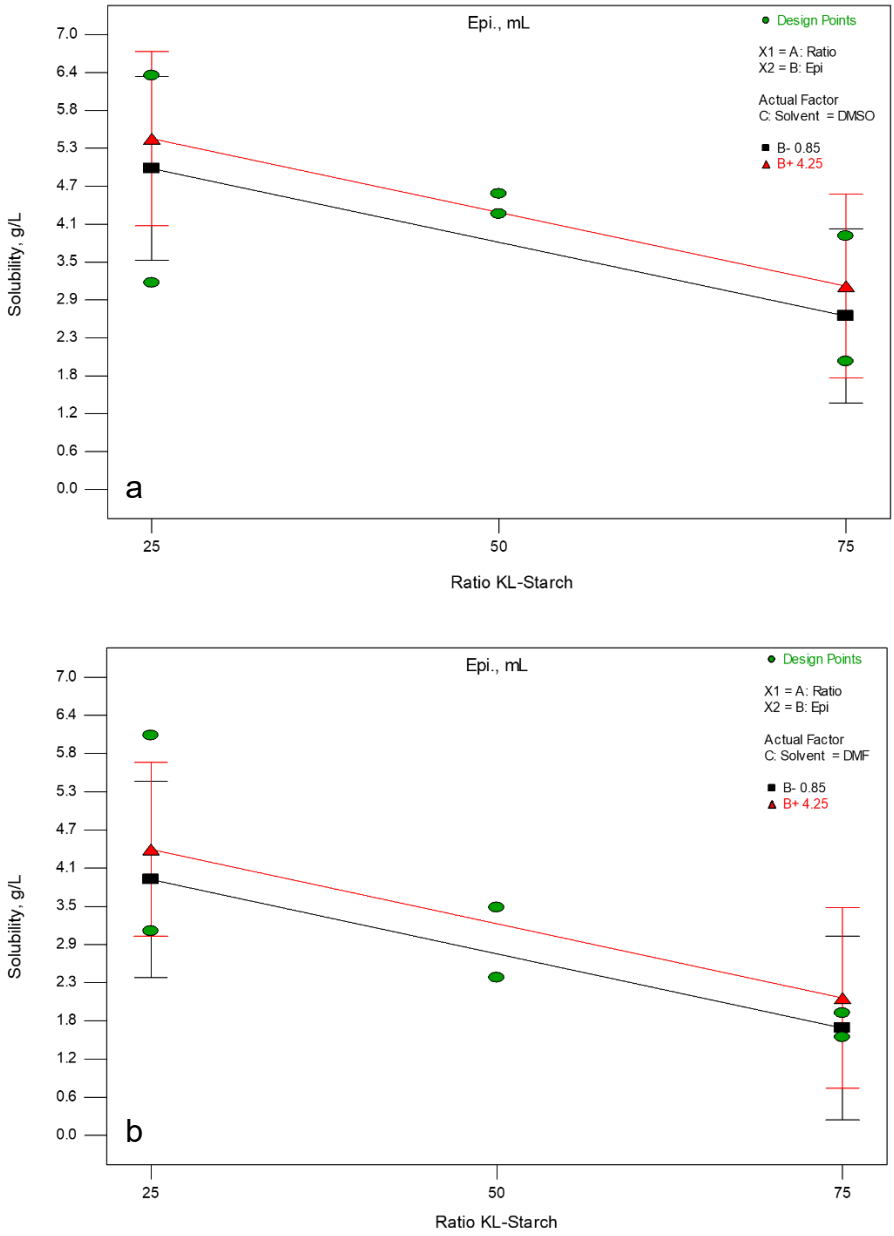

Figure S5.2. Interaction plot for (a) the effect of KL to starch ratio, ECH concentration and DMSO. (b) the effect of KL to starch ratio, ECH concentration and DMF on the solubility of KLS copolymers. Correspondingly green colored circles represent the actual experimental values.

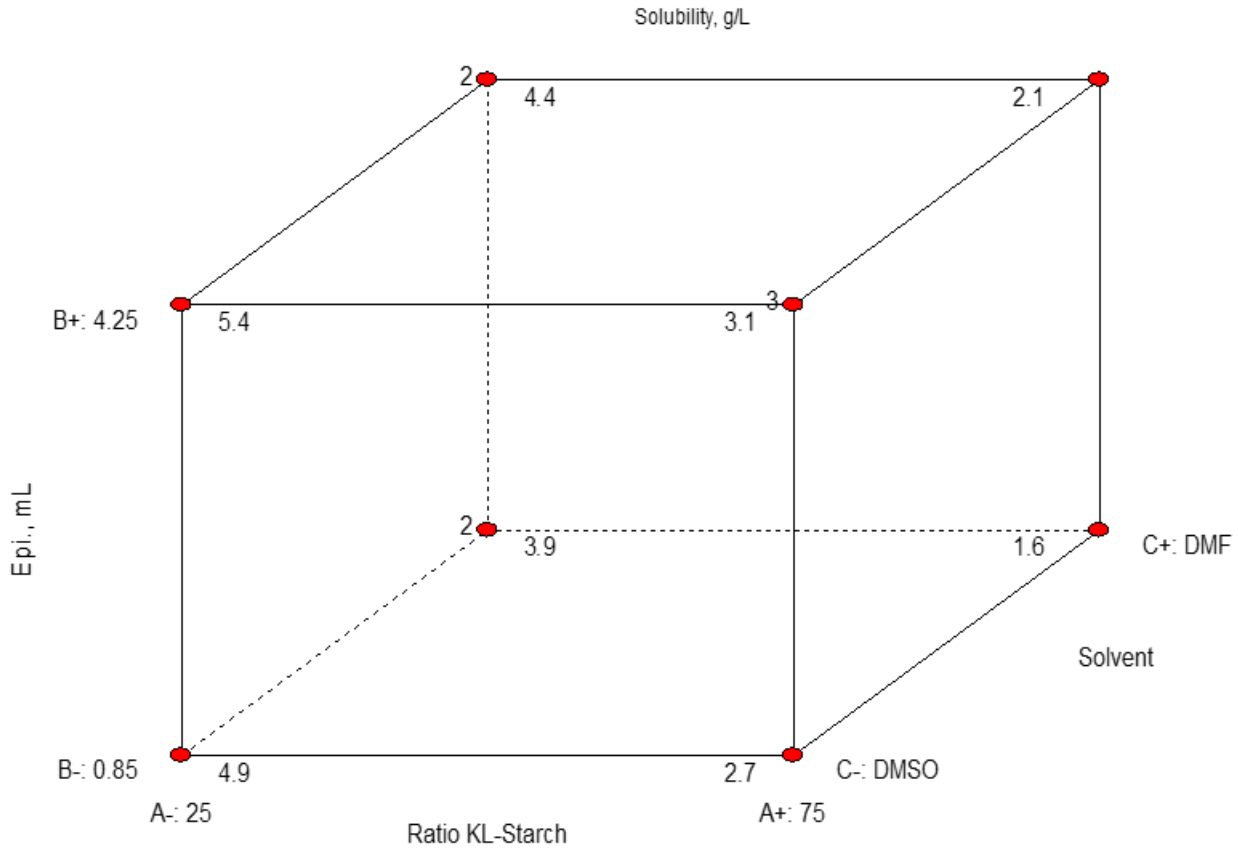

Figure S5.3. Cube plot for the solubility of KLS copolymers under the interaction of factors A (ratio KL to starch), B (Epi. volume) and C (solvent).

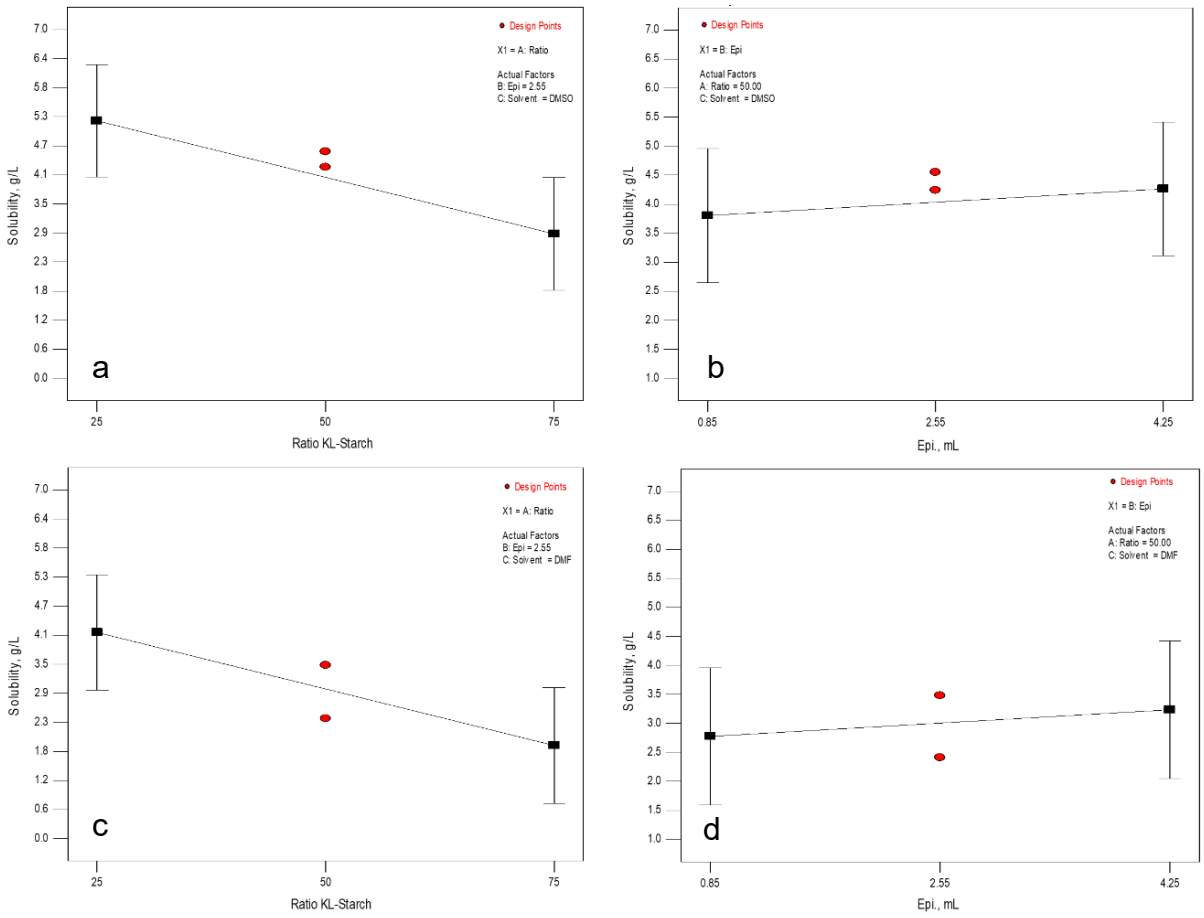

Figure S5.4. Main effects plot of two-factor interaction for the solubility of KLS copolymers. Factors A (ratio KL to starch), B (Epi. volume) and C (solvent). (a) Factor A when B=2.55 and C=DMSO. (b) Factor B when A=50 and C=DMSO. (c) Factor A when B=2.55 and C=DMF. (d) Factor B when A=50 and C=DMF.

Table S5.1. The experimental parameters, solubility, charge density and phenolic hydroxyl group content of KL, starch and KLS co-polymers.

Sample	Yield after purification, %	Solubility, g/L	Total charge density, mmol/g	Ph–OH group, mmol/g
KL	N/A	2.35	-0.5	1.54 ± 0.14
Starch	N/A	0.96	-0.5	N/A
KLS-5	47.2	3.18	-0.1	0.27 ± 0.14
KLS-1	89.3	3.12	-0.1	0.31 ± 0.05
KLS-7	92.1	6.37	-0.2	0.42 ± 0.07
KLS-3	82.2	6.11	0.0	0.51 ± 0.20
KLS-6	60.7	3.90	-0.1	0.73 ± 0.13
KLS-2	60.1	1.87	0.0	0.65 ± 0.05
KLS-8	45.2	1.97	-0.2	0.32 ± 0.12
KLS-4	79.9	1.50	0.0	0.35 ± 0.06
KLS-9	45.5	4.55	-0.3	0.37 ± 0.09
KLS-11	59.1	3.48	-0.1	0.28 ± 0.08
KLS-10	79.0	4.24	-0.2	0.22 ± 0.05
KLS-12	69.1	2.41	0.0	0.23 ± 0.08

± standard error

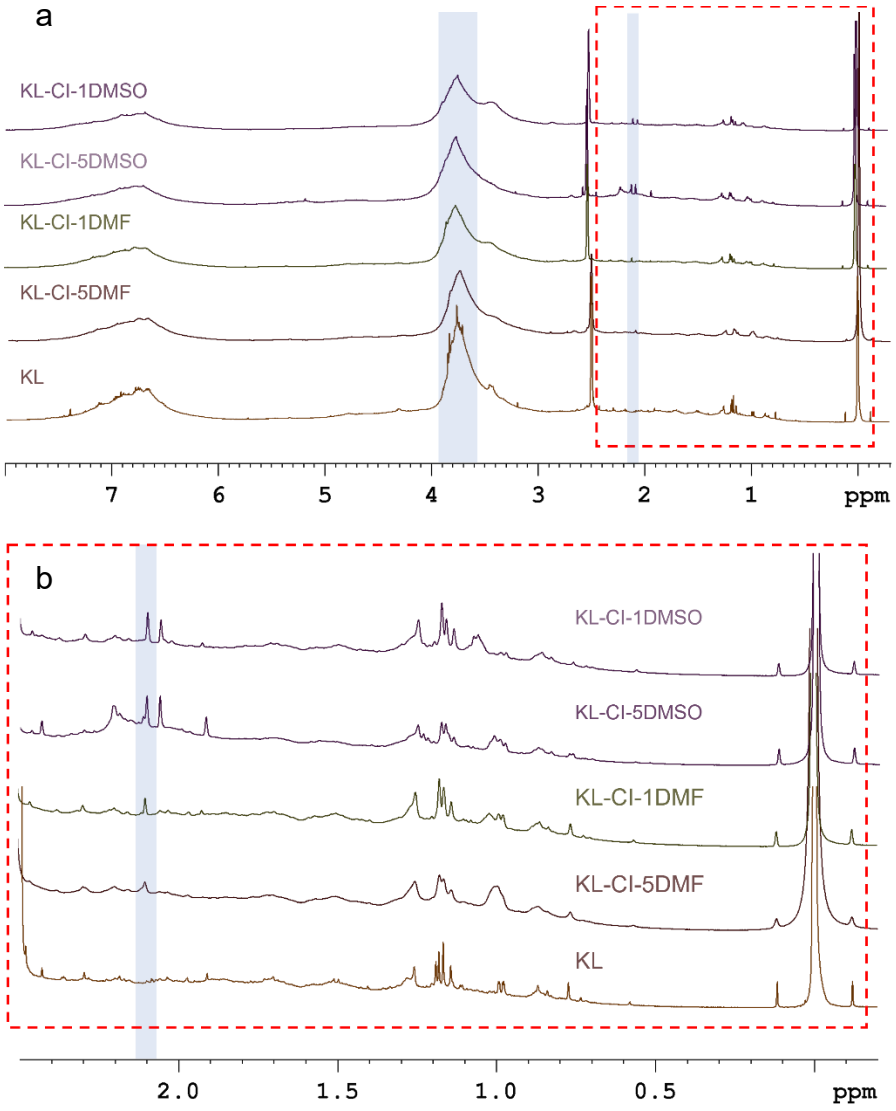

Figure S5.5. (a) ^{1}H-NMR of KL-CI intermediate products from the 1st step of the copolymerization reaction. (b) Zoom view of the ^{1}H-NMR from KL-CI samples.

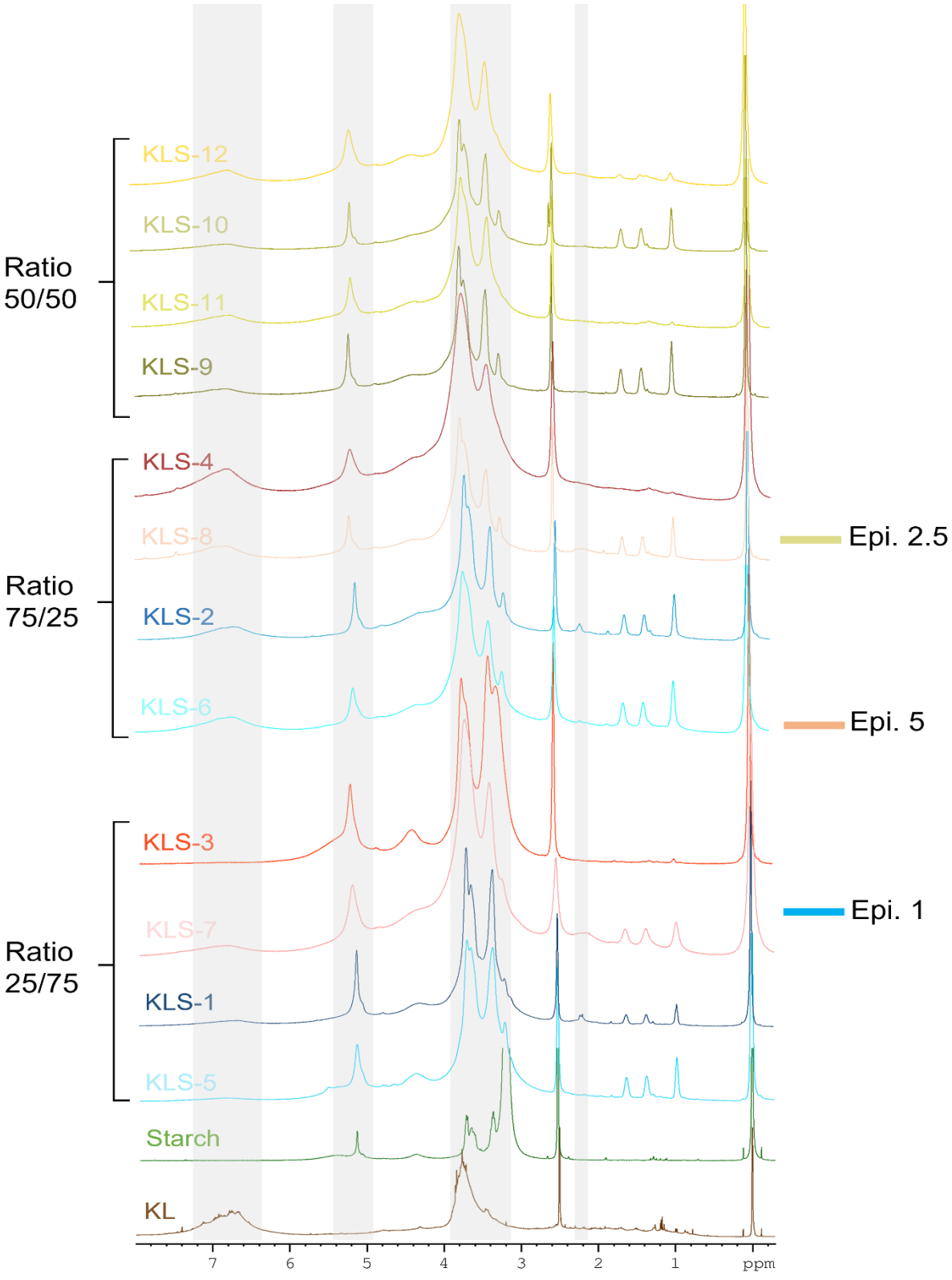

Figure S5.6. ^{1}H-NMR spectra of KL, starch, and KLS products. The order of the spectra goes from the 25/75 KL/starch ratio starting bottom to top and color coded for the ECH concentration.

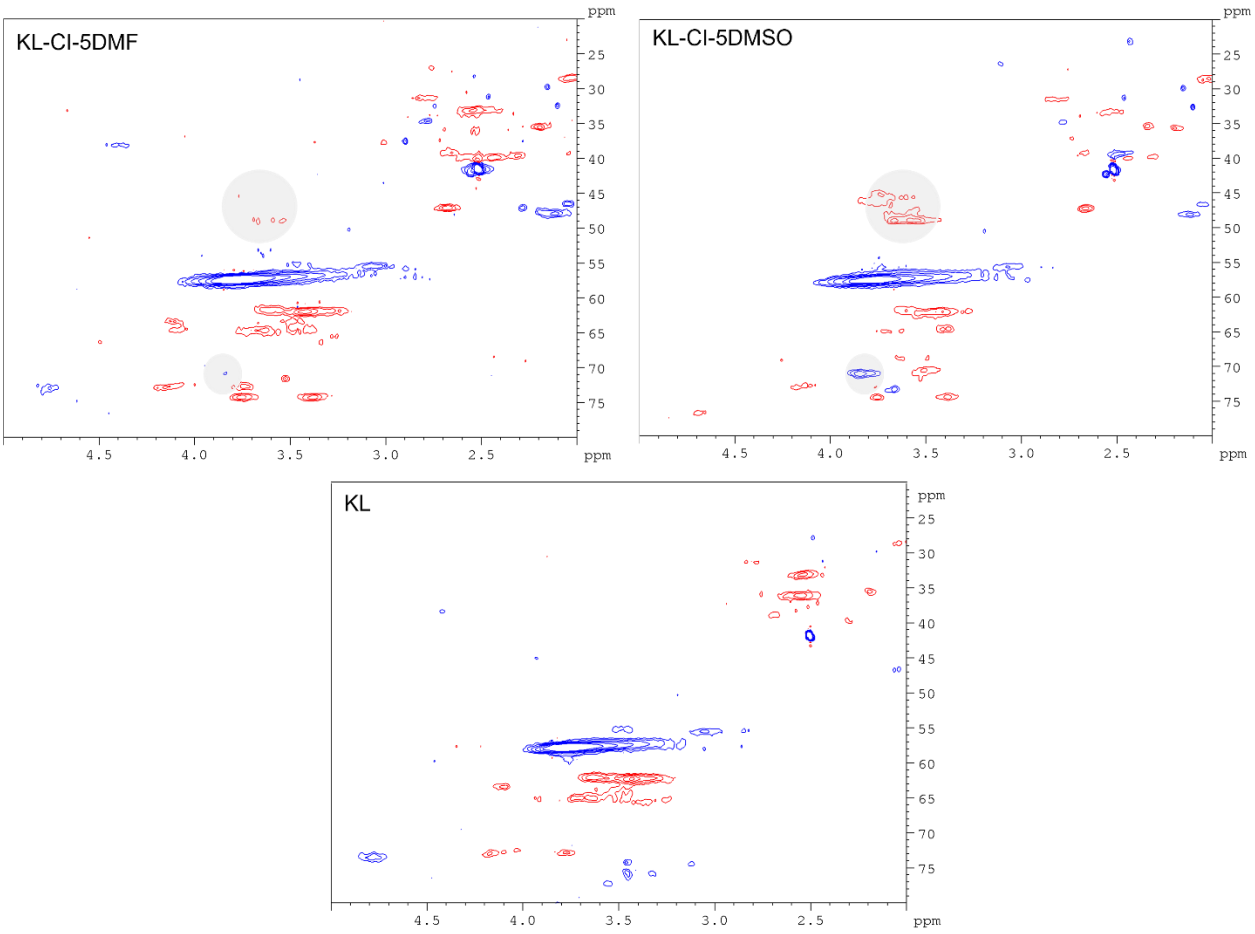

Figure S5.7. HSQC NMR spectra of KL and KL-CI from the 1st step of the copolymerization reaction. Comparing KL-CI-5DMSO and KL-CI-5DMF shows that a more significant decrement of –OH functional groups were obtained with DMSO (2.13 mmol/g), resulting in the most efficient solvent for the etherification of KL.

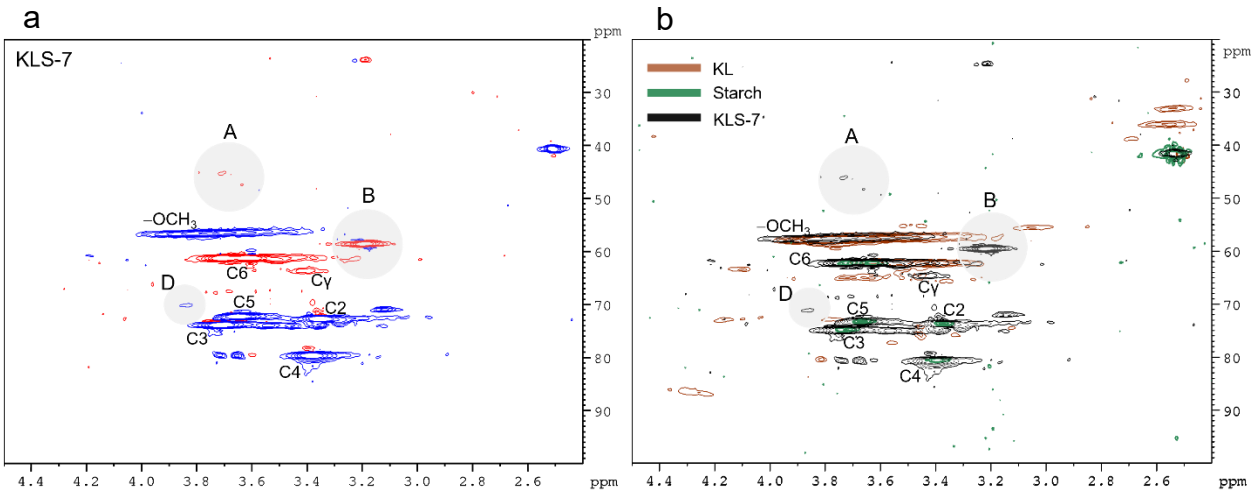

Figure S5.8. (a) ^{1}H-^{13}C HSQC NMR spectra of KLS-7. Cross-peaks corresponding to CH_1 or CH_3 groups appears in blue (positive region), while cross-peaks from CH_2 appear in red (negative region). (b) Overlapped ^{1}H-^{13}C HSQC NMR spectra of KL, starch, KLS-9 (c). The labels are assigned as described in Figure 5.1.

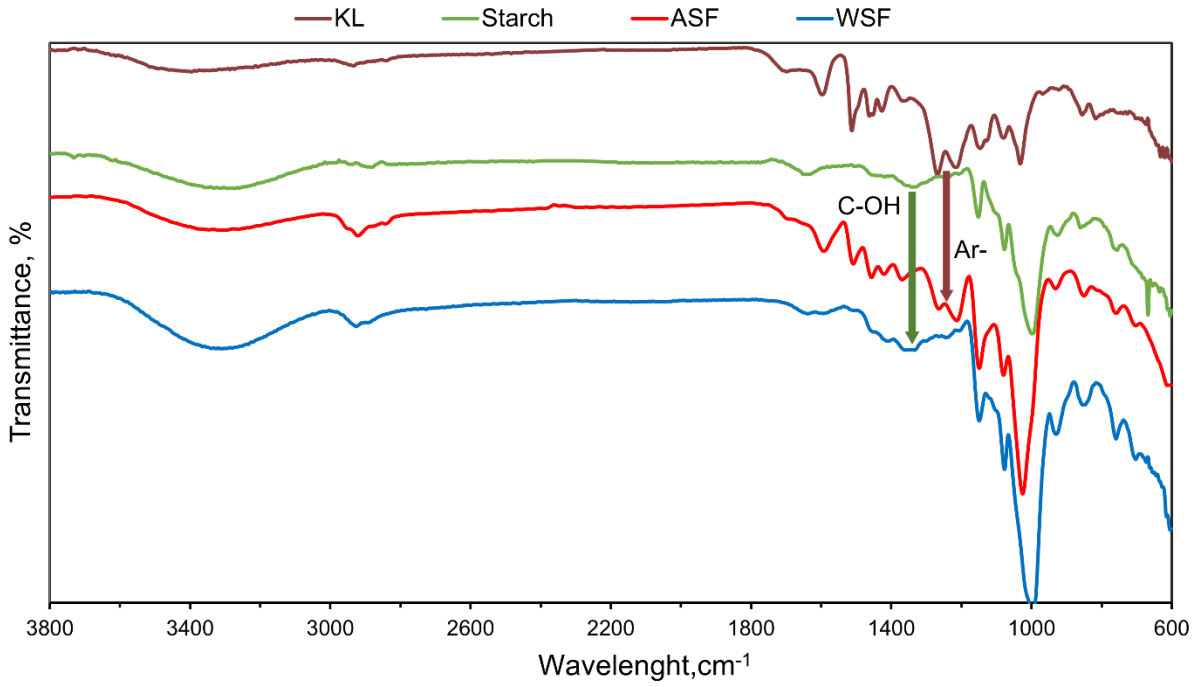

Figure S5.9. FT-IR spectra of KL, starch, washing products ASF (acetone soluble fraction) and WSF (water soluble fraction). Green arrow indicates the band related to the bending vibration of starch molecule (C-OH) at 1338 cm^{-1}. Brown arrow indicates the band related to vibrations of the aromatic (Ar-) units in KL at 1268 cm^{-1}.

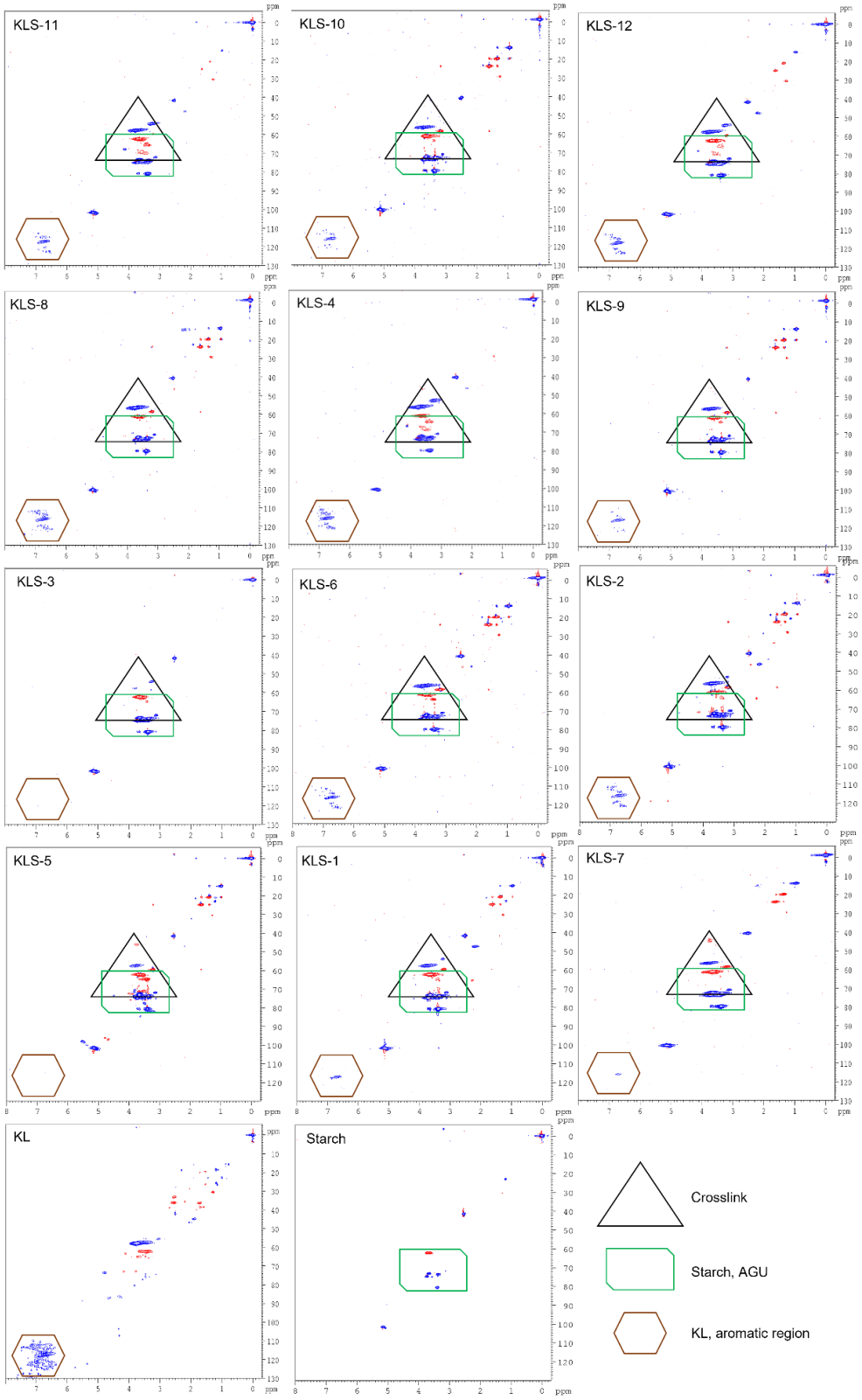

Figure S5.10. ^{1}H-^{13}C HSQC NMR spectra of KL, starch, and KLS products. The identified cross peaks are: brown hexagon (Guaiacyl, Syringyl), green rectangle (starch's AGU), black triangle

(crosslink). The cross-peaks corresponding to CH_1 or CH_3 groups appears in blue (positive region), while cross-peaks from CH_2 appear in red (negative region).

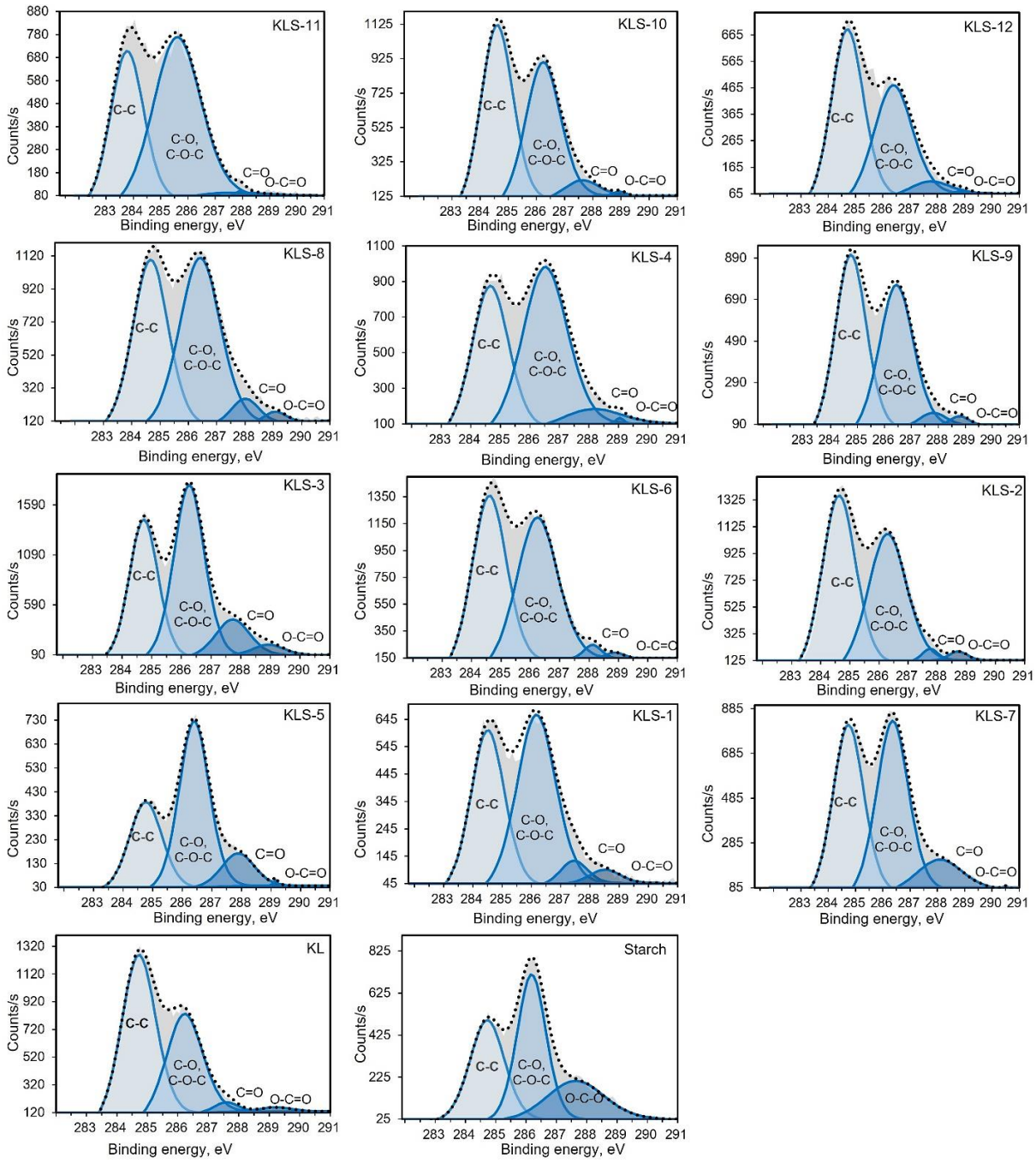

Figure S5.11. XPS spectra of C1s for KL, starch, and KLS products. Dotted line represents the fitted curve and shaded peaks represent the envelope.

Table S5.2. Quantitative chemical bonds at the surface of KL, starch, and KLS products determined via XPS analysis.

Sample	C 1s mass concentration, %			
	C1 (C-C)	C2 (C-O, C-O-C)	C3 (O-C-O)	C4 (O-C=O)
KL	59.1 ± 1.9	37.2 ± 1.8	2.3 ± 0.9	1.3 ± 1.0
Starch	35.4 ± 2.2	42.3 ± 2.2	22.3 ± 2.4	-
KLS-5	32.5 ± 2.0	55.5 ± 2.2	11.7 ± 1.7	0.3 ± 0.1
KLS-7	44.0 ± 1.9	44.7 ± 2.0	11.2 ± 1.8	0.2 ± 0.1
KLS-4	40.4 ± 1.9	52.9 ± 2.0	6.4 ± 2.0	0.3 ± 0.2

± standard error

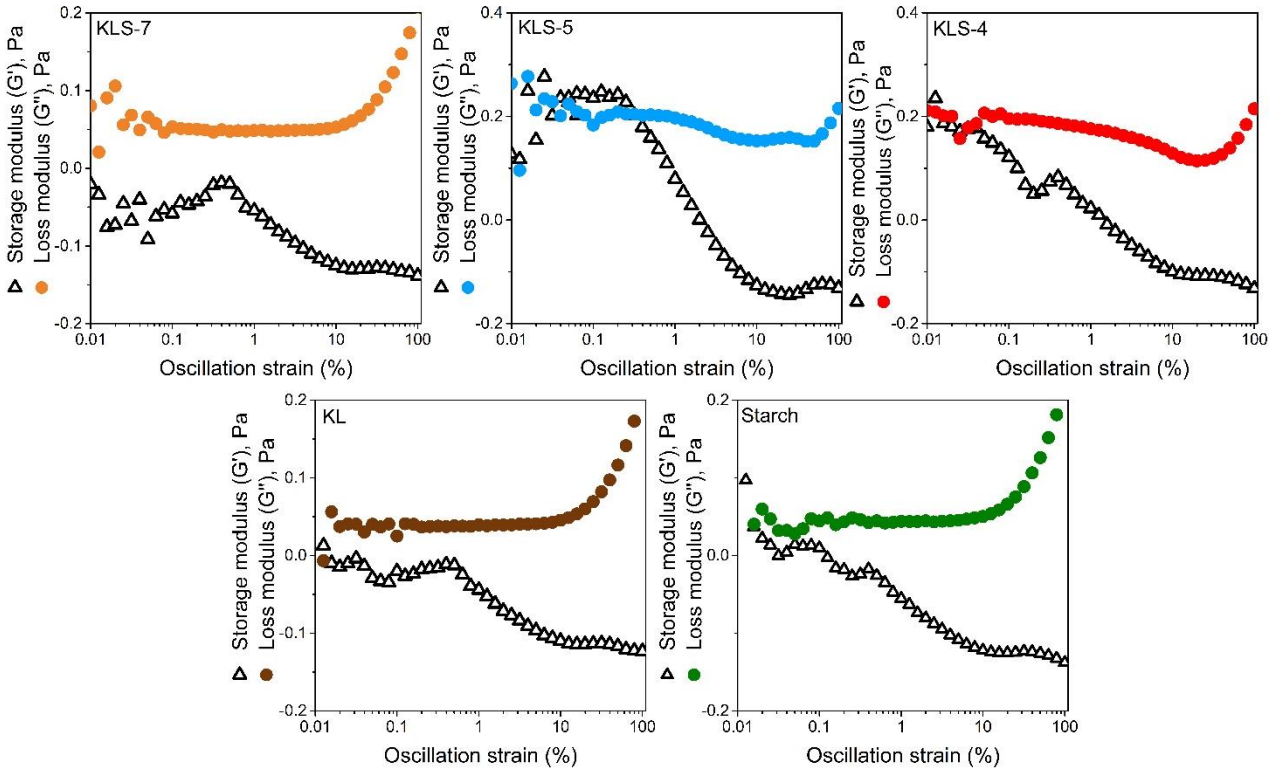

Figure S5.12. Oscillatory strain sweep (0.01 to 100 %) of 2 wt.% water dispersions of KL, starch and selected KLS copolymers at 25 °C.

Chapter 6: Conclusion and Recommendations

6.1. Summary of conclusions

In the literature review study, the chemical modification pathways and characterization methods of starch-lignin material were critically reviewed. The combination of starch with lignin is an effective strategy to generate composite matrices and biobased materials containing the advantageous properties of both biopolymers in a single reinforced material. Lignin confers desirable properties, such as hydrophobicity, thermal stability, UV blocking and antioxidant capacity, to the starch matrices. However, the starch-lignin materials are primarily produced with minimum lignin contents because the higher lignin contents often caused uneven lignin distribution, formation of aggregates, incompatibility, and phase separation, producing brittle and cracking materials. The chemical and structural characterization of starch-lignin materials is also challenging, because of their low solubility in traditional solvents. Moreover, starch-lignin materials are promising as matrices for the controlled release of bioactive molecules yet more comprehensive studies are needed. Finally, practical and commercial applications of starch-lignin materials are in the initial stages, and several scientific and technological gaps are to be filled.

In the first research study presented in this thesis, the LignoTall process was introduced as a new method for isolating lignin (TOL) in the kraft pulping operation. Furthermore, a comprehensive characterization of TOL was performed and compared to kraft lignin (KL) to assess similarities, differences, and potential applications. In comparison with KL, TOL possesses a higher sulphur content, higher carboxylate-OH concentration, and higher molecular weight. The results confirmed the possibility of generating lignin with new properties in the kraft pulping process following the LignoTall process. The characteristics and properties of TOL are attractive for its application as a reinforcer of rubber composites, and as an additive in the manufacturing of epoxy resins.

In the following research study, TOL and starch were successfully copolymerized with a sulphonate-containing monomer to produce water-soluble TOL-starch polymers. Ternary anionic TOL-starch copolymers (ALS-1 and ALS-5) were produced via radical polymerization, and their structures were investigated by comprehensive NMR analysis. The presence of the phenylcoumaran units with β-5' linkages from TOL, the anhydroglucose units and the glycosidic linkages from starch, and the propene unit from MPSA were confirmed by 1D (^{1}H-NMR) and 2D (COSY, HSQC, HSQC-TOCSY, and HMBC) NMR analyses. Moreover, the molecular weight of ALS-1 and ALS-5 was 1800×10^3 and 11000×10^3 g/mol, respectively. The flocculation performance of ALS-1 and ALS-5 was investigated. Because of their large molecular weight, tridimensional structure, and negative charge density, ALS-1 and ALS-5 demonstrated excellent flocculation performance for aluminum oxide-suspended particles. Overall, ALS-5 exhibited the best flocculation performance among all samples due to its larger molecular weight, charge density and extended and coil-like conformation.

In the last research study of this thesis, KL-starch macromolecules (KLS) were generated by covalently crosslinking KL with epichlorohydrin and starch. The macromolecules were successfully produced with high (75 wt.%), medium (50 wt.%) and low (25% wt.%) KL content. The crosslinking reaction was confirmed by NMR and XPS analysis, showing the presence of the glycerol ether linkages between KL and starch. The crosslinked KLS macromolecules had many hydroxyl groups capable of forming hydrogen bonds in water, stable at low temperatures but easily disrupted at high temperatures, displaying temperature-responsive properties. Additionally, the KLS macromolecules presented a globular conformation with different degrees of compactness and molecular weight as high as 4.16×10^5 g/mol. When KLS was dispersed in water, it formed a more structured network than KL and starch, as found by rheological characterization. Also, the

higher molecular weight and extended shape of KLS-5, prompted the formation of a gel-like structure stabilized by the hydrophobic interactions and hydrogen bonds, showing temperature-responsive viscoelastic properties after heating-cooling treatments.

Overall, the results of this thesis confirmed that although TOL and KL have the same botanical source and a similar isolation method, their properties differed considerably, mainly because of the fractionation procedure in LignoTall process. In addition, it was confirmed the feasibility for producing water-soluble and high molecular weight lignin-based polymers by covalently coupling lignin (TOL or KL) and starch. In the coupling reactions, either polymerization or crosslinking, the main functional groups involved in the reaction were the phenolic-OH of lignin and C6-OH of starch. The lignin-starch materials studied in this thesis showed no signs of incompatibility between lignin and starch even though they were composed with a proportion of lignin up to 75 wt.%, which is considerably higher in comparison with that previously reported. It was also demonstrated that lignin-starch polymers can have various properties depending on the reaction pathways and copolymer design. ALS-1 and ALS-5 were anionically charged, soluble in water and presented a larger molecular weight than KLS. Whereas KLS were non-ionic polymers, and in general, presented lower water solubility than ALS. However, KLS showed gel and film formation properties. Ultimately, the coupling of lignin and starch provides interesting new properties worth to be further explored for different applications where water solubility, gel and film formation, and thermo-responsiveness are important.

6.2. Recommendations for future work

The fundamental knowledge about the interaction of lignin and starch is still limited, and the starch-lignin materials' performance needs to be enhanced. Therefore, it is imperative to implement more comprehensive studies of starch-lignin materials and to compare the results against

traditional and commercial formulations; so that their potential use, challenges, and benefits are identified and addressed to comply with international standards. Moreover, the use of tailor-made solvent mixtures is recommended for improving the outcomes in methodologies, such as NMR or molecular weight analysis. Furthermore, the biodegradability and environmental impact of the starch-lignin materials must be closely studied. Based on the analysis of the existing literature, it is proposed to develop future studies around starch-lignin-controlled delivery systems, and to assess the applications of solution-based lignin-starch systems.

Regarding the LignoTall process and TOL, it is encouraged to investigate the use of TOL for manufacturing high-performance soft rubber materials, particularly those requiring hydrophobic properties. Also, it is advised to assess the economic viability of integrating the LignoTall technology into the kraft pulping process and to investigate suitable applications for all fractions obtained in the LignoTall process.

Although the flocculation performance of sulphonated TOL-starch polymer on aluminum oxide particles was promising, it is suggested that the sulphonated TOL-starch polymers are tested in industrial wastewater systems (e.g., mining tailing water), and compared against industrially used flocculants, such as polyacrylamide. Also, the utilization of other monomers, for instance, nitrogen-containing monomers, could be investigated for the copolymerization of TOL and starch. Moreover, future studies on the application of the thermo-responsive crosslinked KLS polymers are recommended, as hydrogel matrices, for the controlled delivery of bioactive molecules. Finally, to follow up with the United Nations' sustainable development agenda, it is advisable to revise the chemical methodologies presented in this thesis and try to implement greener methods in future research works, avoiding the use of organic solvents and opting for water-based aqueous reaction systems.

Publication Lists

(1). Diaz-Baca, J. A.; Fatehi, P. Production and Characterization of Starch-Lignin Based Materials: A Review. Submitted to *Chem. Eng. J.* **2022**

(2). Diaz-Baca, J. A.; Fatehi, P. Temperature Responsive Crosslinked Lignin-Starch Macromolecule. Submitted to *Carbohydr. Polym.* **2022**

(3). Diaz-Baca, J. A.; Salaghi, A.; Fatehi, P. Generation of Sulfonated Lignin-Starch Polymer and its Use as a Flocculant. Submitted to *Biomacromolecules.* **2022**

(4). Soliman, A.; Diaz-Baca, J. A.; Liao, B.; Fatehi, P. One-Pot Synthesis of Magnetic Cellulose Nanocrystal and Its Post-Functionalization for Doxycycline Adsorption. Submitted to *Carbohydr. Polym*. **2022**

(5). Salaghi, A.; Diaz-Baca, J. A.; Fatehi, P. Enhanced Flocculation of Aluminum Oxide Particles by Lignin-Based Flocculants in Dual Polymer Systems. J. Environ. Manage. **2023**, 328, 116999. https://doi.org/10.1016/j.jenvman.2022.116999

(6). Diaz-Baca, J. A.; Fatehi, P. Process Development for Tall Oil Lignin Production. *Bioresour. Technol.* **2021**, *329*, 124891. https://doi.org/10.1016/j.biortech.2021.124891